THE C-F BOND AS A CONFORMATIONAL PROBE IN AGONIST RECEPTOR INTERACTIONS

Poh Wai Chia

A Thesis Submitted for the Degree of PhD
at the
University of St Andrews

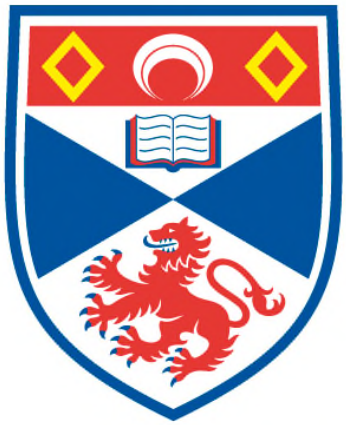

2012

The C-F bond as a conformational probe in agonist receptor interactions.

University
of
St Andrews

A thesis presented for the degree of Doctor of Philosophy to the School of Chemistry- University of St Andrews

Poh Wai Chia
December 2011

Submission of PHD and MPHIL thesis required declarations

1. Candidate's declarations:

I, Poh Wai Chia, hereby certify that this thesis, which is approximately 96,088 words in length, has been written by me, that is the record of work carried out by me and that it has not been submitted in any previous application for a higher degree. I was admitted as a research student I September 2008 and as a candidate for the degree of Doctor of Philosophy in August 2009; the higher study for which this is a record was carried out in the University of St. Andrews between 2008 and 2011.

Date…… Signature of candidate…….

2. Supervisor's declaration:

I hereby certify that the candidate has fulfilled the conditions of the Resolution and Regulations appropriate for the degree of Doctor of Philosophy in the University of St. Andrews and that the candidate is qualified to submit this thesis in application for that degree.

Date…… Signature of supervisor……

3. Permission for electronic publication:

In submitting this thesis to the University of St. Andrews I understand that I am giving permission for it to be made available for use in accordance with the regulations of the University library for the time being in force, subject to any copyright vested in the work not being affected thereby. I also understand that the title and the abstract will be published, and that a copy of the work may be made and supplied to any bona fide library or research worker, that my thesis will be electronically accessible for personal or research use unless exempt by award of a embargo as requested below, and that the library has right to migrate my thesis into new electronic forms as required to ensure continues access to the thesis. I have obtained any third-party copyright permission that may be required in order to allow such access and migration, or have requested the appropriate embargo below. The

following is an agreed request by candidate and supervisor regarding the electronic publication of this thesis: Embargo on both hard and electronic copy for the same fixed period of 2 years on the following ground: Publication would preclude future publication.

Date…… Signature of candidate……

Date…… Signature of supervisor……

Acknowledgements

I would like to express my deepest sense of gratitude and sincere thanks to my supervisor, Professor David O'Hagan for his constant encouragement, keen interest and thoughtful suggestion during this three years. I am also delighted to express my heartiest gratitude to all the members of David O'Hagan's group for their positive attitude and co-operation.

I would like to offer my sincere thanks to the science officers for their co-operation in obtaining the spectral data: Mrs Melanja Smith and Dr Tomas Lebl for the NMR service, Mrs Caroline Horsburgh and Dr Catherine H. Botting for the Mass Spectroscopy and Dr Philip Wormald for Chemical Hazard Risk Management.

I wish to express my hearty gratitude to my parents, brother and sister for their constant encouragement and sacrifice during all the years of my education.

Finally, I am grateful to Su-yin for her loving support and inspiration during the course of this higher study.

Abbreviation

α	alpha
Å	amstrong
Bn	benzyl
B	beta
Boc_2O	tert-butoxycarbonyl anhydride
br	broad
cat.	catalytic
CNS	Central Nervous System
CI	chemical ionization
COSY	correlation spectroscopy
de	diastereomeric excess
Deoxofluor™	(bis(2-methoxyethylamino) sulfur trifluoride)
DFT	density functional theory
DMAP	4-dimethylaminopyridine
DMF	dimethylformamide
ee	enantiomeric excess
EI	electron impact
GABA	γ-aminobutyric acid
GABA-AT	γ-aminobutyric acid aminotransferase
GCMS	gass-chromatography mass spectroscopy
HMBC	heteronuclear multiple bond correlation
Hz:	Hertz
J:	coupling constant

m:	multiplet
NMDA:	*N*-methyl-D-aspartate
NMR:	Nuclear magnetic resonance
ppm:	parts per million
singlet:	singlet
triplet:	triplet
TBAF:	*N*-tetrabutylammonium fluoride

Abstract

Chapter 1 gives an introduction on the physical and electronic properties of fluorine and the C-F bond. The application of fluorine in organic chemistry, which is mainly attributed to the electronic properties of fluorine is described. The role of fluorine in neuropsychiatric drug development and for influencing the conformational study of bioactive amines is also illustrated.

Chapter 2 of the thesis describes the synthesis of the two fluorinated stereoisomers (2*R*, 3*S*) and (2*S*, 3*S*) 3-fluoro *N*-methyl–D-aspartate (NMDA). These were prepared as analogues to study the binding conformation of NMDA on the glutameric NMDA receptor. The (2*S*, 3*S*)-3-fluoro NMDA D-**72** was successfully prepared from diethyl D-tartrate. The (2*S*,3*R*)- stereoisomer was prepared by separation of diastereoisomers generated by reaction of a *meso*- epoxide with an enantiomerically pure amine, followed by fluorination. Both the (2*S*,3*R*)- and (2*R*,3*S*)- enantiomers were prepared separately, however assignment of the absolute configuration to each enantiomer could not be unambiguously proven. The fluorinated 3F-NMDA stereoisomers were assessed by dose response analysis and TEVC analysis in the rat glutamate receptor. The biological results show that the (2*S*, 3*S*)-3F NMDA D-**72** is a good agonist, whereas (2*R*, 3*S*)- and (2*S*, 3*R*)-3-fluoro NMDA are inactive stereoisomers. The result of this study indicates that (*2S, 3S*)-3F NMDA D-**72** is the only relevant agonist that can access a conformation for binding to NMDA receptor.

Chapter 3 describes the preparation of fluorinated analogues of the calcium receptor agonist Cinacalcet. The (2*R*,1'*R*)-**123** and (2*S*,1'*R*)-**124** fluoro Cinacalcet diastereoisomers were prepared from 3'-(trifluoromethyl)cinnamic acid and 3''-SF_5-**137** Cinacalcet was synthesized from pentafluorosulfanyl benzyl alcohol. The biological assessment in the calcium receptor (CaR) revealed that both (2*R*,1'*R*)-**123** and (2*S*,1'*R*)-**124** fluoro Cinacalcet is slightly lower in potency compared to the non-fluorinated Cinacalcet 117. This suggests that the Cinacalcet 117 adopts an extended conformation when bound to the receptor. The 3''-SF_5-**137** Cinacalcet possesses equipotent activity with Cinacalcet **117**.

Contents

Chapter 2: Synthesis of 3-fluoro *N*-methyl-D-aspartate acid (NMDA) from Diethyl-D-tartrate.

Chapter 1: Fluorine in organic chemistry.

1.1 Introduction

The introduction of one or more fluorine atoms in an organic molecule can significantly alter its chemical and biological nature, including its stability, lipophilicity and bioavailability.[1] To date, around 30-40% of agrochemicals and 20% of pharmaceuticals contain a fluorine atom.[1] The exploration of introducing fluorine into a lead structure can enhance pharmacokinetics and affinity and is a general strategy of product development in medicinal chemistry.[2] In a recent survey, it is estimated that three out of 10 drugs of the leading 100 drugs by sales, sold in 2010, contained fluorine.[1]

Fluorine is not only a popular tool for tweaking a drug candidate's biological properties, its applications have also expanded to other fields, ranging from agrochemicals to fine chemicals. In the field of materials chemistry, flat screen technology would not be possible without the application of fluorine in the liquid crystals.[3] In the last decades, fluoropolymers such as Teflon™ **1** and CYTOP **2** have emerged as the fluorinated materials of choice for microchip manufacture and fiber optics.[3] In just over 100 years, the development of fluorine chemistry has been remarkable and fluorine building blocks are becoming increasingly important in all aspect of materials science.

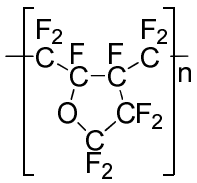

1

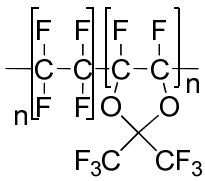

2

Figure 1.0 Structures of fluoropolymers Teflon™ **1** and CYTOP **2**.

1.2 Physical properties of fluorine

1.2.1 Electronic effects

Most of the profound effects resulting from fluorine incorporation come from its electronic properties. Fluorine is the most electronegative element in the periodic table, consequently fluorine forms a highly polarized bond with carbon. The high electronegativity of fluorine, introduces significant ionic character to the C-F bond. This C-F bond presents a significant polar character, which makes it the strongest bond between carbon and all other elements.[4] The small size of fluorine means that it is a good replacement for hydrogen without dramatically altering the molecular size.[5] **Table 1.0** summarizes the length and bond dissociation energy of some key bonds in organic compounds.

Bond	C-H	C-C	C-F	C-O	C-S	C-Cl	C-Br	C-I
Length [Å]	1.09	1.54	**1.39**	1.42	1.82	1.79	1.94	2.13
Energy (KJ/mol)	416	347	**485**	326	259	326	64	50

Table 1.0. Bond length and bond dissociation energy for atoms bonded with carbon.[4]

Although fluorine is very electronegative it can also be electron donating due to the mesomeric effect. Fluorine will stabilize carbocations and destabilize carbanions when placed α- to the charged centre as illustrated in **Figure 1.2**.[6] The stabilization of a carbocation arises from the back bonding of the fluorine lone pairs into the empty p-orbital. In the case of a carbanion, α- fluorine destabilization occurs due to lone pair-charge repulsion.

Resonance effect (stabilizing)

Lone pair-charge repulsion (destabilizing)

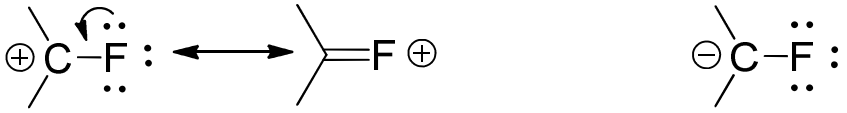

Figure 1.2 α- Fluorine stabilise carbocations and destabilizes carbanions.

While lone pair repulsion destabilises α-fluoro carbanions, a β-fluorine is found to stabilize carbanions by both inductive and hyperconjugation effects. This hyperconjugation effect arises due to electron donation into the electron deficient σ^* C-F anti-bonding orbital as illustrated in **Figure 1.3**. In contrast, a β-fluorine destabilizes carbocations by the inductive effect.

Negative hyperconjugation (stabilizing)

Inductive effect (destabilizing)

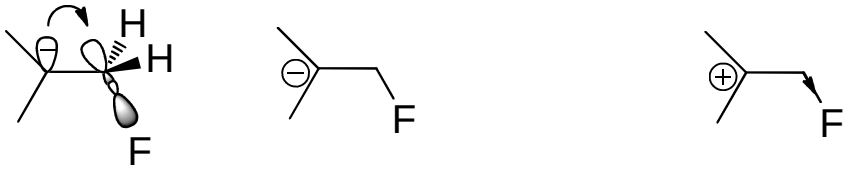

Figure 1.3 β- Fluorine stabilize carbanions by negative hyperconjugation and destabilize carbocations by the inductive effect.

1.2.2 Lipophilicity

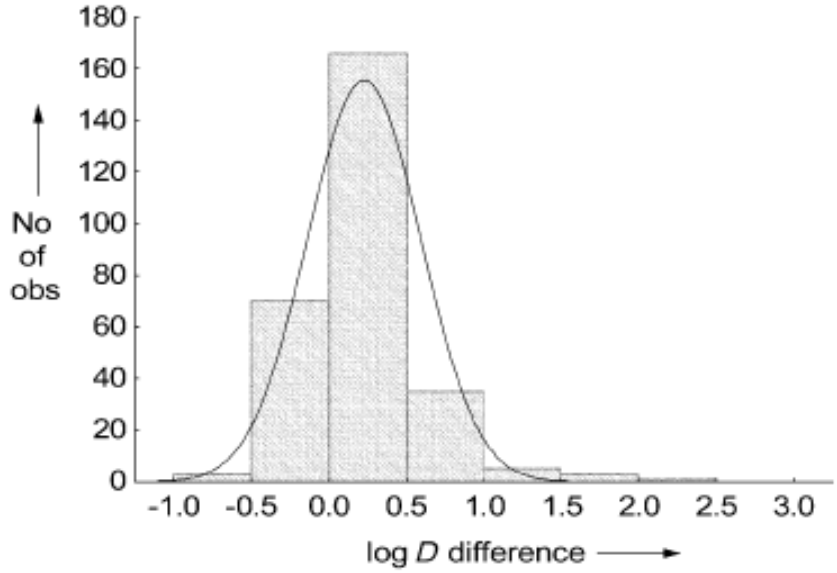

Figure 1.4. Histogram of lipophilicity change observed after H/F exchange. Reprinted with permission of H. J. Böhm, *ChemBioChem*., 1994, **5**, 637-643. Copyright 1994 WILEY-VCH Verlag GmbH & Co. KGaA, Weinheim.

Lipophilicity is an important parameter in the pharmacokinetics of drug design.[7] In order to tune this parameter, fluorine is considered to be a good tool for influencing the overall polarity of a molecule. This aspect has been examined systematically in several studies.[7] An early investigation by Roche was carried out on 293 pairs of molecules that differ by just one fluorine atom. The Log D is the logarithmic coefficient of the distribution of the compound between octanol and water at a pH 7.4. A histogram of changes in log D upon exchange of one fluorine for hydrogen was plotted (**Figure 1.4**). The histogram reveals that, on average the substitution of a hydrogen atom by fluorine increases the lipophilicity by about 0.25 log units, however in some cases it reduces the lipophilicity as evidenced by the distribution around Log D = 0 in **Figure 1.4**.[7]

1.2.3 Fluorine as an Isostere for hydrogen and oxygen.

Fluorine has a Van der Waals radius of 1.47 Å and is a reasonable steric replacement for hydrogen (1.20 Å) or oxygen (1.52 Å) as it causes minimal steric changes to the host molecules. Although the size of fluorine is only slightly bigger than hydrogen, it is the smallest atom after hydrogen to form a stable covalent bond to carbon. In terms of bond length, the C-F bond (1.39 Å) is more similar to the C-O bond (1.42 Å) than the C-H (1.09 Å) bond. Moreover, oxygen is the most electronegative element after fluorine. This suggests that fluorine could be considered as a good steric and electronic mimic of oxygen. A diversity of studies have explored fluorine in place of other functional groups, such as the carbonyl and hydroxyl groups.[8]

Bond	Van der Waals radius
C-F	1.47 Å
C-O	1.52 Å
C-H	1.20 Å
C-Cl	1.75 Å
C-Br	1.85 Å
C-I	1.98 Å

Table 1.1. Carbon-fluorine bond relative to other heteroatom bonds.[8]

Bioisosterism is a very important concept in medicinal chemistry, in which the interchange of a functional group does not affect the potency against the biological target of a drug candidate, but can affect the pharmacokinetics. A nice example is demonstrated by napthyl-fused diazepines (**Figure 1.5**).[9] Replacement of hydrogen in an *ortho* position of the phenyls **3a** and **4a** to give **3b** and **4b** respectively, resulted in enhanced affinity and efficacy. It is thought that the improvement was due to the C-F dipole interacting with an N-H residue in the binding site.

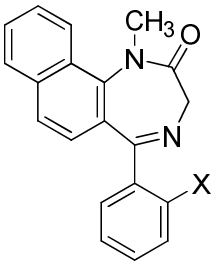

3a = H, IC_{50} = 1000 nM
3b = F, IC_{50} = 260 nM

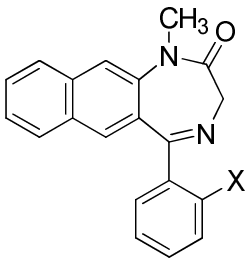

4a = H, IC_{50} = 1000 nM
4b = F, IC_{50} = 55 nM

Figure 1.5 Napthyl-fused benzodiazepine and their binding affinities.

Examples of this were also found in hydroxyl substitution by fluorine-18 in *β*-phenethanolamines as a possible strategy for *in vivo* Positron Emission Tomography (PET) imaging.[10] This work explored the effect of stereospecific replacement of the β-hydroxyl group of biogenic *β*-phenethanolamines with fluorine and at the same time was aimed at developing radiotracers for mapping the sympathetic nervous system of the heart by PET. Preliminary biodistribution studies in mice showed that both tracers exhibited good stability toward metabolic defluorination *in vivo*, with the (*1R,2S*) isomer FDE **5** showing a 3-fold higher radioactivity compared to the (*1S,2S*) isomer FDP **6**. This suggests that fluorine-18 labelling could be applied to radiolabelling of biologically important compounds such as phenthanolamines and catechoamines.

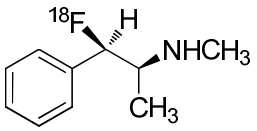

(*1R,2S*)-1-Fluoro-1-deoxyephedrine (FDE) **5**

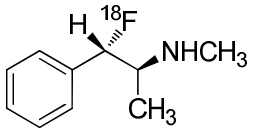

(*1S,2S*)-1-Fluoro-1-deoxypseudoephedrine (FDP) **6**

Figure 1.6. FDE **5** and FDP **6** in PET labeling study.

The metabolic stability of a drug candidate is a central concern in many drug discovery programmes and many lipophilic compounds have a tendency to be oxidized by liver cyctochromes P450 enzymes. One of the strategies used to overcome this is to employ fluorine substitution to block a metabolic site. A successful example is demonstrated by the cholesterol absorption inhibitor Ezetimibe **8**.[11] Drug modification was initiated from SCH48461 **7**, a moderately potent compound, with two metabolically labile sites. Introduction of fluorine atoms prevents the oxidation of the phenyl ring to phenol and dealkylation of the methoxy group, leading to a successful drug candidate.

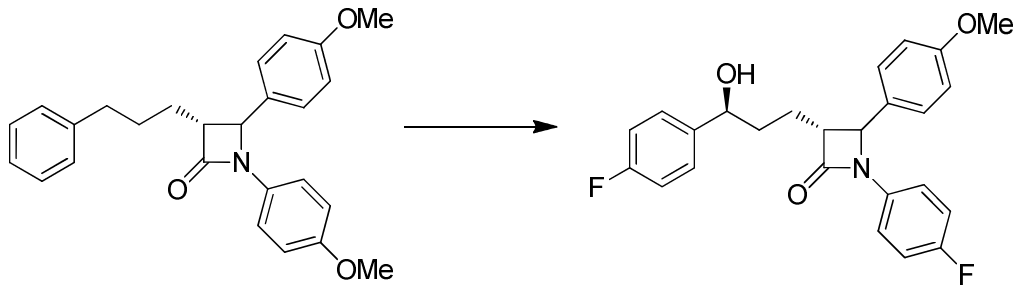

SCH 48461 **7**
ED_{50} (hamster)= 2.2 mg Kg^{-1}

Ezetimibe **8**
ED_{50} (hamster)= 0.04 mg Kg^{-1}

Figure 1.7. Development of Ezetimibe **8** from SCH48461 **7**.[11]

1.2.4 Acidity and Basicity

Fluorine substitution influences the acidity or basicity of nearby functional groups. The pK_a shift of several fluorinated analogues of carboxylic acids, alcohols and imides have been evaluated. Increasing the acidity (pK_a) and lowering the basicity (pK_b) of organic compounds is a general effect of nearby fluorine due to its inductive influence. **Table 1.2** shows the changes of pK_a and pK_b observed in a range of fluorinated and non-fluorinated organic compounds.[12]

Acid	pK_a
C_6H_5COOH	4.21
C_6F_5COOH	1.75
CH_3CH_2OH	15.9
CF_3CH_2OH	12.4
C_6H_5OH	10
C_6F_5OH	5.5
Base	pK_b
$CH_3CH_2NH_2$	10.7
$CF_3CH_2NH_2$	5.9

Table 1.2. Acidities (pK_a) of and basicity (pK_b) of organic compounds in comparison with their fluorinated analogues.[12]

Medicinal chemists have utilized fluorine to fine tune the pK_a of amines and acids in drug candidates. This has led to better solubility and oral absorption of drug candidates.[13] However, the effect of fluorine on the oral absorption can be unpredictable. In medicinal chemistry, a change of pK_a can have a major effect on the pharmacokinetics of a drug. For fluorinated indole derivatives of $5HT_{1D}$ ligands, the low bioavailability due to their limited capacity to pass through membranes was overcome by selective introduction of fluorine. As a result, the incorporation of fluorine was found to reduce the basicity and at the same time led to improved oral absorption. The monofluorinated analogue **10** remained a good receptor binding drug, but with increased bioavailability. However, the difluoro compound **11** had a lower binding affinity compared to **9** and **10**, most probably due to a change of pK_a making it less basic.[13]

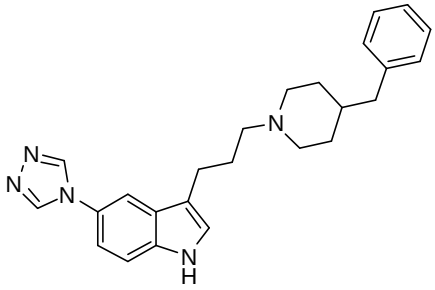

9

IC_{50} = 0.3 nM
pK_a = 9.7
very low bioavailability

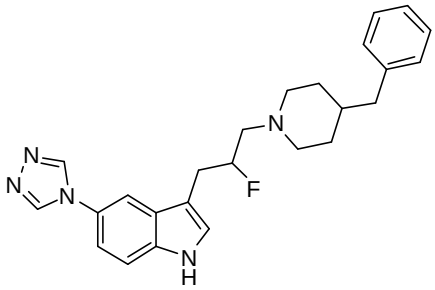

***rac*-10**

IC_{50} = 0.9 nM
pK_a = 8.7
medium bioavailability

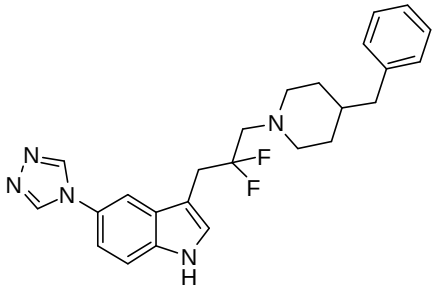

11

IC_{50} = 78 nM
pK_a = 6.7

Figure 1.8. Indole agonists to $5HT_{1D}$ receptors and some pharmacokinetic data.[13]

1.2.5 Hydrogen bonding

In general, fluorine is a very weak hydrogen bond acceptor due to its low polarisability and high electronegativity. The strength of hydrogen bonding for $C(sp^3)$-F---O-H has been estimated to be ~2.4 Kcal mol^{-1}, less than half of the strength of C-X---O-H (5-10 Kcal mol^{-1}), in which X is an electronegative element such as oxygen or nitrogen.[14] Another important aspect which requires into consideration is hybridization. Further evaluation on the $C(sp^2)$-F---O-H bond strength found that it was half that of the $C(sp^3)$-F---O-H and was measured to be (1.48 Kcal mol^{-1}), significantly lower than the

C(sp^3)-F---O-H. The decreased donor ability of allylic bound fluorine as shown in **Figure 1.9** was suggested to be due to the lone pairs of fluorine which are involved in π conjugation with the double bond and therefore are less available to participate in hydrogen bonding.

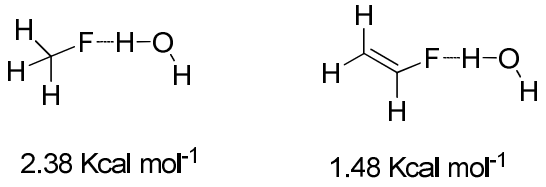

Figure 1.9 The F---OH bond for C(sp^3)-F---O-H is stronger than the C(sp^2)-F---O-H bond.[14]

As discussed above, organo-fluorine compounds form weak hydrogen bonds. This weakening in hydrogen bonding may influence the binding affinity of certain inhibitors and sometimes can have a profound effect on the reactivity of the compound. One notable example was demonstrated with the serine protease inhibitor factor Vlla (TF/Vlla).[15-17] The replacement of the carbonyl group of pyrazole **13** (k_i = 0.34 μm) with fluorine to give **12** was found to have good activity (k_i = 340 nm) with (TF/Vlla).

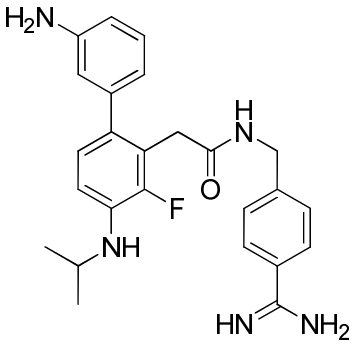

12

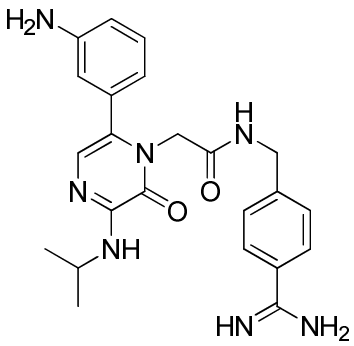

13

A similar observation was reported with a pair of serine protease inhibitors with antithrombotic activity, which just differ by one fluorine atom.[7] Their comparative investigation has led to the discovery of a novel serine protease inhibitor, where the

fluorinated analogue **15** (K_i = 260 nM) is six times more potent than the non-fluorinated inhibitor **14** (K_i = 1.6 μM). Interestingly, an X-ray co-crystal structure study revealed that there was a conformational change when **15** is bound to human thrombin, relative to **14** (**Figure 1.10**). The C-F unit of **15** favors a dipole interaction with the N-H residue of Gly 216, which leads to a different binding mode as observed in the co-crystal structure. This provided an insight that the C-F bond orients towards an electrophilic centre, resulting in enhanced binding affinity.

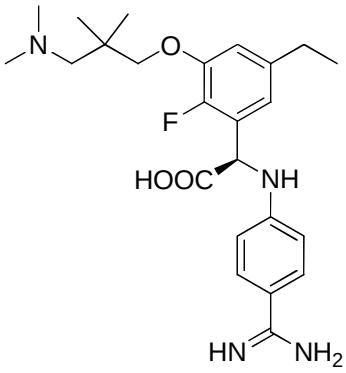

15
K_i = 1.6 μM

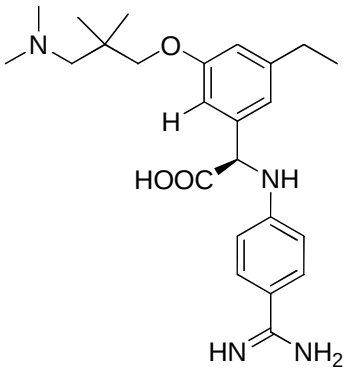

14
K_i = 260 nM

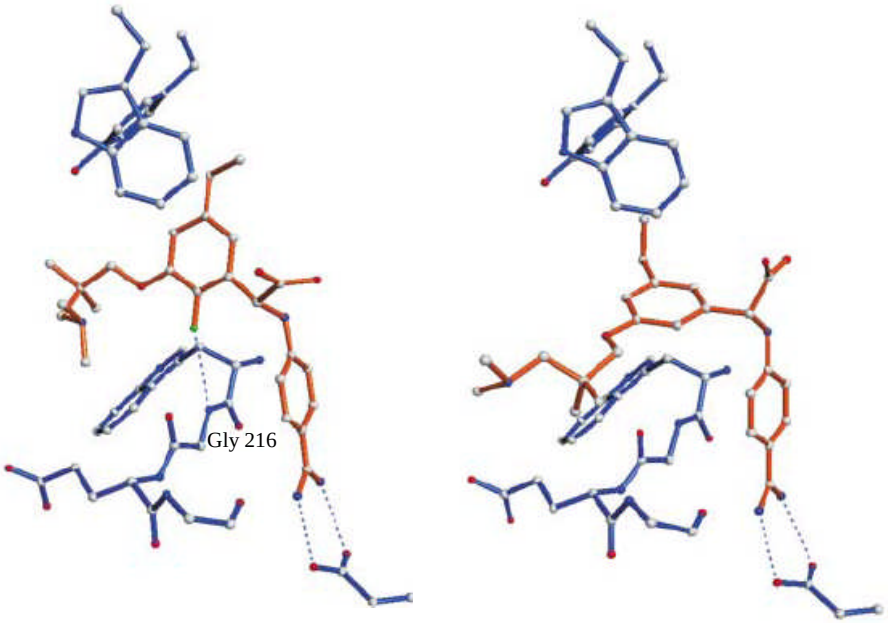

Co-crystal with **15** Co-crystal with **14**

Figure 1.10 Structure of two inhibitors with **15** and without fluorine **14** bound to thrombin. In the left hand structure, the F---N distance is 3.47 Å. Reprinted with permission of H. J. Böhm, *ChemBioChem*., 1994, **5**, 637-643. Copyright 1994 WILEY-VCH Verlag GmbH & Co. KGaA, Weinheim.

1.3 Effect of fluorine on molecular conformation

1.3.1 Stereo-electronic effects

Fluorine substitution can significantly alter the conformation of a molecule due to stereo-electronic effects derived from the polar C-F bond. In general, such stereo-electronic effects can be considered in three categories. These are hyperconjugation, dipole-dipole interactions and charge-dipole interactions. These effects will influence molecular conformation relative to hydrogen and the understanding of these fundamental properties is relevant to the research described in this thesis.

1.3.2 Hyperconjugation.

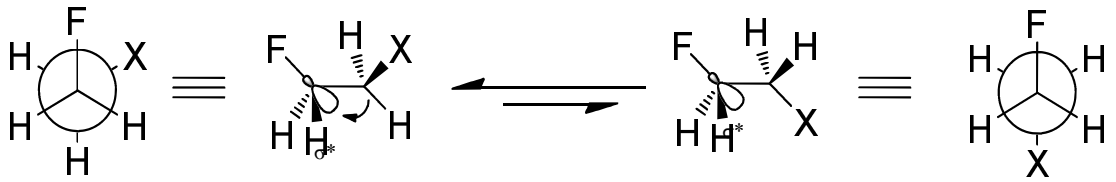

16 (X = F ; 0.8 Kcal mol^{-1})
17 (X = OAc ; 0.95 Kcal mol^{-1})
18 (X = NH_2 ; 1.0 Kcal mol^{-1})
19 (X = NHAc ; 1.8 Kcal mol^{-1})

Figure 1.11 *Gauche* effect associated with fluoroethanes. Values indicate the difference in energy between the *gauche* and anti conformers.

The "*gauche effect*" is the most widely discussed stereoelectronic effect associated with organic fluorine. It is observed when fluorine is placed vicinal to another electron withdrawing group such as amine, amide, acetoxy or fluorine.[18-21] Either *anti* or *gauche* staggered conformations are favoured. However, it is found that fluorine generally prefers a *gauche* rather than an *anti* conformation for most of these functional groups, as this conformation is stabilized by hyperconjugation.[22] This can be best explained by donation of electron density from the electron rich C-H σ-orbital into the electron-deficient C-F anti-bonding σ^* orbital, which occurs if the C-F bond is anti-periplanar to the C-H bond. For example when *erythro*- and *threo*-2,3-difluorobutanes were studied, it emerged that the *gauche* conformation was the more stable in both gas and solution (**Figure 1.12**). In the case of *erythro*-2,3-difluorobutane **20**, the *gauche* conformation **20b** is the most stable. Similarly, a combination of hyperconjugation and steric effects favors conformation **21a** for the *threo* isomer.[23]

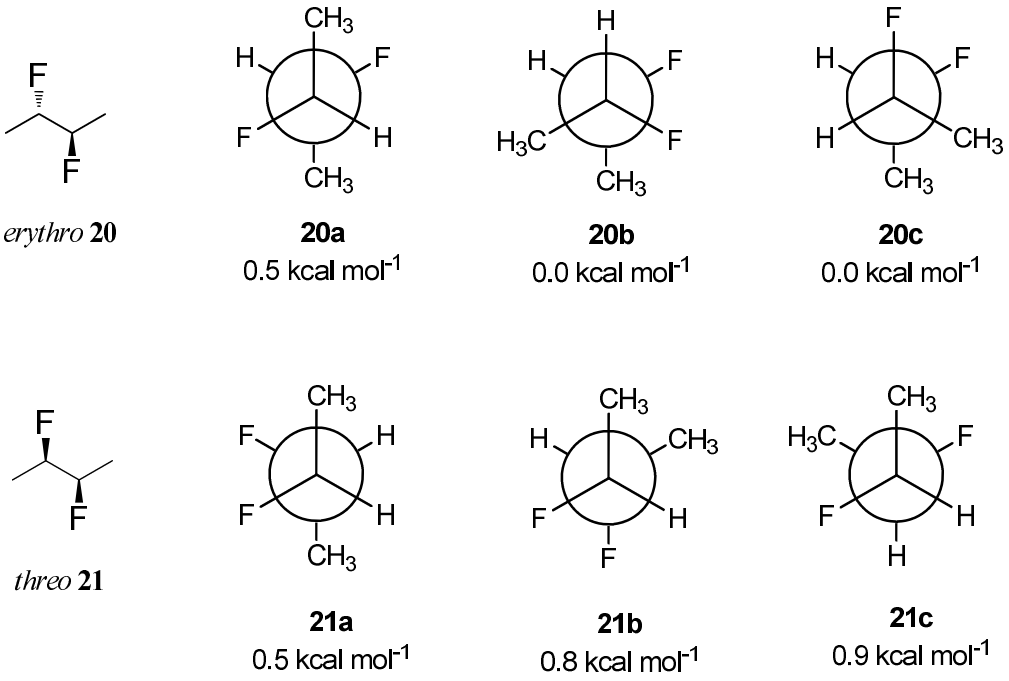

Figure 1.12 Newman projection of *erythro*- **20** and *threo*-2,3-difluorobutane **21**.

It should be noted that the *gauche* effect is not limited to a hyperconjugative explanation. Wiberg has proposed a "bent-bond" analysis. By this analysis, a covalent bond is represented by the direction of maximum electron density. In the *trans*-isomer of 1,2-difluoroethene the electron density of the central C-C sigma bond is distorted in opposite directions resulting in a reduced overlap and weakening of the σ C-C bond. Whereas, in the case of the *cis*-isomer, the electron density bends towards each other improving the overlap.[24] However, recent theorectical comparisons indicate that hyperconjugation is the major effect.[25]

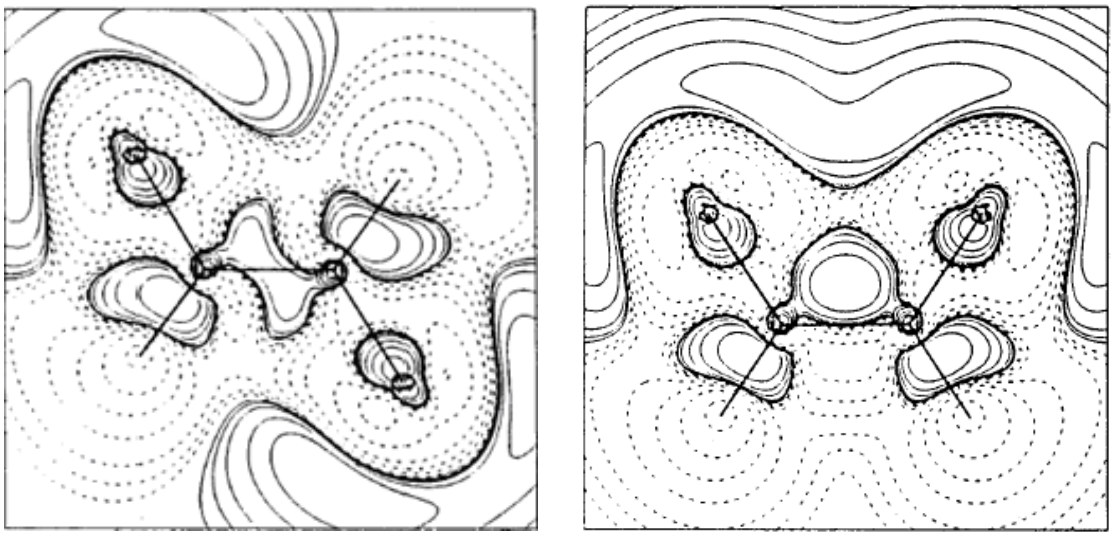

Figure 1.13 Difference between the electron density map for *trans*-1,2-difluoroethene (left) and *cis*-1,2-difluoroethene (right) using 6-31+G basic sets.[24] Reproduced with permission of K. B. Wiberg, *Acc. Chem. Res.*, 1996, 29, 229-234. Copyright 1996 American Chemical Society.

1.3.3 Dipole-dipole interactions

It is becoming increasingly apparent that the C-F bond of fluorinated drug type molecules interact with their binding site through dipole-dipole interactions. Indeed, Dederich *et al.* [26] studied these dipole-dipole interactions by examining the crystal packing of tricyclic phenylamidinium inhibitors of thrombin. The X-ray crystal structures revealed that the C-F bond is orientated towards the electropositive carbon of the amide, as shown in **Figure 1.14** The analysis extends to other weak dipole-dipole interactions such as to nitrile and fluoroaryl groups. This interaction was later exploited in a lead optimization program, in the case of the tricyclic thrombin inhibitor **22** (**Figure 1.14**).

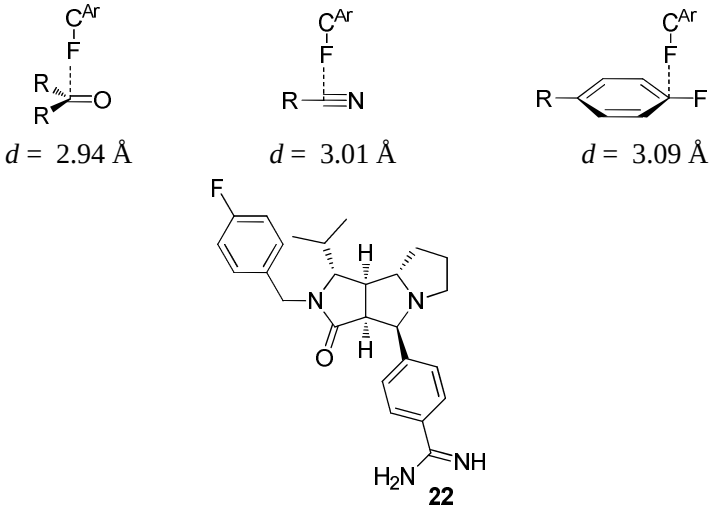

Figure 1.14 Dipole-dipole interactions of tricyclic thrombin inhibitor **22**.[26]

1.3.4 Charge dipole N^{+}….$^{\delta-}$F-C interactions.

The C-F bond will orient towards positive charge due to the negative dipole moment at fluorine. Such a charge dipole interaction which is electrostatic in nature, is a much stronger interaction compared to those interactions described so far. Synder and Lankin first reported that 3-fluoropiperidinium **23** had a preference for the C-F bond to lie axial **23a** rather than equatorial **23b**. Their study has been extended to explore the structural conformation of 3-fluorodimethylpiperidinium **24a**. Despite the large steric influence of the methyl groups, there remained a strong preference for the C-F bond to orient axial rather than equatorial as shown in **Figure 1.15**.[27]

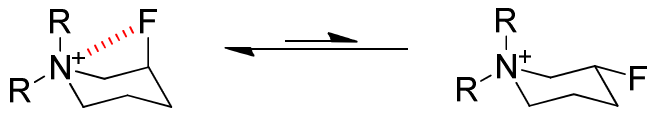

23a (R = H; 5.4 kcal/mol) **23b**

24a (R = CH_3; 4.0 kcal/mol) **24b**

axial equatorial

Figure 1.15 The axial conformations of 3-fluoropiperidinium **23** and 3-fluorodimethyl piperidinium **24** are stabilised by C-F--- N^{+} interactions.

The charge dipole interaction has subsequently been studied by different groups. 2-Fluoroethylammonium has a strong preference to align *gauche* **25a** rather than *anti* **25b** with respect to fluorine. DFT calculations have estimated this preference to be 5.8 kcal mol^{-1}, favoring the *gauche* conformation as shown in **Figure 1.16**.[28] The energy in favour of the *gauche* preference is much larger that the stereoelectronic *gauche* preference found in 1,2-difluoroethane (**Figure 1.11**).

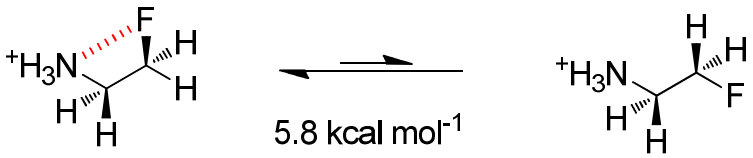

25a
gauche

25b
anti

Figure 1.16 The *gauche* conformation of 2-fluoroethylammonium **25** is stabilised by 5.8 kcal mol^{-1} over the *anti* conformation.

Other systems such as 3-fluoropyridinium salts **26** have been studied by NMR, *ab* initio calculations and X-ray crystallography. Consistent with the observation above, a strong preference for the *gauche* conformation is observed due to the electrostatic charge-dipole interaction.[29]

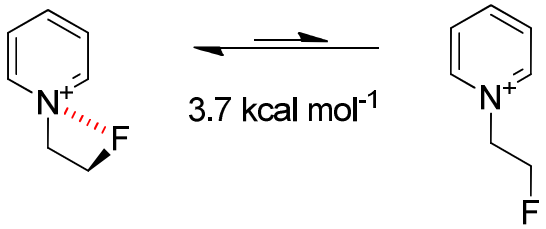

26a
gauche

26b
anti

Figure 1.17 The *gauche* conformation of 3-fluoropyridinium **26a** stabilised by F-C-C-N^+ over the *anti* conformation **26b**.

1.4 Fluorine in neurodegenerative diseases.

In the past, the positron emitting isotope F-18 has been used extensively in imaging for the purpose of detection of brain tumors, Alzheimer's and Parkinson's diseases in the CNS. More generally, introduction of fluorine improves the pharmacokinetics and lipophilicity of drug molecules as discussed earlier, thereby allow their absorption across the blood brain barrier. Many fluorinated drugs have been developed based on these properties. [30]

1.4.1 Drugs for depressive disorders.

Organofluorine compounds continue to make an impact in the development of neuroleptic drugs. Lately, fluorine was incorporated into drug molecules for the treatment of many Central Nervous System (CNS) diseases, such as depression, anxiety, Alzhimer's and Parkinson disease. A notable example is found in the development of the anti-depressant drug Lexapro **28**, an inhibitor for serotonin reuptake.[31] Neuropsychological processes in humans such as appetite, mood, muscle contraction and learning are modulated by serotonin **27**. Serotonin is found mainly in the enterochromaffin cells in the gut, brain and CNS.[31] Over the years, serotonin receptors have been the research target for many psychiatry and neurology disorders. Lexapro™ **28** in (*S*)-enantiomer form is one of the large class of serotonin reuptake inhibitors (SSRIs) that are on the market today.

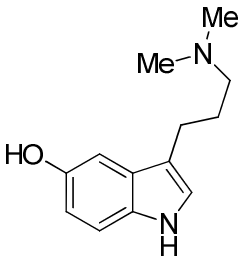

27

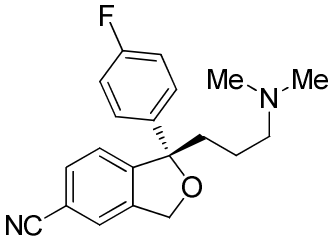

28

1.4.2 Drugs for anxiolytics and sedatives.

Fluorobenzodiazepines **29** is another representative class of important drugs in neurology. They work by controlling ion channel permeability to Cl^- ions and as a consequence modulate cell polarization controlled by $GABA_A$ receptors. To date, about thirty fluorinated analogues have been developed and marketed. These include Haloxazolam™ (*rac*-**30)**, Flutazolam™ **31** and Midazolam™ (*rac*-**32)** which act in a similar manner but are reported to be different in terms of pharmacokinetics and pharmocodynamics.[32]

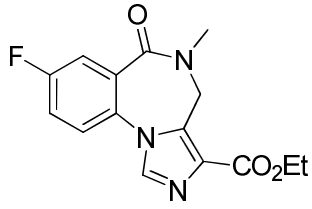

29

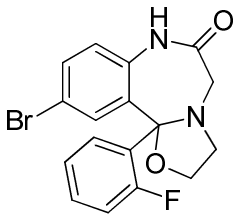

30

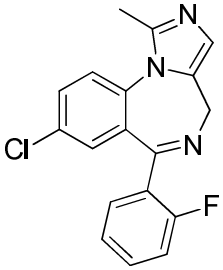

31

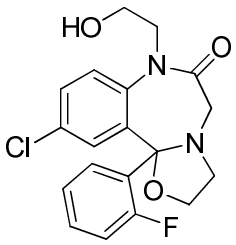

32

Rufinamide™ **33** is a drug developed by Norvatis for the treatment of epilepsy. It has currently advanced into Phase III clinical trials as an antiepilectic agent.[32] Sodium-dependent neuronal action is targeted by this antagonistic drug. As a result, the frequency of stimulation was reduced and thus patients were relieved from epilepsy.

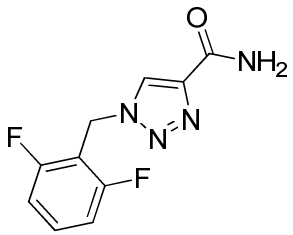

33

1.4.3 Drugs for Alzhimer's and Parkinson's disorders.

Flupirtine™ **34** developed by Viatris in 1986 is prescribed to treat migranes. Further evaluation of this drug indicated that it has the potential to treat Alzhimer's disease. Lately, it has been classified as a neuroprotector in neurodegenerative disease, especially in Alzheimer's and Parkinson's diseases.

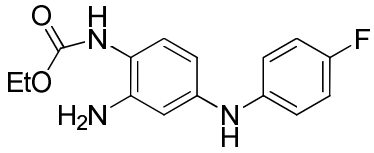

34

FK-960™ **35** developed by the Fujisama company was a drug candidate (Phase II) for treatment of Alzhimer's disease. This drug has however been abandoned, as an Alzhimer's candidate but it is still being evaluated for use in Schizopherenia disorders.[32] HCT-1026 (nitroflurbiprofen) (*rac*-**36)** was initially developed for the treatment of Alzhimer's disease, and is currently in advanced clinical trials for the treatment of overactive bladder and osteoporosis.

Overall, the cause of Alzhimer's and Parkinson's diseases still remain unknown. To date, the most successful drugs developed for the treatment of Parkinson's are

E-2007™ **37** and Safinamide™ **38**. E-2007™, developed by the Eisai company is currently being evaluated in Phase II clinical trials. It is an AMPA receptor antagonist targeting multiple diseases such as epilepsy and sclerosis. Safinamide™ **38** developed by the Newron company is currently in Phase III clinical trials for Parkinson's and Phase II for epilepsy.[32]

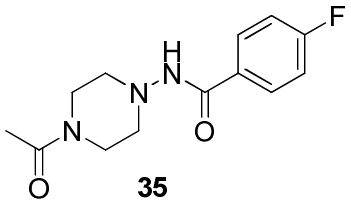

35

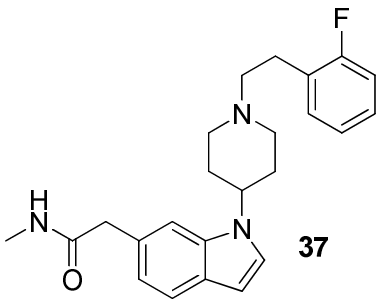

37

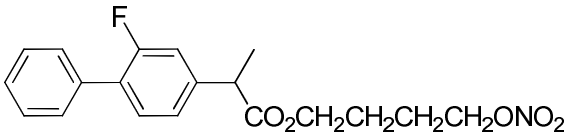

(*rac*-**36**)

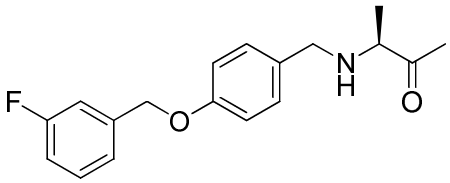

38

1.5 Conformational influence of the C-F bond.

The conformational effect of fluorine substitution has not been extensively studied and is only now emerging. The HIV protease agonist Indinavir **39** presents a good example in this case. For Indinavir **39**, the fluorinated analogue **40** is equipotent, while compound **41** is less potent. The potency of each of the fluorinated analogues could be attributed to the "*gauche* effect", with the vicinal OH group, which either reinforces or destabilizes a preferred binding mode for these molecules to their receptor.[33]

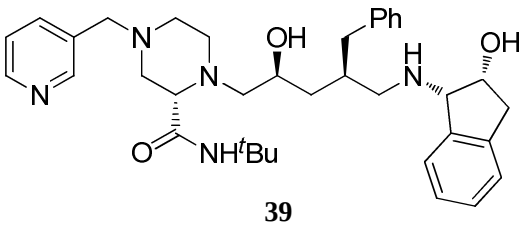

39

Indinavir, K_i = 1.9 nM

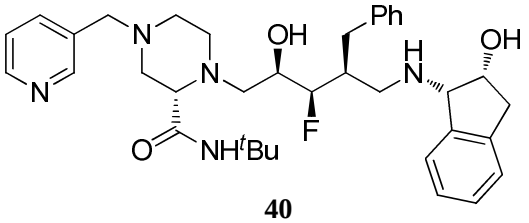

40

K_i = 2.0 nM

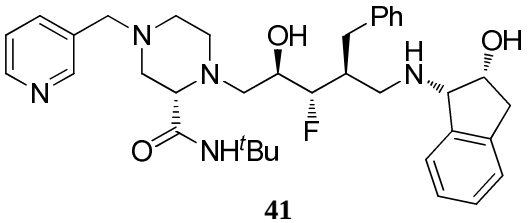

41

K_i = 27 nM

Figure 1.18 Fluorinated analogues of HIV protease inhibitors.

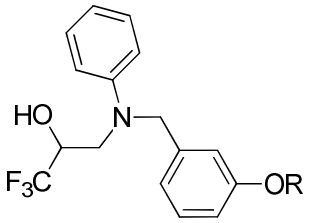

R = Et, *rac*-**42**.
R = CF_2CF_2H, *rac*-**43**

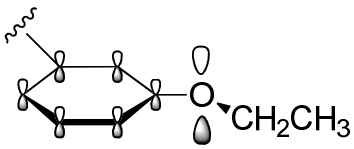

42

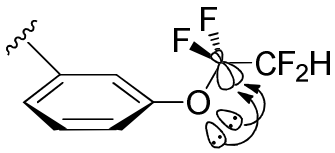

43

Figure 1.19 Cholesteryl ester transfer protein inhibitors **42** and **43**. In the fluorinated analogue **43**, $n_o \rightarrow \sigma^*_{CF}$ hyperconjugation leads to an out-of-plane orientation of the fluoroalkyl sidechain, resulting in improved binding affinity.

An interesting observation is found for compounds **42** and **43**.[34] Both are known to be inhibitors of the cholesteryl ester transfer protein and they are of potential value in the treatment of coronary heart disease. The fluorinated analogue **43** was found to be 8-fold more potent compared to the non-fluorinated **42**. The ether oxygen in **42** is significantly sp^2 hybridized to allow conjugation with the aryl π-system. This in turn forces the ethoxy group to align in the plane of the aryl ring. On the other hand, the fluorinated analogue **43** is essentially sp^3 hybridized and adopts an out-of plane conformation. Electron density from the two lone pairs donate into the two σ^*_{CF} anti-bonding orbital. As a consequence of the steric impact of the R group, the orthogonal orientation is preferred when binding to the target protein.

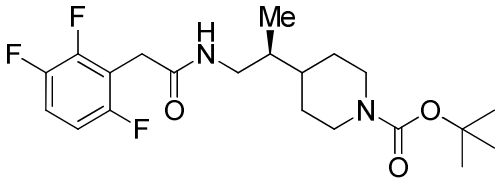

(*R*)-**44**

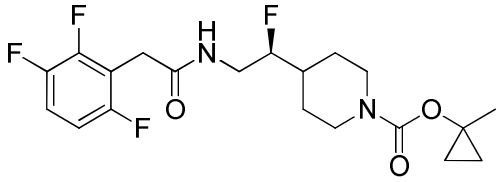

(*S*)-**45**

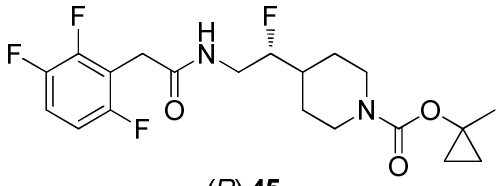

(*R*)-**45**

GPR119 (*R*)-**44** is an agonist of the human G-protein coupled receptor found in human enteric L-cells and in pancreatic β-cells. It plays an important role in regulating glucose homeostasis and is therefore a highly desirable drug candidate for the treatment of Type 2 diabetes. A drawback of this compound was found to be its high lipophilicity (E Log D = 4.3) which causes oxidative turnover in human liver microsomes (HLM). This led to evaluation of the fluorinated enantiomers (*S*)- and (*R*)-**45** GPR119.[35] These compounds now have a stereogenic centre containing fluorine with the fluorine *β* to the nitrogen of an amide. Such amides are known to display a *gauche* preference found more generally in N-*β*-fluoroethylamides.[35] Assay results have indicated that (*S*)-**45** has good agonist potency, and reduced lipophilicity and oxidative metabolism in HLM. By contrast, (*R*)-**45** has reduced potency, most likely due to a less compatible solution-phase conformation and unfavourable binding.[35]

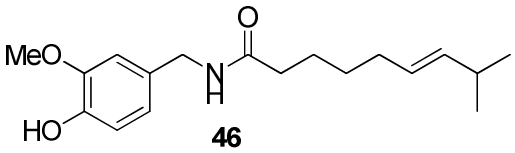

46

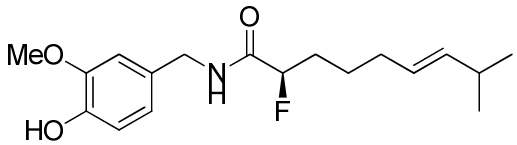

(*R*)-**47**

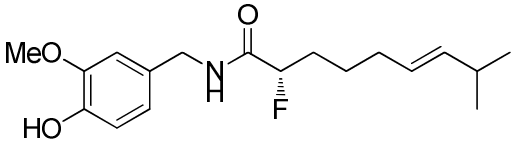

(*S*)-**47**

Capsaicin **46** is an active pain stimulant that is responsible for the pungency in chili peppers. Capsaicin is currently used as an analgesic and there is a continuous effort to develop analogues as potent painkillers. However, the binding mode of capsaicin to its receptor, TRPV1 remains unknown. Enantiomers of the α-fluorinated analogues of Capsaicin have served as a tool to explore the binding conformation by comparing the relative efficacy of the two enantiomers. It emerged that the two enantiomers (*R*)-**47** and (*S*)-**47** have the same efficacy as Capsaicin.[36] As a result, it is suggested that the two fluorinated analogues bind to TRPV1 in an extended conformation as shown in **Figure 1.20**. This conclusion was also in agreement with a previous model study, which concluded the extended chain of capsaicin aligned parallel to the lipid chain of the membrane.[36]

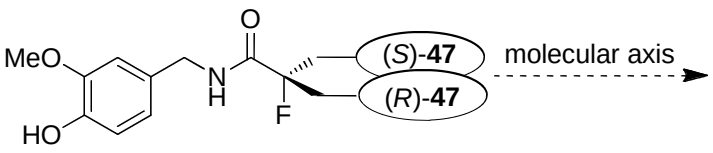

Figure 1.20 The suggested binding mode of capsaicin as deduced by comparison of α-fluorinated enantiomers of **47**. [36]

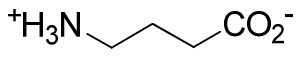

48

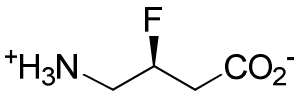

(*S*)-**49**

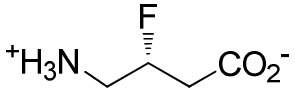

(*R*)-**49**

(*γ*-Aminobutyric acid) GABA **48** is an inhibitory neurotransmitter found in the mammalian central nervous system. It plays an important role in regulating human muscle tone. As discussed above, when the C-F bond is introduced *β* to an ammonium group it will orient *gauche* to the C-N^+ bond due to a stabilizing charge dipole interaction. Thus, fluorine induces a bias favouring conformations where the C-F and C-$^+NH_3$ bonds are *gauche* rather than *anti*. In order to understand more thoroughly the binding of GABA to its receptors, both 3-fluoro-GABA enantiomers have been used as conformational probes. Staggered conformations are illustrated by Newman projections in **Figure 1.21**. The relative efficacy of the two enantiomers was explored with $GABA_A$ and $GABA_C$ receptors and also the metabolising enzyme, GABA aminotransferase, an enzyme that degrades GABA. Evaluation of both (3*R*)- and (3*S*)-fluoro **49** showed that they had the same efficacy with the $GABA_A$ receptors, suggesting that the preferred binding conformation of GABA to the receptor is conformation **A** as shown in **Figure 1.21.**[37]

For $GABA_C$ receptors, the (*S*)-3F-GABA **49** was more potent that (*R*)-**49**.[38] This suggests that conformation **C** is the binding mode rather than **A**. This is clearly different from that observed in $GABA_A$ receptors, in which both isomers bind as conformation **A** in an extended conformation as shown in **Figure 1.21**.

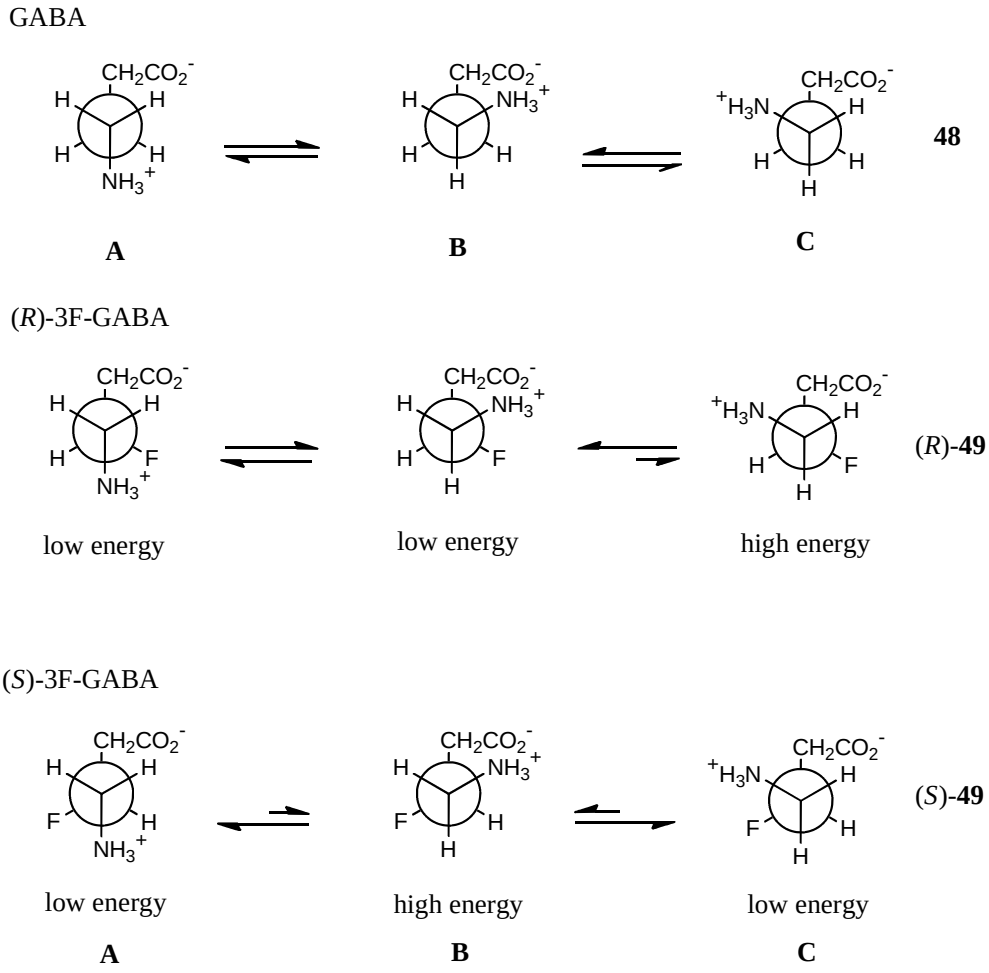

Figure 1.21 Newman projections illustrating staggered conformations A, B and C of GABA **48** and the enantiomers of (*R*)- and (*S*)-3F GABA **49**.

In a molecular docking study, (*R*)-3F-GABA **49** and (*S*)-3F-GABA **49** were docked into the receptor binding site of the p_1 $GABA_C$ subunit as shown in **Figure 1.22**. The $GABA_C$ receptor used in this study was developed based on homology to the X-ray structure of the *Lymnae stagnalis* acetylcholinesterase binding protein (AChBP).[38] Based on the molecular docking study, a different binding mode in $GABA_C$ has been observed to the previous study with $GABA_A$. **Figure 1.23** summarizes the two different binding modes of GABA for the $GABA_A$ and $GABA_C$ receptors.

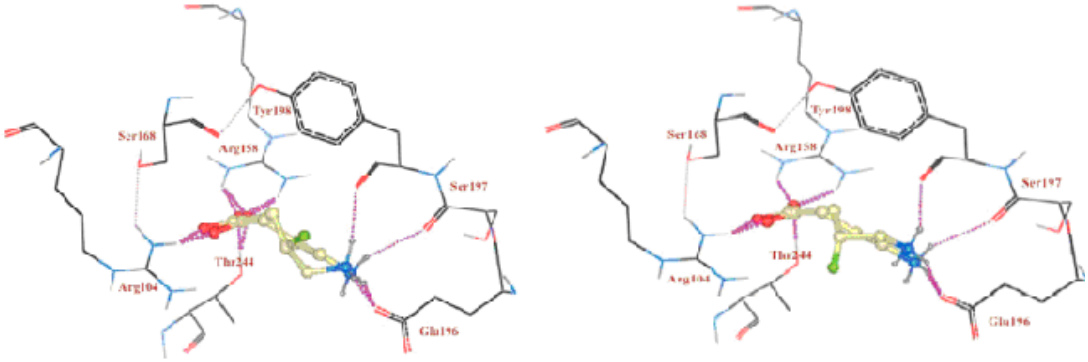

Figure 1.22. (*S*)- and (*R*)-3F-GABA **49** docked into the p_1 $GABA_C$ receptor ligand binding site.[38]

$GABA_A$ receptor binding mode

$GABA_C$ receptor binding mode

Figure 1.23. Comparison of the preferred binding mode of GABA to $GABA_A$ and $GABA_C$ receptors.

On the other hand, when both enantiomers were analysed with GABA aminotransferase, only (*3R*)-fluoro GABA **49** had high efficacy as a substrate for the enzyme. From this experiment, it was deduced that the preferred binding conformation of GABA to GABA-transaminase was conformation **B** (**Figure 1.21**).[37]

1.6 Towards predicting the conformational activity relationship on glutameric-NMDA receptors.

Evidence emerging from animals and receptor binding studies has shown that overactivation of the glutamate receptor leads to numerous neurological disorders.[39] *N*-Methyl-D-aspartate (NMDA) is an agonist of the glutamate receptor which induces reasonable activity in electrophysiological studies and was the focus in this conformational-activity study to gain an insight into binding at the glutamate receptors. The current tools used to explore binding conformation include co-crystallization of the corresponding receptors with agonist or by preparing a series of analogues to understand key binding residues. However, some of these techniques have limitations or drawbacks. The C-F bond as the most polar bond was envisioned as a conformational tool to explore the binding mode of different bioactive molecules. Numerous examples have shown that the C-F bond can influence the conformation of an organic molecule, especially when incorporated adjacent to other functional groups. As a consequence of this, two bioactive molecules were chosen as the targets in this study. Our first target involves the preparation of 3F-NMDA diastereoisomers **72** and **73** to explore the glutamateric NMDA receptors. The synthesis of 3F-NMDA **72** and **73** diastereoisomers and their biological study on glutamate receptors are described in the chapter 2.

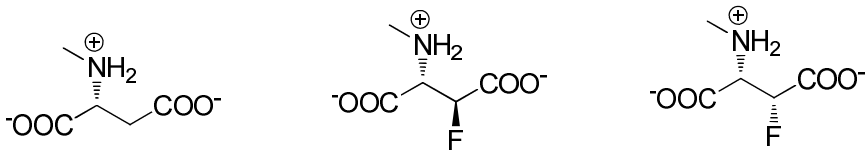

NMDA **52** | (*2S,3S*)- **72** | (*2S,3R*)- **73**

Another lead molecule which was selected for study is the Cinacalcet HCl, a calcimimetic drug that inhibits the production of parathyroid hormone (PTH) when bind to the allosteric site of the calcium sensing receptor. The binding mode of this molecule is unknown. In light of this, the C-F bond could serve as a tool to reveal the

important binding mode of this drug, for future drug development program. As part of this study, the CF_3-substituent of Cinacalcet HCl **117** will be swapped with the SF_5-substiuent to generate **137** to explore the relative efficacy between these two substituents.

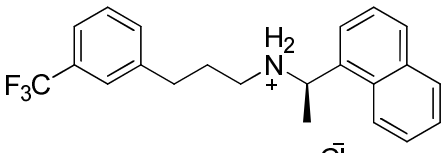

117

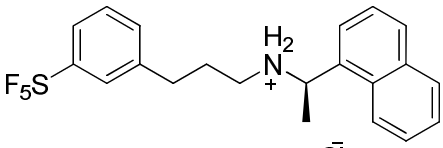

137

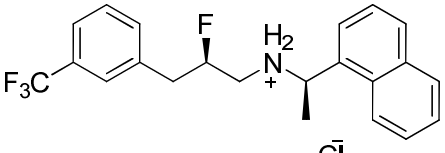

123

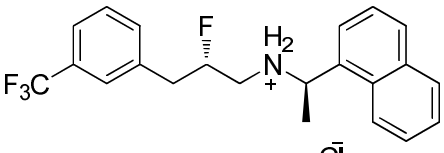

124

References:

[1] D. O'Hagan, *J. Fluorine Chem.*, 2010, **11**, 1071-1081.

[2] A. M. Thayer, *Chem. Eng. News*, 2006, **84**, 15-24.

[3] W. R. Dolbier, Jr., *J. Fluorine Chem.*, 2005, **2**, 157-163.

[4] P. Beier, A. M. Z. Slawin and D. O'Hagan, *Tetrahedron: Asymmetry*, 2003, **15**, 2447-2449.

[5] J. Mann, *Chem. Soc. Rev.*, 1987, **16**, 381-426.

[6] P. Kirsch, In *Modern Fluoorganic Chemistry*, Wiley-VCH, 2004.

[7] H. J. Boehm, D. Banner, S. Bendels, M. Kansy, B. Kuhn, K. Muller, U. Obst-Sander and M. Stahl, *ChemBioChem*, 2004, **5**, 637-643.

[8] K. Müller, C. Faeh and F. Diederich, *Science*, 2007, **317**, 1881-1886.

[9] G. A. Patani and E. J. LaVoiel, *Chem. Rev.*, 1996, **96**, 3147-3176.

[10] E. V. D. Marcian, W. J. Yong, S. S. Philip, R. K. Michael and M. W. Donald, *J. Med. Chem.*, 1995, **38**, 810-815.

[11] J. W. Clader, *J. Med. Chem*., 2004, **47**, 1-9.

[12] B. E. Smart, *J. Fluorine Chem.*, 2001, **109**, 3-11.

[13] M. B. V. Niel, I. Collins, M. S. Beer, H. B. Broughton, S. K. F. Cheng, S. C. Goodacre, A. Heald, K. L. locker, A. M. Macleod, D. Morison, C. R. Moyes, D. O'Connor, A. Pike, M. Rowley, M. G. N. Russell, B. Sohal, J. A. Stanton, S. Thomas, H. Verrier, A. P. Watt and J. L. Castro, *J. Med. Chem.*, 1999, **42**, 2087-2104.

[14] J. A. K. Howard, V. J. Hoy, D. O'Hagan and G. T. Smith, *Tetrahedron*, 1996, **52**, 12613-12622.

[15] J. J. Parlow, A. M. Stevens, R. A. Stegeman, W. C. Stallings, R. C. Kurumbail and M. S. South, *J. Med. Chem.*, 2003, **46**, 4297-4312.

[16] J. J. Parlow, R. G. Kurumbail, R. A. Stegeman, A. M. Stevens,W. C. Stallings and M. S. South, *Bioorg. Med. Chem. Lett*., 2003, **13**, 3721-3725.

[17] J. J. Parlow, R. G. Kurumbail, R. A. Stegeman, W. C. Stallings and M. S. South, *J. Med. Chem.*, 2003, **46**, 4696-4701.

[18] C. R. Briggs, M. J. Allen, D. Tozer, D. O'Hagan, A. M. Z. Slawin, A. E. Goeta and J. A. K. Havard, *Org. Biomol. Chem.*, 2004, **2**, 732-740.

[19] K. B. Wiberg, M. A. Murcko, K. E. Laidig and P. J. Macdougall, *J. Phys. Chem*, 1990, **94**, 6956-6959.

[20] D. O'Hagan, C. Bilton, J. A. K. Howard, L. Knight and D. J. Tozer, *J. Chem. Soc. Perkin Trans*, **2**, 2000, 605-607.

[21] R. C. Briggs, D. O'Hagan, H. S. Rzepa, A. M. Z. Slawin, *J. Fluorine Chem*., 2004, **25**, 19-25.

[22] D. O'Hagan, *Chem. Soc. Rev*., 2008, **37**, 308-319.

[23] G. Angelini, E. Gavuzzo, A. L. Segre and M. Speranza, *J. Phys. Chem*., 1992, **94**, 8762-8766.

[24] K. B. Wiberg, *Acc. Chem. Res*., 1996, **29**, 229-234.

[25] L. Goodman, H. B. Gu and V. Pophristic, *J. Phys. Chem A*, 2005, **109**, 1223-1229.

[26] J. A. Olsen, D. W. Banner, P. Seiler, B. Wagner, T. Tschopp, U. O-Sander, M. Kansy, K. Müller and F. Diederich, *ChemBioChem*, 2004, **5**, 666-675.

[27] J. P. Synder, N. S. Chandrakumar, S. N. Rao, D. P. Spangler and D. C. Lankin, *J. Am. Chem. Soc.*, 1993, **115**, 3356-3387.

[28] C. R. Briggs, M. J. Allen, D. O'Hagan, A. M. Z. Slawin, A. E. Goeta and J. A. K. Havard, *Org. Biomol. Chem*., 2004, **2**, 732-740.

[29] N. E. J. Gooseman, D. O'Hagan, M. J. G. Peach, A. M. Z. Slawin, D. J. Tozer and R. J. Young, *Angew. Chem.*, 2007, **119**, 6008-6012.

[30] B. Gaye and A. Adejare, *Future Med. Chem*., 2009, **5**, 821-833.

[31] M. Berger, J. A. Gray and B. L. Roth, *Annu. Rev. Med*., 2009, **60**, 355-366.

[32] J. P. Bēguē and D. B. Delpon, In *Bioorganic and Medicinal Chemistry of Fluorine*, Wiley-VCH, New York, 2008, 300-305.

[33] A. G. Myers, J. K. Barbay and B. J. Zhong, *J. Am. Chem. Soc.*, 2001, **123**, 7207-7219.

[34] M. A. Massa, D. P. Spangler, R. C. Durky, B. S. Hickory, D. T. Connoly, B. J. Witherbee, M. E. Smith and J. A. Sikorski, *Bioorg. Med. Chem. Lett.*, 2001, **11**, 1625-1628.

[35] V. Mascitti, B. D. Stevens, C. C. Kim, F. McClure, C. R. W. Guimaräes, K.A. Farley, M. J. Munchhof, R. P. Robinson, K. Futatsugi, S. Y. Lavergne, B. A. Lefker, P. Cornelius, P. D. Bonin, A. S. Kalgutkar, R. Sharma and Y. Chen, *Bioorg. Med. Chem. Lett.*, 2011, **21**, 1306-1309.

[36] M. Wrinkler, T. Moraux, H. A. Khairy, R. H. Scott, A. M. Z. Slawin and D. O'Hagan, *ChemBioChem*, 2009, **10**, 823-828.

[37] G. P. Deniau, A. M. Z. Slawi, T. Lebl, F. Chorki, J. P. Issberner, T. V. Mourik, J. M. Heygate, J. J. Lambert, L.–A. Etherington, K. T. Sillar and D. O' Hagan, *ChemBioChem*, 2007, **8**, 2265-2274.

[38] I. Yamamoto, G. P. Deniau, N. Gavande, M. Chebib, G. A. R. Johnston and D. O' Hagan, *Chem. Comm*., 2011, **47**, 7956-7958**.**

[39] A. Bernareggi, Z. Duenas, J. M. R. Ruiz, F. Ruzzier and R. Miledi, *Proc. Nat. Acad. Sci.*, 2007, **8**, 2956-2960.

Chapter 2: Synthesis and biological studies of 3-fluoro NMDA stereoisomers.

2.1 Introduction

Neurodegenerative disorders, such as Ischemia, Alzhimer's, Parkinson's and Huntington's are diseases associated with progressive memory impairment, paranoia, delusion and decline in language function.[1] All these physiological functions including memory and learning, are modulated by brain regions in which glutamate is the principal excitatory neurotransmitter. Evidence from *in vivo* and *in vitro* studies indicated that GluR-induced toxicity is associated with Alzhimer's disease.[1]

2.1.1 The glutamate receptor in the mamalian CNS.

The glutamate receptor falls into two categories, namely the metabotropic receptors (mGluR) and the ionotropic receptors (iGluR). The iGluRs can be further divided into three sub-classes, namely the *N*-methyl-D-aspartate (NMDA), kainic acid (Kainate) and α-amino-3-hydroxy-5-methyl-4-isoxazole propionic acid (AMPA) receptors.[2] These three sub-classes are cation permeable and are thought to be involved in key processes, such as learning and memory.[2] The mGluRs which comprise subclasses I-III are found to conduct slow modulating responses through G-protein-coupled receptors by depolarization of the membrane potential. It is generally agreed that mGluRs and iGluRs are responsible for many neurodegenerative diseases in the CNS, and all of these subunits have important potential for therapeutic interventions.[2] The structures of iGluR agonists, namely the AMPA **50**, kainate **51**, NMDA **52** and glutamate **53** are shown in **Figure 2.1**.

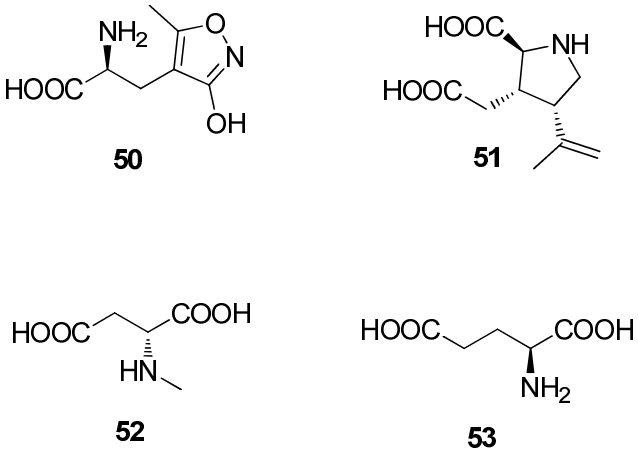

Figure 2.1 Structure of iGluR agonists: AMPA **50**, Kainate **51**, NMDA **52** and Glutamate **53**.

Structurally, the iGluR and mGluR receptors are composed of heterogenous protein subunits. For example, four sub-units (GluA1-4) for AMPA and five sub-units (GluK1-5) for Kainate receptors. The NMDA receptor has up to seven sub-units, namely the GluN1, Glu2A-D and Glu3A-B. The mGluR are similarly complex as illustrated in **Figure 2.2**.[2]

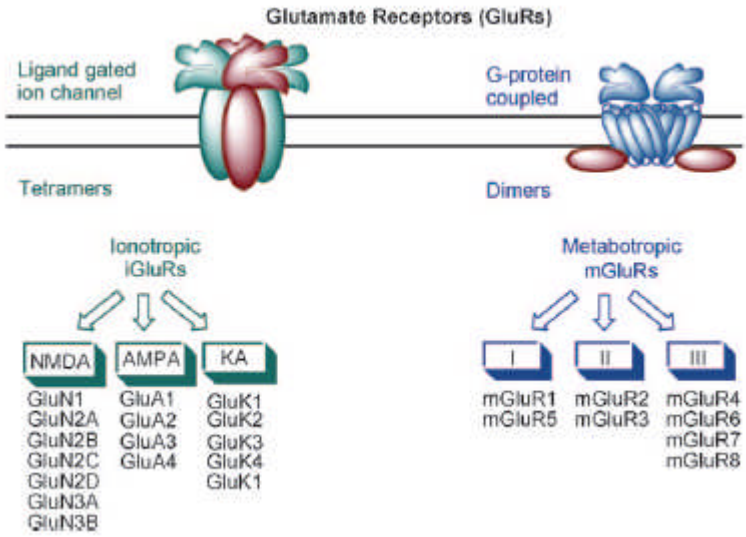

Figure 2.2 Sub-units identified in NMDA, AMPA, KA receptors and mGluRs.[2]

2.1.2 The binding domain of glutameric NMDA receptors.

Activation of glutamate receptors requires the binding of both glycine and glutamate **58**, where GluN1 and GluN2 contain the binding sites of glycine and glutamate respectively. The glutamate receptors are both ligand and voltage sensitive. Once activation occurs, the ion channel allows the flow of Na^+ and Ca^{2+} into cells while releasing K^+. The influx of Ca^{2+} through the receptor to postsynaptic cells, allows the conversion of an electrical to a biochemical signal to trigger a synaptic response.[3] The depolarization of the ion-channel is subsequently carried out by the inhibition of magnesium on glutamate receptors.

Ionotropic glutamate receptors comprise different functional domains as illustrated in **Figure 2.3**, namely the amino terminal domain, the ligand binding domain, the membrane associated region and the intracellular carboxyl domain. Armstrong *et al*. reported that the ligand binding domain is formed of S1 and S2 protein regions which are thought to form a hinged clamshell-like structure.[4] Chen *et al*. reported that the AMPA and kainate subunits in bacterial glutamate receptors have a very high degree of similarity to those observed in human NR2 NMDA receptor subunits.[5]

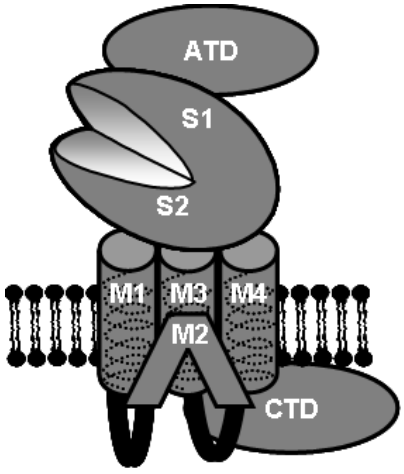

Figure 2.3. Cartoon structure of an ionotropic glutamate receptor comprising ligand binding domains S1 & S2, re-entrant loop (M2), amino terminal domain and the carboxyl terminal domain.[6]

Before that, the mechanism of binding of glutamate to the NR2 subunit was not well understood. Most of the partial and full agonism studies were conducted using site directed mutagenesis to identify key binding residue in the binding pocket. Indeed, the result of these studies showed that the NR2 subunits had a higher degree of homology that the corresponding AMPA subunits. In 2005, Furukawa *et al*. reported the first X-ray crystal structure of the NR2A agonist binding site co-crystallized with glutamate as shown in **Figure 2.4**.[7] This X-ray structure was interrogated by molecular modelling to further explore the different residues involved in the binding of glutamate to the NR2A subunit.

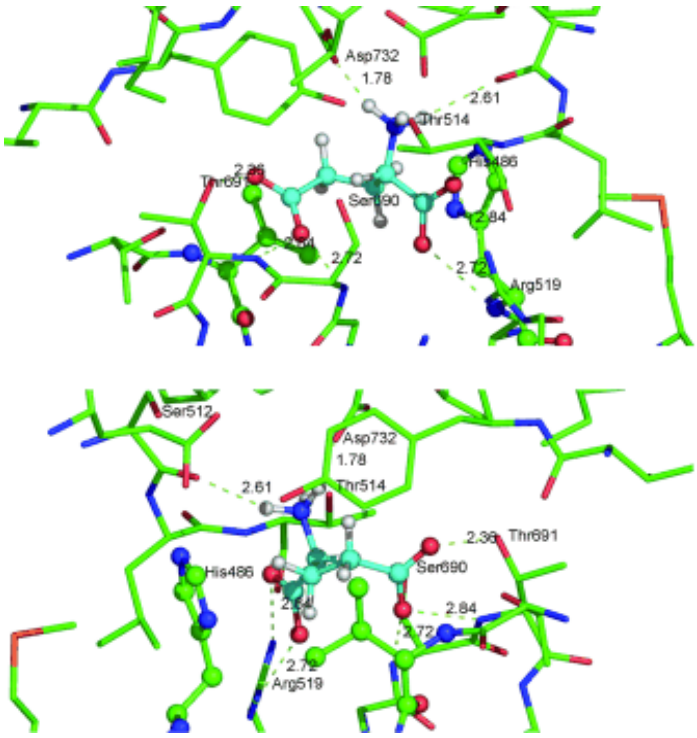

Figure 2.4 The X-ray derived structure of NR2 with bound glutamate viewed from two different angles.[7]

The glutamate is shown to bind to the receptor in an extended conformation, with the carboxylic groups forming ionic interactions with the N-H residue from Arg11A, Thr 116A, Asp215 A and Thr 174A. The protonated amine contacted two residues of the

binding site, namely Thr 116A and Ser 114A (**Figure 2.5 A**). During the later stages of this research, the structure of NMDA co-crystallized with GluN1/N2D NMDARs was reported by Furukawa *et al*. in 2011.[8] Interestingly, the structure with NMDA shows that it adopts a different binding mode, with its methylamine group and one of the carboxylates forming ionic interactions with Thr 116A. The other residues Thr 174A, Ser 173A and Arg 121A form ionic interactions with the carboxylic groups of NMDA (**Figure 2.5 B**). Overall, the receptor induces a folded binding mode for NMDA. **Figure 2.6** summarizes the binding mode of glutamate and NMDA into the GluN1/N2D receptor.

A

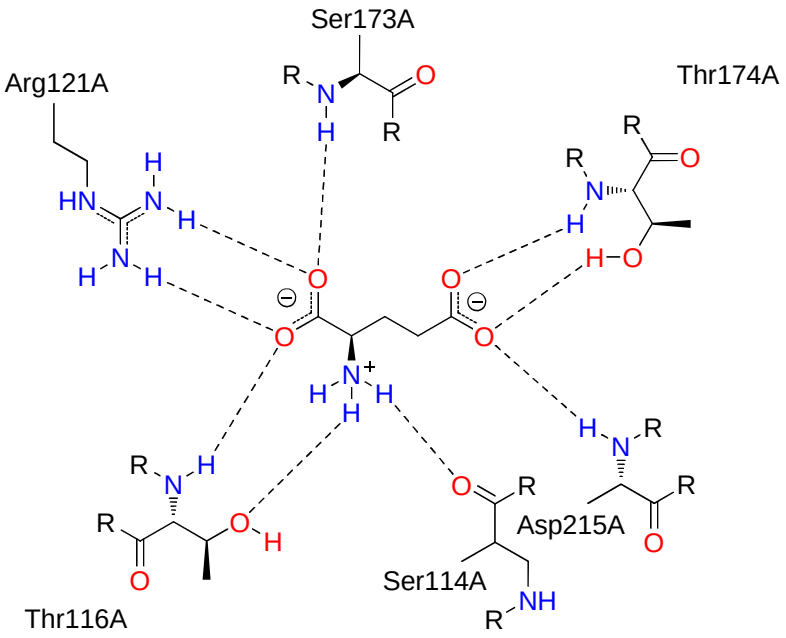

B

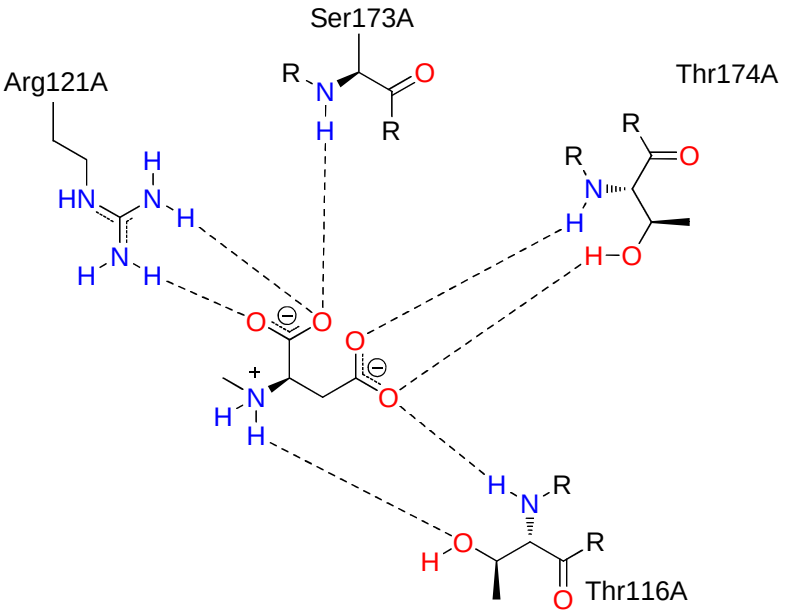

Figure 2.5 The extended conformation of glutamate (A) and folded conformation (B) for NMDA when bound into the active site of the GluN1/N2D receptor.

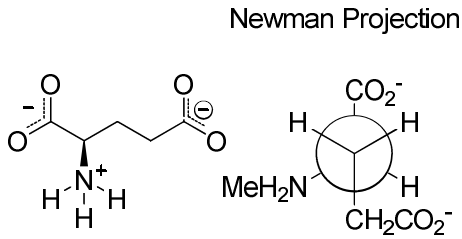

Binding conformation of glutamate **53** into GluN1/N2D receptor

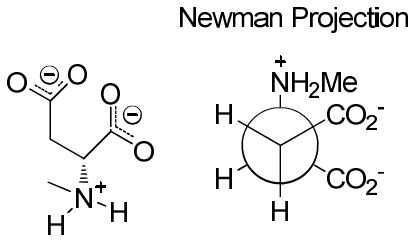

Binding conformation of NMDA **52** into GluN1/N2D receptor

Figure 2.6 The preferred binding mode of glutamate and NMDA when bind into the GluN1/N2D receptor.

2.1.3 Agonists and antagonists of glutamate receptors.

The pharmacological description of the various glutamate receptors derive from the structure of agonists and antagonists. Such excitatory amino acids (EAA) are important for modulating different glutamate receptors and they serve as pharmacological tools and are useful therapeutics for the future.

Over the decades, a large number of potent agonists and antagonists have been discovered. The glutamate structure can often be identified within these compounds. Among these, (*S*)-2-amino-3-(*N*-oxalylamino)propionic acid (*β*-ODAP) **54**, *rac*-tricholomic acid **56**, ibotenic acid **55**, willardiine **57** and quisqualic acid **58** are very potent, but unselective agonists.[9] These amino acids have acted as model structures for lead development of neuroactive drugs.

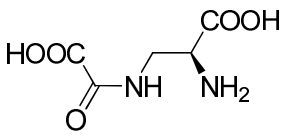

54

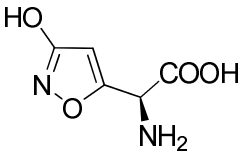

55

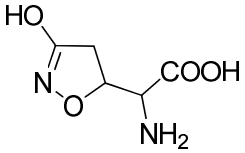

(*rac*)-**56**

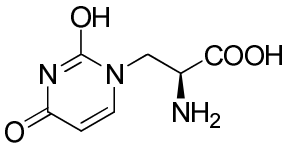

57

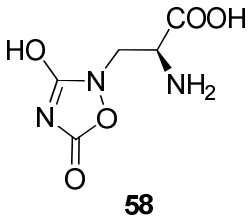

58

A range of glutamate receptor antagonists have been developed and are in early clinical trials for the treatment of stroke. Relevant antagonists are the non-competitive channel blocker aptiganel **59**, the competitive glycine site antagonist ACEA-1021 **60**, the competitive glutamate antagonist Selfotel **61** and the Ifenprodil analogue Eliprodil **62**. These compounds were hampered by unwanted side effects, such as respiratory depression and cardiovascular dysregulation. Furthermore, Selfotel and Eliprodil have shown reduced side effects but these compounds were withdrawn during the early clinical stage due to a lack of efficacy at tolerable doses.[10-11]

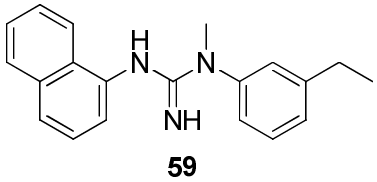

59

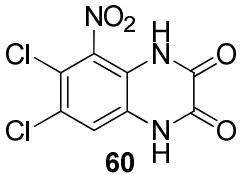

60

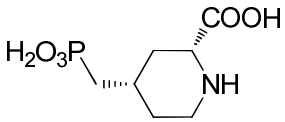

61

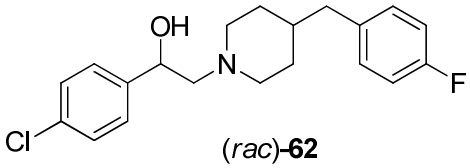

(*rac*)-**62**

2.1.4 The pharmacology of NMDA receptors and it subunits.

There are many well documented examples showing that NMDA or related compounds are found to be neurotoxic to glutamate receptors. Neuronal death linked to epilepsy appears to be highly dependant on NMDA receptor activation, while neuronal degeneration such as ischemia is caused by both NMDA and AMPA receptors.[12] It is important to note that the NMDA receptor plays a number of roles associated with crucial physiological and pathological brain processes. More recently, it has been shown that different subunits correspond to different expression levels, with NR2B restricted to the forebrain, NR2C to the cerebellum and NR2D is much rarer than the other subtypes. This differential subunit assembly allows sub-unit

selective compounds to be developed, for instance NR2B is selectively blocked by Ifenprodil.[13] On top of this, Zn^{2+} was also reported to be a natural antagonist to the NR2A subunit.[14] The sub-type selective ligands that bind to the NMDA receptors are illustrated in **Figure 2.7.**

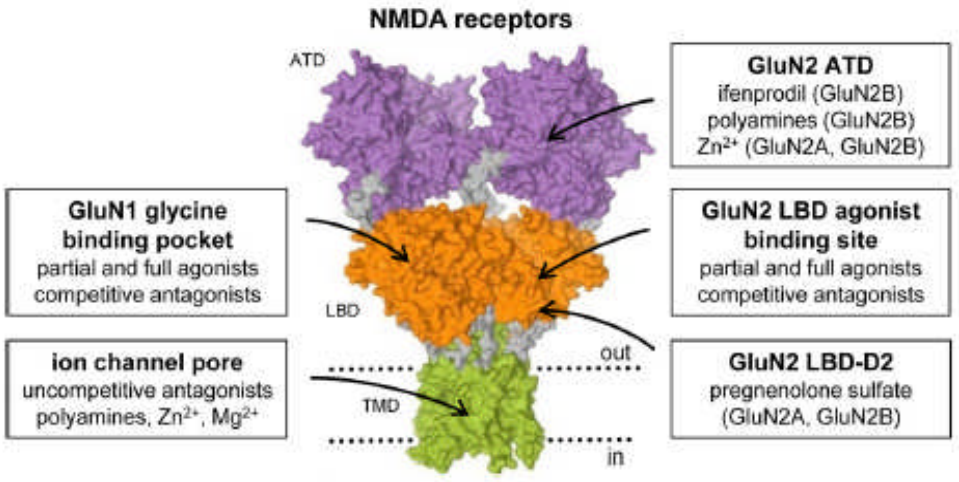

Figure 2.7 Sub-units selective antagonists ligands of the NMDA receptors.[15]

Although NMDA receptors subtype have been known for 30 years, details of the exact binding mode of glutamate and NMDA are only emerging from X-ray structural biology (Figure 28). Early studies involved comparing the relative efficacy of ring systems of restricted rotation. For example Erreger *et al*, prepared glutamate agonists of type **63-71**[16]. Compound **64** was as potent as glutamate on the NR2A and NR2B subuits, but it exhibited a much higher potency in the nano-molar range with NR2C and NR2D subtypes. However, the increase of the ring size from cyclobutyl to cyclopentyl was found to decrease potency and efficacy, with a 10 fold decrease for cylcobutyl and a 20 fold decrease for cyclopentyl. Similarly, compounds **69-71** were found to be biologically inactive probably due to unfavorable binding modes. In this experiment, it is very clear that low molecular weight molecules are ideal compounds for glutamate receptor binding.

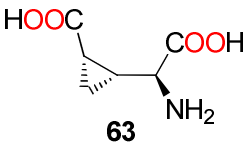

63

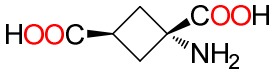

64

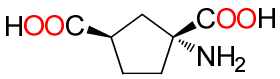

65

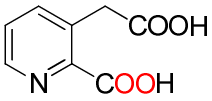

66

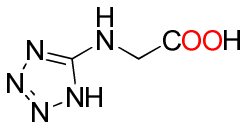

67

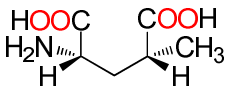

68

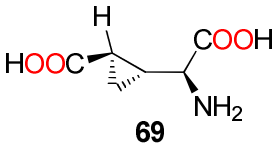

69

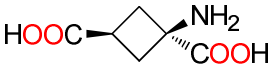

70

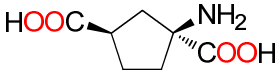

71

2.1.5 Therapeutic prospects of NMDA analogues.

A substantial amount of research has shown that the NMDA receptor is a promising target for preventing the progression of neurodegeneration. Diseases such as Alzheimer's, Parkinson's, Huntington and Ischemia are associated with glutamate toxicity, therefore novel NMDA antagonists are of interest. Unfortunately, most of the current NMDA antagonists induce side effects, which also suppress learning and memory. Therefore, there is value in studying the binding conformation of both the NMDA agonist and antagonist to their pathologically active receptors.

2.2 Aim of this Project

Following the 3F-GABA research in St. Andrews,[17-18] it became an objective to explore the influence of the C-F bond on the conformation of NMDA and thus explore the conformational requirement for NMDA binding to its receptors. **Figure 2.8** shows that each 3F-NMDA stereoisomer is limited to a set of three staggered conformations. It is anticipated that the C-F---NH_3^+-C interaction will bias the conformation such that the C-F and C-N^+ bonds are *gauche*. The Newman projections show that the diastereoisomers **72** and **73** are likely to show different levels of activity, as they are predicted to adopt different favoured conformers in solution.

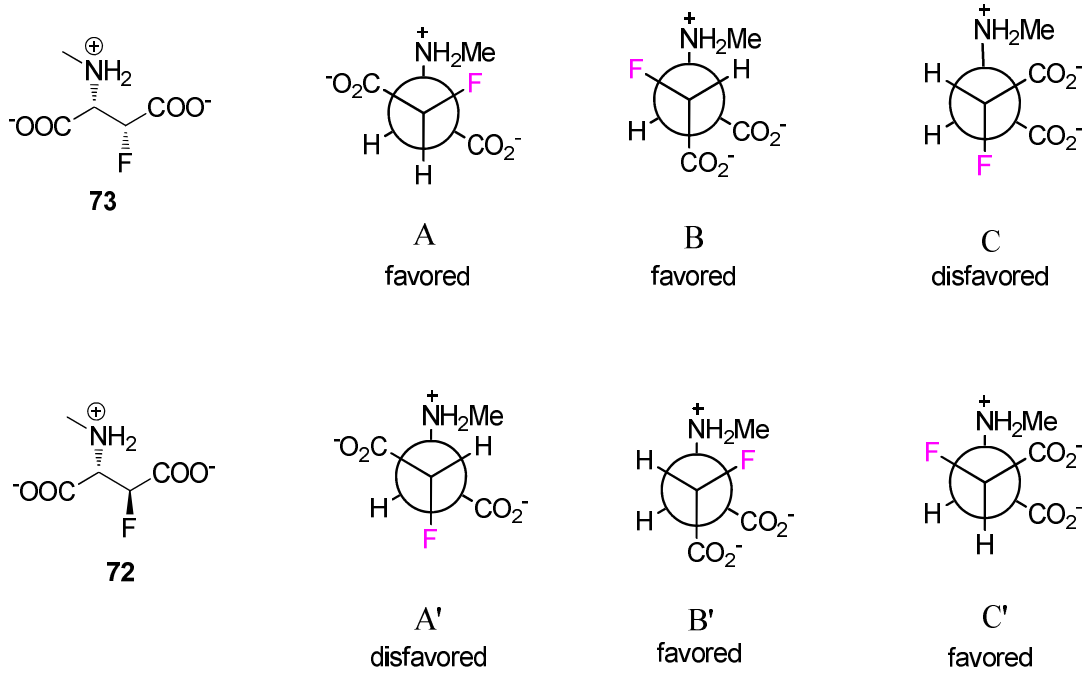

Figure 2.8 Newman projection of D-3F-NMDA diastereoisomers.

The aim of this project was to develop a method for the synthesis of individual diastereoisomers of D-3F-NMDA and to assess their efficacy as glutamate receptor agonists. There are four possible stereoisomers of 3F-NMDA which are shown in **Figure 2.9**. Stereoisomers D-(2*S*,3*S*) **72** and **73** (2*S*,3*R*) were the key targets in this research programme as they have the required D-configuration.

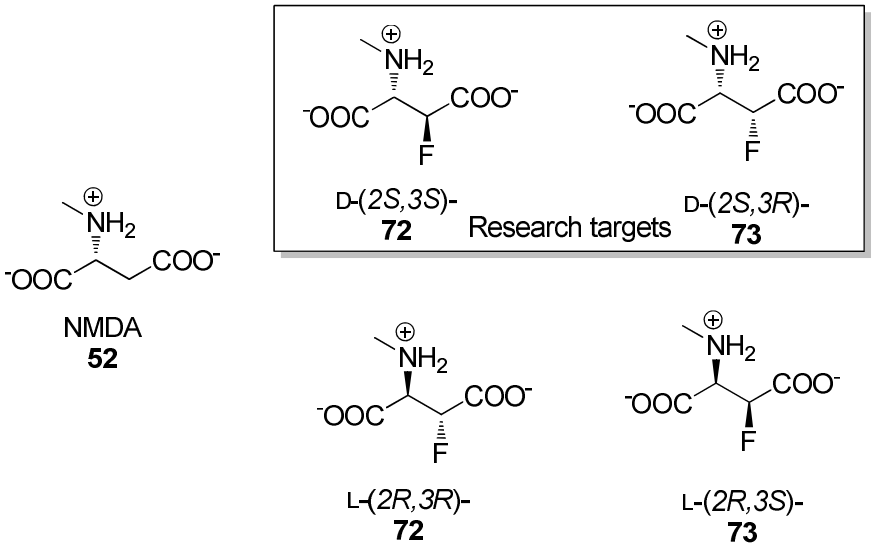

Figure 2.9 The four possible stereoisomers of 3F-NMDA.

2.3 Background on the synthesis of 3F-NMDA.

3-Fluoro D-aspartate is a close structural analogue of 3F-NMDA.[19-20] An enantiomeric pure synthesis of 3-fluoro D-aspartate was reported by Charvillion *et al*.[21] In this route (Sceheme 1), (*2S,3S*)-3F-D-aspartic acid **78** was prepared from (*2S,3S*)-epoxy succinate **74** in three steps. The key step involved a deoxofluorination reaction of **75** to obtain **76**, a reaction that proceeds by a double inversion of configuration. This was achieved with DAST™ or Deoxofluor™. The mechanism of formation of **76** is thought to proceed *via* a three member aziridinium ring, followed by ring opening with fluoride ion to generate **76**.

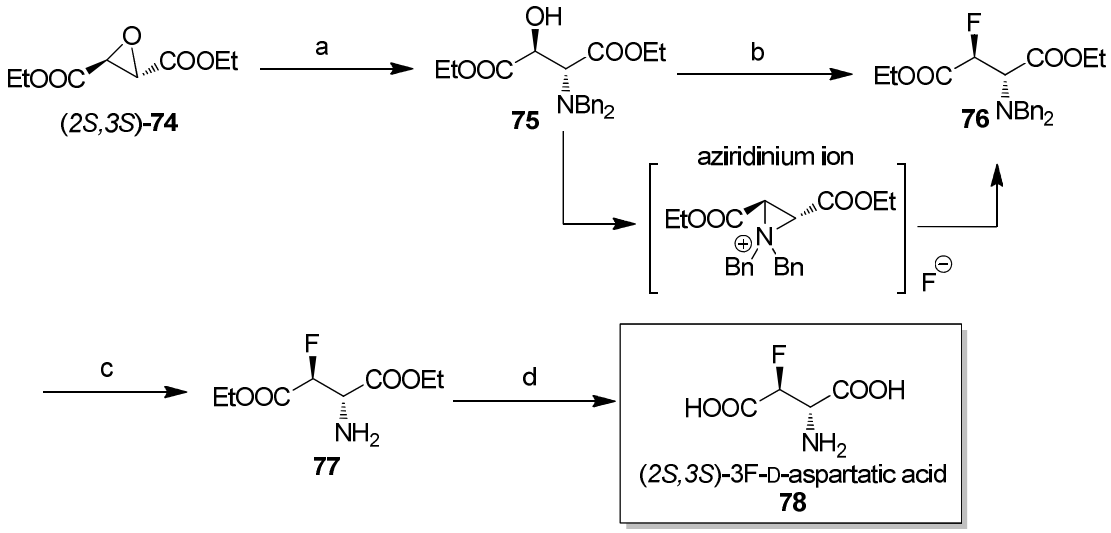

Scheme 2.1 Reagents and conditions: a) $HNBn_2$, $LiBF_4$, CH_3CN, reflux, 72 h, 62%; b) Et_2NSF_3, THF, RT, 2 h, 94 %; c) H_2, (1atm) Pd/C, EtOH, 4 h, quant.; d) HCl 4N, reflux, 48 h, 40 %.[22]

By contrast, the *syn* isomer (*2S,3R*)- **83** (Scheme 2) was accessed by forming cyclic sulfate **79**, which was derived from diisopropyl D-tartrate. Ring opening of the cyclic sulfate by TBAF proceed with an inversion of configuration to generate fluorohydrin **80**, which was then converted to the corresponding triflate. Displacement of the triflate with sodium azide, followed by hydrogenation to the amine and then acid hydrolysis gave (*2S,3R*)-3F **83** as a single enantiomer.

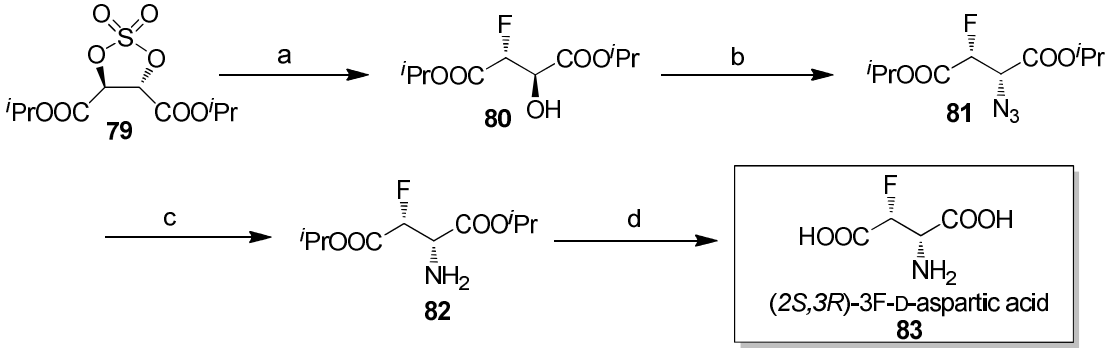

Scheme 2.2 Reagents and conditions; a) 1. Et_4NF, acetone, RT, 6 h; 2. H_2SO_4, 20% aqueous solution, RT, 7 h, 88%; b) 1. Tf_2O, CH_2Cl_2, -65 °C, 5 min then 2, 6-lutidine; 2. NaN_3, DMF, -5 °C, 56%; c) H_2, (1 atm) Pd/C, EtOH, 4 h, quant.; d) HCl 4N, reflux, 20 h, 53 %.[22]

2.4 Result and Discussion

2.4.1 Retrosynthetic analysis of 3F-NMDA.

Our retro-synthetic approach to diastereoisomer (2*S*,3*S*)-3F-NMDA D-**72** is shown in Scheme 2.3. Target D-**72** is accessible by hydrolysis of diethyl ester **90.** Access to **90** was envisaged by deprotection of *N*-benzyl or *N*-para-methoxy groups. The key step in this route lies in the fluorination of alcohol **88** to give **89** and then ring opening of epoxide **87** with an appropriate methylamine. The preparation of epoxide **87** follows from the literature.[22] The retrosynthetic analysis of (2*S*,3*R*)-3F-NMDA D-**73** differ from the above, with **96** synthesized as an intermediate to facilitate the single fluoride inversion leading to **97**. The rest of the route will be the same as that reported for D-**72**. The envisaged synthetic route towards the first single diastereoisomer D-**72** is outlined in Scheme 2.4.

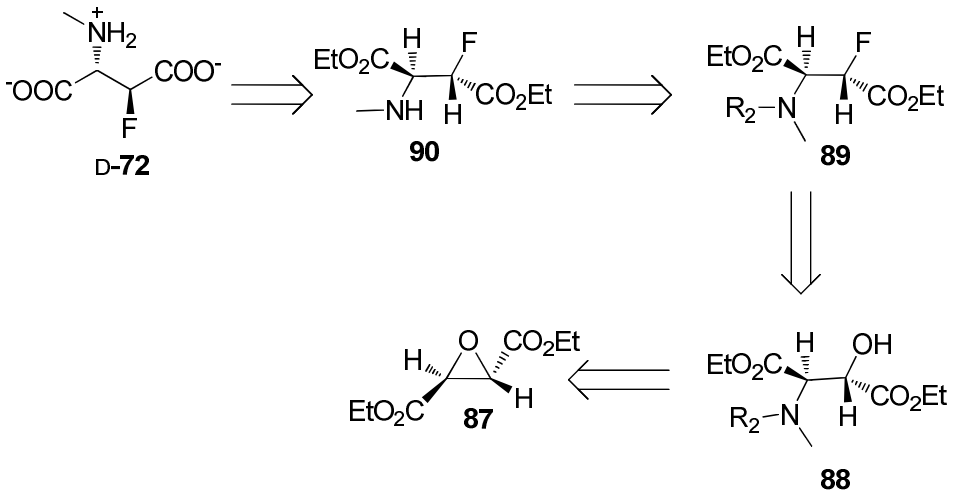

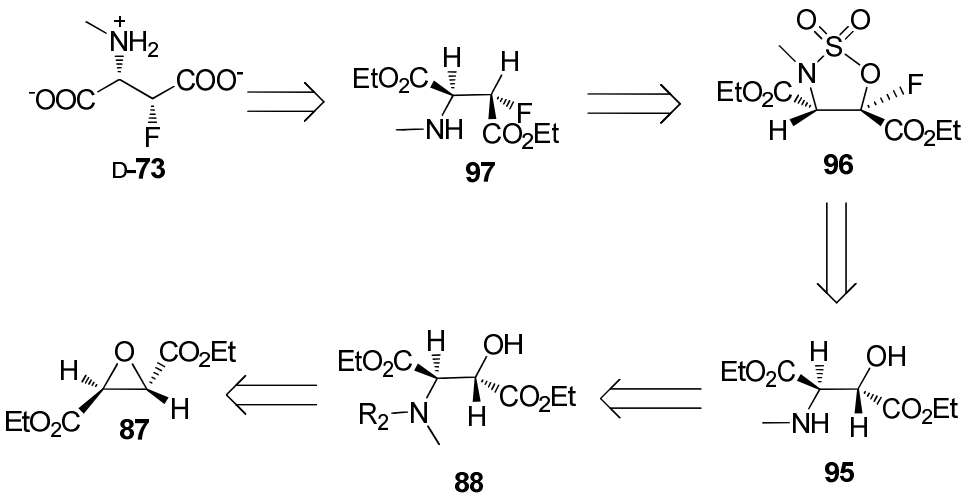

Scheme 2.3 Retrosynthetic analysis of 3F-NMDA diastereoisomers of D-**72** and D-**73**.

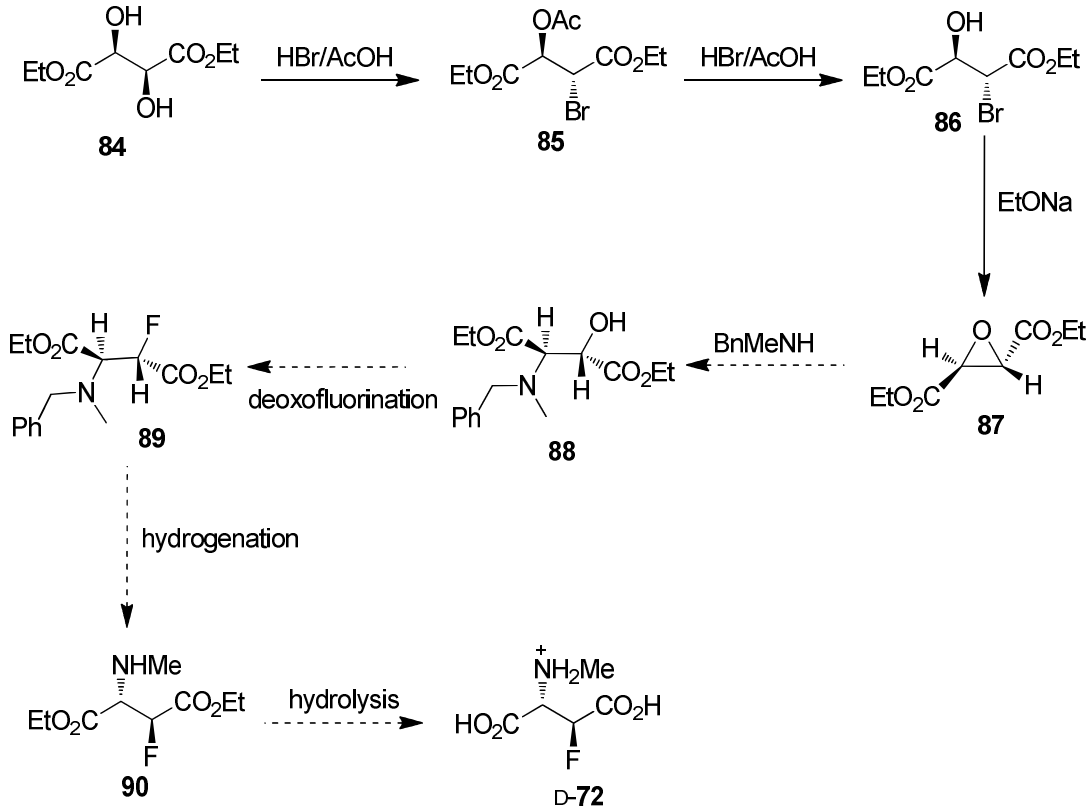

Scheme 2.4 Proposed strategy towards the (2*S*, 3*S*)-3F NMDA D-**72.**

2.4.2 Synthesis of (*2S, 3S*) 3-fluoro NMDA D-72.

Epoxy succinyl dipeptides have gained considerable attention due to their novel applications as cystein-protease inhibitors.[23] Accordingly, this has further encouraged the optimization of synthetic protocols for the synthesis of epoxy succinyl moieties. The *trans*-epoxy succinic ester **87** could be accessed from diethyl (-) D-tartrate **84** in three steps following the procedure of Korn *et al*.[22] In this route, bromoacetoxy ester **85** was prepared by treating **84** with hydrobromic acid in acetic acid. The mechanism for the formation of **85** is proposed by Golding *et al*. to proceed as illustrated in Scheme 2.6.[24] Fractional distillation afforded **85** in good yield (94%). This product was then treated with sodium ethoxide in ethanol to give a satisfactory yield (52 %) of epoxide **87**.

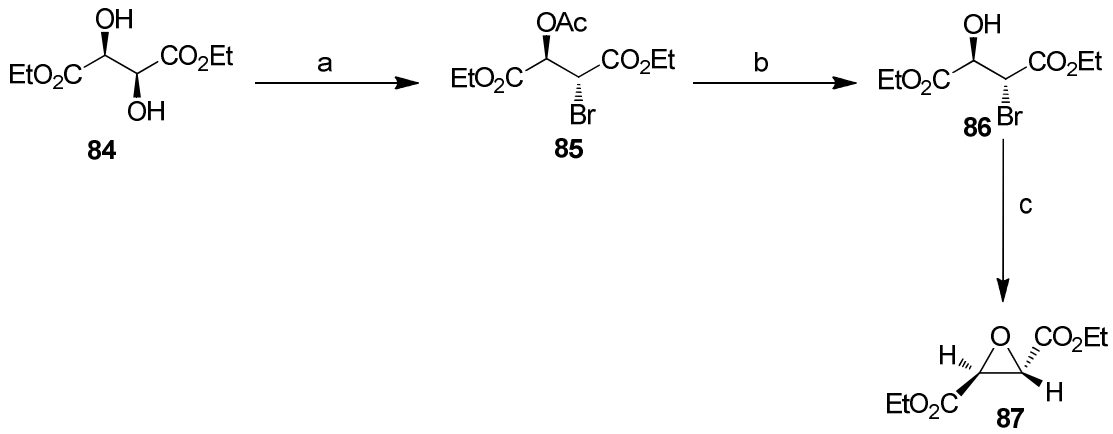

Scheme 2.5. Synthesis of epoxy succinate **87** from **84**. Reagent and conditions: a) HBr/AcOH, RT, 4 h ; b) HBr/AcOH, EtOH, 85 °C, 97%; c) EtONa, EtOH, rt, 2 h, 57 %.

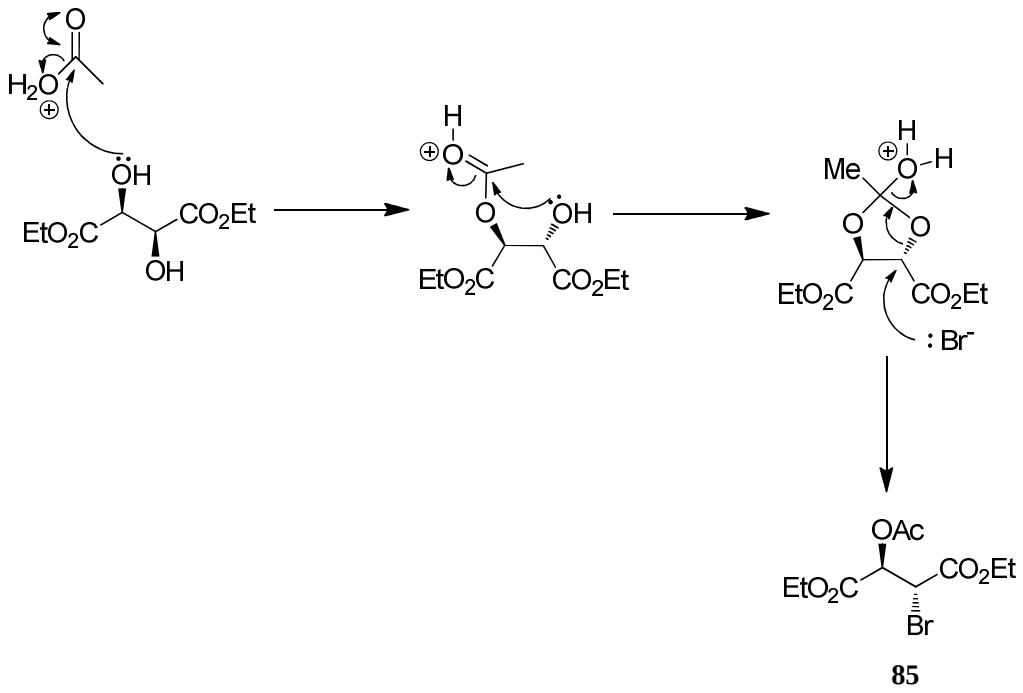

85

Scheme 2.6. Proposed mechanism by Golding *et al*. for the formation of **85**.[24]

A key step in the synthesis of (2*S*,3*S*)-3F **72** lies in the ring opening of epoxide **87** with an appropriate amine. Several attempts were explored. This included treating epoxide **87** with methylamine in ethanol under reflux. However, this proved unsuccessful due to methylamine attacking the ester to generate diamide **92** as illustrated in Scheme 2.7 a. Upon repeating the same reaction, but with the diisoproyl ester **93** to suppress amide formation, it was found that only the monoamide **94** was generated, but no ring opening occurred as illustrated in Scheme 2.7 b. Finally, success was achieved by reacting diethyl ester **87** with the less nucleophile amine, benzylmethylamine (Scheme 2.7 c). This time the reaction gave **88** in 85% yield after chromatography. This proved satisfactory and allowed preparation of an appropriate substrate for the important fluorination reaction.

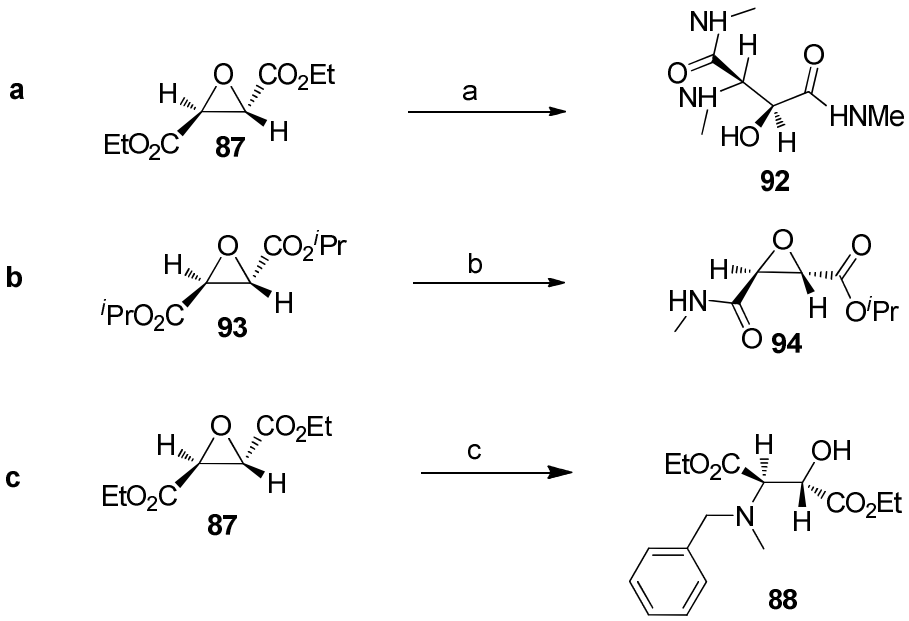

Scheme 2.7 Reagent and conditions: CH_3NH_2, EtOH, 85 °C, a) 74%; b) 50%. c) BnMeNH, EtOH, 85 °C, 85%.

Dehydroxyfluorination of alcohol **88** proved to be a straightforward reaction. Treatment with Deoxofluor^{TM} afforded the fluorinated product **89** in 93 % yield and as a single diastereoisomer. Substitution of the hydroxyl group with fluorine is anticipated to proceed by a double inversion process, and thereby with an overall rentention of stereochemistry. Ring opening of the aziridinium (Scheme 2.9) by pathway (a) and (b) give an identical product. Indeed, the ^{19}F NMR only showed one peak (at –195.0 ppm) consistent with a single isomer **89**. A proposed mechanism for the formation **89** is outlined in Scheme 2.9. In order to establish that the reaction did indeed proceed with a retention of configuration, it was desirable to prove relative stereochemistry by X-ray crystal structure analysis. However, this proved difficult, as product **89** reacts with HCl in ether to form a rearrangement product (**Figure 2.12)** and the proposed mechanism of the rearranged product is illustrated in Scheme 2.10. Another attempt was made to make the cyclohexylamine derivative of **89**. Disappointingly, defluorination occurred again. The stereochemical proof of this synthesis step will be discussed later.

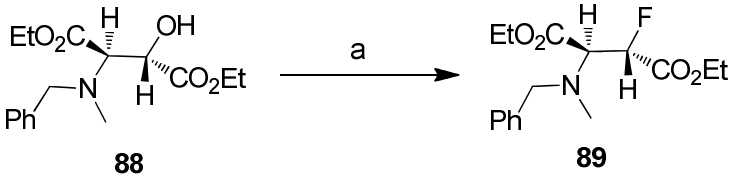

Scheme 2.8 Synthesis of fluoro analogue **89** from **88**. Reagent and conditions: a) Et_2NSF_3 (3 equiv), DCM, RT, 2 h, 93%.

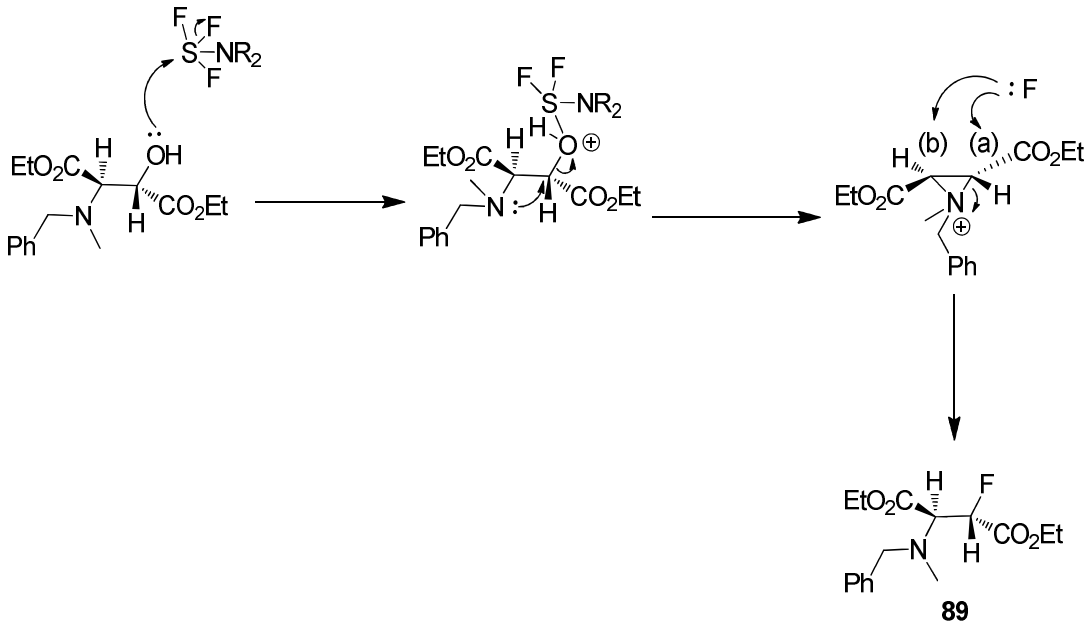

Scheme 2.9 Proposed mechanism for the formation of **89** proceeding *via* an aziridinium intermediate and with overall retention configuration at C-3. Ring opening by either pathway (a) and (b) gives an identical stereoisomer.

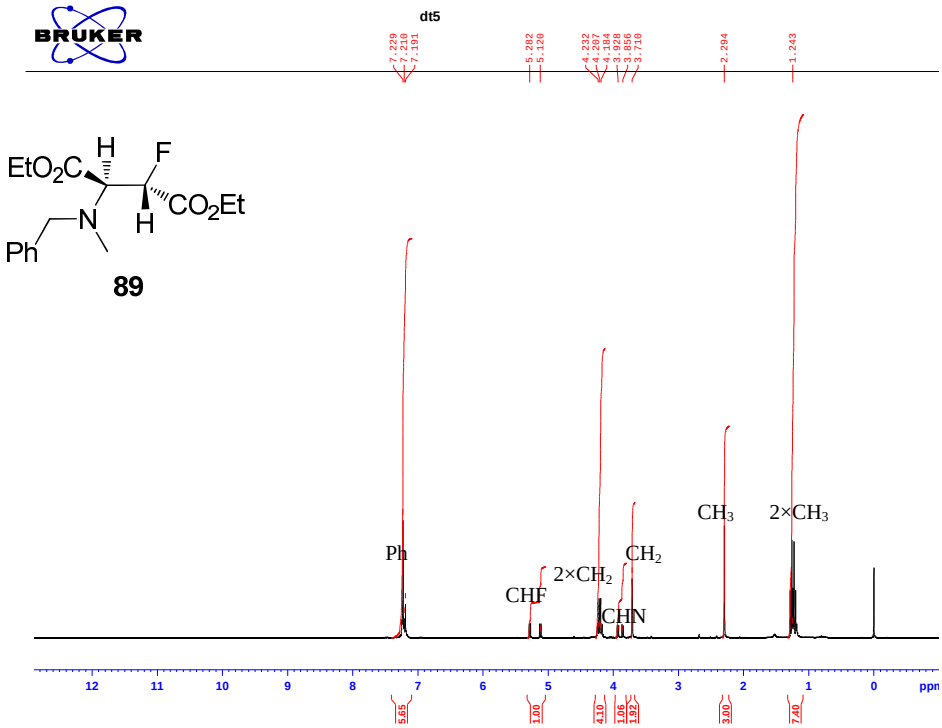

Figure 2.10 ^{1}H-NMR of fluorination product **89**.

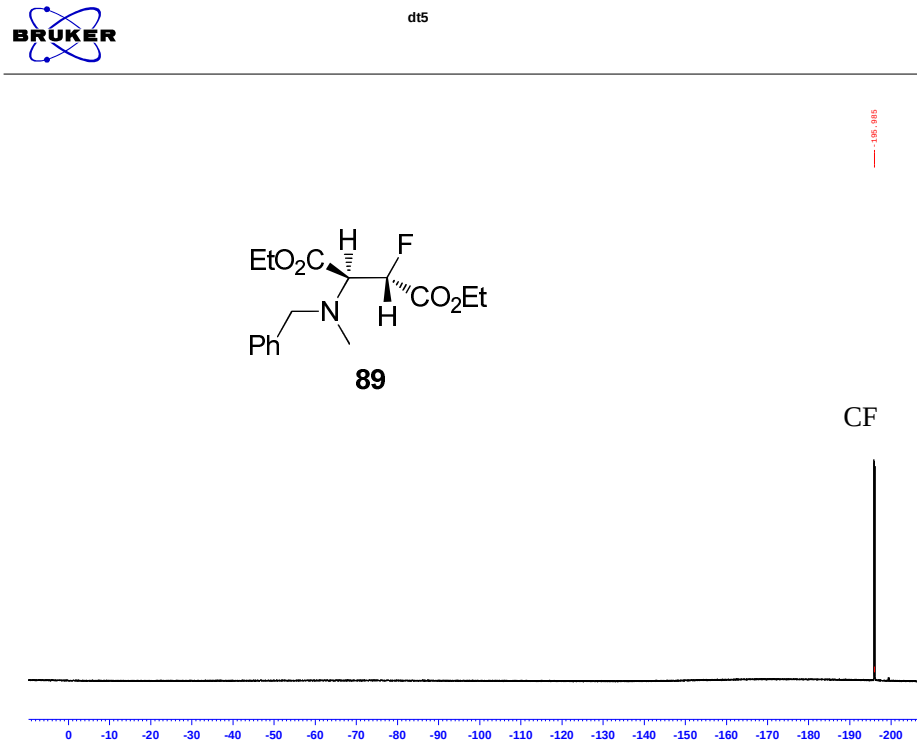

Figure 2.11 ^{19}F-NMR of fluorination product **89** indicating a single stereoisomer.

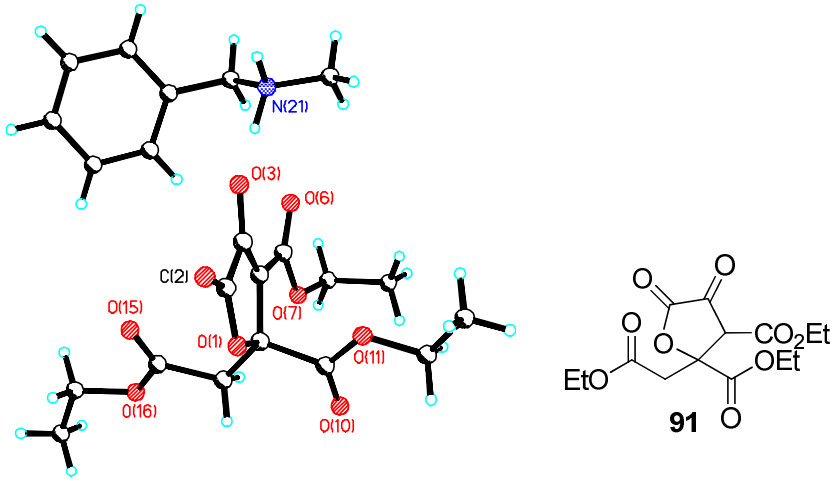

Figure 2.12 X-ray crystal structure of **91** the product resulting from the reaction of **89** in HCl-ether.

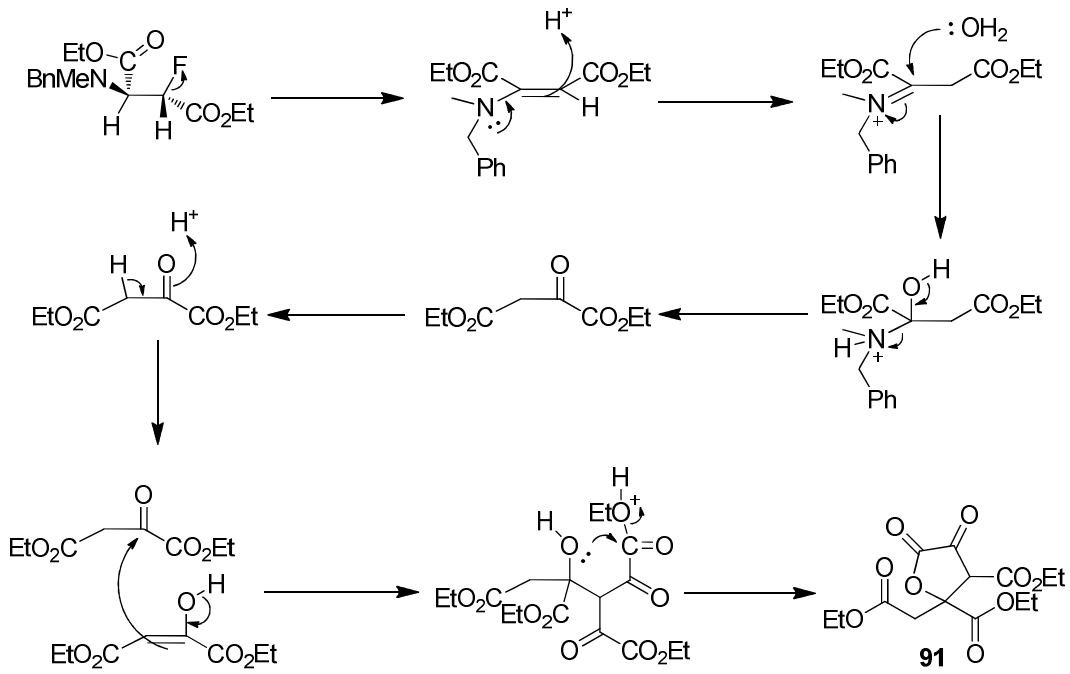

Scheme 2.10 Proposed mechanism for the formation of triethyl oxalocitrolactone ester **91** in HCl-ether.

With the fluorine successfully in place, deprotection of the benzyl group of **89** was investigated by hydrogenation as shown in Scheme 2.11. The deprotection was performed with hydrogen using palladium on activated carbon as a catalyst in ethanol.

The reaction was followed by TLC until the starting material was consumed. Work up afforded product diester **90** in a good yield and this product was used for subsequent reaction without further purification.

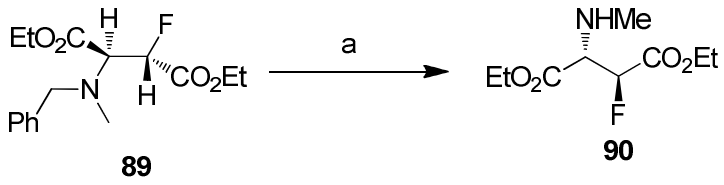

89 **90**

Scheme 2.11 Deprotection of **89** by hydrogenation. Reagent and condition: a) H_2, Pd/C, EtOH, RT, 2 h, 97%.

The final step in the synthesis of (*2S, 3S*)-3F D-**72** involved acid catalyzed hydrolysis of diethyl ester **90**. The experiment was successfully carried out by treating diester **90** with HCl (4M) at 80 °C for 48 hours.

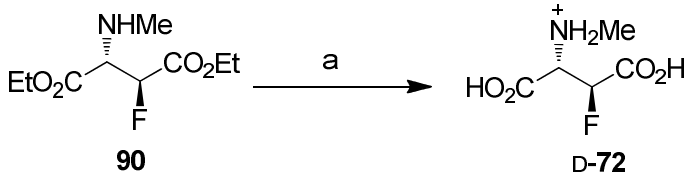

90 D-**72**

Scheme 2.12 Synthesis of (2*S*, 3*S*)- **72** from **90**. Reagent and condition: a) 4 M HCl/H_2O, 85 °C, 50 %.

With the completed synthesis of *erythro* (2*S*, 3*S*)-3F NMDA HCl D-**72**, this gave the first sample of a 3F-NMDA diastereoisomer. The optical rotation of D-**72** was measured and compared to that of *erythro* (2*S*, 3*S*)-3F aspartic acid **78**. Interestingly both have the same sense of rotation, with the $[\alpha]_D$ for D-**72** and **78**, found to be -7.2° and -18.0°, respectively. ^{19}F-NMR analysis of both D-**72** and **78** showed signals at -198.5 ppm and -198.5 ppm respectively, suggesting that these are the related stereoisomers. The ^{19}F-NMR of *threo* is -196.0 ppm, which is 2 ppm difference

between the diastereoisomer series. With D-**72** in hand, it was now important to prepare the second diastereoisomer.

2.4.3 Synthesis of (2*S*, 3*R*) 3-fluoro NMDA D-73.

The synthetic route to (2*S*, 3*R*) 3-fluoro NMDA D-**73** is outlined in Scheme 2.13. The route is a modification of the above pathway, but designated to attempt a single inversion of configuration during the fluorination reaction, rather than a double inversion. To achieve this, nucleophilic ring opening of a cyclic sulfamate was envisaged to generate (2*S*,3*R*) 3-fluoro NMDA D-**73**.

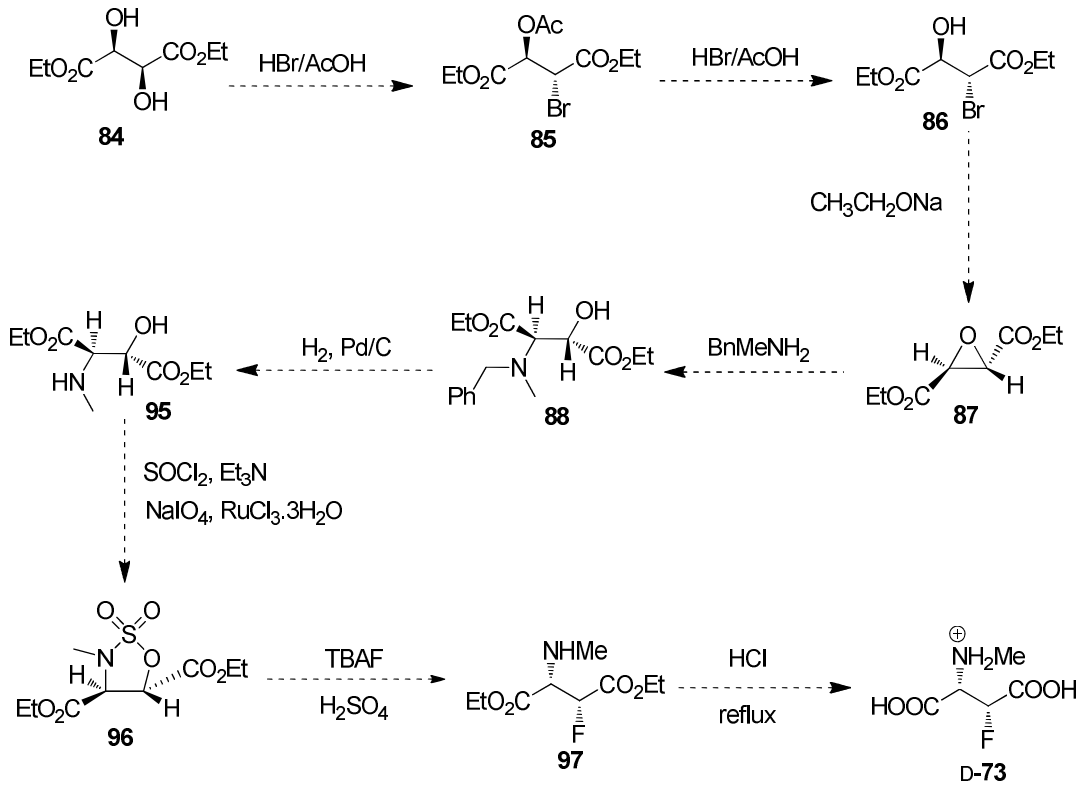

Scheme 2.13. Proposed route to (2*S*, 3*R*)- D-**73.**

The routes to the two stereoisomers diverge at alcohol **88**. Amino alcohol **95** was readily accessed by hydrogenation of **88** as shown in Scheme 2.14. The procedure for the hydrogenation was straightforward and the reaction was followed by TLC until complete conversion had occurred. Simple filtration and solvent removal afforded **95** in good yield.

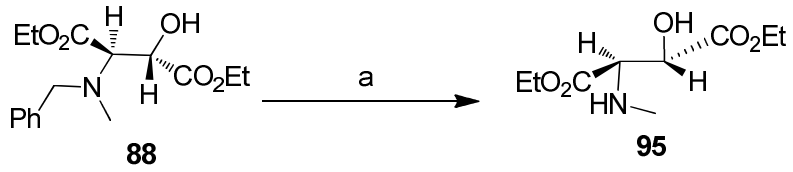

88 **95**

Scheme 2.14 Reagent and condition: a) H_2, Pd/C, EtOH, RT, 2 h, 97%.

The route was progressed by subjecting amino alcohol **95** to treatment with thionyl chloride and sodium meta periodate and cat. $RuCl_3.3H_2O$. The reaction was carried out according to the method of Marcian *et al*.[25] This generated the cyclic sulfamate **96** as illustrated in Scheme 2.15.

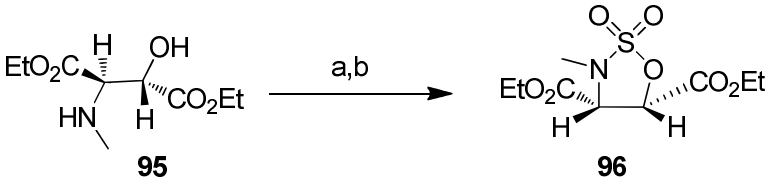

95 **96**

Scheme 2.15. Synthesis of **96** from **95.** Reagents and conditions: a) Et_3N (2 equiv), $SOCl_2$ (1.2 equiv), DCM, – 78 °C, 2 h, RT, 16 h; b) $NaIO_4$ (2.0 equiv), $RuCl_3.3H_2O$, CH_3CN/H_2O (1:1), 0 °C, 4 h, 75%.

It was envisaged that cyclic sulfamate **96** could then be treated with a fluoride ion source to generate **97**. However, this proved unsuccessful with TBAF. All of the starting material was converted into a new product, but no fluorine was incorporated. The actual product could not be characterized, however it presumably arose due to a fluoride ion promoted elimination reaction. Therefore, this synthetic route was discontinued and a new approach to this *threo* stereoisomer was considered.

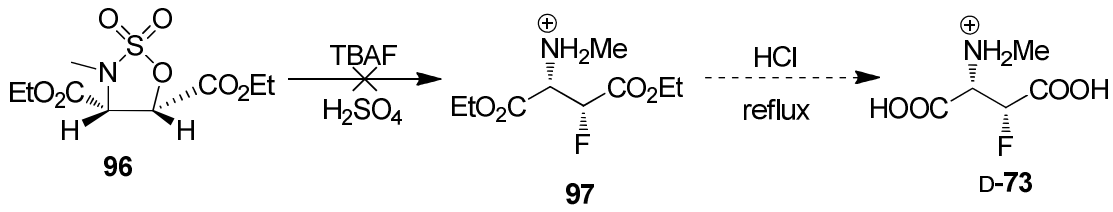

Scheme 2.16. Unsuccessful attempt towards the synthesis of **97.**

2.4.4 Synthesis of *threo* (±)(2*SR*,3*RS*)-3F NMDA from diethyl maleate 98.

An alternative approach to the *threo* stereoisomer of 3F-NMDA was explored as shown in Scheme 2.17 from the *meso*-epoxy succinate **99**.[26] Accordingly, diethyl maleate **100** was treated with *t*-BuOOH and nBuLi and the excess of peroxide was quenched with sodium sulfide. Work-up gave the *meso*-epoxide **99** after column chromatography, in about 50 % yield.

In order to explore whether this epoxidation reaction proceeded stereospecifically to generate only the *cis*-epoxide, the ^{1}H NMR of this product was compared to that of a reference sample of the *trans*-epoxide. The spectra are shown in **Figure 2.13**, and they are clearly different entities. To be conclusive both *cis* and *trans* epoxides were add- mixed as shown in the lower spectrum of **Figure 2.14**. The result was very clear indicating that both **87** and **99** are different geometric isomers, and that the basic peroxide reaction was stereospecific.

Ring opening of epoxide **99** in an ethanol with benzylmethylamine gave racemic alcohol **100** in good yield (92%). With *rac*-**100** in hand, a deoxofluorination reaction was performed and as anticipated, fluorination afforded **101** also in good yield (84%).

Subsequently, deprotection of *rac*-**101** was performed by hydrogenation and *β*-fluoroamine *rac*-**102** was recovered in a straight forward manner in 87% yield. Finally hydrolysis of diethyl ester *rac*-**102** was performed in 4M HCl. Examination of the literature[21] found that acid hydrolysis under reflux gave the best yield, however, this turned out to be a sluggish reaction and the yield is not always good (30%). The

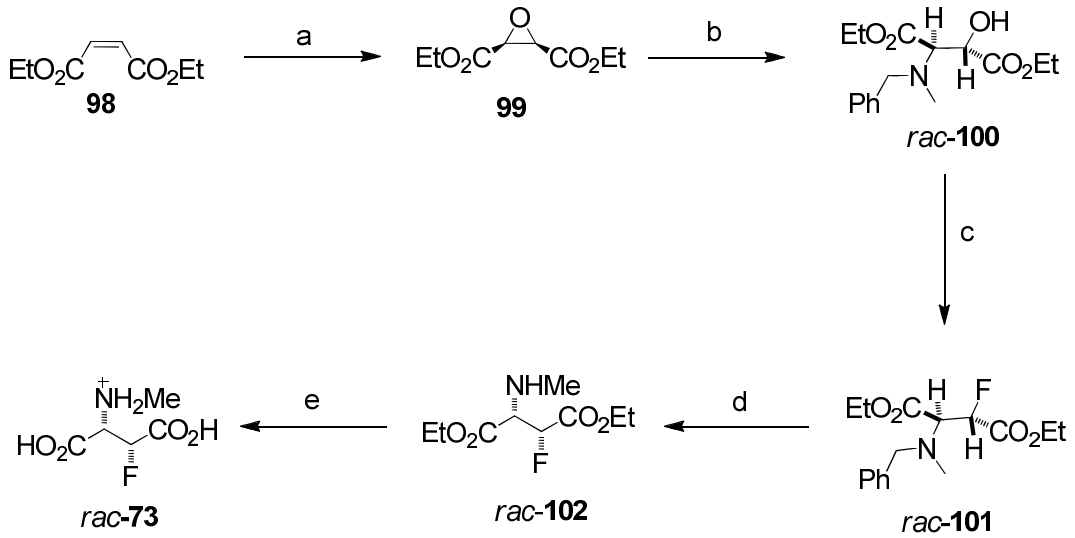

overlay of ^{1}H-NMR spectrum of D-**72** and *rac*-**73** were shown in **Figure 2.14**.

Scheme 2.17. Reagents and conditions: a) tBuOOH (2 equiv), *n*BuLi (1.2 equiv), THF, – 78 °C, 30 min, RT, 16 h, 50%; b) $BnMeNH_2$, EtOH, 85 °C, 92%; c) Et_2NSF_3 (3 equiv), DCM, RT, 2 h, 87%; d) H_2, Pd/C, EtOH, RT, 2 h, 87%; e) 4 M HCl/H_2O, 85 °C, 48 h, 30%.

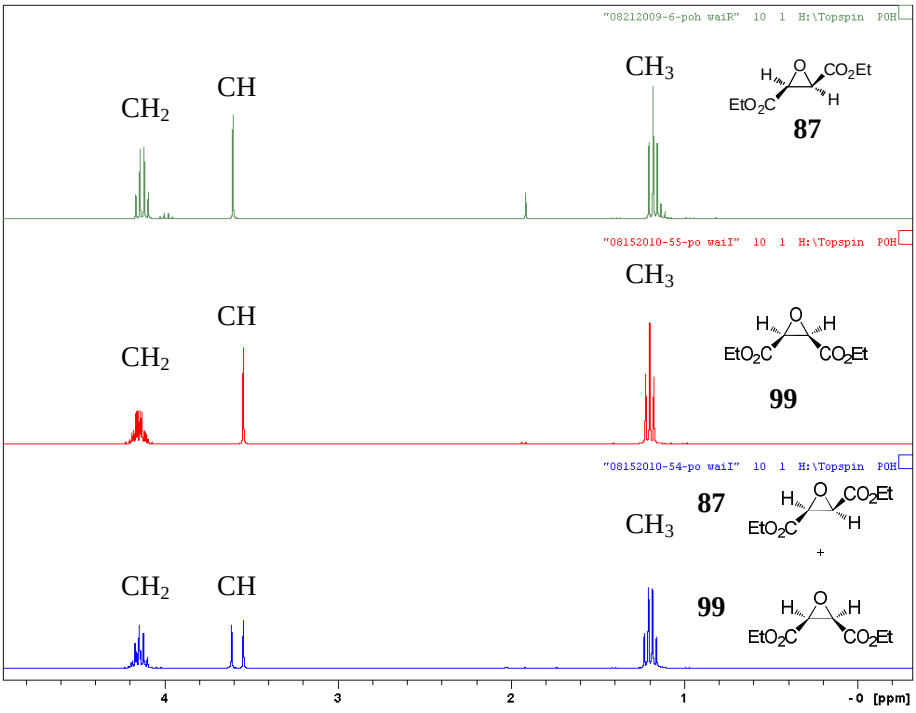

Figure 2.13. The ^{1}H-NMR of (2*S*,3*S*)-**87**, (±)(2*SR*,3*RS*)- **99** and the mixture of both isomers spectrum recorded in $CDCl_3$ at 300 MHz**).**

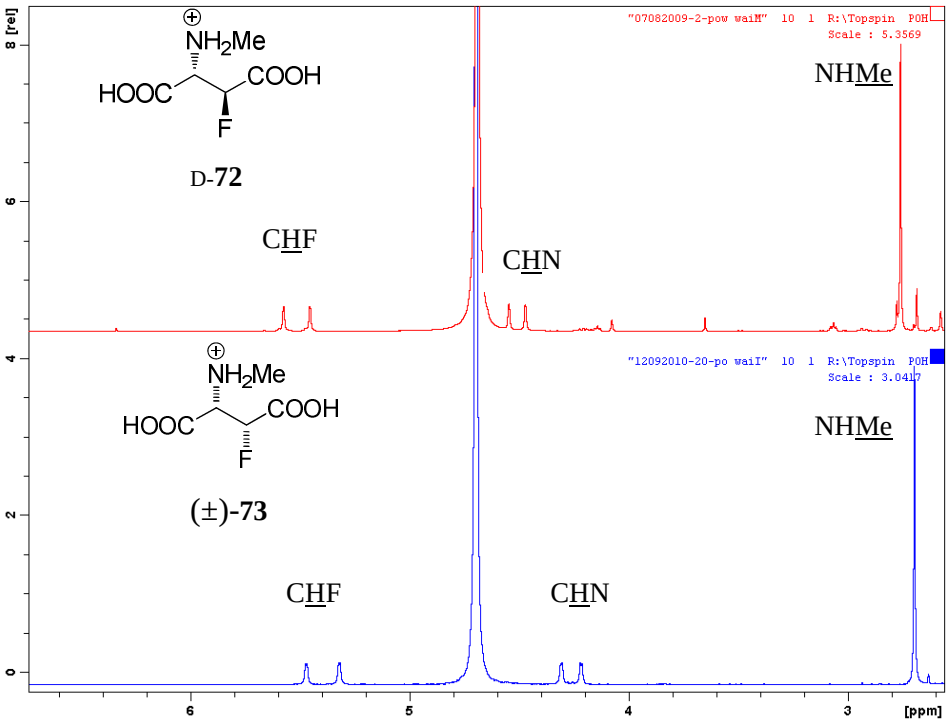

Figure 2.14. ^{1}H-NMR of D- (2*S*,3*S*)- **72** and (±)(2*SR*,3*RS*)-3F NMDA HCl **73** spectra recorded in D_2O at 400 MHz**.**

2.4.5 Improved synthesis of *threo* (±) 73.

A new approach to *threo* (±)-**73** was considered. This was required as *threo* (±)-**73** prepared from the diethyl maleate was subject to decomposition and low yields in the last step after long reaction times in concentrated HCl. As a result, an improved route leading to a higher yield of *threo* (2*SR*,3*RS*)-3F (±)-**73** was developed and is outlined in Scheme 2.18. This time *threo* (±)-**73** was prepared from the dibenzyl ester rather than the diethyl ester. Accordingly, diacid **103** was treated with oxalyl chloride and triethylamine to generate the diacid chloride, which was used without purification.[27] It was then treated with 2.1 equivalents of benzyl bromide. A catalytic amount of DMF and pyridine afforded epoxide **104** as colorless oil in 86% yield.

Ring opening of epoxide **104** with benzylmethylamine, *via* the now established method gave rise to **105** in good yield (92%) and then subsequent deoxofluorination of **105** afforded fluoroamine **106**. With **106** in hand, the final hydrogenation reaction, to remove all three benzyl groups, was explored with Pd/C and hydrogen. Celite filtration and concentration under reduce pressure afforded (±)-**73** in a high yield (86%). Overall, this dibenzyl maleate synthetic route gave a more satisfactory yield of (±)-**73** in comparison to the diethyl ester approach.

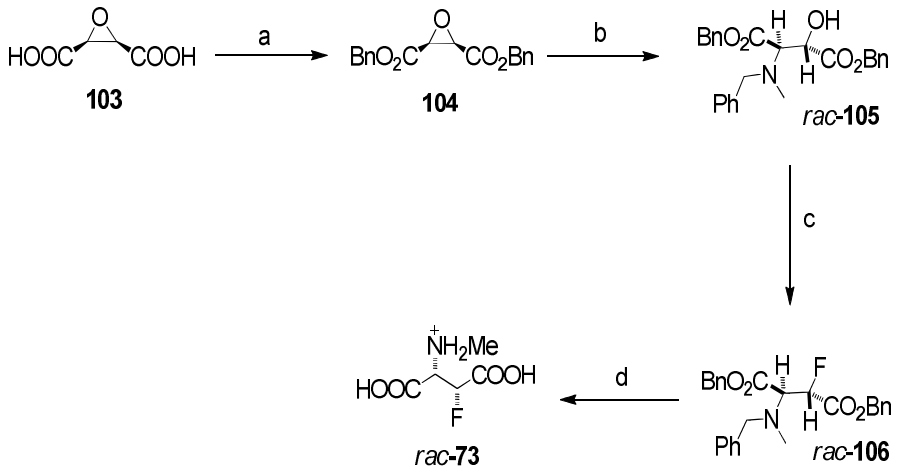

Scheme 2.18 Improved route to *threo* (±)-**73** involving benzyl deprotection. Reagents and conditions: a) (i) $(COCl)_2$ (1.2 equiv), DMF, Et_3N (2 equiv), THF, –78 °C, 30 min, reflux 2 h, 86% ; (ii) BnOH (2.1 equiv), py, THF, RT, 16 h, 92%; b) BnMeNH, EtOH, 85 °C, 84%; c) Et_2NSF_3 (3 equiv), DCM, RT, 2 h, 84%; d) H_2, Pd/C, EtOH, RT, 2 h, 86%.

2.4.6 Enantiomer resolution from racemic (2*SR*,3*RS*)-3F NMDA HCl 73.

Resolution of a single enantiomer of *threo* **73** was investigated involving diastereoisomeric separation of a suitable intermediate. The approach taken is outlined in Scheme 2.19 and 2.21. Diastereosiomers (*S*)-**107** and (*S*)-**108** were prepared by treating the *meso* **104** with the enantiomerically pure base, (*S*)-(-)-*N*, α-dimethylbenzylamine as shown in Scheme 2.19 to generate two diastereoisomers. Fluorination of this diastereoisomeric mixture was then carried out with Deoxofluor™. Neighbouring group participation during the deoxofluorination generates an aziridium ring which has two electrophilic sites. Attack by fluoride ion at each of these centres affords a different diastereoisomer in each case as shown in Scheme 2.20. Therefore, the diastereoisomeric mixture of alcohol (*S*)-**107** and (*S*)-**108** was used directly in the deoxofluorination reaction without separation as shown in Scheme 2.21. The

chromatographic separation of the resultant fluorinated diastereoisomers (*S*)-**109** and (*S*)-**110** after deoxofluorination was difficult, but a single diastereosiomer was isolable after careful chromatography. The second diastereosiomer could not be purified as a single compound, as the separation was always accompanied by the other stereoisomer. Therefore, in order to obtain a pure sample of the second stereoisomer, **104** was treated with (*R*)-(+)-*N*, *α*-dimethylbenzylamine, the other enantiomer of the base, and the protocol repeated.

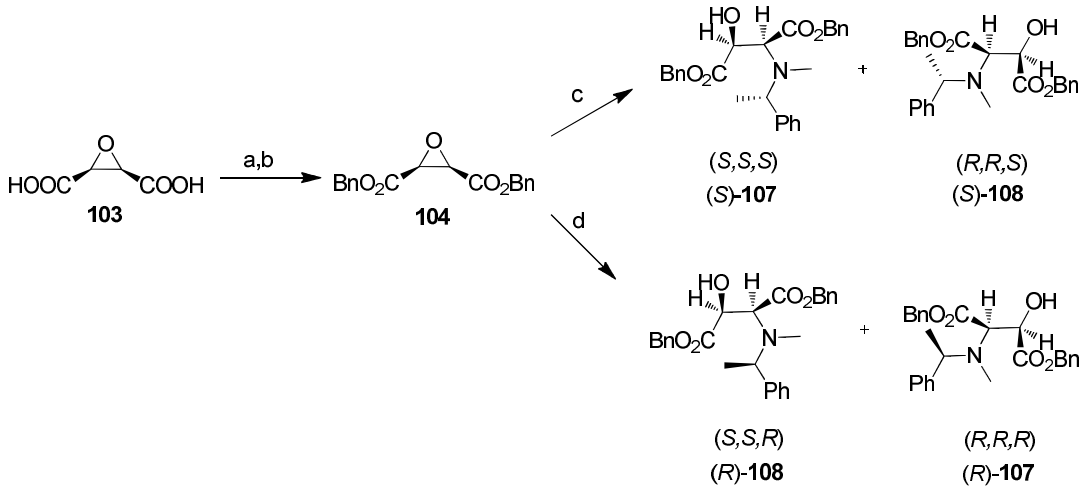

Scheme 2.19 Reagents and conditions: a) $(COCl)_2$ (1.2 equiv), Et_3N (2 equiv), THF, –78 °C, 30 min, reflux 2 h ; b) BnOH (2.1 equiv), DMF, py, THF, RT, 16 h, 86%; c) (*S*)-(-)-*N*,*α*-dimethylbenzylamine, DMF, 160 °C, 85%; d) (*R*)-(+)-*N*,*α*-dimethylbenzylamine, DMF, 160 °C, 89%

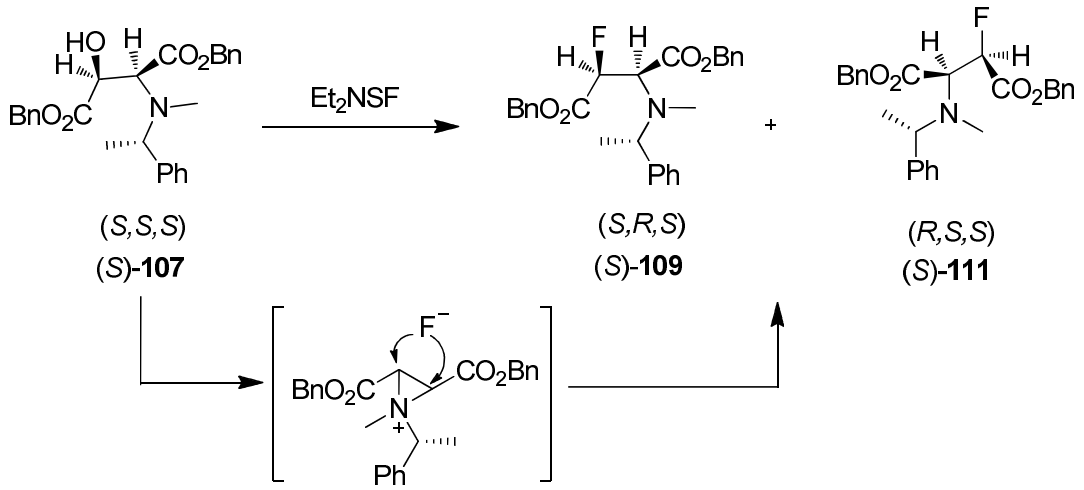

Scheme 2.20 Deoxofluorination of single diastereoisomer (*S*)-**107** leading to diastereoisomers (*S*)-**109** and (*S*)-**111**.

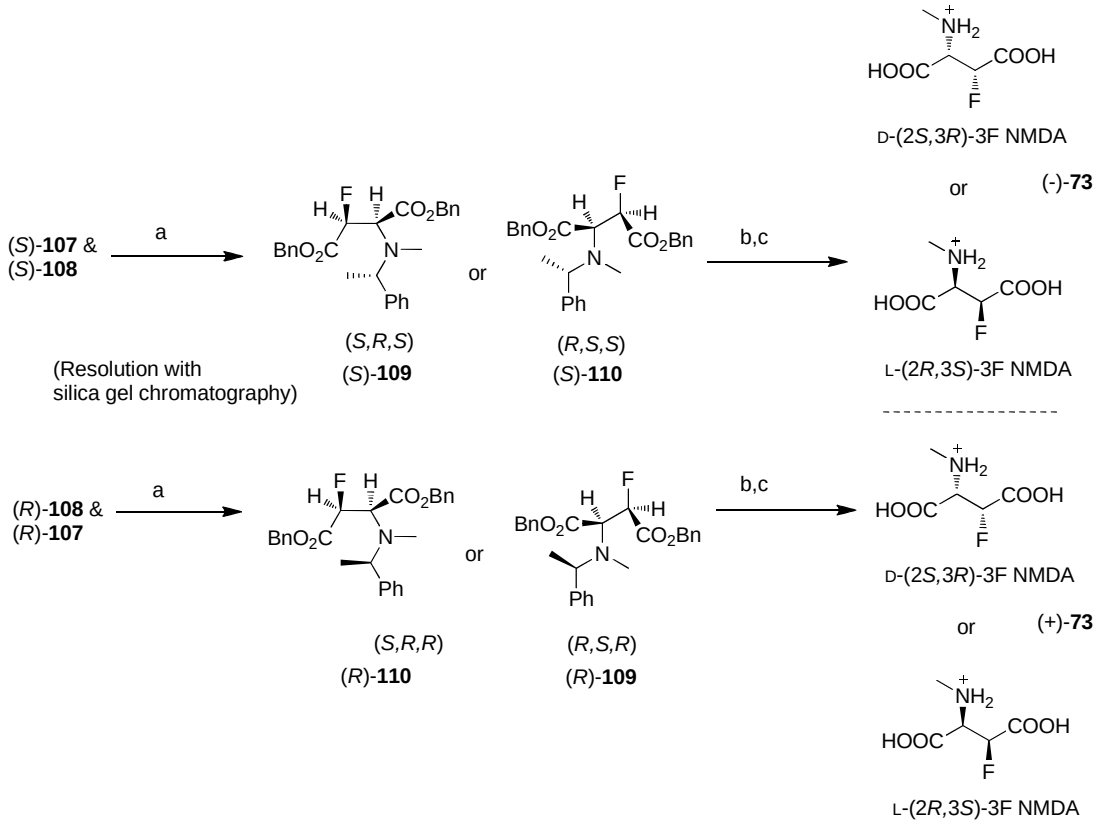

Scheme 2.21 Preparation of enantiomers (-)-**73** and (+)-**73**. Reagents and conditions: a) Et_2NSF_3 (3 equiv), DCM, RT, 2 h, 43%, resolution by silica column chromatography; b) H_2, Pd/C, EtOH, RT, 2 h, 85%; c) 1 M HCl.

In this way, both stereoisomers could be obtained as pure compounds, however the absolute configuration of each diastereoisomer **109** or **110** could not be determined. Stereoisomers **109** and **110** were subjected to hydrogenation to furnish the end-product (2*S*,3*R*)- and (2*R*,3*S*)-3F- NMDA HCl with the absolute stereochemistry yet to be confirmed. The ^{1}H- and ^{19}F- NMR of the enantiomers were of course identical, and identical too to racemic *threo*, with $^{3}J_{HH}$ and $^{3}J_{HF}$ coupling constants found to be 27.0 Hz and 45.0 Hz, respectively. X-ray crystal analysis of a suitable crystal of (-)-**73** confirmed the relative stereochemistry and showed that 3F-NMDA clearly adopts a *gauche* relationship between C-F—C-N^{+} with a dihedral angle of 62.7°.[28] The structure had an extended conformation with the carboxylate groups anti-periplanar to each other as illustrated in **Figure 2.15**.

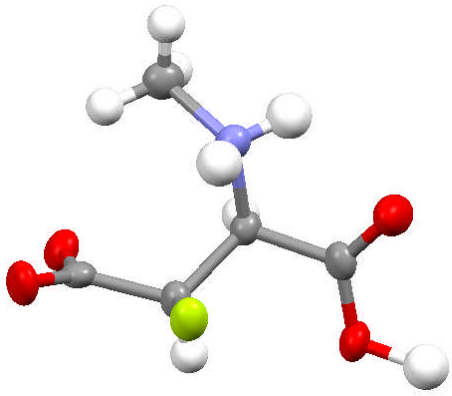

Figure 2.15 X-ray structure of (-)-**73** showing an extended conformation and a C-F to C-N^{+} dihedral angle of 62.7°. The absolute stereochemistry is arbitrarily shown.

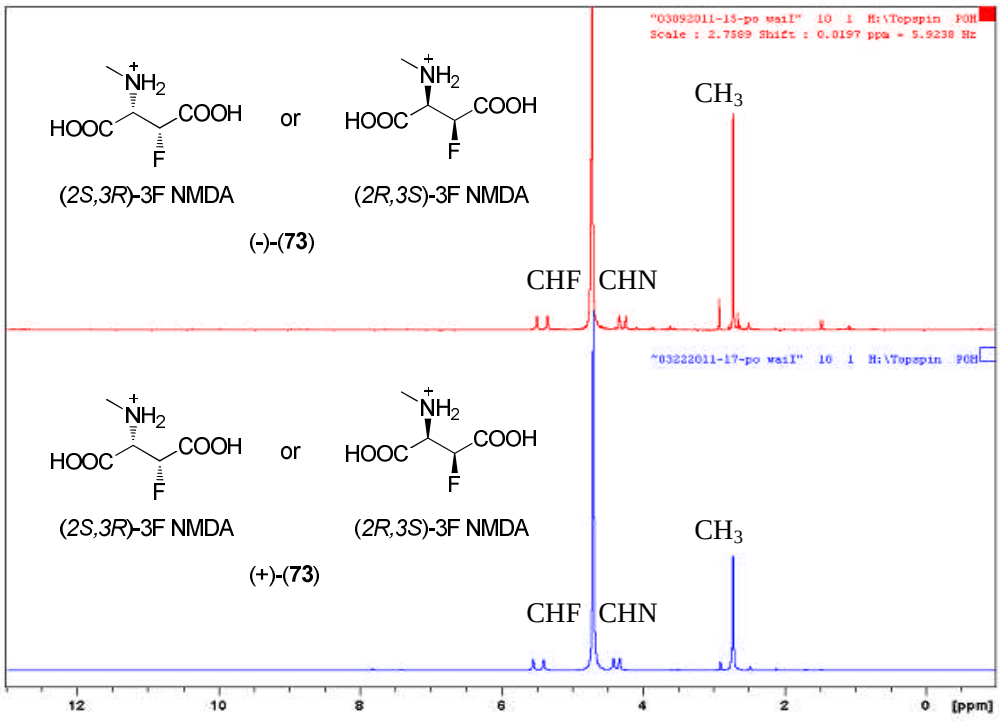

Figure 2.16 ^{1}H NMR spectra of (-)-**73** and (+)-**73** recorded in D_2O at 300 MHz**.**

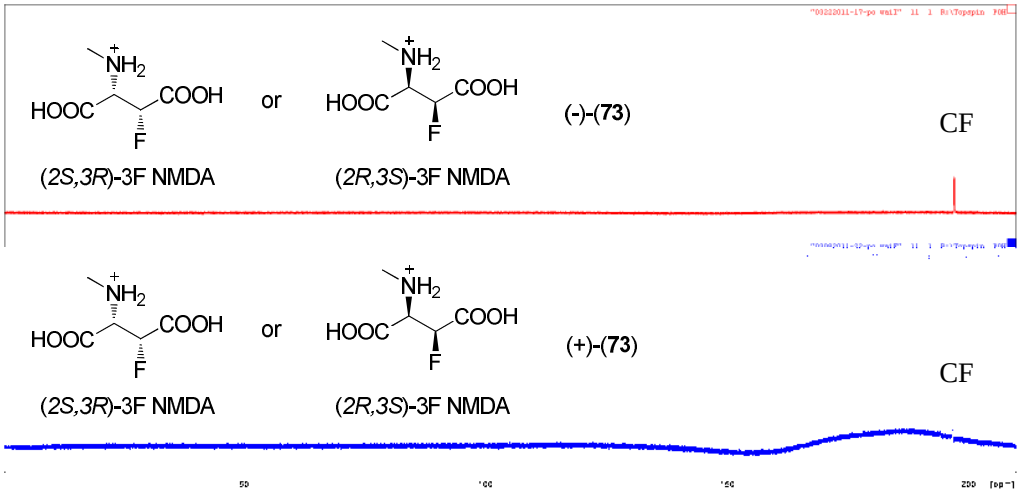

Figure 2.17 ^{19}F NMR spectra of (-)-**73** and (+)-**73** recorded in D_2O at 300 MHz

Stereosiomers (-)-**73** and (+)-**73** were explored in a diastereomeric ratio study to assess if even minor levels of the opposite diastereomers **72** could be present in the sample. The signal at -198.6 ppm corresponds to *erythro*-**72**, while that at -196.4 ppm corresponds to the *threo*-**73**. The chemical shift differences are consistent with two separate diastereoisomers, and neither sample was contaminated with the other, indicating a very high diastereomeric ratio of *erythro*-**72** and *threo*-**73**.

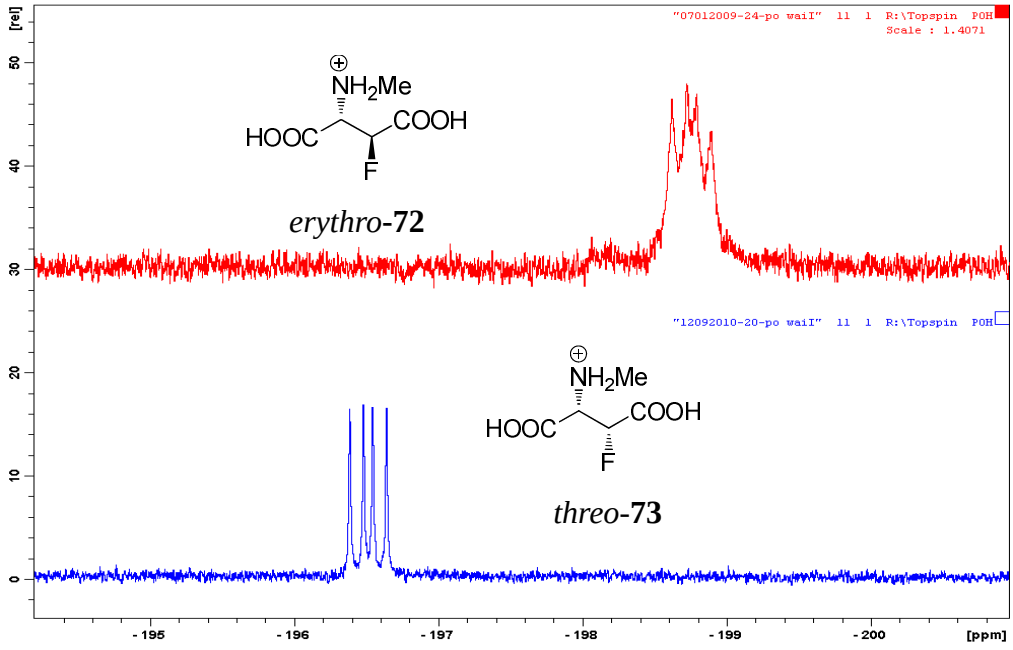

Figure 2.18. ^{19}F NMR spectra of *erythro*-**72** and *threo*-**73** recorded in D_2O at 300 MHz**.**

2.4.7 pKa studies

The high electronegativity of fluorine will clearly affect the pKa of the adjacent functional groups (NH_2 and COOH) relative to NMDA. It is well documented that the pKa of carboxylic acids, alcohols and amines are reduced by fluorine substitution α or *β* to the functional groups.[29] This is illustrated in **Table 2.0** for fluoroalanines. The successive introduction of fluorine increases the acidity of the carboxylic groups by upto 0.9 of a pKa unit, while it causes the amine to become less basic by upto 4.0 pKa units as we progress along the series from $–CH_3$ to $–CF_3$.[29]

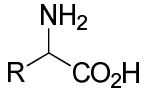

R	CH_3	CH_2F	CHF_2	CF_3
pK_a (CO_2H)	2.3	2.4	1.5	1.2
pK_a (NH_2)	9.9	9.8	8.4	5.3

Table 2.0. pKa of fluoroalanines.[28]

Similarly, it is therefore relevant to measure the pKa of 3F-NMDA HCl D-**72**, as the fluorine will influence the electronics relative to NMDA. In particular lowering the pKa of the amine could affect the protonation status *in vivo*. A potentiometric titration of NMDA HCl **52** was established as a control. The measurement was carried out in deionised water (2 ml) at 25° C, in a (2.3 mmolar) solution of **52** in a temperature controlled water bath. A pH electrode designed for small volumes was calibrated using standard solutions of pH 4 and pH 7. The NaOH solution (2.3×10^{-2} mol.L^{-1}) was calibrated with a known concentration of tartaric acid using phenolphthalein as an indicator. The pKa values for NMDA HCl can be read from the curve as show in the **Figure 2.19 (i)**. The pKa values for NMDA HCl were found to be 2.63 (pKa^1), 4.02 (pKa^2) and 10.22 (pKa^3). The same analysis was then carried out for (2*S*,3*S*)-3F NMDA **72** and the resultant curve is shown in **Figure 2.19 (ii)**.

(i) Potentiometric titration of NMDA HCl 52

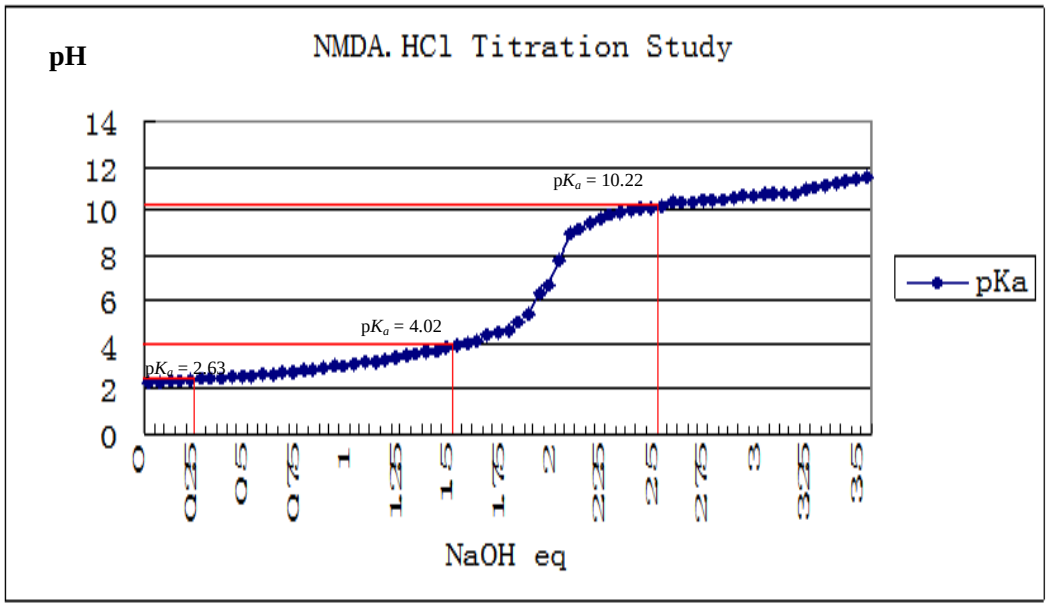

(ii) Potentiometric titration of (2*S*,3*S*)-3F D-72

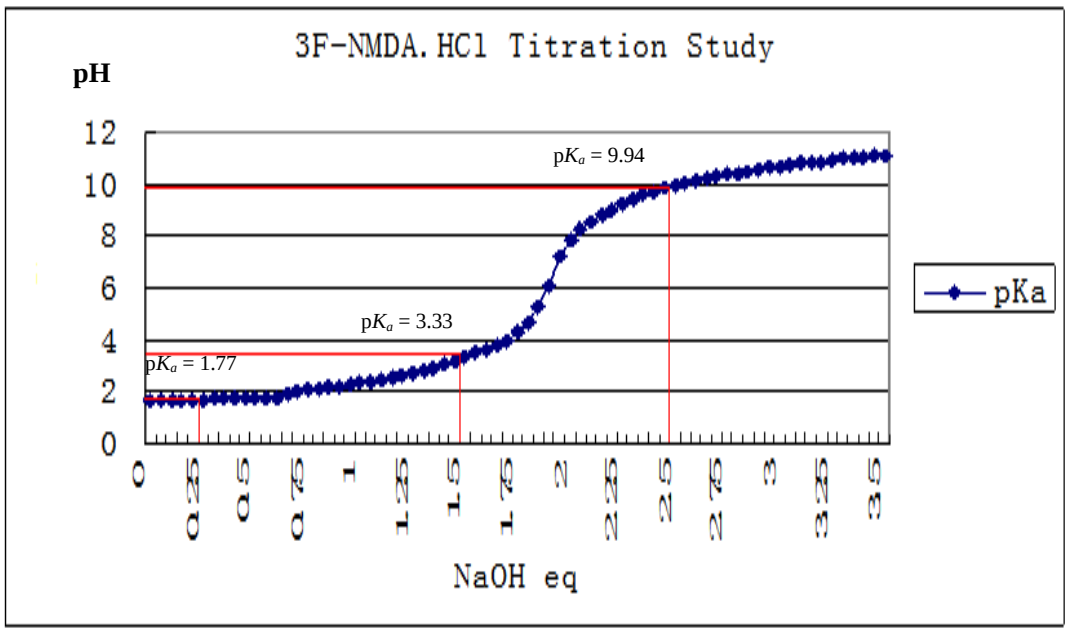

Figure 2.19 pKa titration curve for NMDA and (2*S*,3*S*)-3F D-**72** at 25 °C.

Table 2.1 summarizes the pKa values of NMDA HCl compared to (2*S*,3*S*)-3F NMDA HCl D-**72**. The fluorine substituent has lowered the pKa of both carboxylic acids and the amine group as expected. The pKa^1 of D-**72** was lowered by 0.86 pKa of a unit and pKa^2 was lowered by 0.69 of a pKa unit, while the pKa^3 was lowered by 0.28 of a pKa unit. It would be expected that 3F-NMDA D-**72** is a zwitterion form and overall negative charge at neutral pH.

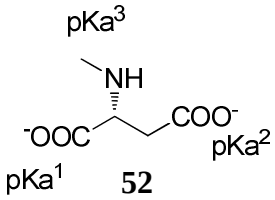

52

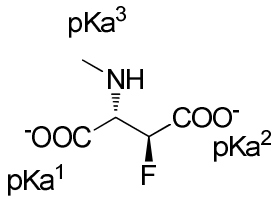

D-**72**

	pKa^1	pKa^2	pKa^3
NMDA.HCl **52**	2.63	4.02	10.22
(2*S*,3*S*)-3F NMDA D-**72**	1.77	3.33	9.94

Table 2.1. Comparison of the pKa values of NMDA.HCl **52** and (2*S*,3*S*)-3F NMDA HCl D-**72**.

2.5 Biological Studies

2.5.1 Receptor assays with NMDA GluN1/N2A and GluN1/N2B.

Biological evaluation of the 3F-NMDA stereoisomers was performed at the Cellular Neurophysiology and Pharmacology Centre for Integrative Physiology, at the University of Edinburgh. The fluorinated NMDA HCl salts were tested on rat NR1/NR2A and NR1/NR2B subunits of the glutamate receptor, expressed in *Xenopus laevis* frog oocytes. A patch clamp assay was performed after 72 h injections. Two electrode voltage clamp current recordings were set up in a solution containing 90 mM NaCl, 3 mM KCl, 10 mM HEPES, 0.5 nM $BaCl_2$, 0.01 mM EDTA (10 μM) and 0.05 mM glycine. The patch clamp analysis was carried out at 23 °C and pH 7.3.

Extra-cellular contaminants such as Zn^{2+} ions were chelated by adding 10 μM of EDTA. The current responses were recorded at a holding potential at –40 mV. Responses and data acquisition were recorded by two electrode voltage-clamp amplifiers and the responses by the agonists to the subunits were expressed from 0 to 1. The E_{max} below refers to the maximal current produced during the saturated concentration of the agonist, while EC_{50} refers to the concentration of the agonist required to produce 50 % of the response in E_{max}.

Based on the concentration response study (**Figure 2.20**) on the NR1/NR2A subunits, the results clearly show that the (2*S*,3*S*)-3F NMDA HCl **72** stereoisomer is almost as active as NMDA. In **Figure 2.20**, the maximum responses for NMDA **52** and (2*S*,3*S*)-3F NMDA D-**72** have been normalized relative to L-glutamate. NMDA gives a response equivalent to 0.78 of that produced by glutamate whereas the corresponding value for (2*S*,3*S*)-3F D-**72** is 0.64 as shown in the **Table 2.2**. By contrast, the unresolved enantiopure (-)- and (+)-3F-NMDA **73** were found to be below the threshold of detection. A further analysis of the 3F-NMDA HCl enantiomers with the GluNR1/NR2B subunit was conducted. In this case (**Table 2.3**),

the relative maximum response of NMDA was found to be 0.96 and the (2*S*,3*S*) 3F-NMDA D-**72** to be 0.54 as shown in **Figure 2.21**. Again, the resolved but not configurationally assigned (-)-**73** and (+)-**73** were both below the detection threshold and were essentially inactive.

Agonist	E_{max}	EC_{50}
Glutamate **53**	1.0	5.9 ± 0.3
NMDA **52**	0.78	105 ± 6
(2*S*,3*S*)-3F NMDA D-**72**	0.64	150 ± 2

Table 2.2. Potency and relative efficacy of 3F-NMDA derivatives at GluN2A NMDARs

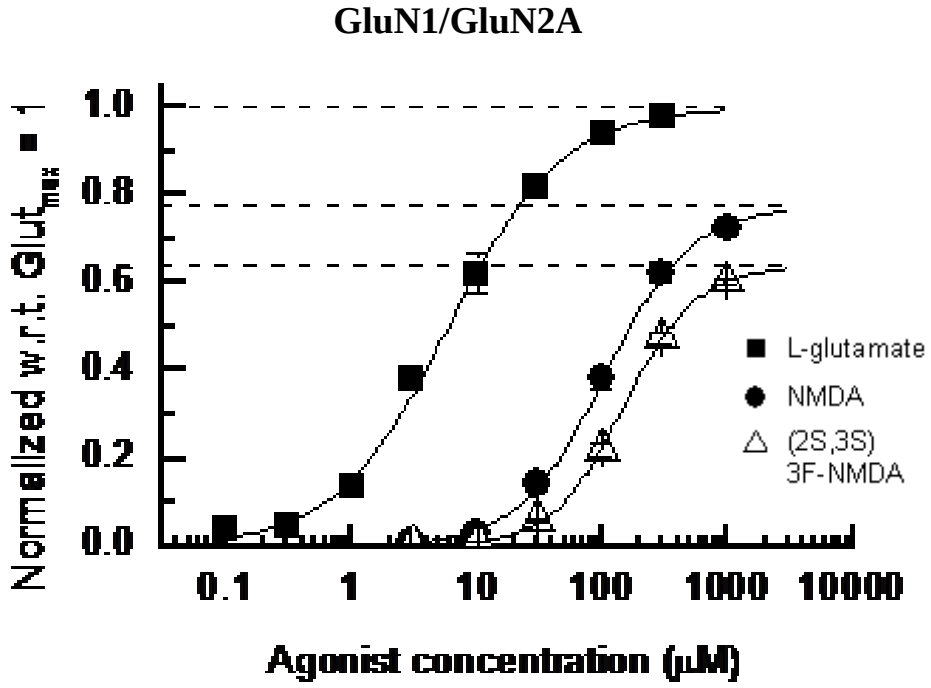

Figure 2.20. Activities of (2*S*,3*S*)-3F NMDA **72** on NR1/NR2A subunit. Both (-)- and (+)-3F NMDA **73** were found to be inactive.

Agonist	E_{max}	EC_{50}
Glutamate **53**	1.0	4.0 ± 0.3
NMDA **52**	0.96	48 ± 3
(2*S*,3*S*)-3F NMDA D-**72**	0.53	55 ± 1

Table 2.3. Potency and relative efficacy of 3F-NMDA derivatives at GluN1/N2B NMDARs

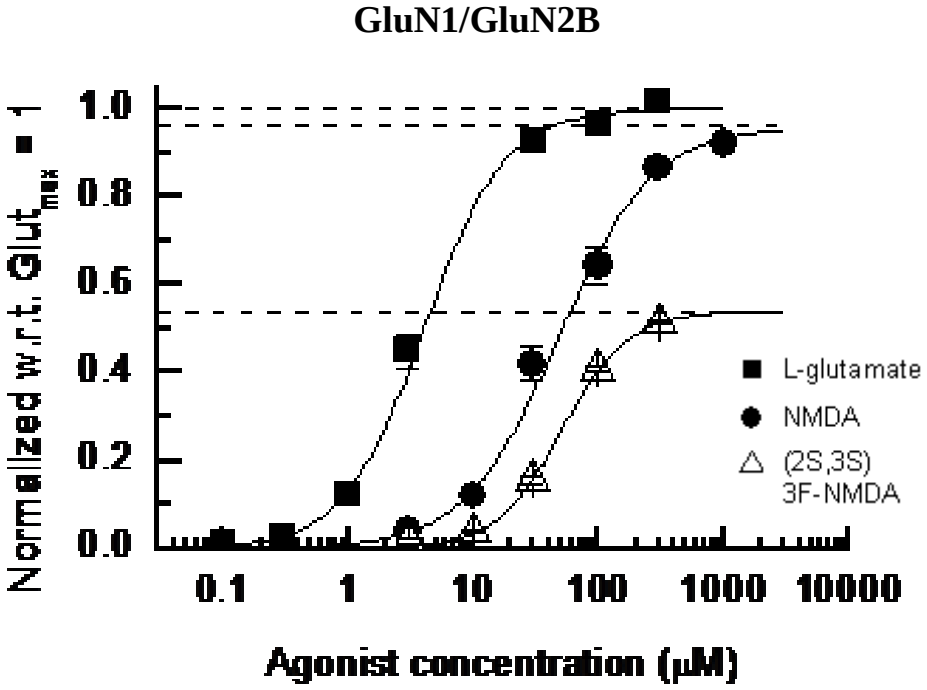

Figure 2.21. Activities of (2*S*,3*S*)-3F NMDA **72** on NR1/NR2B subunit. Both (-)- and (+)-3F NMDA **73** were found to be inactive.

The data was once again normalized relative to the maximum response for NMDA, itself compared with that produced by a maximal concentration of glutamate. By this measure, NMDA gives a response of 1 whereas the corresponding value for (*2S,3S*) 3F-NMDA **72** is 0.72. The other diastereoisomer series (-)-**73** and (+)-**73** gave very low response as shown in **Table 2.4**.

	GluN2A Agonist @ 100 mM	GluN2B Agonist @ 50 mM
NMDA **52**	1.0	1.0
(2*S*,3*S*)-3F NMDA D-**72**	0.72 ± 0.03	0.45 ± 0.01
(+)-3F NMDA **73**	0.009 ± 0.0009	0.0031 ± 0.0009
(-)-3F NMDA **73**	0.001 ± 0.0005	Not detected (n.d).

Table 2.4. NMDA and 3F-NMDA potencies at the GluN2A and GluN2B receptor.

2.5.2 Two-electrode voltage-clamp (TEVC) analysis.

The relative potencies of the 3F-NMDA enantiomers were then compared by the alternative two-electrode voltage-clamp (TEVC) analysis. The TEVC currents were recorded from an oocyte expressing GluN1/GluN2A subunits. All agonists were applied at 100 μM. NMDA **52** and (2*S*,3*S*) 3F-NMDA **72** each elicit large inward currents as illustrated in **Figure 2.22**. By contrast, (-)- and (+)-3F NMDA **73** evoke very low currents which are only resolvable on a higher (×100) gain setting (blue traces)(**Figure 2.22**). All of the currents have been normalized to the response produced by NMDA when it is applied at its EC_{50} concentration at either GluN1/GluN2A or GluN1/GluN2B subunits (100 μM or 50 μM, respectively).

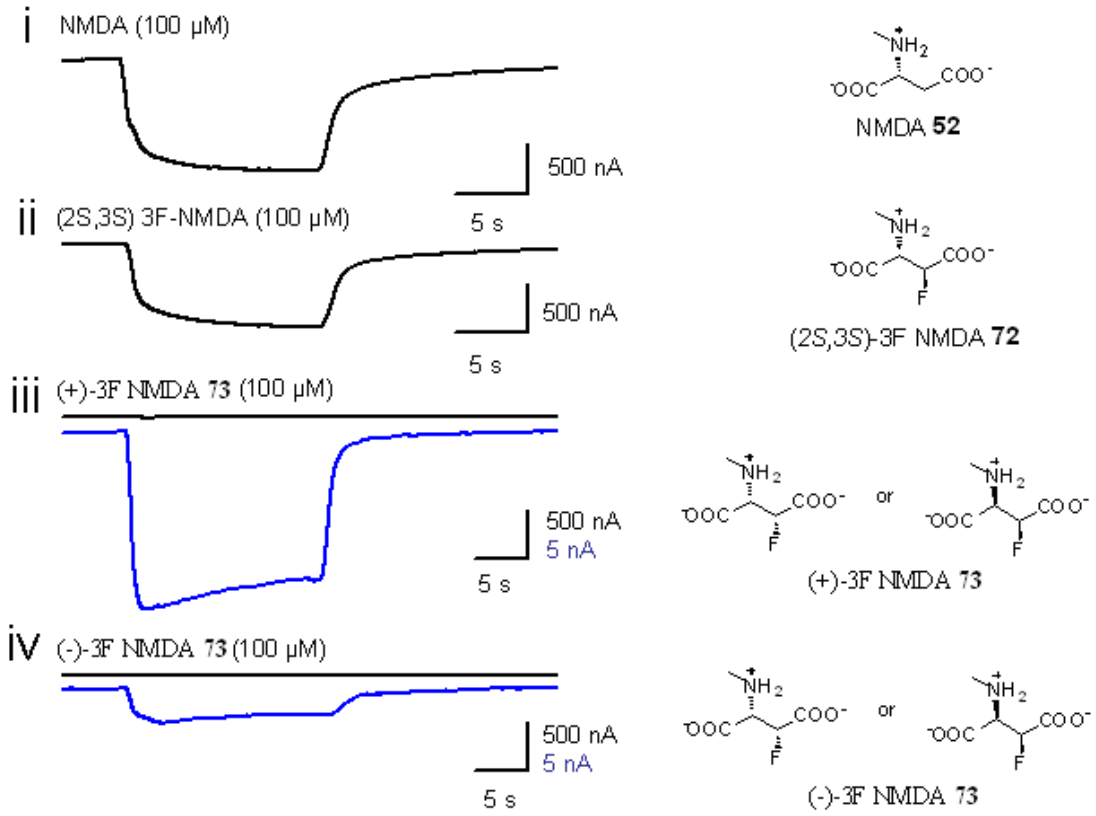

Figure 2.22 The TEVS analysis on 3F-NMDA stereoisomers. All the currents were recorded from an oocyte expressing GluN1/GluN2A subunits.

The data extracted from that in **Figure 2.22**, but on an expanded scale to indicate the low responses evoked by either (-)- and (+)-3F NMDA **73,** is reformatted in histogram form in **Figure 2.23**. Although the absolute stereochemistry of both (-)- and (+)- 3F NMDA **73** could not be distinguished in this study, the biological assessment has shown that these enantiomers and this relative stereochemistry do not act as agonists, and thus achieve the wrong binding mode relative to NMDA.

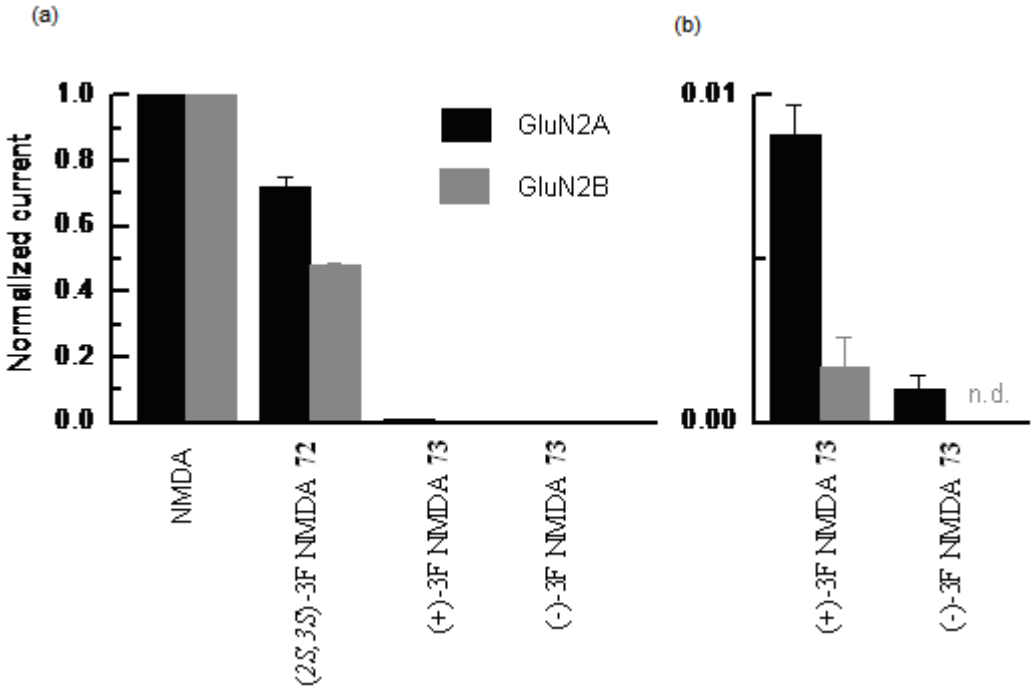

Figure 2.23. (a) TEVS analysis on 3F-NMDA enantiomers (b) All the currents were recorded from an oocyte expressing GluN1/GluN2A subunits.

2.5.3 Binding conformation analysis of NMDA.

The above findings suggest that the (2*S*,3*S*)-3F NMDA D-**72** is the sole stereoisomer that can access the correct binding conformation for GluNR1/NR2A and GluN1/NR2B NMDARs. The data also indicates that (-)- and (+)-3F NMDA **73** stereoisomers do not bind to the receptors. The preferred conformations of D-**72** and D-**73** in solution were deduced to be those highlighted in the blue boxes (**Figure 2.24**) based on Karplus relationship. Accordingly, the $^{3}J_{HF}$ coupling constants for the *syn* H-C-C-F were known to be around 0-18 Hz whereas mixtures of *syn*- and *anti*-periplanar relationship were found around 30.0 Hz. In this case, $^{3}J_{HF}$ of **72** was found to be 29.9 Hz, indicating that the fluorine prefers a *syn*- or *anti*-periplanar orientation to hydrogen. In addition, the $^{3}J_{HH}$ of **72** were found to be 2.0 Hz, suggesting that the vicinal methylene hydrogens are *gauche* or close to 90 ° to each other. These data

suggest that the major solution conformation in **72** is a folded conformation with the carboxylates *syn* to each other, which means either conformation **B** or **C** is the preferred solution conformation. The X-ray crystallography of Furukawa enables the assignment of **C** (highlighted in blue) as the major binding conformation. Conformation **A** is less relevant as this conformation will be high in energy, with the fluorine *anti* to protonated amine. The same analysis was applied to **73** in which the $^{3}J_{HF}$ value shows a large coupling constant, about 26.0 Hz and a small $^{3}J_{HH}$ value 0.0 Hz, indicating that **73** prefers extended conformation **A** with the carboxylate groups *anti*-periplanar to each other (highlighted in blue) as shown in the Newman projection in **Figure 2.24**. Indeed, an X-ray crystal structure of **73** also has this extended conformation (**Figure 2.15**).

(i) (*2S,3S*)-3F NMDA (72)

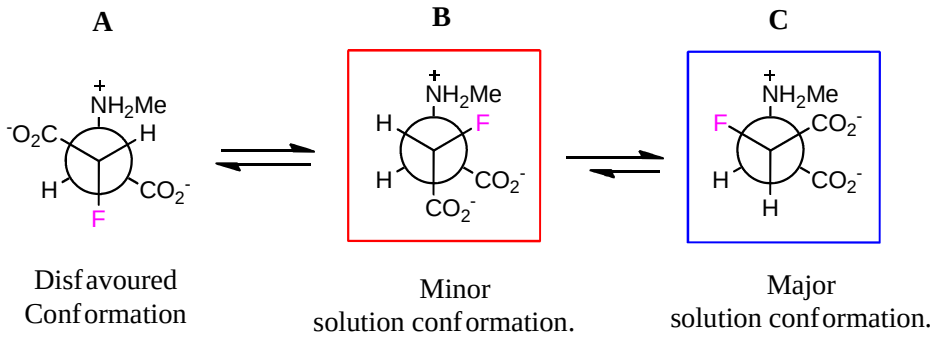

(ii) (*2S,3R*)-3F NMDA (73)

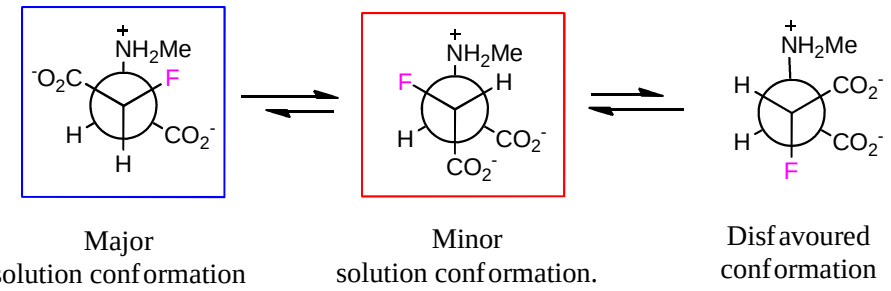

Figure 2.24 The Newman projection of the 3F diastereoisomers. Coupling constants of (i) D_2O, ^{2}J(H,F) = 44.0 Hz and ^{3}J(H,F) = 26.0 Hz; (ii) D_2O, ^{2}J(H,F) = 47.9 Hz, ^{3}J(H,F) = 29.9 Hz.

The biological results indicated that (2*S*, 3*S*)-3F **72** is inactive and (2*S*, 3*R*)-3F **73** is not. The X-ray crystal structure of NMDA bound to the glutamate receptor (GluN2D) (**Figure 2.25**) indicates that conformer **C** is the active binding conformation. The (2*S*, 3*R*)-3F **73** NMDA cannot easily adopt this conformation **C** as the fluorine and $NMeH_3^+$ substituent would be *anti*-periplanar and high in energy relative to conformer **A** and **B**. However, in the case of isomer (2*S*, 3*S*)-3F **72**, conformer **C,** a major one in solution can be accessed as the fluorine and $NMeH_3^+$ are *gauche* to each other, a relative low energy conformation.

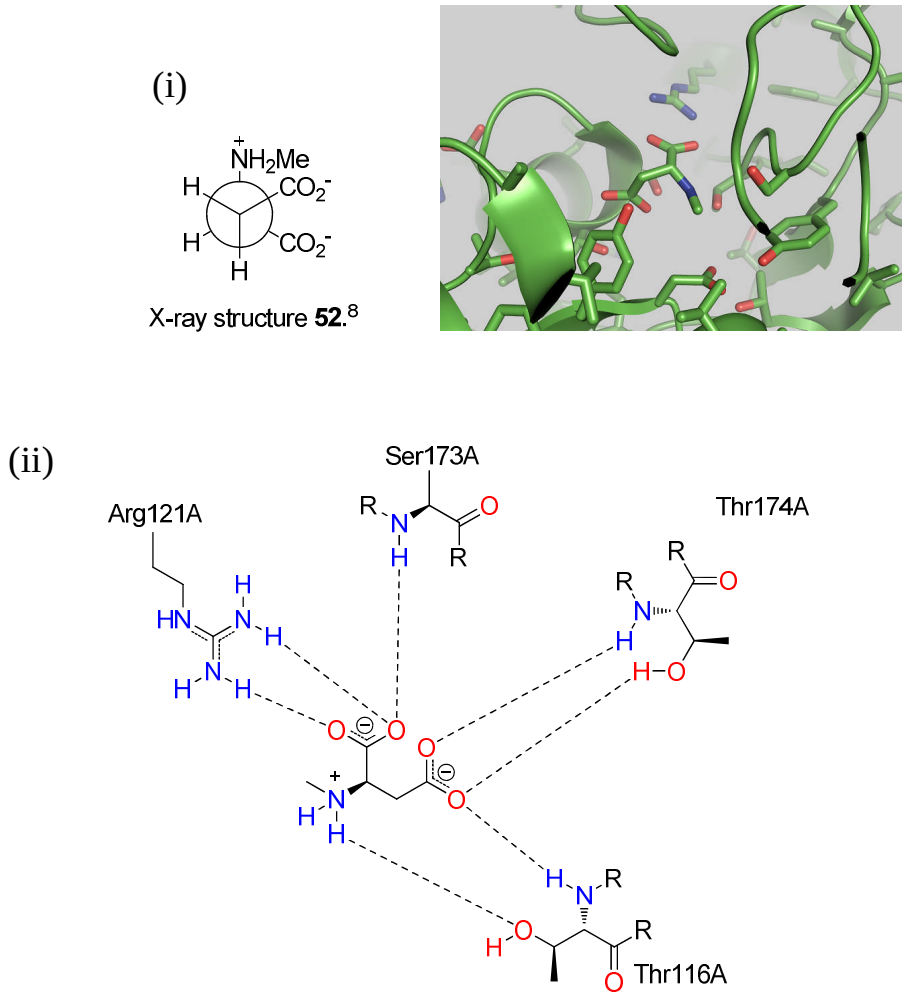

Figure 2.25 (i) The crystal structure of GluN2D in complex with *N*-methyl-D-aspartate (NMDA) reported by Furukawa *et al*. (ii) NMDA is bound in this folded conformation which was supported in this study.[8]

In solution, the minor solution conformation **B** is in equilibrium with **C**. In order to trigger a response, the NMDA has to orientate conformation **C**. The active solution conformation of NMDA **52** deduced from our study is consistent with the X-ray structure study (**Figure 2.26)**.

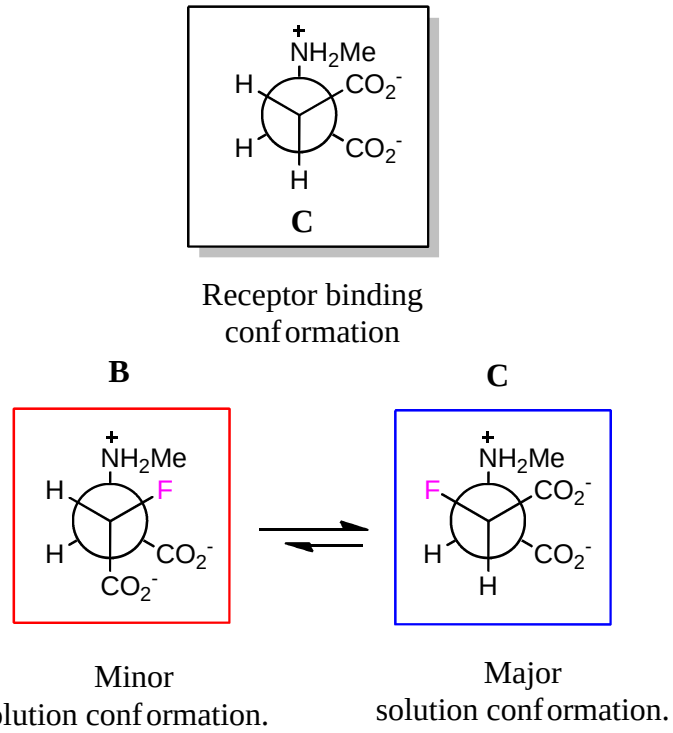

Figure 2.26 The active binding conformation was deduced to be conformation **C** based on $^{3}J_{HF}$ values and biological assays.

2.6 Conclusions

The (2*S*, 3*S*)-3-fluoro NMDA D-**72** was successfully prepared from diethyl D-tartrate. The (2*S*, 3*R*)- stereoisomer was prepared by separation of diastereoisomers generated by reaction of a *meso*- epoxide with an enantiomerically pure amine, followed by fluorination. Both the (2*S*,3*R*)- and (2*R*,3*S*)- enantiomers were prepared separately, however assignment of the absolute configuration to each enantiomer could not be unambiguously proven. The results of this study demonstrate that the active binding conformation is the major solution conformation of (2*S*, 3*S*)-3F NMDA D-**72**. It is this conformation that NMDA adopts when bound to GluNR1/2A and GluNR1/2B sub-units. The other 3F-diastereoisomer cannot easily adopt that binding conformation. This led to the conclusion that NMDA binds to the receptor with the carboxylate groups *gauche* to each other, with the major solution acting as preferred conformation. The study reinforces the recent finding of Furukawa *et al*, where they solved an X-ray crystal structure of NMDA bound to the GluNR1/N2D subunits.[8] The study indicates that such comparative studies with fluorine stereoisomers of bioactives can be utilized to explore the binding conformation of small molecules on proteins.

References:

[1] A. Bernareggi, Z. Duenas, J. M. R. Ruiz, F. Ruzzier and R. Miledi, *Proc. Natl. Acad. Sci.*, 2007, **8**, 2956-2960.

[2] R. Risgaard, K. B. Hansen and R. P. Clasen, *Chem. Eur. J*., 2010, **16**, 13910-13918.

[3] F. Fondum, *J. Neurochem*., 1984, **42**, 1-11.

[4] N. Armstrong, Y. Sun, G. Q. Chen and E. Gouaux, *Nature (Lond.)*, 1998, **395**, 913-917.

[5] L. C. Anson, P. E. Chen, D. J. A. Wylie and R. Schoepfer, *J. Neurosci*., 1998, **18**, 581-589.

[6] P. E. Chen, M. T. Geballe, P. J. Stansfeld, A. R. Jonhston, H. J. Yuan, A. L. Jaacob, J. P. Synder, S. F. Traynellis and D. J. A. Wylie, *Mol. Pharmacol*., 2005, **67**, 1470-1484.

[7] H. Furukawa, S. K. Singh, R. Mancusso and E. Gouaux, *Nature*, 2005, **438**, 185-192.

[8] K. M. Vance, N. Simorowski, S. F. Traynelis and H. Furukawa, *Nat. Commun*., 2011, **2**, 294-294.

[9] H. B. Osborne, J. Egebjerg, E. Ø. Nielsen and P. K. Larsen, *J. Med. Chem*., 2000, **9**, 2609-2645.

[10] G. F. Morris, R. Bullock, S. B. Marshall, A. Marmarou, A. Mass and L. F. Marshall, *J. Neurosurg*., 1999, **91**, 737-743.

[11] R. J. Hargreaves, R.G. Hill and C.C. Iversen, *Acta Neurochir. Suppl (wien)*, 1994, **60**, 15-9.

[12] B. S. Meldrum, *J. Nutr.*, 2000, 1007S-1015S.

[13] K. Williams, *Mol. Pharmacol*., 1993, **44**, 851-859

[14] S. F. Traynellis, M. F. Burgess, F. Zheng, P. Lyuboslavsky and J. L. Powers, *J. Neurosci.*, 1998, **18**, 6163-6175.

[15] M. F. Davies, P. A. Maguire and G. H. Leow, *Mol. Pharmacol*., 1993, **44**, 876-881.

[16] K. Erreger, M. T. Geballe, A. Kristensen, P. E. Chen, K. B. Hansen, C. J. Lee, H. Yuan, P. Le, P. N. Lyuboslavsky, N. Micale, L. JØrgensen, R. P. Clausen, D. J. Wyllie, J. P. Synder, S. F. Traynelis, *Mol. Pharamcol*., 2007, **72**, 907.

[17] G. Deniau, A. M. Z. Slawin, T. Lebl, F. Chorki, J. P. Issbern, T. V. Mourik, J. M. Heygate, J. J. Lambert, L. A. Etherington, K. T. Sillar and D. O'Hagan, *ChemBioChem*, 2007, **8**, 2265-2274.

[18] I. Yamamoto, G. P. Deniau, N. Gavande, M. Chebib, G. A. R. Johnston and D. O' Hagan, *Chem. Comm*., 2011, **586,** 227-245.

[19] M. J. Wanner, J. J. M. Hageman, G. J. Koomen and U. K. Pandit, *J. Med. Chem*., 1980, **23**, 85-87.

[20] A. M. Stern, B. M. Foxman, A. H. Tashjian, Jr. and R. H. Abeles, *J. Med. Chem*., 1982, **25**, 544-550.

[21] F. B. Charvillon and R. Amouroux, *Tetrahedron Lett.*, 1996, **37**, 5103-5106.

[22] A. Korn, S. R. Böhner and L. Moroder, *Tetrahedron*, 1994, **28**, 8381-8392.

[23] T. Schirmeister and A. Klockow, *Mini Rev. Med. Chem.*, 2003, **3**, 585-596.

[24] B. T. Golding, D. R. Hall and S. Sakrikar, *J. Chem. Soc. Perkins Trans.*1, 1973, 1214-1220.

[25] M. E. V. Dort, Y. W. Jung, P. S. Sherman, M. R. Kilburn and D. M. Wieland, *J. Med. Chem.*, 1995, **38**, 810-815.

[26] O. M. Cohn, C. Moore and H. C. Taljaard, *J. Chem. Soc. Perkins Trans.*1, 1988, **9**, 2663-2674.

[27] R. Cysewski, M. Kwit, B. Warzajtis, U. Rychlewska and J. Gawroński, *J. Org. Chem*., 2009, **74**, 4573-4583.

[28] D. O'Hagan, C. Bilton, J. A. K. Howard, L. Knight and D. J. Tozer, *J. Chem. Soc., Perkin Trans*. 2, 2000, 605-607.

[29] Kukhar, V. P., *J. Fluorine Chem.*, 1994, **69**, 199-205.

Chapter 3: Fluorinated Cinacalcet analogues.

3.1 Introduction

Parathyroid hormone (PTH) is an important hormone produced by the thyroid gland. Elevation of PTH level caused by abnormal calcium homeostasis is the main cause of chronic kidney disease and in some cases can contribute to metabolic bone disease.[1] Therapies such as administration of vitamin D sterols and phosphate binders have been outlined to decrease PTH secretion. However, these treatments generate side effects such as hypercalcemia and hyperphosphatemia.[1] Lately, the calcium-sensing receptor (CaSR) has emerged as a target of therapeutic interest to circumvent these side effects.[1]

3.1.1 The calcium-sensing receptor (CaSR) in the parathyroid.

Accumulated research in structural biology has shown that the CaSR consists of seven transmembrane (TM) helices. It is a member of G-protein-coupled receptor (GPCR) family.[2-6] The primary role of CaSR is to maintain constant blood Ca^{2+} levels by regulating PTH secretion. PTH normalises the Ca^{2+} level in bone, kidneys and intestines and it also regulates the vitamin D receptor (VDR).

When Ca^{2+} levels are high (hypercalcemia), parathyroid cell proliferation and PTH gene expression are suppressed, and the VDR is then upregulated. In addition, high Ca^{2+} levels are inhibited by calcitonin (CT) and the 1,25 $(OH)_2D_3$ production decreases. In response to the high calcium level, the activity of bone-resorbing osteoclasts is suppressed. As a consequence, the net Ca^{2+} level is normalized by reduction of Ca^{2+} release from bone. At the renal tubular level, an increase of Ca^{2+}

reduces calcium reabsorption in both cortical thick ascending limb (cTAL) and distal convulated tubule (DCT) into the blood plasma.[7-9]

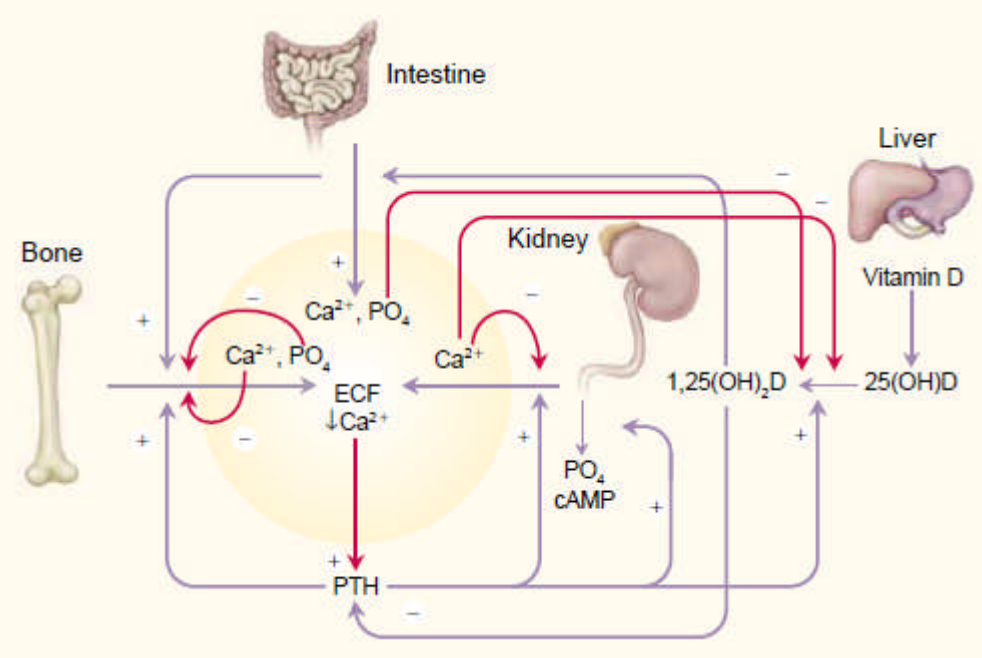

Figure 3.1 Calcium homeostasis regulated in three organs; kidney, bone and intestine, by transport of the calcium in or out of the extracellular fluid (ECF).[10]

3.2 Allosteric modulators and CaSR ligands.

The function of the CaSR is mediated by exogenous ligands. Two types of ligands have been recognized, namely orthosteric and allosteric modulators. Orthosteric ligands are capable of activating the CaSR directly. Examples are divalent and trivalent cations, such as the Ca^{2+}, Mg^{2+}, Al^{3+}, Ni^{2+} and Ba^{2+}. By contrast, an allosteric modulator is only capable of activating the receptor if it is accompanied by the binding of primary orthosteric ligands. Orthosteric and allosteric modulators are classified as type I and type II agonists, respectively.

3.2.1 Orthosteric ligands (Type I agonists).

Orthosteric ligands (types I agonists) of the CaSR have been studied extensively and it is generally agreed that these exogenous ligands offer more benefit than harm. Among these are metal ions strontium and aluminium (Sr^{2+} and Al^{3+}). Studies on the effect of Sr^{2+} has shown that it is effective in osteoporosis treatment and is widely used for this purpose.[11] Sr^{2+} activates the CaSR and thereby promotes osteoblasts in bone formation. By contrast, osteoclasts promote brittle bone or bone resorption of Ca^{2+}. Osteoblasts and osteoclasts are involved in physiology processes that control bone tissues. In hypercalcemia, bone resorption is inhibited controlling the break down of the bone. As a result, blood calcium levels are restored as Ca^{2+} is no longer transferred from bone to the blood. Sr^{2+} also works by stimulating the production of osteoprotegerin from osteoblasts, thus inhibiting the formation of osteoclasts from preosteoclasts in a similar manner.[12-14] However, orthosteric ligands (type I agonists) can have negative side effects.[15] The aminoglycoside antibiotics, namely neomycin **111**, gentamicin **112** and tobramycin **113** (**Figure 3.2**) were reported to increase Ca^{2+} levels upon binding to CaSR and were responsible for renal toxicity.[15]

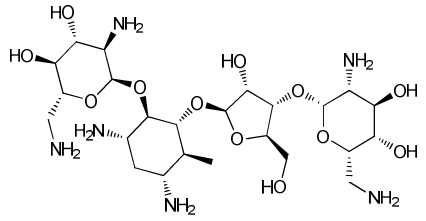

111

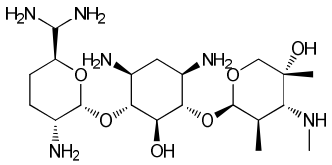

112

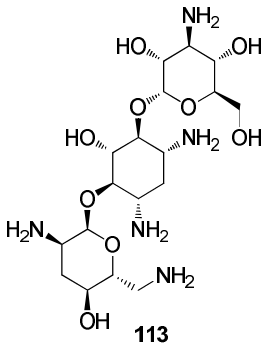

113

Figure 3.2 The aminoglycoside antibiotics are type I orthosteric agonists of the CaSR.

Polyamines are known to activate the CaSR and have been demonstrated to inhibit PTH secretion. These cationic compounds (spermine **114**, spermidine **115** and putrescine **116**, **Figure 3.3**) inhibit PTH secretion. Further biological evidence has shown that spermine **114** has other physiological roles, such as the regulation of gastrointestinal epithelia function and stimulation of gastrin release in stomach through activation of the CaSR.[16-17]

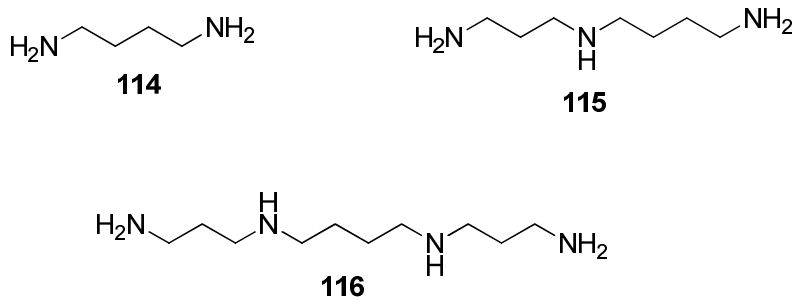

Figure 3.3 Polyamines belong to the Type I orthosteric agonists of the CaSR.

3.2.2 Allosteric modulators (Type II agonists).

The phenylalkylamine drugs including Cinacalcet **117**, NPS R-568 **118**, NPS R-467 **119** and calindol **120** (**Figure 3.4**) are allosteric modulators displaying calcimimetic effects. These compounds are known to inhibit secretion of PTH in patients with hyperparathyroidism through binding to an allosteric site of the CaSR. The calcimimetics influence Ca^{2+} release leading to the inhibition of PTH secretion. Cinacalcet **117** emerged as a more potent allosteric modulator than NPS R-568 **118** and NPS R-467 **119**. Cinacalcet **117** is undergoing clinical trials for treating parathyroid cancer patients.[18] The calcimimetic Calindol **120** is another in this series developed for the same purpose with a similar structure but with an indole ring.[19]

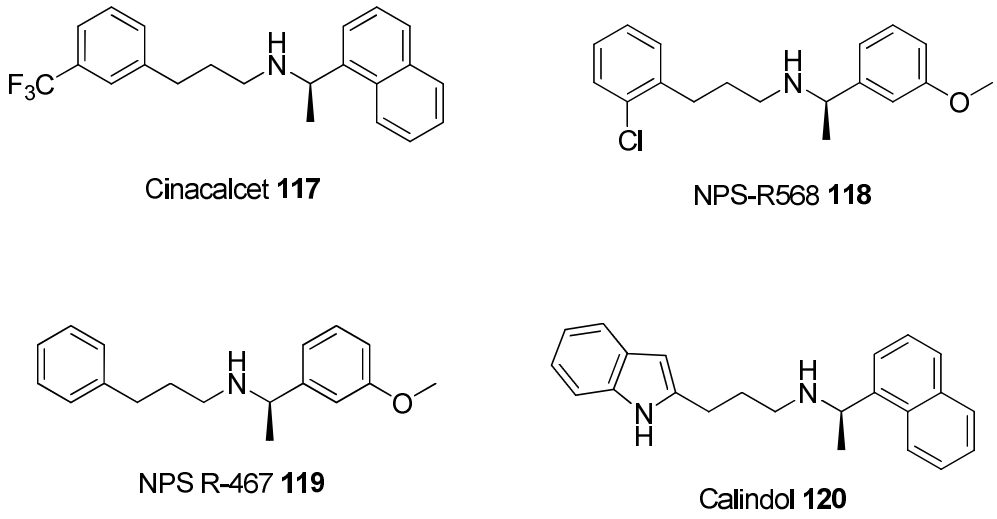

Figure 3.4 Phenylalkylamines type II allosteric modulators CaSR.

Compound **121** acts opposite to the calcimimetics but also binds the allosteric site of the CaSR.[20] This compound is a calcilytic, or a negative allosteric modulator. It interacts by elevating PTH secretion. This negative allosteric modulator recently came to attention due to its potential for osteoporosis treatment. Furthermore, **121** has been demonstrated to regulate PTH levels and thereby emerges as a potential lead candicate for drug development. Another calcilytic which has been identified recently is Calhex 231 **122**. As a class, their mechanism of action of these drugs involves binding to an CaSR allosteric site, the location of which is still under investigation.

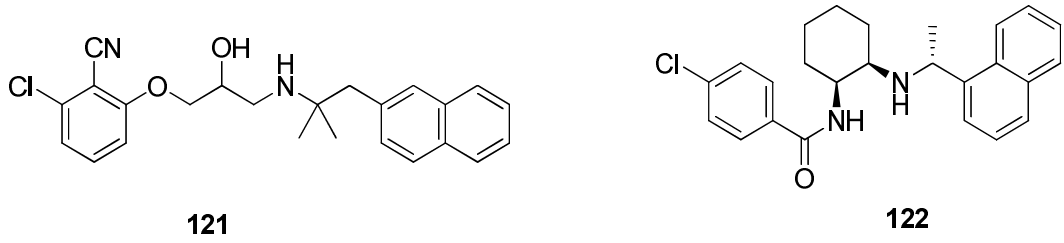

Figure 3.5. The calcilytics belong to the type II CaSR allosteric modulators.

3.3 Binding conformation of calcimimetic and calcilytics on the CaSR.

Some effort has gone into understanding the binding of the phenylalkylamines, including the calcilytic compounds to CaSR. A structural feature common to both NPS R-568 **118** and NPS 2143 **121** is the presence of a phenylalkyl amine. The amine is protonated and positively charged at physiological pH. Recent homology modeling using the crystal structure of G-protein coupled receptor bovine rhodopsin bRho as a template, has displayed that the both **118** (calcimimetic) and **120** (calcilytic) bind to the 7TM of CaSR as illustrated in **Figure 3.6**.[21] Furthermore, this finding has also indicated that the protonated amine forms an ionic interaction with the Glu 837 residue. This further implies that the location of binding for calindol **120** and NPS R-568 **118** is the same, however their unique binding modes at this site are different. This homology data remains speculative and the working hypothesis requires to be verified by experimental data. In the most recent study from Bristol-Meyers Squibb, "BMS compound 1" **125** was found to stimulate PTH secretion when administrated orally.[22] This compound emerges as a potential drug for the treatment of osteoporosis. Interestingly, **125** was found to have a different binding site compared to NPS 2143 **121** and other phenylalkylamines. The binding does not appear to involve the Glu837 residue, instead deletion of the Ile841 residue eliminated the potency of **125**.[23] Further identification of improved chemical entities which are capable of modulating the agonism and antagonisim on the CaSR is needed. This project is focused on exploring the binding mode of cinacalcet on the CaSR by comparative and stereospecific C-F bond modification to generate two diastereoisomers **123** and **124**.

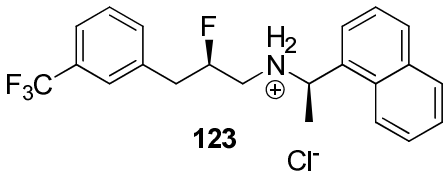

123

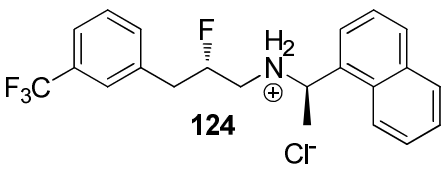

124

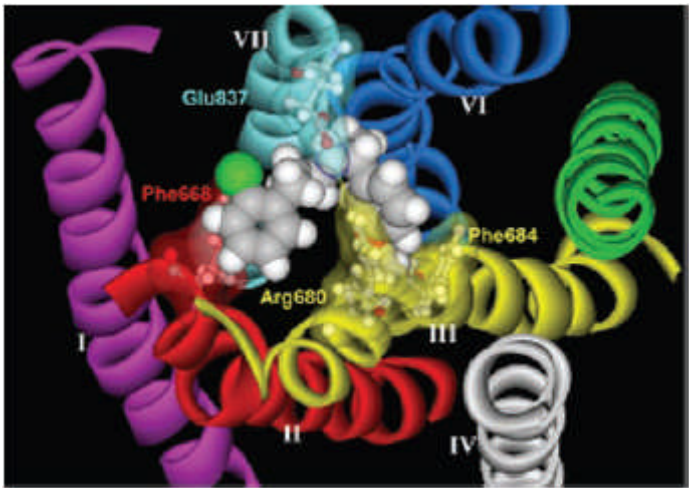

Figure 3.6. Homology modelling for NPS R-568 **118** indicates that the N-H forms a hydrogen bond with Glu837.[24]

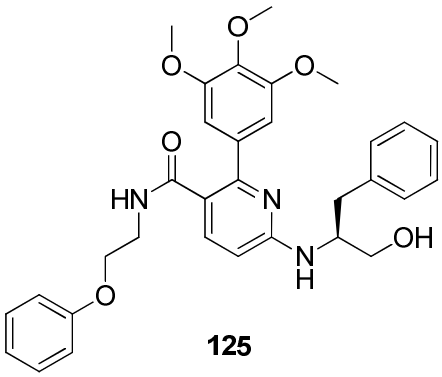

125

3.4 The pentafluorosulfanyl group (SF_5), a new substituent for medicinal chemistry.

The physical properties and electronegativity of the SF_5 group has attracted a lot of attention in recent years. The interest in the SF_5 group is derived from its physical properties, which include high chemical resistance, thermal stability, electron withdrawing nature and hydrophobicity which make it an attractive substituent for modifying pharmacokinetic properties.[25] Moreover, these combined properties suggest that it may be an alternative to the trifluoromethyl group, a widely used substituent in pharmaceutical development.[26] In terms of size, the pentafluorosulfanyl group is slightly smaller than the *tert*-butyl group, but it is clearly larger than the trifluoromethyl group.[29] Pentafluorosulfanyl is more electronegative than the trifluoro group, 3.65 D *vs*. 3.36 D in terms of electronegativity.[17]

There are a limited number of examples involving incorporation of SF_5 group into bioactive molecules. This is due to the limited number of SF_5 building blocks. P. Wipf *et al*., reported the synthesis of analogues of SF_5 mefloquine.[27] Mefloquine **126** is an orally administrated drug used for the treatment of malaria. However, its application has been hindered recently by many side effects such as depression, anxiety, hallucination and seizures. In this work, efforts have been carried out to re-engineer the molecule by substituting the CF_3 group to different positions, and placing SF_5 on the aromatic ring. Direct comparison of the SF_5 analogues to the original mefloquine in mammalian cell lines (Pf 235) showed the IC_{50} of **127** and **128** to be more potent, than **126** (9.8 and 10.0 *vs*. 18 ng/mL respectively). Analogues **127** and **128** were more potent against some cell lines, suggesting that the CF_3 and SF_5 group could be interchangeable, sometimes to advantageous effects.[27]

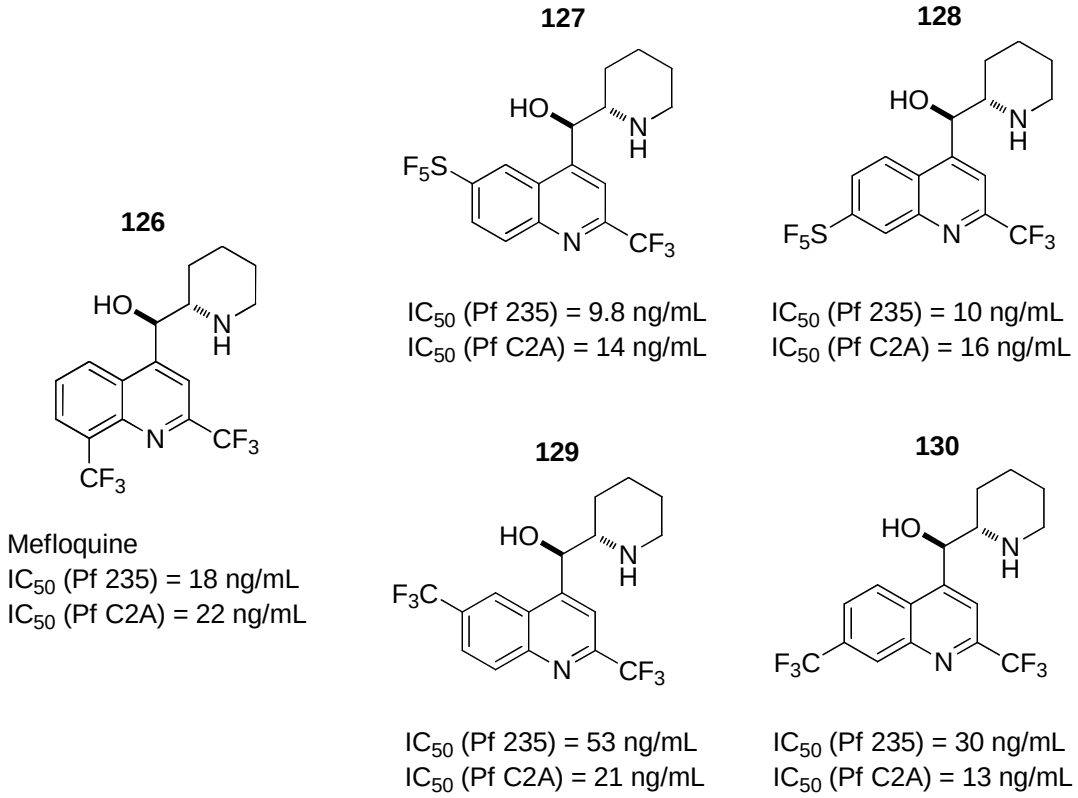

Figure 3.7.Antimalaria activity exhibited by SF_5 and CF_3 analogues of mefloquine.

Drug discovery programmes targeting modifications of fluoxetin (*rac*)-**131**, fenfluramine (*rac*)-**132** and norfenfluramine (*rac*)-**133** (**Figure 3.8**) obtained an interesting outcome when the trifluoromethyl group was replaced by the pentafluorosulfanyl group. This led to enhanced potency against the 5-hydroxytryptamine (5-HT) receptor.[28] Fluoxetin (*rac*-**131**) and fenfluramine (*rac*-**132**) were first introduced as clinical agents in 1974 as selective serotonin reuptake inhibitors. The 5-HT receptors are well known to control human physicology. Fluoxetin is the market leaders with profit margins of more than $3 billion per year, while fenfluramine (*rac*-**132**) and norfenfluramine (*rac*-**133**) have been withdrawn from the drug market due to detrimental side effects on appetite.

The pentafluorosulfanyl analogues of fenfluramine (*rac*)-**135** and norfenfluramine (*rac*)-**136** were prepared from pentafluorosulfanylbenzene building blocks.[28] Binding and inhibition assays showed that both (*rac*)-**135** and (*rac*)-**136** have ten-fold increased affinity for the 5-HT_6 receptor. More strikingly the pentafluorosulfanyl analogues showed binding selectivity between different receptor subtypes.

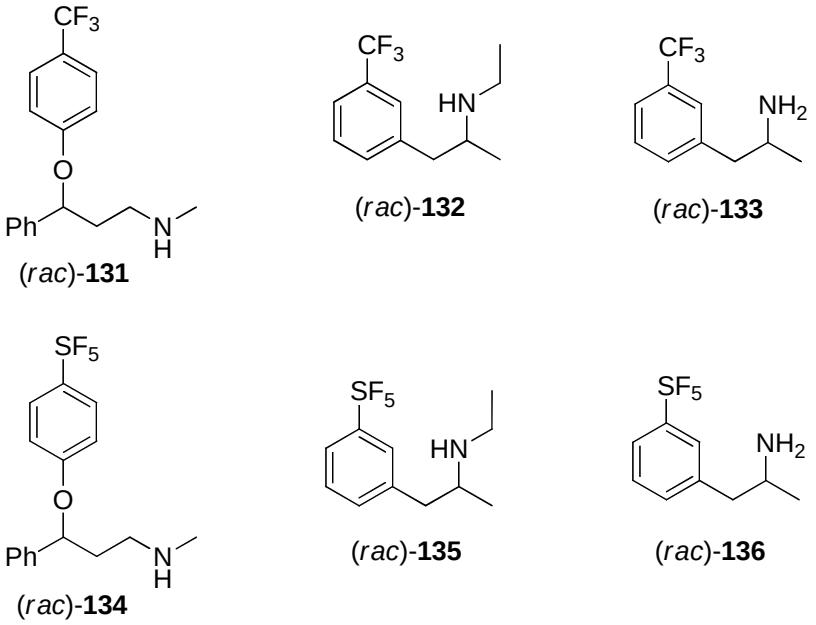

Figure 3.8. Fluoxetin (*rac*)-**131**, fenfluoroamine (*rac*)-**132**, norflenfluroamine (*rac*)-**133** and some pentafluorosulfanyl analogues.

3.5 Aims of this project

The study can be divided into two parts. The first objective involved the synthesis of the individual diastereoisomer (2*R*,1'*R)*-**123** and (2*S*,1'*R*)-**124** of fluoro cinacalcet HCl to study the relative efficacy of these compounds on the calcium sensing receptor as shown in **Figure 3.9**. This concept is similar to that described in the 3-fluoro NMDA research discussed in the previous chapter. It is anticipated that the C-F---NH_3^+-C interaction will favour a *gauche* conformation with a low population of *anti* conformation in solution. In order to explore the preferred binding conformation of Cinacalcet HCl **117**, assays and relative potency of these fluorinated diastereosiomers should allow an assessment of the preferred binding conformation, based on our understanding of fluorine chemistry.

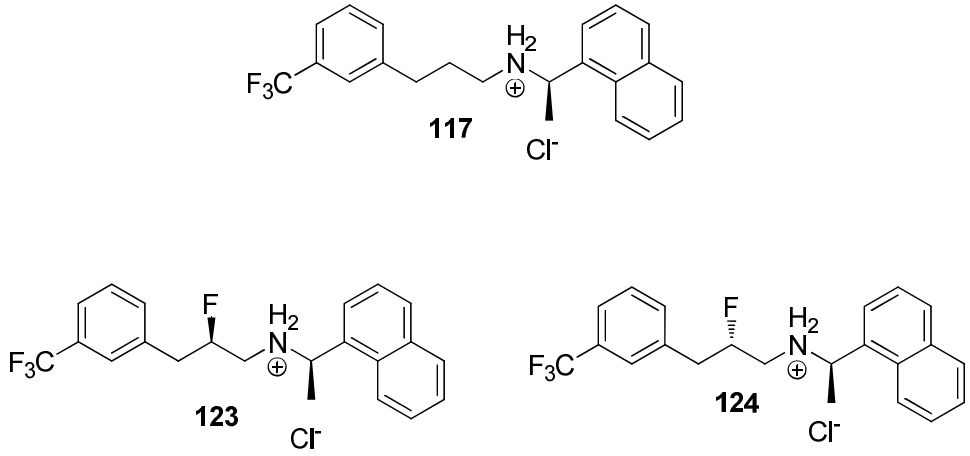

Figure 3.9 Cinacalcet and the two fluorinated diastereoisomers **123** and **124**.

The second objective will focus on the synthesis of a pentafluorosulfur 3''-(SF_5-) analogue of Cinacalcet as shown in **Figure 3.10**. It is anticipated that replacing CF_3- for SF_5- should increase the lipophilicity of this substituent.

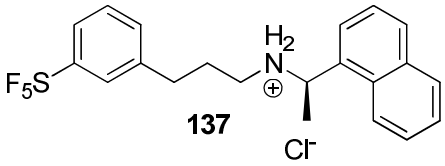

137

Figure 3.10 3''-SF_5-Cinacalcet HCl **137** a synthetic target.

3.6 Background on the synthesis of Cinacalcet.

In the past, a number of reports have appeared on the synthesis of Cinacalcet. Most of these routes rely on a reductive amination with sodium cyanoborohydride or sodium triacetoxyborohydride. An example of this is illustrated in Scheme 3.0 using 3-arylpropionaldehyde condensed with arylethylamine followed by a one-pot reduction.[29]

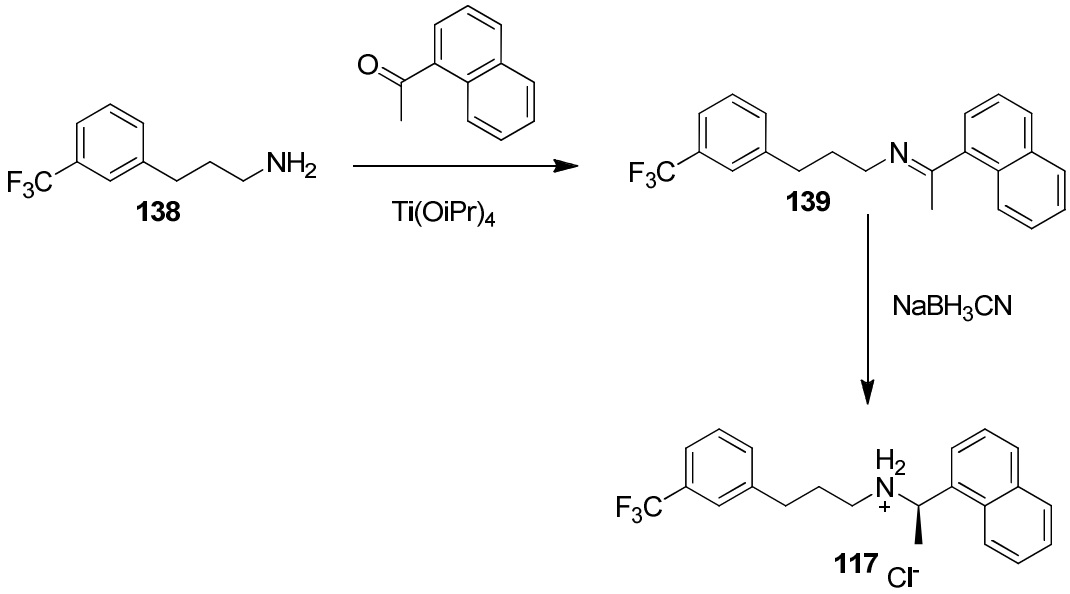

Scheme 3.0 Previous synthetic study on the route to **117**.[29]

Alternatively, the synthesis of **117** has been assessed from 3'-(trifluoromethyl)cinnamic acid **140**. Successful hydrogenation on the olefinic carbon of **140** in the presence of palladium hydroxide and hydrogen, gave **141**, which could be coupled with (*R*)-1-(1-napthyl)ethylamine **142** to generate amide **143**. Acid chloride or peptide coupling reagents have been used to activate the carboxylic group. It has been reported the amide can also be generated *via* direct condensation of the carboxylic acid with the amine without any solvent, as shown in Scheme 3.1.[30] Removal of the amide carbonyl with sodium borohydride in the presence of boron trifluoride and then recrystallization afforded **117.**

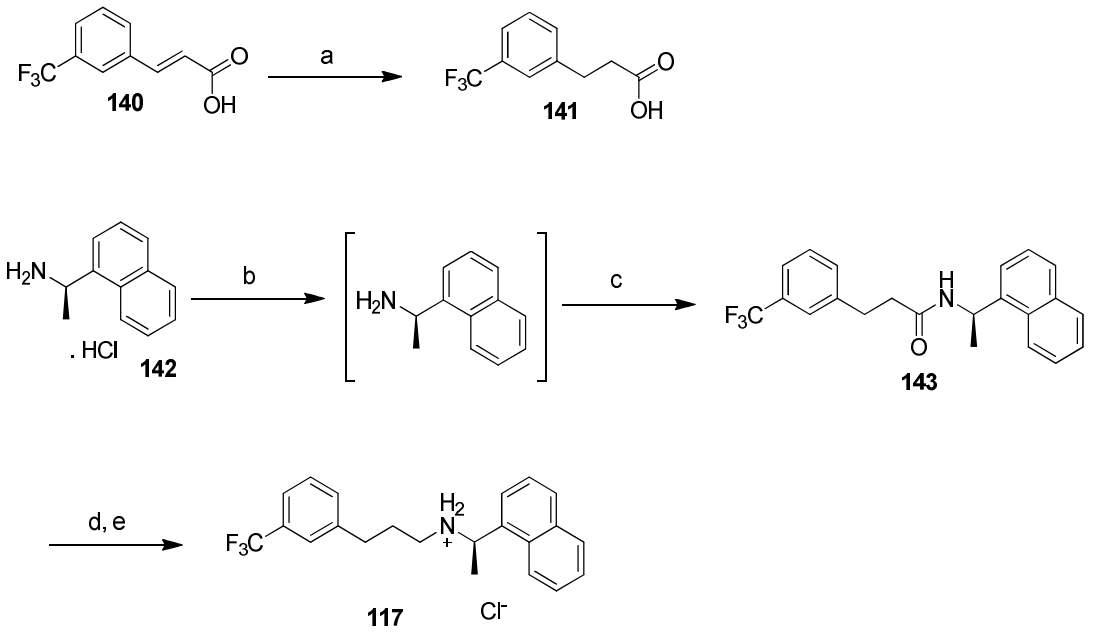

Scheme 3.1 Direct condensation of carboxylic acid **141** with amine **142**. Reagents and conditions: a) $Pd(OH)_2/C$, H_2 (3-4 bar), 40-60 °C, quantitative; b) toluene, NaOH, quantitative; c) **142**, 140-150 °C, 95%, d) $NaBH_4$, BF_3.THF, THF.diglyme, 45-60 °C, 2. toluene, HCl, 95%; e) $MeOH/H_2O$, 95%.

3.7 Results and Discussion.

3.7.1 Retrosynthesis of fluoro Cinacalcet HCl.

The synthetic approach to cinacalcets **123** and **124** was explored as shown in Scheme 3.2 This route contains two important steps which involve a Macmillan asymmetric fluorination followed by a reductive amination.[30] The retrosynthetic analysis indicates that both (2*R*,1'*R*)-**123** and (2*S*,1'*R*)-**124** could be accessed by displacement of the triflates of (*R*)-**149** and (*S*)-**149** with (*R*)-1-(1-napthyl)ethylamine **142**. These triflates could be prepared from alcohols (*R*)-**148** and (*S*)-**148**. The fluoro alcohol (*R*)-**148** and (*S*)-**148** could reasonably be obtained from aldehyde **146** by a Macmillan fluorination protocol, involving reductive amination with (*R*)-1-(1-napthyl)ethylamine **142** and then treatment with sodium borohydride or lithium aluminium hydride in a one pot reaction. The different enantiomers can be achieved by utilizing different enantiomers of the Macmillan organo-catalyst (*R*)- or (*S*)-**150**. Finally, aldehyde **146** can be prepared as previously described in three steps from 3'-(trifluoromethyl)cinnamic acid **140**. The envisaged route towards (2*R*,1'*R*)-**123** is outlined in Scheme 3.3.

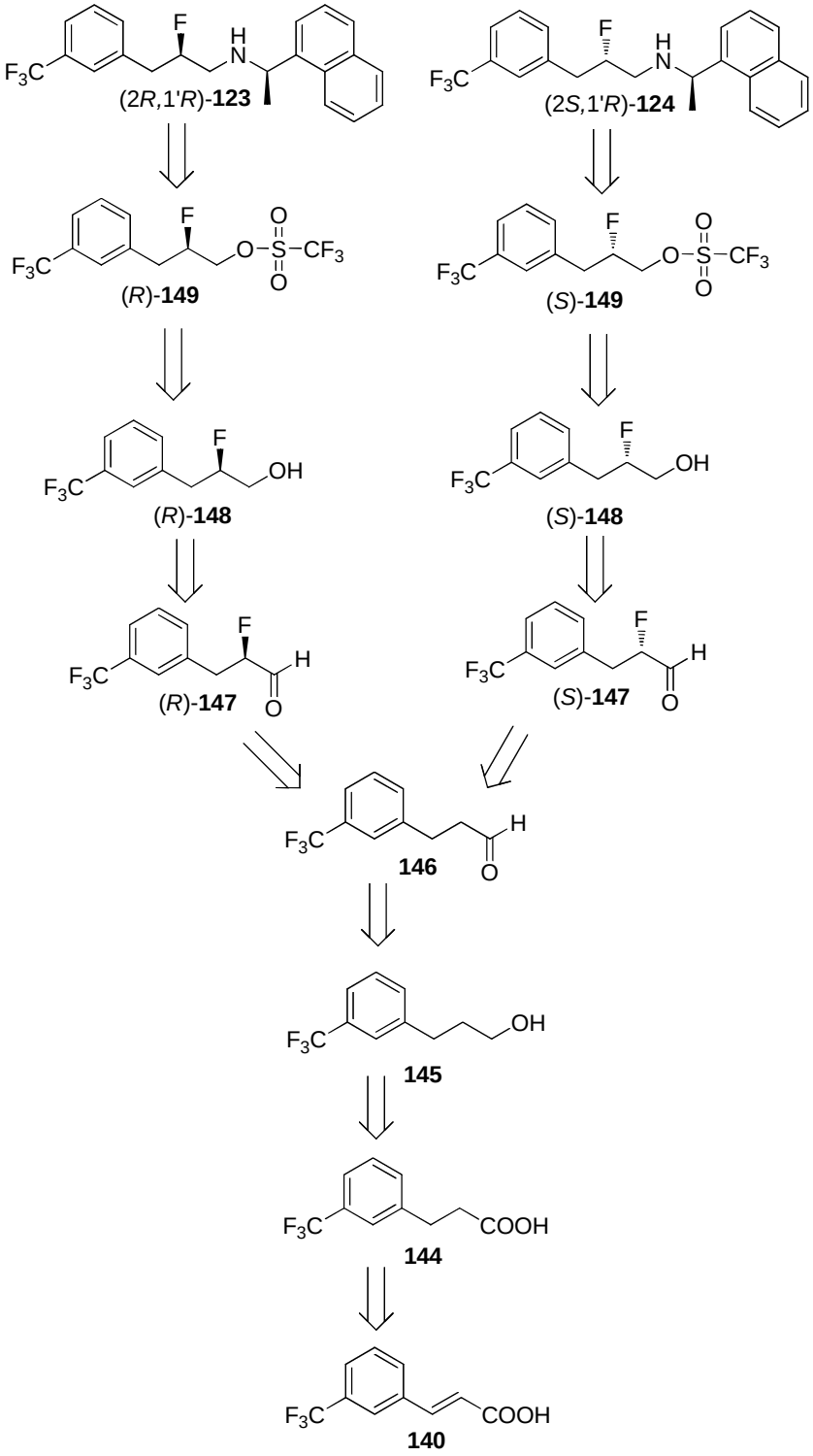

Scheme 3.2 Retrosynthetic routes of the two fluorinated diastereoisomers of Cinacalcet.

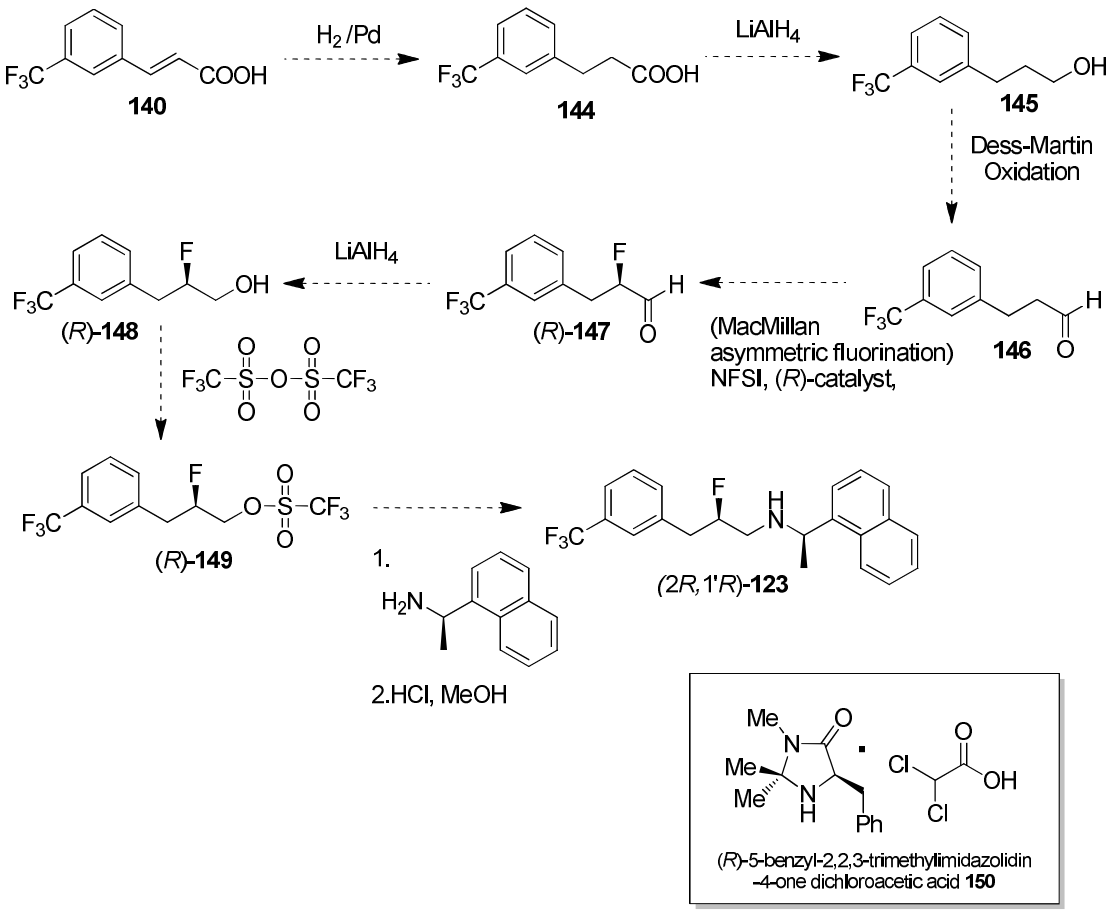

Scheme 3.3 Proposed synthesis of 2F-(2*R*,1'*R*)-**123**.

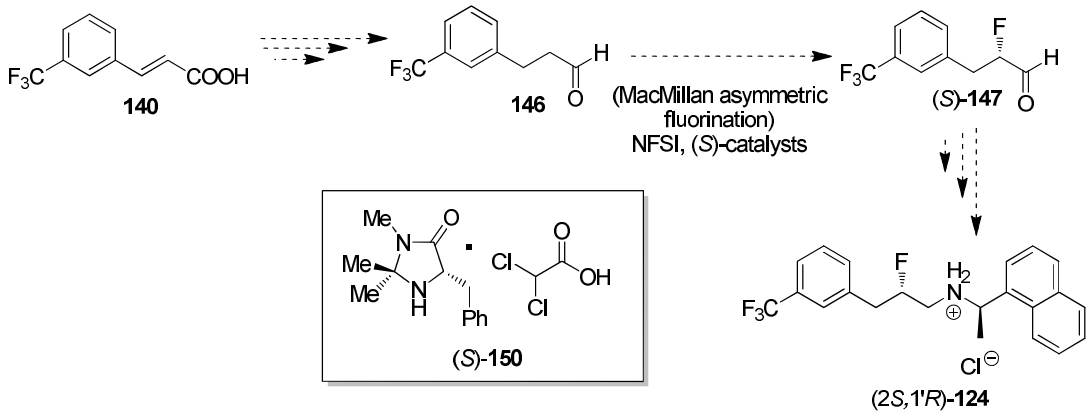

Scheme 3.4 Proposed synthesis of 2F-(2*S*,1'*R*)-**124**.

3.7.2 Synthesis of (2*R*,1'*R*)-2F Cinacalcet 123.

The successful preparation of **146** involved three individual steps starting from hydrogenation of olefin **140**. Further reduction of carboxylic acid group gave alcohol **145.** Oxidation of **145** by a Dess-Martin periodinane reaction generate aldehyde **146**, which was then subjected to a Macmillan asymmetric fluorination.[31] Accordingly, **146** was treated with 2.5 equivalent of NFSI and 10 % mol of (+)-Macmillan catalyst (5*R*)-**150** in THF/isopropanol (9:1) at -15 °C. This solvent combination plays a significant role due to the polar protic nature of isopropanol, which can solvate the fluoride ion. Another factor that influences the formation of **147** is the temperature which was kept around –15 °C to obtain an optimum yield of the mono-fluorinated aldehyde.

The reaction was stirred at low temperature and the production of (*R*)-**147** was monitored by GC-MS until the consumption of the starting material (> 99%). Most of the substrate is converted to the mono-fluorinated aldehyde (*R*)-**147**, however about 5-10 % of the difluoro aldehyde **151** was recovered from the reaction. Measurement of the enantiomeric excess (ee) was carried out by mixing both (*R*)- and (*S*)-**147** followed by chiral phase GC-MS analysis. The chromatogram is shown in **Figure 3.13**. Clearly, the mixture of both (*R*)- and (*S*)-**147** shows two distinctive signals which are consistent with the two enantiomers injected into GC-MS. The enantiomeric excess of (*R*)-**147**, measured by chiral phase GC-MS, was found to be 99%ee (**Figure 3.11**). Subsequently, the reduction of fluoro aldehyde (*R*)-**147** was carried out with lithium aluminium hydride. The difluoro alcohol **152** contaminant could be separated by careful chromatography to afford (*R*)-**148** in a reasonable yield (80%). The proposed mechanism for the formation of (*R*)-**147** is depicted in Scheme 3.5. The same procedure was then applied to the synthesis of (*S*)-**147** in which the Macmillan catalyst (5*S*)-**150** was employed and the reaction was again monitored by the GC-MS. The resultant analysis is shown in **Figure 3.12**. The enantiomeric excess of the resultant (*S*)-**147** was measured also to be 99%ee by chiral phase GC-MS.

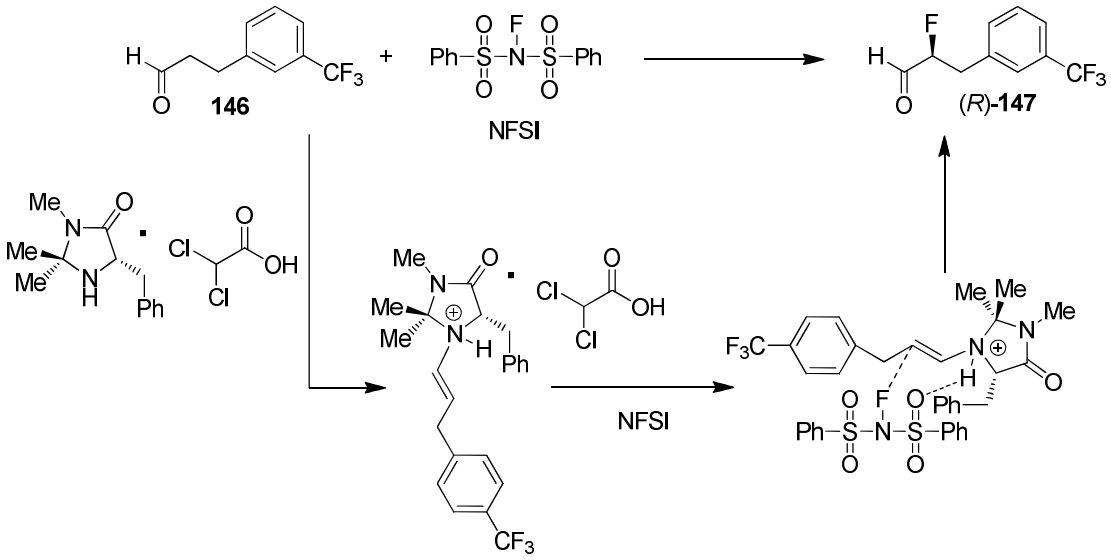

Scheme 3.5 Proposed intermediates for the Macmillan asymmetric fluorination.[40]

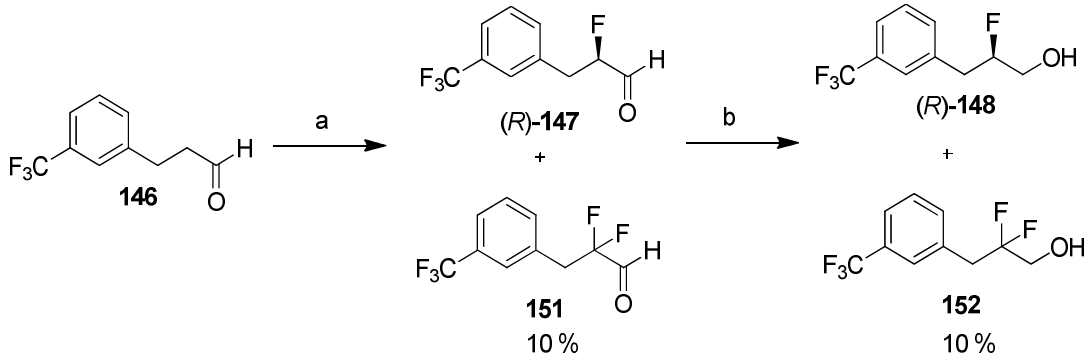

Scheme 3.6. Reagents and conditions: a) NFSI (2.5 equiv), (5*R*)-(+)-2,2,3-trimethyl-5-benzyl-4-imidazolidinone dichloroacetic acid salt (10% mol), THF/Isopropanol (9:1), - 15 °C; b) $LiAlH_4$ (2.0 equiv), - 15 °C, 80%.

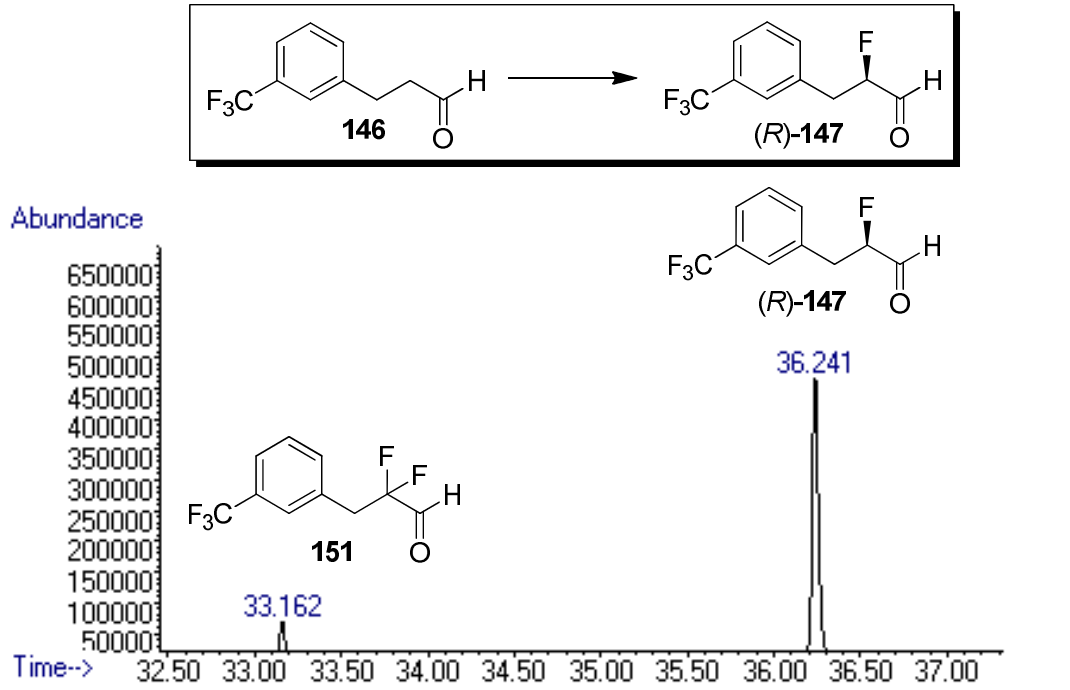

Figure 3.11 Chiral phase GC analysis of the crude (*R*)-**147** (99 % ee) achieved by Betadex^{TM} 120 fused silica capillary column (30 m × 0.25 mm i.d., 0.25 μM film thickness). Oven start at 80 °C held for 20 min, the gradient at 20 °C/min to 150 °C), 250 °C injector temperature, 100:1 split ratio, 1.0 mL/min flow.

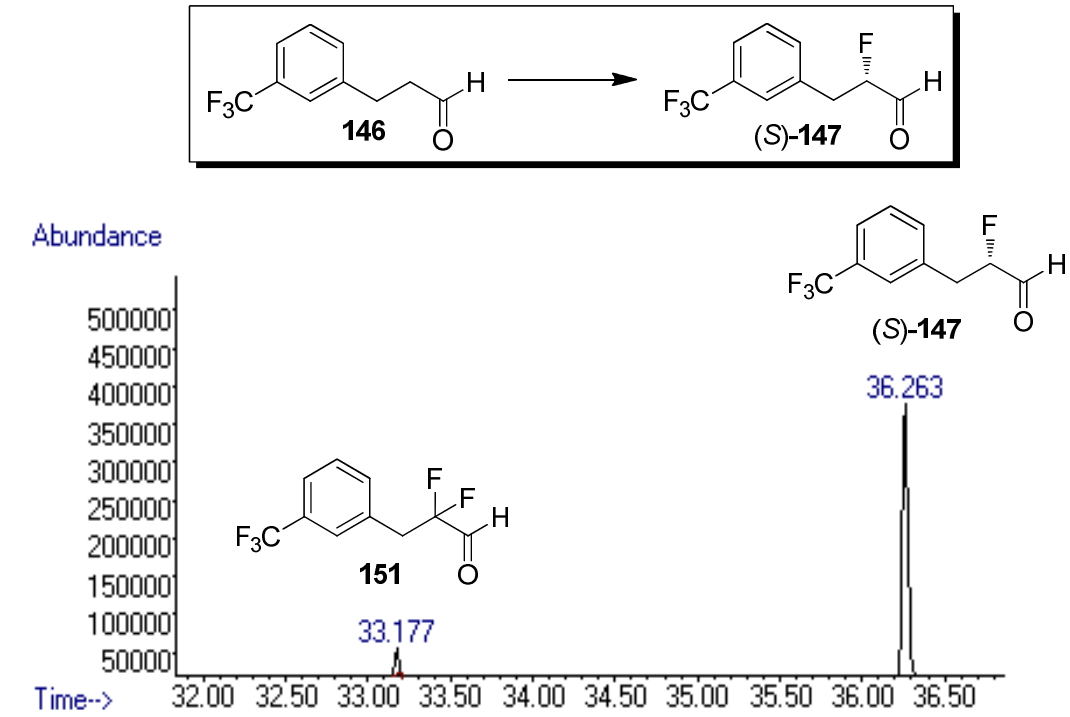

Figure 3.12 Chiral phase GC analysis of the crude (*S*)-**147** (99 % ee) achieved by Betadex^{TM} 120 fused silica capillary column (30 m × 0.25 mm i.d., 0.25 μM film thickness) . Oven start at 80 °C held for 20 min, the gradient at 20 °C/min to 150 °C), 250 °C injector temperature, 100:1 split ratio, 1.0 mL/min flow.

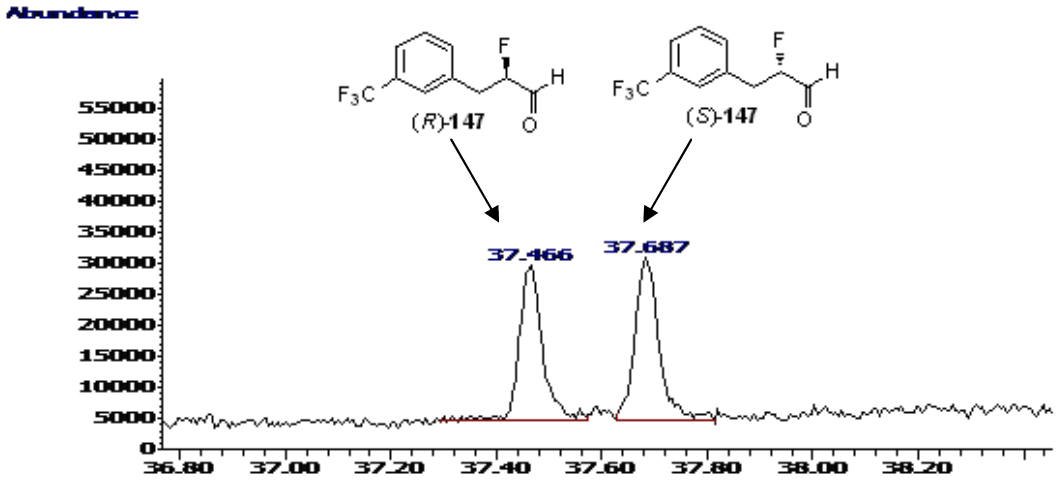

Figure 3.13 Chiral phase GC chromatogram of a mixture of (*R*)- and (*S*)-**147.**

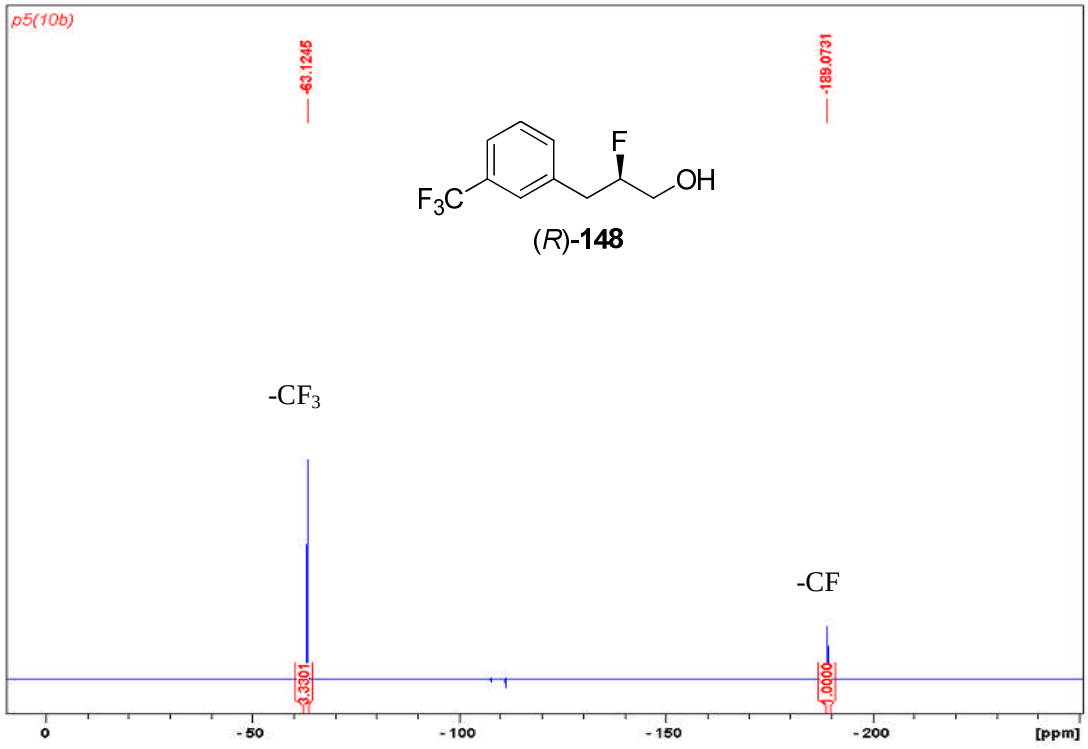

Figure 3.14 ^{19}F NMR spectrum of (*R*)-**148** in $CDCl_3$.

In the ^{19}F-NMR spectrum (**Figure 3.14**) of (*R*)-**148** displayed two distinctive signals, in which the peak at -63.1 ppm corresponds to the -CF_3 group and the peak at -189.0 ppm corresponds to the -CF group of (*R*)-**148**.

With (*R*)-**148** in hand, a conversion to the triflate was required. Accordingly, (*R*)-**148** was transferred through cannula into a reaction mixture containing triethylamine, DMAP and trifluoromethanesulfonic anhydride. The reaction was left stirring under argon for 16 h. Work-up and concentration gave a very good conversion to product as indicated by ^{1}H-NMR. This product was used for the subsequent step without further purification. The final step involved the displacement of the triflate group of (*R*)-**149** with (*R*)-1-(1-napthyl)ethylamine **142** to generate the (2*R*,1'*R*)-**123** as shown in Scheme 3.7. By this method, the first fluorinated Cinacalcet diastereoisomer was obtained in a good yield (95%). The second diastereoisomer was obtained after repeating the same procedure for (*S*)-**147**. In order to study the diastereoisomeric relationship between (2*R*,1'*R*)-**123** and (2*S*,1'*R*)-**124**, the overlay of their ^{1}H- and ^{19}F NMR spectra shown in **Figure 3.15** and **Figure 3.16** respectively. Indeed, the signals for the methylene and methyl groups are shifted slightly when compared to each other, consistent with a set of diastereosiomers.

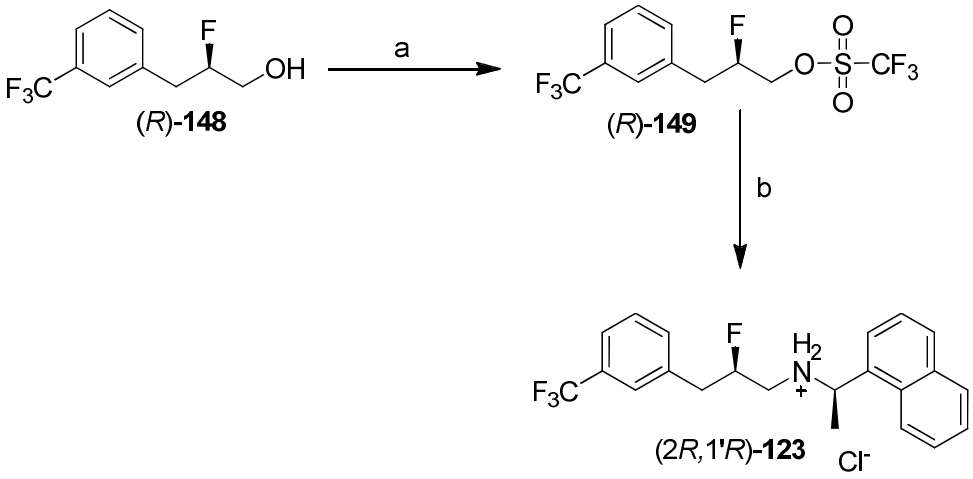

Scheme 3.7 Synthesis of (2*R*,1'*R*)-fluoro Cinacalcet **123**. Reagents and conditions: a) $(CF_3SO_2)_2O$ (1.2 equiv), Et_3N (2 equiv), DMAP (10% mol), 0 °C- RT, 16 h, 76%. b) (*R*)-1-(1-napthyl)ethylamine (1.2 equiv), toluene, 140 °C, 95%.

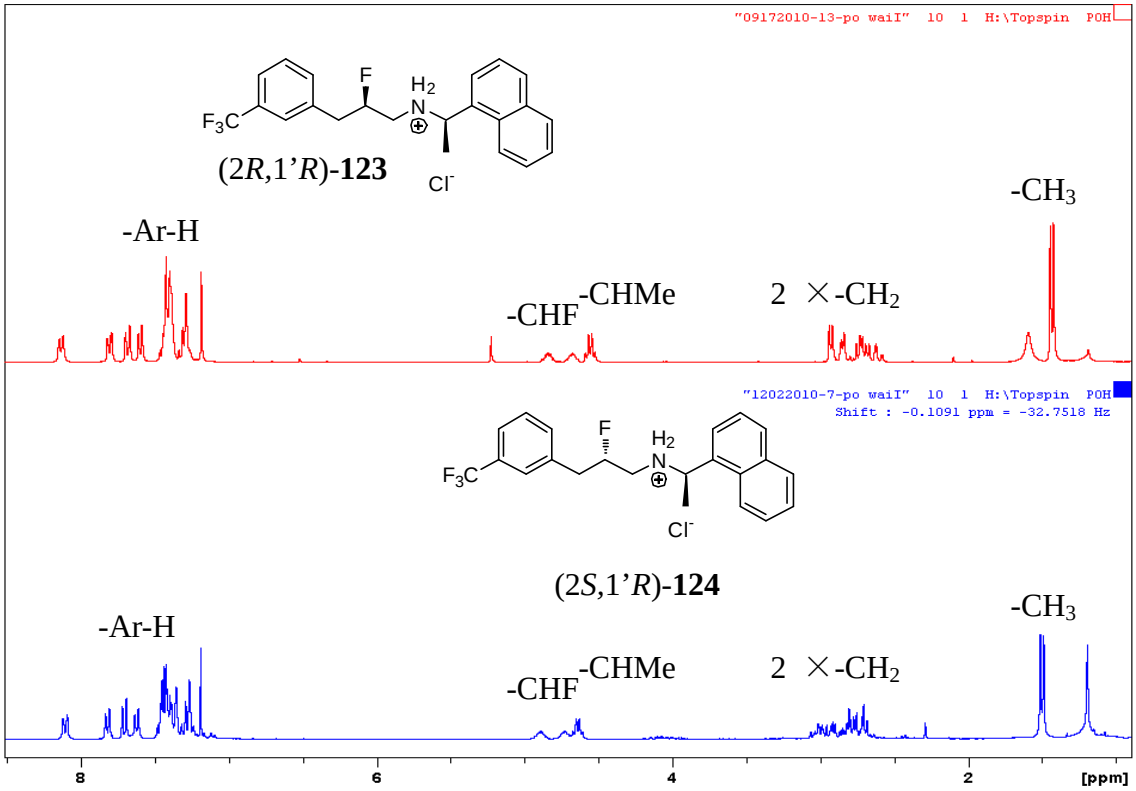

Figure 3.15. A set of diaseteoisomers observed by the overlay of ^{1}H-NMR spectrum of (2*R*,1'*R*)-**123** and (2*S*,1'*R*)-**124**.

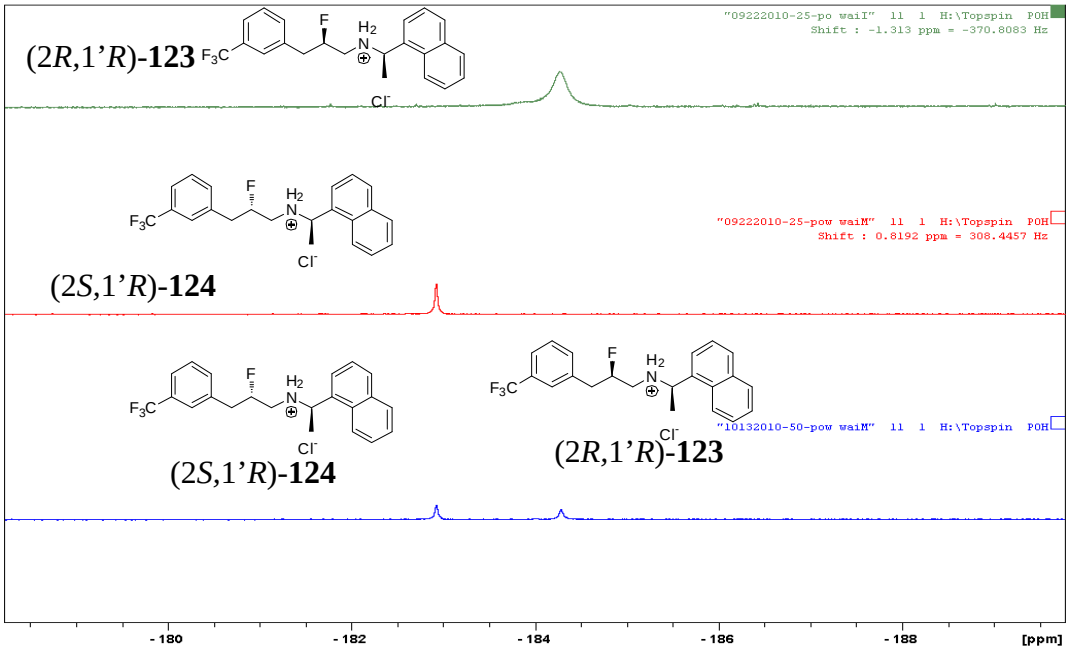

Figure 3.16. Overlay of the ^{19}F-NMR spectra of (2*R*,1'*R*)-**123** and (2*S*,1'*R*)-**124** and a mixture of both diastereoisomers.

The diastereomeric purity was determined by ^{19}F-NMR as shown in **Figure 3.16**. From the ^{19}F NMR analysis, it is very clear that only one set of peaks is observed in a single spectrum. The lower spectrum shows the mixture of diastereoisomers (2*R*,1'*R*)-**123** and (2*S*,1'*R*)-**124**. The ^{19}F NMR analysis indicates a very high diastereomeric ratio for each of these end-products. Subsequently, a suitable crystal of the (2*R*,1'*R*)-**123** was obtained from crystal structure analysis. The X-ray crystal structure confirms the absolute configuration as (2*R*,1'*R*)-**123.** A dihedral angle of 53.0 ° was measured for the C-F---N^+-C angle, consistent with a *gauche* conformation. Examination of the X-ray crystal structure of (2*R*,1'*R*)-**123** reveals that the fluorinated Cinacalcet adopts a similar alkyl chain conformation to the non-fluorinated Cinacalcet[32] as showed in **Figure 3.17**.

(i)

(ii)

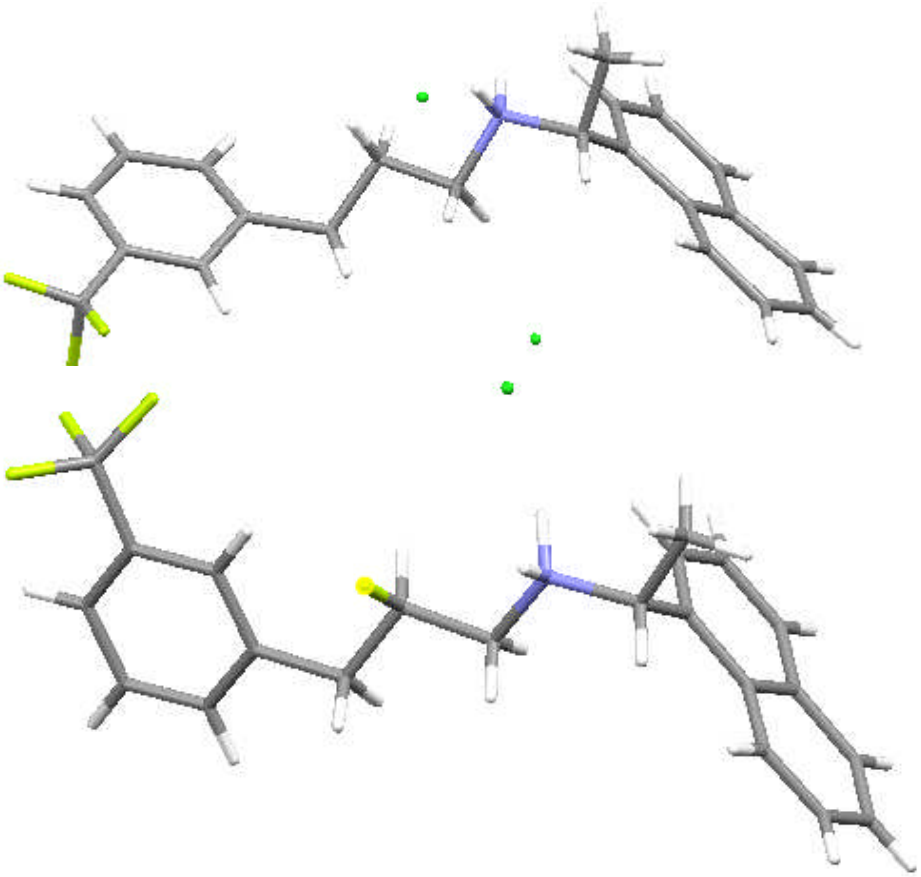

Figure 3.17 Comparison of the X-ray crystal structure of (i) Cinacalcet[32] **117** and (ii) (2*R*,1'*R*)-**123**.

3.7.3 Synthesis of Cinacalcet HCl 117.

A synthesis of Cinacalcet was carried out as a control for biological assessment. The synthesis followed the literature protocol of Wang *et al.*[33] Carboxylic acid **140** was used as the starting material. The synthesis was similar to that previously described, except that the last step involved amination with simultaneous reduction, as summarized in Scheme 3.8. The ^{1}H NMR spectrum of Cinacalcet is shown in **Figure 3.18** and was identical to that reported for Cinacalcet HCl **117**.

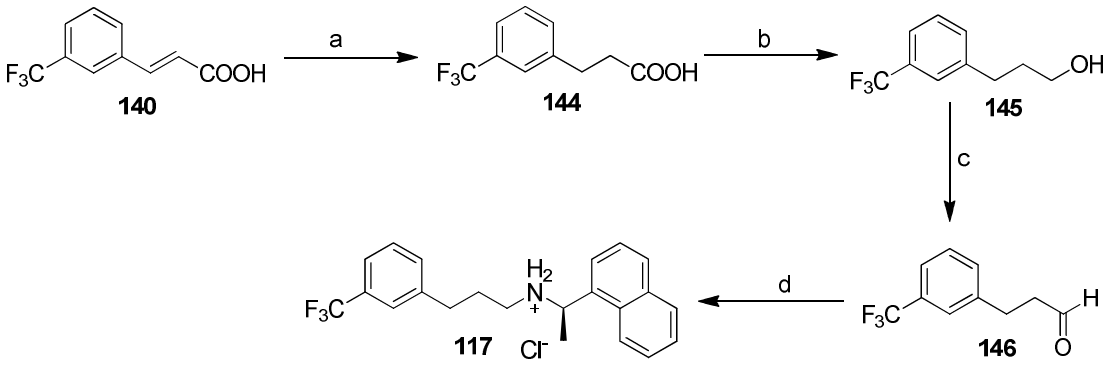

Scheme 3.8. Synthesis of Cinacalcet. Reagents and conditions: a) Pd/C, H_2, EtOH, RT, 2h, 98 %; b) $LiAlH_4$ (1.5 equiv), THF, 75 °C, 1 h, 95%; c) DMP (2 equiv), DCM, RT, 1 h, 80 %; d) 1. (*R*)-1-(1-napthyl)ethylamine, RT, 5 h; 2) $NaBH(OAc)_3$, RT; 3) HCl ether, methanol, 80%.

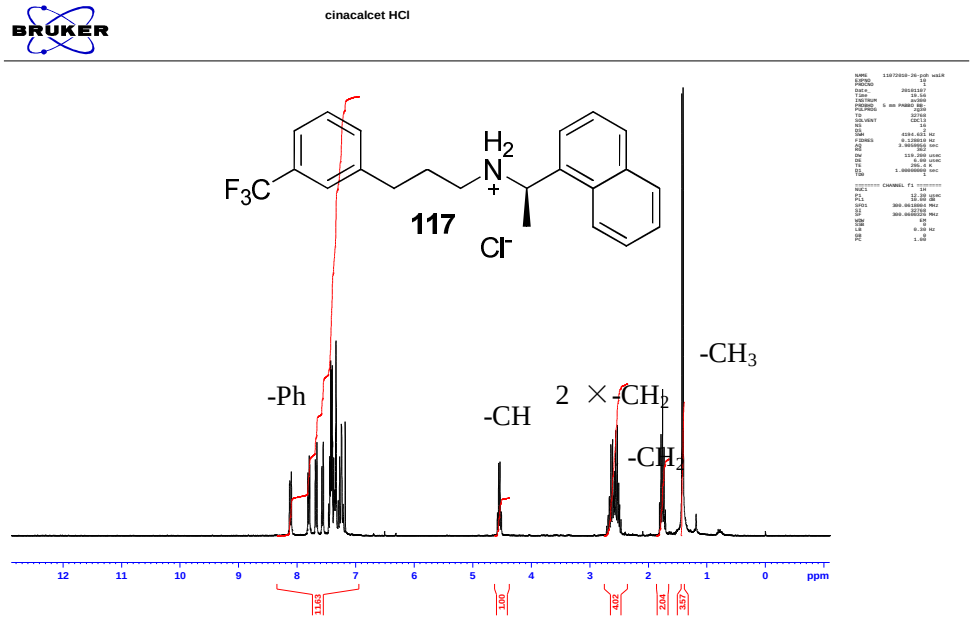

Figure 3.18 ^{1}H NMR spectrum of synthetic Cinacalcet **117** ($CDCl_3$).

3.8 Solution conformation analysis of the fluorinated Cinacalcet diastereosiomers.

The coupling constants from ^{1}H- and ^{19}F- NMR offer information on the solution conformation for the 2F-Cinacalcets. The NMR simulation software DAISY which is part of the processing package in Topspin proved to be useful as it can be employed to simulate the ^{2}J, $^{3}J_{\text{H-H and H-F}}$ coupling constants. The coupling constants allow an assessment of the conformation of these molecules in solution. Accordingly, the approximate coupling constants associated with the conformation of (2*R*,1'*R*)-**123** were entered into the DAISY program and the software refined the values. After several iterations, the software generates a good match between the simulated and experimental spectra. The coupling constants retrieved from this process were found to match the ^{1}H- and ^{19}F- NMR spectra recorded at 500 MHz as shown in **Figure 3.20** and **Figure 3.21**. The same analysis was conducted on (2*S*,1'*R*)-**124** (**Figure 3.22** and **Figure 3.23**), the coupling constants in each analysis are displayed in **Table 3.0** and **3.1**.

Figure 3.19 illustrates the Newman projections for both (2*R*,1'*R*)-**123** and (2*S*,1'*R*)-**124** and the dihedral angles deduced from the DAISY program were consistent with the angle of fluorine to adjacent protons. In **Figure 3.19 (i)**, the $^{3}J_{\text{HF}}$ value of the fluorine *cis* to H^{4} was found to be 17.5 Hz, consistent with a small dihedral angle and the coupling constant of fluorine *anti* to the H^{3} was found to be a large value, 30.8 Hz. Similarly, **Figure 3.19 (ii)** displayed that the the fluorine *cis* to H^{2} $^{3}J_{\text{HF}}$ value was found to be 20.9 Hz, whereas the the *anti* relationship of fluorine to H^{1} was 31.0 Hz.

The same analytical procedure was applied to (2*S*,1'*R*)-**124** and the Newman projection is illustrated in **Figure 3.19 (iii)** and **(iv)**. The data is consistent with the two fluorinated diastereoisomers adopting an extended conformation in solution with

the amine *anti* to the phenyl group (R_2) bearing a trifluoromethyl group. The solution conformation deduced from this experiment is also reinforced by the X-ray crystal structure of the (2*R*,1'*R*)-**123**, which shows an extended conformation in the solid state (**Figure 3.17)**.

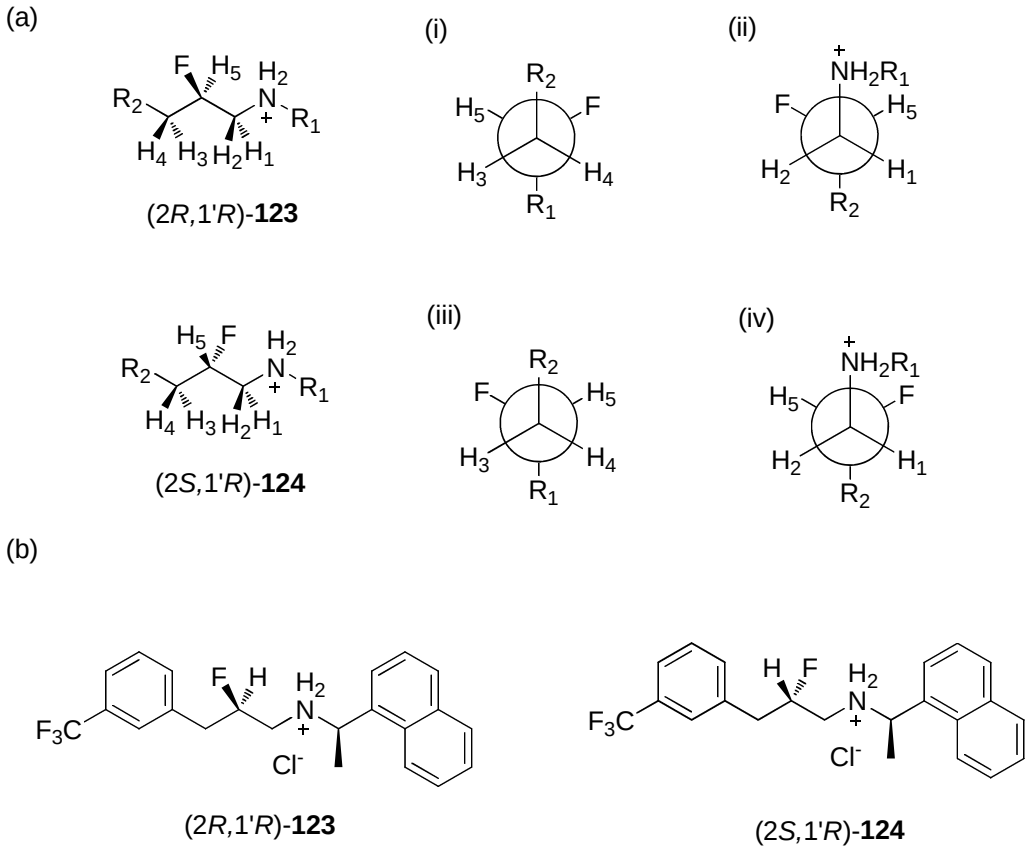

Figure 3.19. (a) Newman projection of the (2*R*,1'*R*)-**123** (2*S*,1'*R*)-**124** deduced from DAISY program. (b) The preferred conformation of (2*R*,1'*R*)-**123** and (2*S*,1'*R*)-**124** in solution phase.

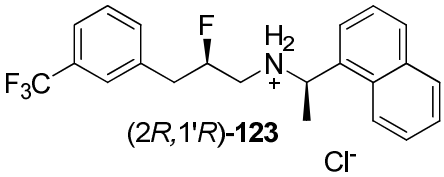

(2*R*,1'*R*)-**123**

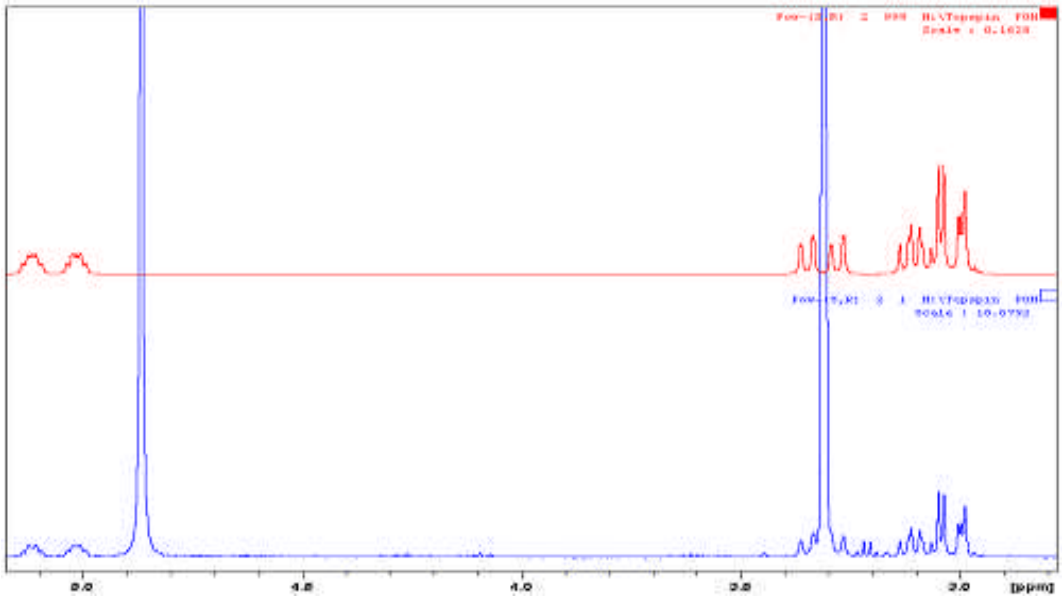

Figure 3.20 The simulated (top spectrum) and experimental (bottom spectrum) ^{1}H NMR spectrum of (2*R*,1'*R*)-**123** at 500 MHz (CD_3OD at 25 °C).

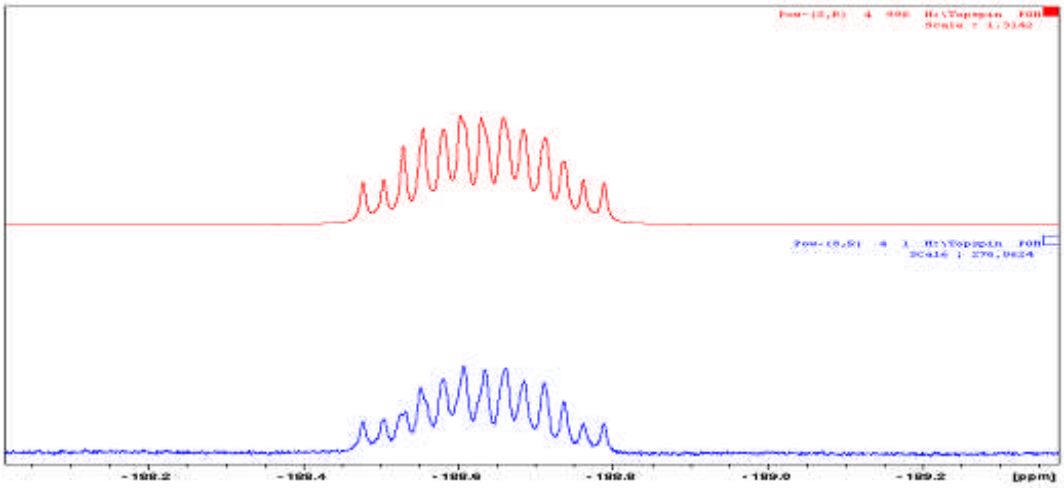

Figure 3.21 The simulated (top spectrum) and experimental (bottom spectrum) ^{19}F NMR spectrum of (2*R*,1'*R*)-**123** at 500 MHz (CD_3OD at 25 °C).

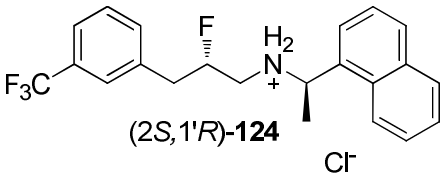

(2*S*,1'*R*)-**124**

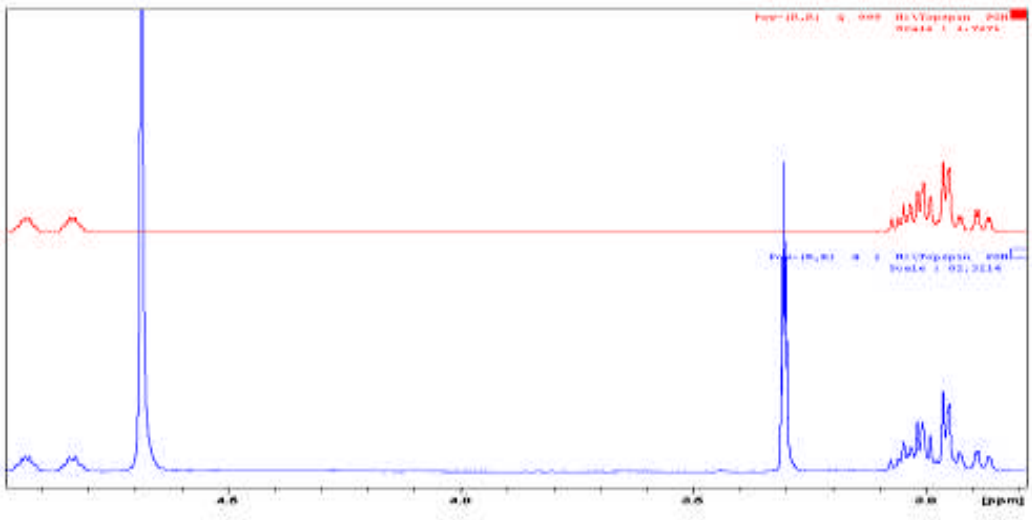

Figure 3.22 The simulated (top spectrum) and experimental (bottom spectrum) ^{1}H NMR spectrum of (2*S*,1'*R*)-**124** at 500 MHz (CD_3OD at 25 °C).

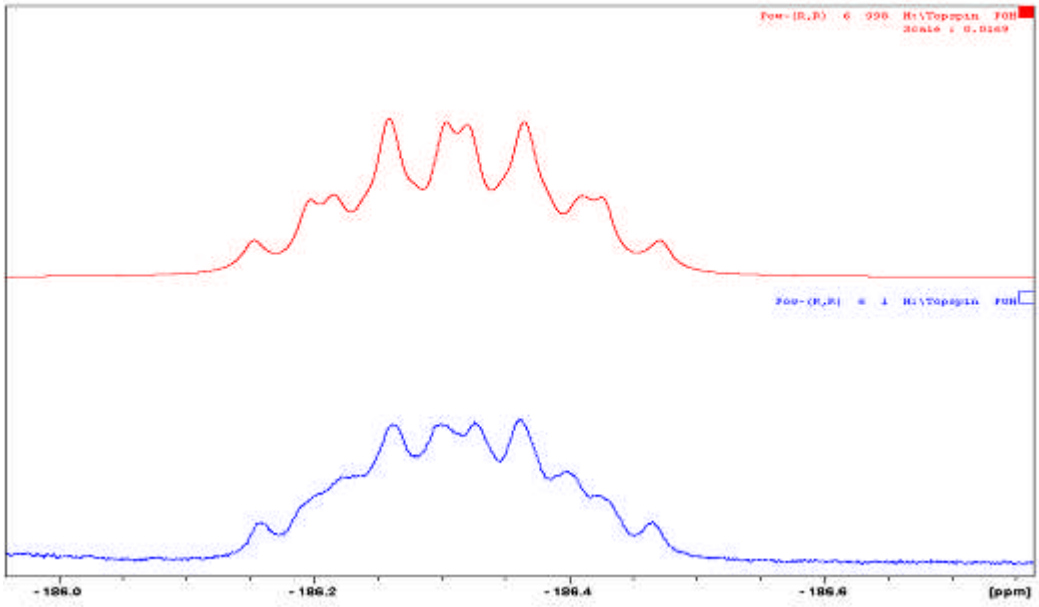

Figure 3.23 The simulated (top spectrum) and experimental (bottom spectrum) ^{19}F NMR spectrum of (2*S*,1'*R*)-**124** at 500 MHz (CD_3OD at 25 °C).

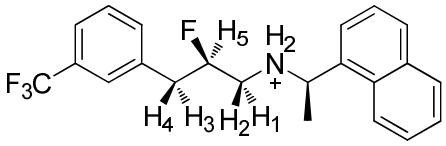

(2*R*,1'*R*)-**123**

	H^1	H^2	H^3	H^4	H^5
F	31.03	20.87	30.77	17.51	-49.85
H^1		-12.60	0	0	3.03
H^2			0	0	6.90
H^3				-14.46	4.20
H^4					8.62

Table 3.0. Coupling constants of (2*R*,1'*R*)-**123** extracted from the simulated NMR spectrum.

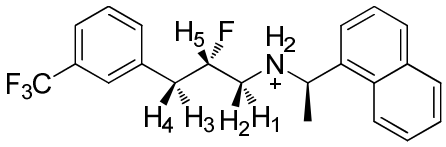

(2*S*,1'*R*)-**124**

	H^1	H^2	H^3	H^4	H^5
F	12.46	34.53	19.49	29.35	-50.52
H^1		-13.73	0	0	9.79
H^2			0	0	1.79
H^3				-15.86	8.24
H^4					3.91

Table 3.1. Coupling constants of (2*S*,1'*R*)-**124** extracted from the simulated NMR spectrum.

3.9 Synthesis of 3''-SF_5-Cinacalcet HCl 137.

As part of our programme exploring Cinacalcet anaogues, we were interested to explore the substituent effect of a Cinacalcet analogue bearing a pentafluorosulfur (-SF_5) group in place of the trifluoromethyl (-CF_3) group. The proposed synthetic route towards this 3'-SF_5-Cinacalcet analogue **137** is outlined in Scheme 3.9.

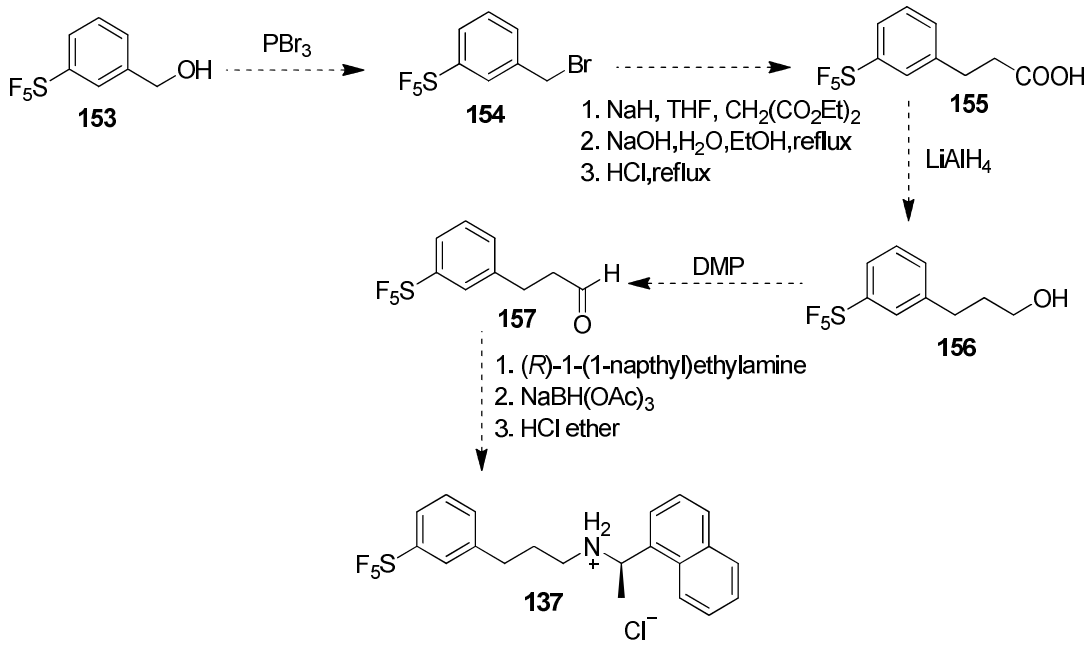

Scheme 3.9 The proposed synthetic route to 3''-SF_5-Cinacalcet HCl **137**.

The synthesis of benzylbromide **154** proved to be straightforward following a published protocol.[34] This involved the treatment of alcohol **153** with PBr_3 in THF at room temperature. After the starting material was consumed, benzyl bromide **154** was purified by chromatography and was recovered in good yield (76%). The next reaction, which involved nucleophilic displacement of the bromide with diethyl malonate and sodium hydride at –78 °C, was followed by ^{1}H-NMR. After all the

starting material was consumed, the crude mixture was treated with NaOH (6 M) in EtOH and the reaction mixture was heated under reflux. The saponification product was then treated with concentrated HCl (4 M) to mediate a decarboxylation of the *in situ* formed malonic acid. Work-up was carried out with sodium hydrogen carbonate and the pH was adjusted to pH=3 to enable the products to be extracted into ethyl acetate. Purification by careful chromatography gave the desired carboxylic acid **155.**

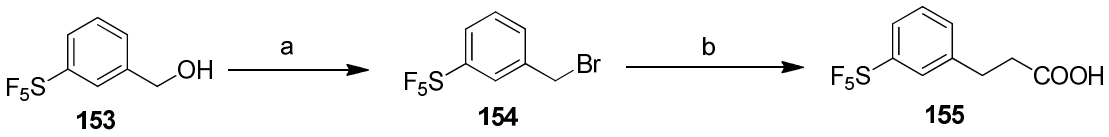

Scheme 3.10. Synthesis of carboxylic **155** from alcohol **153**. Reagents and conditions: a) PBr_3 (1.2 equiv), THF, RT, 3 h, 76%; b) 1. NaH (1.0 equiv), THF, $CH_2(CO_2Et)_2$ (1.0 equiv), - 78 °C- RT, 16 h; 2. NaOH 6M, EtOH, reflux, 16 h; 3. HCl 4 M, reflux 16 h, 50%.

With carboxylic acid **155** in hand, it was treated with lithium aluminium hydride to generate alcohol **156**. As anticipated, the reduction proved to be a straightforward reaction and after work-up, **156** was obtained as a clear oil. This product **156** was used without further purification.

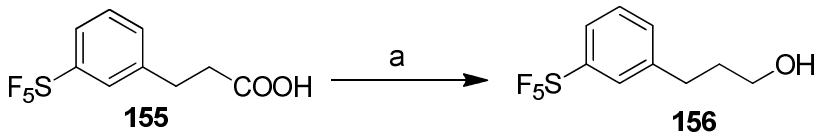

Scheme 3.11 Preparation of alcohol **156**. Reagents and conditions: a) $LiAlH_4$ (1.5 equiv), THF, reflux, 90%.

It was necessary now to oxidize alcohol **156** to an aldehyde. A Dess-Martin oxidation approach was carried out. Column chromatography of the oxidation product afforded **157** in a good yield (90%) and this aldehyde was then treated with (*R*)-1-(1-napthyl)ethylamine **142** in THF for 5 h followed by reductive amination. As expected, **157** was all converted into a single product, as indicated by TLC. Column

chromatography afforded **137** as a free base, which was then dissolved in methanolic HCl in diethyl ether to afford the 3''-SF_5-Cinacalcet HCl salt **137**. The ^{1}H NMR spectrum of **137** is shown in **Figure 3.24**.

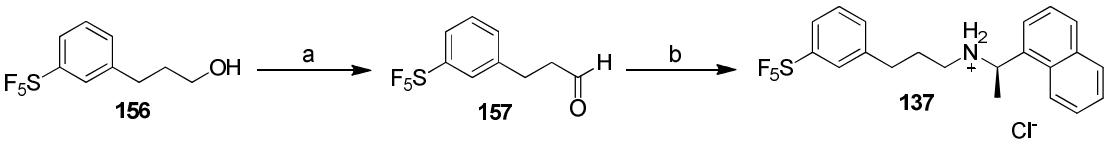

Scheme 3.12 Synthesis of **137** from **157**. Reagents and conditions: a) DMP (1.5 equiv), DCM, RT, 1 h, 90 %; b) 1. (*R*)-1-(1-napthyl)ethylamine (1.2 equiv), THF, RT, 5 h; 2. $NaBH(OAc)_3$, RT; 3) HCl ether, methanol, 90%.

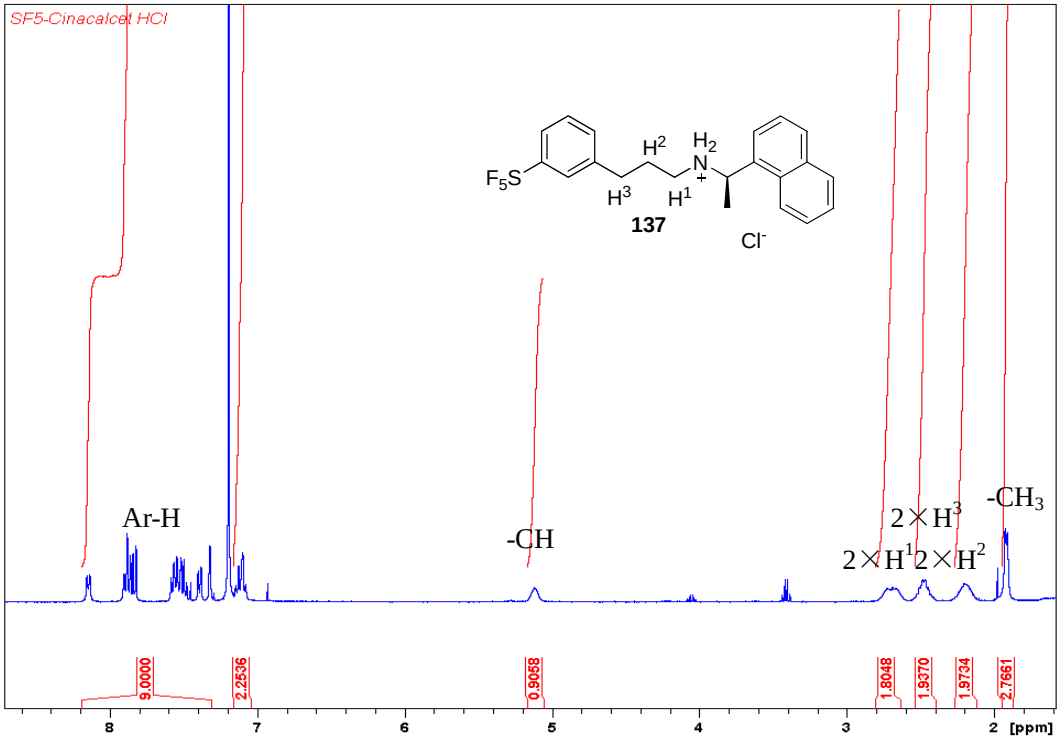

Figure 3.24. The ^{1}H NMR spectrum of **137** in $CDCl_3$.

The ^{1}H-NMR spectrum of **137** has three signals for three sets of methylene protons (2.69 ppm, 2.47 ppm and 2.19 ppm) which corresponded to H^1, H^3 and H^2 respectively. Closer examination of these methyene protons by ^{1}H-^{1}H COSY-NMR (**Figure 3.25**) confirms that H^2 is located between H^1 and H^3. Analysis of the ^{1}H-HMBC spectrum (**Figure 3.26**) indicated that H^3 has a crosspeak with the aromatic carbons at 125.4 ppm which confirms that H^3 is located between H^2 and the phenyl group.

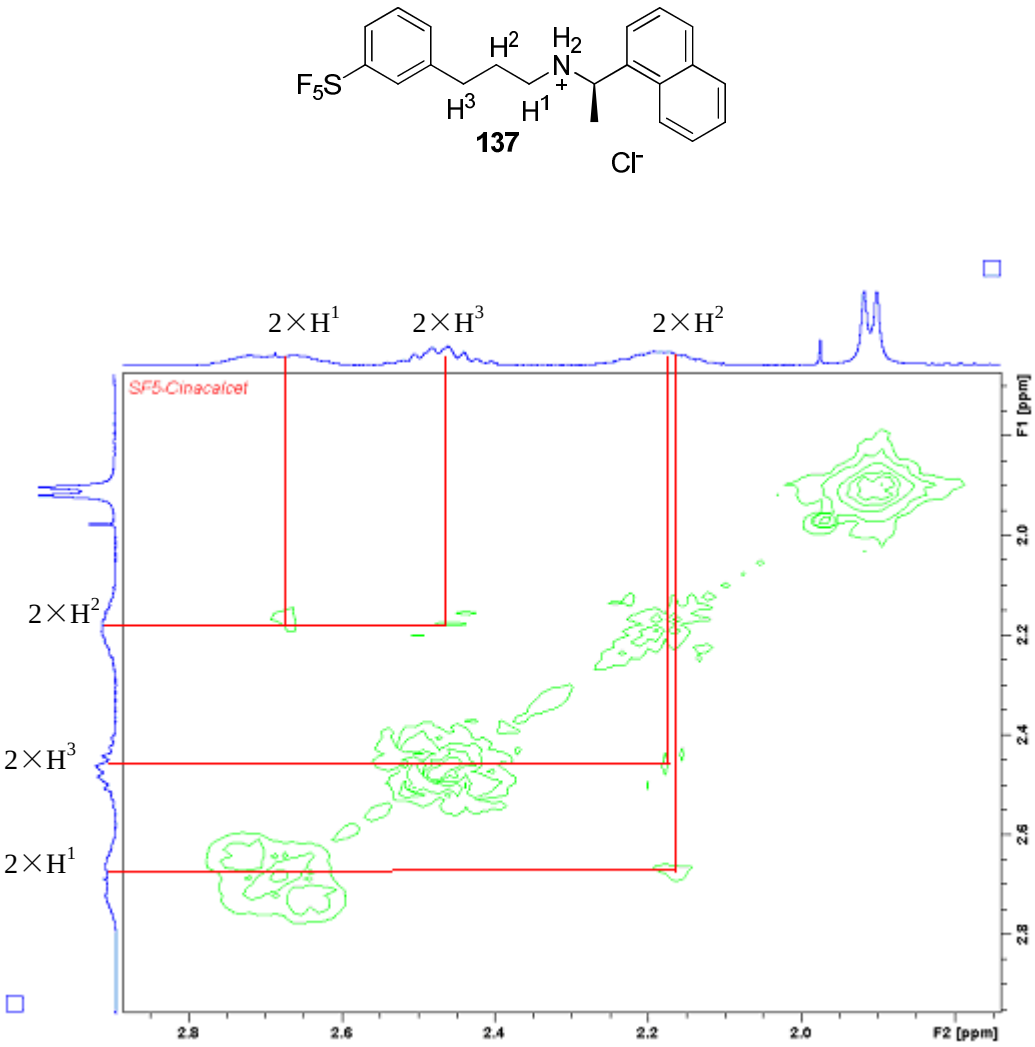

Figure 3.25 The ^{1}H- ^{1}H COSY NMR of 3''-SF_5-**137** in $CDCl_3$.

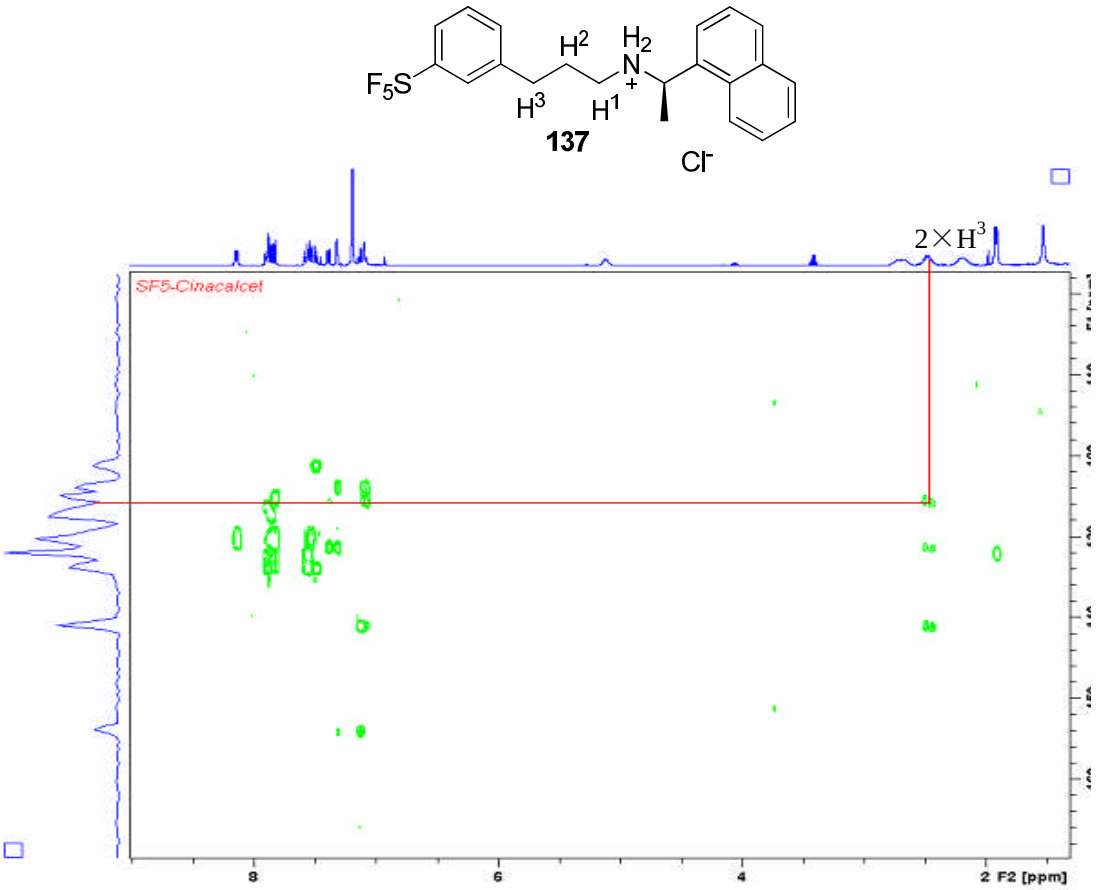

Figure 3.26 ^{1}H-HMBC NMR spectrum of 3''-SF_5-**137** in $CDCl_3$.

The ^{13}C NMR analysis (**Figure 3.27**) of **137** reveals three methylene carbons at 27.3 ppm, 32.6 ppm and 45.4 ppm. Other signals such as that at 21.3 ppm correspond to be the methyl group. The methine carbon is assigned to 53.5 ppm and the aromatic carbons have signals at 121.2 ppm to 141.0 ppm. The 2D-HSQC spectrum (**Figure 3.28**), indicates that H^1 has a crosspeak to the methine carbon at 45.4 ppm. Furthermore, the H^3 and H^2 methylene groups are found to have crosspeaks to carbons at 32.6 and 27.3 respectively, suggesting that the H^2 methylene group is located in between H^1 and H^3, with H^3 assigned to be the aryl carbon, adjacent to that bearing the SF_5 group.

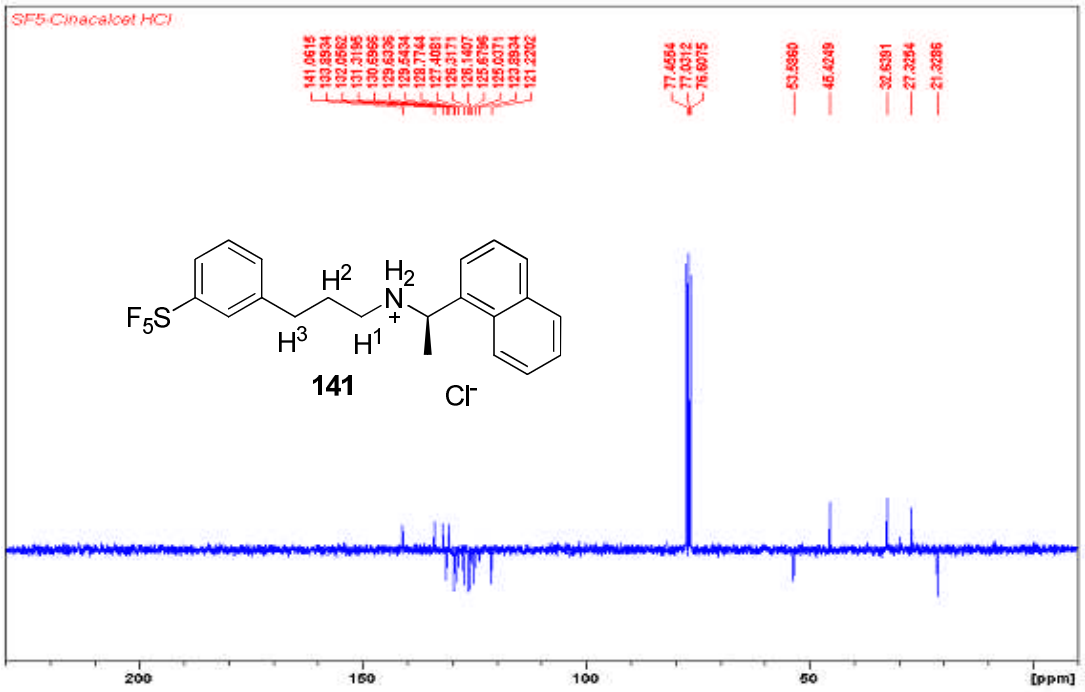

Figure 3.27 The DEPT ^{13}C NMR spectrum of 3''-SF_5-**137** in $CDCl_3$.

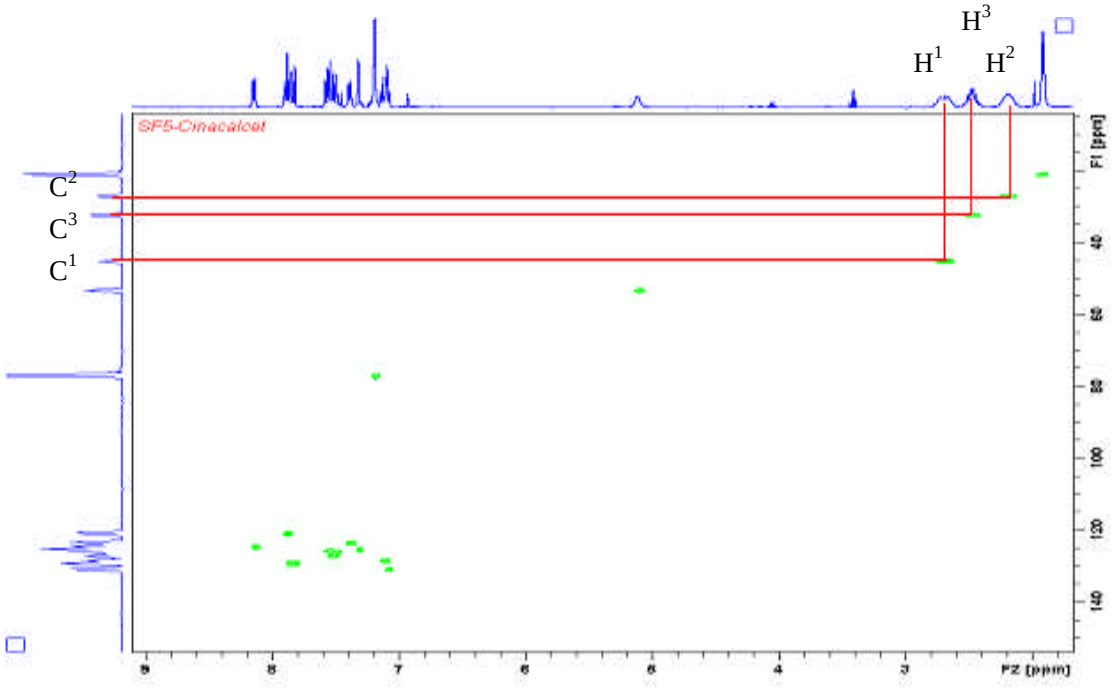

Figure 3.28 The 2D-HSQC NMR spectrum of 3''-SF_5-**137** in $CDCl_3$.

^{19}F NMR spectrum (**Figure 3.29**) of **137** is shown to have two different fluorine populations with signals at 62.1 ppm and 84.8 ppm. Both signals correspond to the fluorines in the SF_5 group. The signal at 62.1 ppm integrated as four and is attributed to all four of the equatorial fluorines coupled to the axial fluorine, to produce a doublet. The signal at 84.8 ppm, which integrated as one is assigned to the axial fluorine, coupled to all four equatorial fluorine and thus the multiplicity is a quintet.

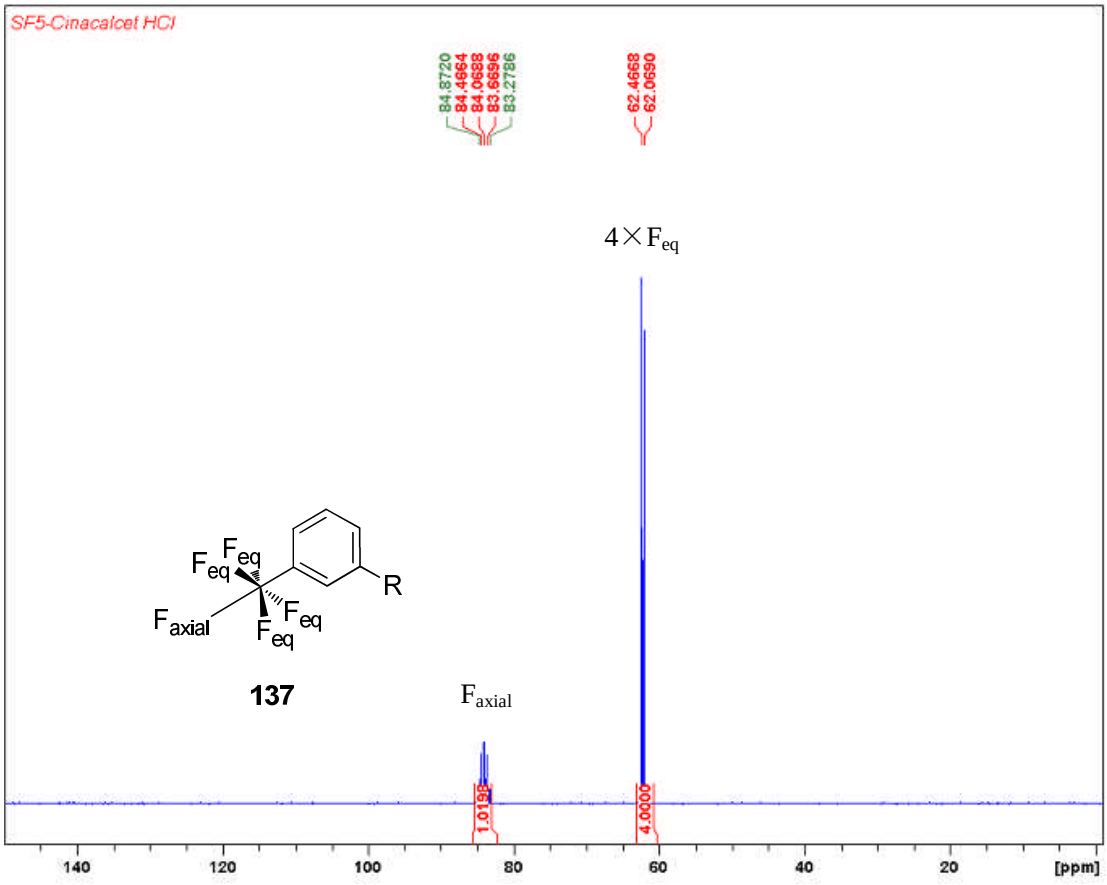

Figure 3.29 The ^{19}F NMR spectrum of 3''-SF_5-**137** showing the axial and equatorial fluorines.

3.10 Biological Result

3.10.1 Biological Assessment of the Fluorinated Cinacalcet Analogues with CaSR.

All the calcimimetics **117**, **123**, **124** and **137** was assessed by using a calcium imaging technique. The free intracellular calcium was visualized by binding to a fluorescent compound, namely Fura-2. Visualization was achieved by exciting the cells at different wavelengths of light, at 340 and 380 nm and the ratio between those two wavelengths is directly correlated with the amount of intracellular calcium. In this experiment, stimulation of the CaR was achieved by using a concentration of 100 nM for all the calcimimetics in a physiological buffer. Each of these calcimimetics was left to stimulate the cells for 2 min and subsequently the cells was left for another 5 min to restore to their normal calcium levels. At the end of each experiment, the calcimimetic was added into the cells as a positive control to ensure that the cells were still responding.[35]

The graph in **Figure 3.30** represents the response for all four calcimimetics fitted into a single plot. On the Y-axis the 340/380 ratio is plotted and on the X-axis the calcimimetics concentration in micromolar is shown. The EC_{50} for each compound is calculated from each individual graph and depicted in **Table 1.3**.

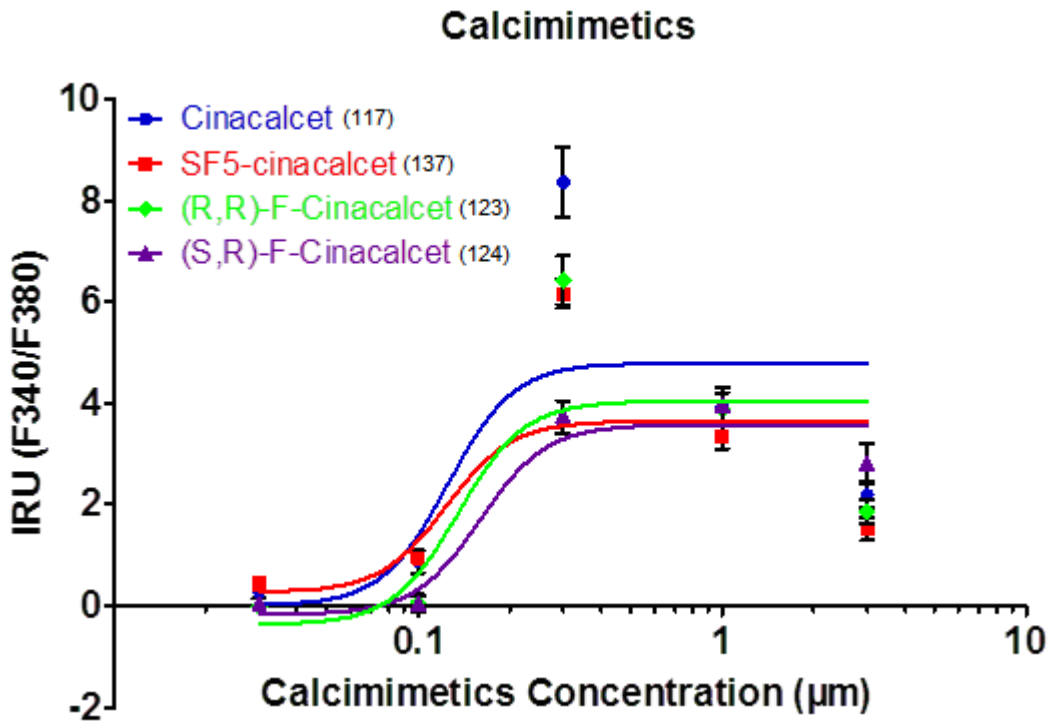

Figure 3.30 Overall dose-response curves represent the all four calcimimetics (**117**,**123**, **124** and **137**) response towards the calcium visualization excited at 340 and 380 nm.

	Cinacalcet HCl **117**	SF_5-Cinacalcet HCl **137**	(2*S*,1'*R*)-2F Cinacalcet HCl **124**	(2*R*,1'*R*)-2F Cinacalcet HCl **123**
Maximum response	4.791	3.646	3.573	4.040
EC_{50} (µm)	0.13	0.12	0.16	0.14

Table 3.2 The maximum response and EC_{50} of the fluorinated and non-fluorinated calcimimetics obtained from individual experiments.

The SF_5-3''-Cinacalcet **137** give a comparable EC_{50} similar to that of Cinacalcet HCl **117**, around 0.13 to 0.12 µm. This means that the substitution of CF_3- by SF_5- group in Cinacalcet **117** can be interchangeable, and this does not lead to decrease in bioactivity as shown in **Table 3.2**. In contrast, the fluorinated calcimimetics (*2R*,1'*R*)-2F **123** and (*2S*,1'*R*)-2F **124** were found to have lower activity compared to

the control **117**. This could be explained in terms of our understanding of fluorine chemistry. Firstly, it is well-understood that the introduction of fluorine will decrease the pKa of a β- amine group. In this case, the reduced of activities in both fluorinated calcimimetics **123** and **124** is perhaps understandable. Secondly, the syntheses of these diastereoisomers will either reinforce or destabilize the active binding conformation of Cinacalcet **117**.[14,17] Therefore, the difference in terms of EC_{50} suggests a preferred binding conformation in solution. From the Newman projection **in Figure 3.31**, this conformation for **117** was deduced to be conformation **A**. Only conformation **A** can be accessed by both diastereoisomers **123** and **124**, with the alkyl group extended to each other. Conformation **C** would be less able to achieve this conformation due to the loss in C-F and C-N^+ stabilization.

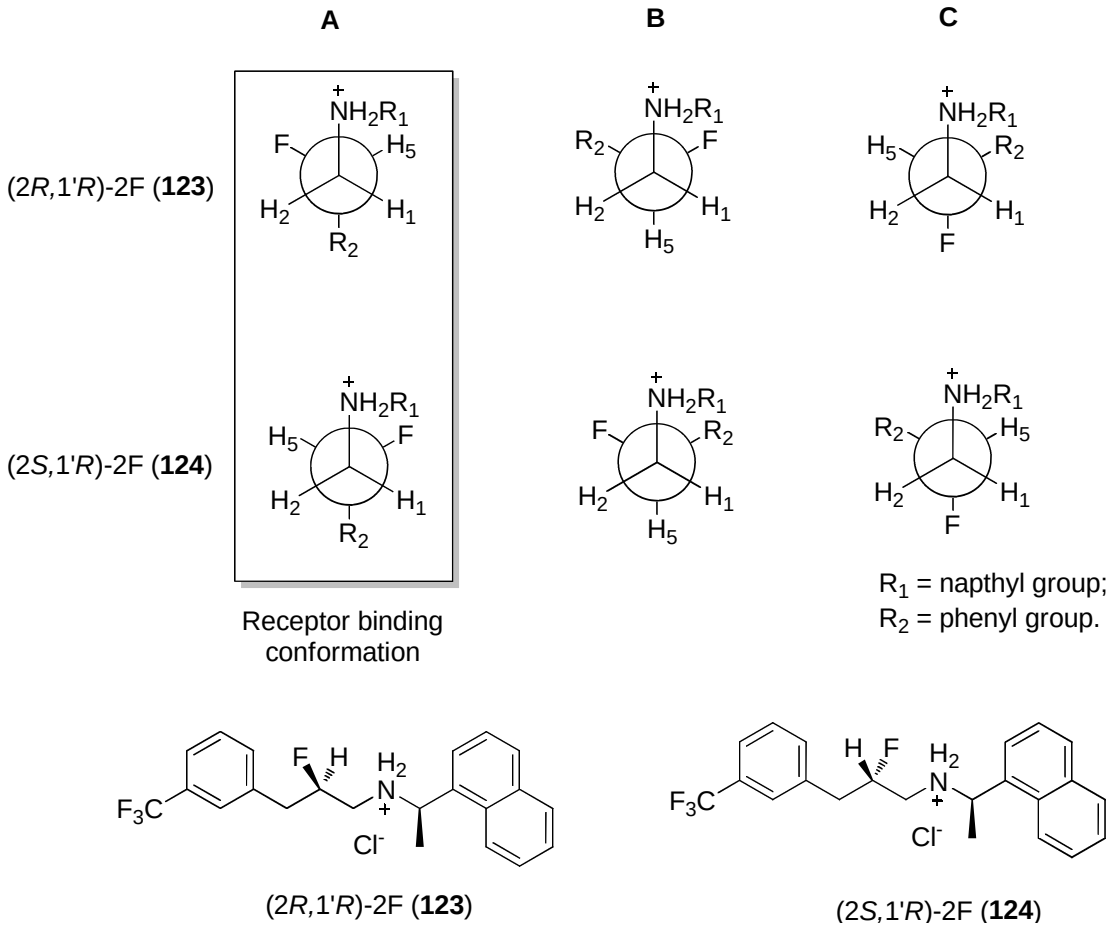

Figure 3.31 The preferred binding conformation of Cinacalcet HCl **117** in solution as represented by Newman projection.

3.11 Conclusion:

Diastereoisomers **123** and **124** of 2F-Cinacalcet HCl have been successfully prepared from 3'-(trifluoromethyl)cinnamic acid in high diastereoisomeric ratio. The 3''-SF_5-derivative **137** of Cinacalcet is also prepared in conjunction with this study. 3''-SF_5-**137** was accessed from pentafluorosulfanyl benzyl alcohol. The major solution conformation of the 2F-Cinacalcet diastereoisomers have been assessed based on the coupling constants that were simulated by DAISY Topspin. They were found to be in an extended conformation for both of the 2F-Cinacalcet HCl diastereoisomers **123** and **124**. In the biological assessment, the relative potency of the non-fluorinated Cinacalcet **117** and fluorinated Cinacalcets diastereoisomers **123** and **124** were studied in CaR. It was found that both fluorinated Cinacalcets **123** and **124** were active at a nano-molar scale, however were slight lower potency compared to the non-fluorinated Cinacalcet **117**. It is therefore concluded that in solution, Cinacalcet binds in an extended conformation with the alkyl chain *anti*-periplanar to each other. This was also supported by a suitable crystal of (2*R*,1'*R*)-2F Cinacalcet **123** and $^3J_{HF}$ values generated for both **123** and **124** by Topspin Daisy analysis, in which both fluorinated diastereoisomers adopt an extended alkyl chain in solution. The biological assessment of 3''-SF-Cinacalcet **137** revealed that the SF_5- substituent has a similar potency to Cinacalcet **117**. The result of this study proves that both substituents can be interchangeable and that the SF_5 group can be used as a bioisosterase for CF_3 in medicinal chemistry.

References:

[1] J. S. Linberg, B. Culleton, G. Wong, M. F. Borah, R. V. Clark, W. B. Shapiro, S. D. Roger, F. E. Husserl, P. S. Klassen, M. D. Guo, M. B. Albiem and J. W. Coburn, *J. Am. Soc. Nephrol*., 2005, **16**, 800-807.

[2] E. M. Brown, *Physiol. Rev*., 1991, **71**, 371-411.

[3] E. M. Brown, G. Gamba, D. Riccardi, M. Lombardi, R. Butters, O. Kifor, A. Sun, M. A. Hediger, J. Lytton and S. C. Hebert, *Nature*, 1993, **366**, 575-580.

[4] E. M. Brown and R. J. Macleod, *Physiol. Rev*., 2001, **81**, 239-297.

[5] J. P. Pin, T. Galyez and L. Prézeau, *Pharmacol. Ther*., 2003, **98**, 325-354.

[6] J. Hu, G. Reyes-Cruz, K. A. Jacobson, A. M. Spigel, *J. Biol. Chem.*, 2002, **277**, 46622-46631.

[7] K. Matsuo and N. Iriel, *Arch Biochem. Biophys*, 2008, **473**, 210-209.

[8] J. G. Hoenderop, B. Nilius and R. J. Blinders, *Physiol. Rev*., 2005, **85**, 373-422.

[9] E. M. Brown, *Biochem. Pharmacol*., 2010, **80**, 297-307.

[10] E. M. Brown, M. Pollak, C. E. Seidman, J. G. Seidman, Y. H. W. Chou, D. Riccardi and S. C. Hebert, *N. Engl. J. Med*., 1995, **333**, 234-240.

[11] D. L. Kendler, J. D. Adachi, R. G. Josse and D. O. Slosman, *Osteoporos. Int*., 2009, **20**, 1101-1106.

[12] M. Pi and L. D. Quarles, *J. Bone Miner. Res*., 2004, **19**, 862-869.

[13] O. Fromigue, E. Hay, A. Babara, C. Petrel, E. Traiffort, M. Ruat and P. J. Marie, *J. Cell Mol. Med*., 2009, **13**, 2189-2199.

[14] E. Bonnelye, A. Chadabel, F. Saltel and P. Jurdic, *Bone*, 2008, **42**, 129-138.

[15] D. T. Ward, D. Maldonado-Pérez, L. Hollins and D. Riccardi, *J. Am. Soc. Nephrol*., 2005, **16**, 1236-1244.

[16] J. Shin, F. Shen and J. R. Huguenard, *J. Neuro-physiol.*, 2005, **93**, 2634-2643.

[17] H. T. Kurata, W. W. Cheng, C. Arrabit, P. A. Slesinger and C. G. Nicholas, *J. Gen. Physiol*., 2007, **130**, 145-155.

[18] E. F. Nemeth, W. H. Heaton, M. Miller, J. Fox, M. F. Balandrin, B. C. Van Wagenen, M. Colton, W. Karbon, J. Scherrer, E. Shatzen, G. Rishton, S. Scully, M. Qi, R. Harris, D. Lacey and D. Martin, *J. Pharmacol. Exp. Ther*., 2004, **308**, 627-635.

[19] A. Kessler, H. Faure, C. Petrel, M. Ruat, P. Dauban and R. H. Dodd, *Bioorg. Med. Chem. Lett.*, 2004, **14**, 3345-3349.

[20] E. F. Nemeth, E. G. Delmar, W. L. Healton, M. A. Miller, L. D. Lambert, R. L. Conklin, M. Gowen, J. G. Gleason, P. K. Bhatnagar and J. Fox, *J. Pharmacol. Exp. Ther.*, 2001, **299**, 321-331.

[21] C. Petrel, A. Kessler, P. Dauban, R. H. Dodd, D. Rognan and M. Ruat, *J. Biol. Chem.*, 2004, **279**, 18990-18997.

[22] B. J. Arey, R. Seethala, Z. Ma, A. Fura, J. Morin, J. Swartz, V. Vyas, W. Yang, J. K. Dickson Jr. and J. H. Feyen, *Endocrinology*, 2005, **146**, 2015-2022.

[23] J. Hu, J. Jiang, S. Costanzi, C. Thomas, W. Yang, J. H. Feyen, K. A. Jacobson and A. M. Spiegel, *J. Biol. Chem*., 2006, **281**, 21558-21565.

[24] S. U. Miedlich, L. Gama, K. Seuwan, R. M. Wolf and G. E. Breitwieser, *J. Biol. Chem*., 2004, **279**, 7254-7263.

[25] G. S. LaI and K. E. Minnich. U. S. Patent 6, 870, 068, 2002.

[26] L. J. Saethre, N. Berrah, J. D. Bozek, K. J. Borve, T. X. Carroll, E. Kukk, G. L. Gard, R. Winter and T. D. Thomas, *J. Am. Chem. Soc.*, 2001, **123,** 10729.

[27] P. Wipf, T. Mo, S. J. Geib, D. Caridha, G. S. Dow, L. Gerena, N. Roncal and E. E. Milner, *Org. Biomol. Chem.*, 2009, **7**, 4163-4165.

[28] J. T. Welch and D. S. Lim, *Bioorg. Med. Chem*., 2007, **15**, 6159-6666.

[29] M. C. Hansen and S. L. Buchwald, *Tetrahedron Lett*., 1999, **40**, 2033-2034.

[30] O. R. Thiel, C. Bernard, W. Tormos, A. Brewin, S. Hirotani, K. Murakami, K. Sato, R. D. Larsen, M. J. Martinelli and P. J. Reider, *Tetrahedron Lett*., 2008, **49**, 13-15.

[31] T. D. Beeson and D. W. C. Macmillan, *J. Am. Chem. Soc*., 2005, **127**, 8826-8828.

[32] D. E. Brawn, D. M. Többens, V. Kahlenberg, J. Ludescher and U. J. Grisser, *Crystal Growth & Design*, 2008, **8**, 4109-4119.

[33] X. Wang, Y. Chen, R. Crockett, J. Briones, T. Yan, C. Orihuela, B. Zhi and J. Ng, *Tetrahedron Lett.*, 2004, **45**, 8355-8358.

[34] J. M. Kim, M. A. Bogdan and P. S. Mariano, *J. Am. Chem. Soc*., 1993, **23**, 10591-10595.

[35] S. J. Mclarnon, D. Holden, D. T. Ward, M. N. Jones, A. C. Elliott, D. Riccardi, 2002, *Biochem. Biophys. Res. Comm*., **297**, 71-77.

Chapter 5. Experimental Section

5.1 General methods

5.1.1 Reagents, solvents and reaction conditions.

All reagents used in synthesis reactions were obtained from commercial supplies as synthetic grade reagents and were used without further purification. Dry tetrahydrofuran, dichloromethane, toluene and diethylether were obtained from the Solvent Purification System MB SPS-800. Isopropyl alcohol was distilled from CaH before used. All moisture sensitive reactions were carried out under a positive pressure of nitrogen in standard vacuum lines. All glassware was flame dried or oven-dried at 140 ° C. Reaction temperatures of 0 °C were obtained using ice or water bath. Reactions of -15 °C to –78 °C were obtained by using an isopropyl alcohol bath together with cooling apparatus LP Technology RP-100-CD. Reactions requiring heating were achieved on a heating block with a thermostatted thermometer. Organic extracts were dried over $MgSO_4$. RT refers to ambient temperature.

5.1.2 Chromatography and mass spectroscopy.

Column chromatography was performed using Apollo Scientific Ltd. silica gel 60 (43-63 micron). Thin layer chromatography (TLC) was performed using Macherey-Nagel Polygram Sil G/UV254 plastic and aluminium plates. Visualization was achieved by inspection under UV light (255 nm) or by use of potassium permanganate stain or molybdenum-based stain. High resolution and low resolution mass spectra were recorded using a Micromass LCT-TOF mass spectrometer using ES ionization in + ve and – ve mode, sometimes the CI was used if inadequate.

5.1.3 Nuclear magnetic resonance spectroscopy (NMR)

NMR spectra were recorded on either Bruker AV-300 (^{1}H at 300.06 MHz, ^{13}C at 75.45 MHz), ^{19}F at 282.34 MHz), or Bruker AV-300 (^{1}H at 300.13 MHz, ^{13}C at 75.48 MHz) or Bruker AV-500 (^{1}H at 499.90 MHz, ^{19}F at 470.33 MHz). Samples were prepared either in deuterated chlorofrom, deuterated methanol or deuterium oxide. Chemical shifts δ are reported in parts per millions (ppm) and quoted relative to internal standard Me_4Si for ^{1}H and ^{13}C and external standard $CFCl_3$ for ^{19}F. Coupling constants (*J*) are given in Hertz (Hz) and the splitting patterns described as: singlet-s, doublet-d, triplet-t, multiplet-m, doublet of doublets-dd or a broad doublet-brd. Spectroscopic data were assigned based on the combination of one- and two-dimensional experiments (COSY, HSQC and HMBC).

5.1.4 Gas chromatography

GC-MS analysis was carried out using an Agilent 6890 gas chromatograph coupled to a 5973 N mass spectrometer detector in EI mode. The carrier gas was helium and injection was achieved on a 7683 series injector. GC-MS chiral phase analysis was carried out with a supelco Betadex^{TM} 120 fused silica capillary column (30 m $\times$ 0.25 mm i.d., 0.25 μM film thickness). Conditions used for chiral phase GC-MS analysis: 80 °C held for 20 min, then a gradient at 20 °C/min to 150 °C), 250 °C injector temperature , 100:1 split ratio, 1.0 mL/min flow.

5.1.5 Other analysis

IR experiments were recorded by the Nicolet Avatar 360 FT-IR by preparing the sample in nujol method. Optical rotations determination was performed using a Perkin Elmer Model 341 polarimeter, $[\alpha]_D$ values are determined at 589 nm and given in 10^{-1} deg.cm^2.g^{-1}. Single X-ray diffraction analyses was carried out by Prof. A.M.Z. Slawin on Robotic Diffractometer consisting of Mo sealed tube X-Ray system. The pKa analysis was measured using a Hamilton pH electrode and the pH changes was recorded by Fisher brand Hydrus 300 pH meter. The pH electrode was calibrated at pH 4 and pH 7 standard buffer solution.

5.1.6 Glutamate receptor assay.

Assessment of 3F-NMDA activity at recombinant NMDARs.

Biological evaluation of the 3F-NMDA stereoisomers was performed at the Cellular Neurophysiology and Pharmacology Centre for Integrative Physiology, at the University of Edinburgh. The agonist activities of NMDA **2** and the 3F-NMDA stereoisomers , D-**3**, D-**4** and L-**4**, were assessed using two-electrode voltage-clamp (TEVC) recordings from *Xenopus laevis* oocytes that had been inject with cRNA coding for GluN1 and either GluN2A or GluN2B NMDAR subunits. 24 – 72 hours following injection TEVC recordings were made at room temperature (18-21ºC) from oocytes that were placed in a solution that contained (in mM): NaCl 115, KCl 2.5, HEPES 10, $BaCl_2$ 1.8, EDTA 0.01; pH 7.3 with NaOH. Current and voltage electrodes were made from thin-walled borosilicate glass and when filled with 0.3 M KCl possessed resistances of between 1 and 2 MΩ. Oocytes were voltage-clamped at –40 mV. Application of solutions was controlled manually and data were filtered at 10 Hz and digitized at 100 Hz. Two separate assessments of agonist potency were made: (i) currents evoked by applying the same concentration of NMDA **2**, D-**3**, D-**4**

and L-**4** to the same oocyte were measured in order to determine the relative potencies of the 3F-NMDA stereoisomers compared to that of NMDA **2** itself. (ii) for D-**3** we determined the concentration required to produce a half-maximal response (EC_{50}) by constructing concentration-response curves using a range of concentrations (3 – 300 μM) so that its EC_{50} value could be compared to that of NMDA **2** at both GluN2A - and GluN2B-containing NMDARs.

5.2 Protocols

Diethyl (2*S*, 3*S*)-3-acetoxy-2-bromosuccinate 85 [1]

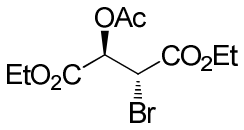

85

Diethyl (2*S*, 3*S*)-3-acetoxy-2-bromosuccinate **85** was synthesized as described previously.[1] 33% HBr/AcOH (40 ml) was added to a stirred solution of diethyl (-)-D-tartrate (25 g) **86**. The mixture was stirred for 4 h at RT. The mixture was then extracted into Et_2O (3 ×50 mL), washed with H_2O and then dried with $MgSO_4$. Concentration under reduced pressure gave diethyl (2*S*, 3*S*)-3-acetoxy-2-bromosuccinate **85** as a pale yellow oil.

[α]$_D$ -6.45 (c 1.0, $CHCl_3$), lit., [1] **[α]$_D$** - 6.60 (c 2.5, $CHCl_3$); **δ_H** (300 MHz, CD_3OD) 5.60 (1H, d, *J* = 5.4 Hz, CHBr), 5.03 (1H, d, *J* = 5.4 Hz, CHOAc), 4.20 (4H, m, OCH_2), 2.14 (3H, s, CH_3) and 1.28 (t, *J* = 7.2 Hz, 2 × CH_3); **δ_c** (300 MHz, CD_3OD) 74.8 (CHOAc), 63.5 (OCH_2), 62.7 (s, OCH_2), 45.4 (CHBr), 14.5 (CH_3) and 14.2 (CH_3). These data were in accordance with the literature.[1]

Diethyl (2*S*, 3*S*)-2-bromo-3-hydroxysuccinate 86.[1]

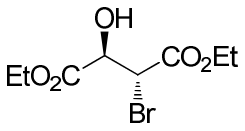

86

Diethyl (2*S*, 3*S*)-3-acetoxy-2-bromosuccinate **85** (25 g) was added to a solution of 33% HBr/AcOH (40 mL) in EtOH (120 mL). The solution was refluxed for 4 h and then the residue was concentrated under reduced pressure. The residue was purified by distillation to give diethyl (2*S*, 3*S*)-2-bromo-3-hydroxysuccinate **86** as a pale yellow oil (24.3 g, 97%).

$[\alpha]_D$ -28.4 (c 1.2, $CHCl_3$), lit.,[1] $[\alpha]_D$ – 29.9 (c 4.51, $CHCl_3$); δ_H (300 MHz, CD_3OD) 4.60 (1H, 2 × d, *J* = 5.0 Hz, CHOH), 4.57 (1H, d, *J* = 5.0 Hz, CHBr), 4.30-4.19 (4H, m, OCH_2) and 1.33 (t, *J* = 7.2 Hz, 2 × CH_3); δ_c (300 MHz, CD_3OD) 171.5 (C=O), 168.5 (C=O), 74.0 (COH), 63.6 (OCH_2), 62.6 (OCH_2), 48.9 (CHBr), 14.5 (CH_3) and 14.3 (CH_3); ***m/z*** (ESI^+) $C_8H_{13}O_5{}^{79}BrNa$, 290.89; $C_8H_{13}O_5{}^{81}BrNa$, 292.89. These data were in accordance with the literature.[1]

Diethyl (2*S*, 3*S*)-epoxysuccinate 87.[1]

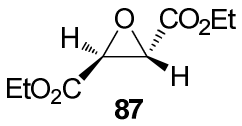

87

Diethyl (2*S*, 3*S*)-epoxysuccinate **87** was synthesized as previously described.[1] A solution of diethyl (2*S*, 3*S*)-2-bromo-3-hydroxysuccinate **86** (24.3 g, 0.09 mol) in EtOH (50 mL) was added dropwise to sodium ethoxide (7.14 mL,0.10 mol) in EtOH (4 mL) and stirred for 2 h at RT. The reaction mixture was then neutralised with glacial acetic acid and extracted into diethyl ether (3 × 30 mL). The combined extracts were washed with saturated brine, dried over $MgSO_4$ and then concentration under reduced pressure to give the title product **87** as a pale yellow oil (9.7 g, 57%).

[α]$_D$ -78.4 (c 1.2, $CHCl_3$), lit.,[1] **[α]$_D$** – 88.5 (c 4.51, $CHCl_3$); **δ_H** (300 MHz, $CDCl_3$) 4.19-4.16 (4H, m, OCH_2), 3.59 (s, 2H, 2 × CH) and 1.24 (t, *J* = 7.2 Hz, 2 × CH_3); **δ_c** (300 MHz, $CDCl_3$) 177.6 (C=O), 62.1 (2 × OCH_2), 51.8 (2 ×CH), 13.7 (2 × CH_3); ***m/z*** (ESI^+) 211.01 [$M+Na^+$] (95). These data were in accordance with the literature.[1]

(+) *Erythro* (2*R*,3*S*)-diethyl 2-(benzyl(methyl)amino)- 3- hydroxyl succinate 88.

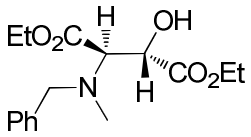

88

A solution of *N*-benzylmethylamine (7.74 mL, 0.06 mol) was added dropwise to a suspension of diethyl (2*S*, 3*S*)-epoxysuccinate **87** (9.7 g, 0.05 mol) in EtOH (60 mL). The solution was stirred at reflux for 15 hours, and then the excess of benzylmethylamine and EtOH were removed under reduced pressure. The residue was purified over silica column (hexane:EtOAc; 6:4) to give the title compound **88** (9.5 g, 85%) as a colourless oil.

$[\alpha]_D$ +50.4 (c 0.9, $CHCl_3$); **δ_H** (400 MHz, $CDCl_3$) 7.24-7.22 (5H, m, Ar-H), 4.51 (1H, d, *J* = 6.6 Hz, CHOH), 4.16 (4H, m, OCH_2), 3.75 (1H, d, *J* = 6.6 Hz, CHN), 3.74 (2H, s, CH_2), 2.32 (3H, s, NCH_3) and 1.23 (6H, t, *J* = 6.6 Hz, 2 $\times CH_3$); δ_c (400 MHz, $CDCl_3$) 172.8 (C=O), 169.9 (C=O), 139.0 (Ar C), 128.7 (Ar CH), 128.7 (Ar CH), 127.1 (Ar CH), 127.1 (Ar CH), 70.9 (CHOH), 68.6 (CHN), 61.8 (OCH_2), 60.8 (OCH_2), 59.4 (CH_2), 39.0 (NCH_3) and 14.4 (2 x CH_3); **IR** (nujol mull) **υ_{max}/cm^{-1}** 3472, 1732, 1572, 1458, 1372, 1258, 1151, 1098 and 1025; ***m/z*** (ESI^+) 332 [$M+Na^+$] (100). HRMS (ES^+): Found 332.1474. Calcd. For $[M+Na]^+$ $C_{16}H_{23}NO_5Na$, 332.1474.

(+) *Erythro* diethyl (2*S*, 3*S*)-fluoro benzylmethylamine succinate 89.

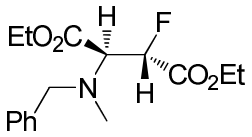

89

Deoxo-fluor^{TM} (6.44 mL, 0.03 mol) was added to a solution of (2*R*,3*S*)-diethyl 2-(benzyl(methyl)amino)-3-hydroxysuccinate **88** (4 g, 0.01 mol) in dry DCM (20 mL) at RT. The solution was stirred for 15 h at RT, and then the excess of Deoxo-fluor^{TM} was quenched with saturated $NaHCO_3$ solution to pH 7. The reaction mixture was extracted into EtOAc (3 x 50 mL) and the combined organic layers were dried with $MgSO_4$. The residue was purified over silica gel (hexane:EtOAc; 9:1) to give the title compound **89** (2.8 g, 90%) as a pale yellow oil.

$[\alpha]_D$ +4.64 (c 0.2, $CHCl_3$); **δ_H** (300 MHz, $CDCl_3$) 7.24-7.19 (5H, m, Ar-H), 5.20 (1H, dd, *J* = 5.8, 48.2 Hz, CHF), 4.21-4.19 (4H, m, CH_2), 3.88 (1H, dd, *J* =5.9, 21.6 Hz, CHN), 3.71 (2H, s, CH_2), 2.29 (3H, s, NCH_3) and 1.28 (6H, t, *J* =6.2 Hz, 2 x CH_3); **δ_c** (300 MHz, $CDCl_3$) 172.8 (C=O), 169.9 (C=O), 137.4 (Ar C), 127.7 (Ar CH), 127.7 (Ar CH), 126.3 (Ar CH), 126.3 (Ar CH), 88.4 (d, *J* = 189.0 Hz, CHF), 65.7 (d, *J* = 24.0, CHN), 60.7 (OCH_2), 60.1 (OCH_2), 58.7 (CH_2), 37.9 (NCH_3), 13.3 (CH_3) and 13.0 (CH_3); **δ_F** {^{1}H} (300 MHz, $CDCl_3$): -195.85 (1F, s, C(3)HF); **IR** (nujol mull) **υ_{max}/cm^{-1}** 1744, 1691, 1576, 1458, 1376, 1270, 1141, 1094, 1037, 796 and 739; ***m/z*** (ESI^+) 334 [M+Na^+] (100). HRMS (ES^+): Found 334.1431. Calcd. For [M+Na]$^+$ $C_{16}H_{22}NO_4FNa$, 334.1434.

(-) *Erythro* diethyl (*2S, 3S*)-fluoro amino alcohol methylamine 90.

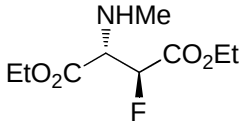

90

10 % Palladium on activated carbon (30 mg) was added to a solution of diethyl (2*S*, 3*S*)-fluoro benzylmethylamine succinate **89** (3.2 g, 0.01 mol) in EtOH (20 mL) and stirred at RT in the presence of hydrogen gas. The reaction mixture was followed by TLC until completion. The catalyst was filtered through celite and the reaction mixture was extracted into EtOAc (3 x 50 mL) and the combined organic layers were dried with $MgSO_4$. Concentration of the reaction crude gave to the title compound **90** (2.1 g, 97%) as a colourless oil.

$[\alpha]_D$ -3.79 (c 0.1, $CHCl_3$); **δ_H** (400 MHz, $CDCl_3$) 5.13 (1H, dd, *J* = 2.8, 47.7 Hz, CHF), 4.22-4.14 (4H, m, CH_2), 3.65 (1H, dd, *J* = 2.9, 24.2 Hz, CHN), 2.43 (3H, s, NCH_3) and 1.28 (6H, m, 2 x CH_3); **δ_c** (400 MHz, $CDCl_3$) 169.4 (C=O), 167.3 (C=O), 90.6 (d, *J* = 191.6, CHF), 64.6 (d, *J* = 21.1, CHN), 61.7 (OCH_2), 61.7 (OCH_2), 35.4 (NCH_3) and 14.0 (2 x CH_3); **δ_F** {^{1}H} (400MHz, $CDCl_3$): -199.63 (1F, s, C(3)HF); **IR** (nujol mull) **υ_{max}/cm^{-1}** 1744, 1691, 1576, 1458, 1376, 1270, 1141, 1094, 1037, 796 and 739; ***m/z*** (ESI$^+$) 222 [M+H$^+$] (40). HRMS (ES$^+$): Found 222.1137. Calcd. For [M+H]$^+$ $C_9H_{17}NO_4F$, 222.1142.

(-) *Erythro* (2*S*, 3*S*) 3-fluoro NMDA HCl D-72.

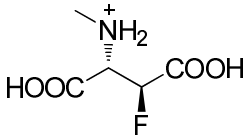

D-**72**

A few drops of EtOH was added to a solution of (2*S*, 3*S*) 3-fluoro amino alcohol methylamine **90** (1.6 g, 7.23 mmol) until complete dissolution followed by adding HCl (4 M, 4 mL). The solution was then heated at reflux for 48 h and the reaction was then diluted with DCM (30 mL) and concentrated under reduced pressure to give the title compound D-**72** (597 mg, 50%) as a pale yellow oil.

[α]$_D$ -7.28 (c 4.1, D_2O); **δ_H** (400 MHz, $CDCl_3$) 5.57 (1H, d, *J* = 48.0 Hz, CHF), 4.70 (1H, d, *J* = 29.0 Hz, CHN) and 2.74 (3H, s, NCH_3); **δ_c** ($CDCl_3$) 169.4 (d, *J* = 22.2, C=O), 86.4 (d, *J* = 189.0, CHF), 62.3 (d, *J* = 22.7, CHN) and 31.8 (NCH_3); **δ_F** {^{1}H}(400MHz, $CDCl_3$): -198.6 (1F, s, C(3)HF); ***m/z*** (ESI^-) 164 [$M\text{-}H^+$] (100). HRMS (ES^-): Found 164.0359. Calcd. For $[M\text{-}H]^-$ $C_5H_7NO_4F$, 164.0365.

Erythro Diethyl (2*S*, 3*S*)-amino alcohol methylamine 95.

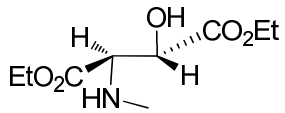

95

10 % mol of Palladium on activated carbon was added into a solution of diethyl (2*S*, 3*S*)-benzylmethylamine **88** (3.0 g, 9.70 mmol) in EtOH (20 mL) and stirred at RT in the presence of hydrogen gas. The reaction mixture was followed by TLC until completion and filtered through celite. The reaction mixture was extracted into EtOAc (3 x 50 mL) and the combined organic layers were dried with $MgSO_4$. Concentration of the reaction crude and purification over silica gel (hexane: EtOAc; 8:2) to give the title compound **95** (2.1 g, 97%) as a colourless oil.

$[\alpha]_D$ +18.9 (c 0.2, $CHCl_3$); **δ_H** (300 MHz, $CDCl_3$) 4.42 (1H, d, *J* = 3.3 Hz, CHOH), 4.18-4.15 (4H, m, OCH_2), 3.49 (1H, d, *J* = 3.6 Hz, CHN), 2.41 (3H, s, NCH_3) and 1.25 (6H, m, 2 x CH_3); **δ_c** (300 MHz, $CDCl_3$) 171.9 (C=O), 170.78 (C=O), 65.7 (CHOH), 65.7 (CHN), 61.7 (OCH_2), 61.2 (OCH_2), 35.4 (NCH_3) and 14.21 (2 x CH_3). **IR** (nujol mull) **υ_{max}/cm^{-1}** 3481, 3338, 2361, 1748, 1634, 1462, 1372, 1266, 1209, 1139, 1090, 947, 865, and 702; ***m/z*** (ESI^+) 242.0 $[M+Na]^+$ (100). HRMS (ES^+) Found 220.1186. Calcd. For $[M+H]^+$ $C_9H_{18}NO_5$, 220.1200.

Cyclic sulfamate 96.

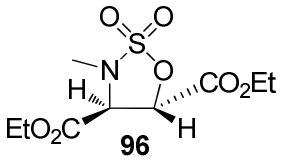

96

$SOCl_2$ (0.59 mL, 8.1 mmol) and Et_3N (1.90 mL, 13.7 mmol) were added dropwise to a stirred solution of **95** (1.5 g, 6.85 mmol) in dry DCM (40 mL) at –78 °C. Stirring was continue at -78 °C for a further 2 h. The resulting solution was slowly warmed to RT and stirred for an additional 16 h. The reaction mixture was concentrated under reduced pressure, and the crude product was partitioned between EtOAc (30 mL) and saturated NH_4Cl solution (30 mL). The aqueous layer was then extracted into EtOAc (3 ×50 mL) and the combined organic layers were dried with $MgSO_4$. Concentration under reduced pressure afforded the crude product as yellow oil.

The crude product was dissolved in CH_3CN/water (1:1) and cooled to 0 °C. $NaIO_4$ (1.1 g) and $RuCl_3.3H_2O$ (5 mg) were added. The resulting solution was slowly warmed to RT and stirred for an additional 4 h, at which point TLC analysis showed the reaction had gone to completion. The reaction mixture was concentrated under reduced pressure, and the product was extracted into EtOAc (30 mL) and the combined organic layers were dried with $MgSO_4$. Concentration under reduced pressure followed by purification over silica gel (hexane: EtOAc ;7:3) gave the title compound **96** (750 mg, 75%) as a pale yellow oil.

$[\alpha]_D$ +52.3 (c 1.0, $CHCl_3$); **δ_H** (300 MHz, $CDCl_3$) 5.18 (1H, d, *J* = 7.0 Hz, CHO), 4.29 (1H, d, *J* = 7.0 Hz, CHN), 4.24-4.19 (4H, m, CH_2), 2.89 (3H, s, CH_3), 1.27 (3H, t, *J* = 7.1 Hz, 2 x CH_3); **δ_c** (300 MHz, $CDCl_3$) 165.0 (C=O), 164.3 (C=O), 74.5 (CHO), 63.4 (CHN), 63.1 (CH_2), 62.7 (CH_2), 32.4 (NCH_3), 13.9 (CH_3) and 13.9 (CH_3); **IR** (nujol mull) **υ_{max}/cm^{-1}** 2721, 2663, 2365, 1752, 1462, 1372, 1262, 1180, 1021 and 739; ***m/z***

(ESI$^+$) 304 [M+Na$^+$] (100). HRMS (ES$^+$): Found 304.0467. Calcd. For [M+Na]$^+$ $C_9H_{15}NO_7SNa$, 304.0467.

meso Diethyl (2*S*,3*R*)- oxirane-2,3-dicarboxylate 99.[2,3]

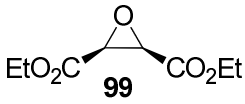

99

n-Butyl lithium (2.5 M in hexane, 5.87 mL, 0.063 mol) was added to a solution of *tert*-butyl hydroperoxide (5.5 M in decane, 11.6 mL, 0.1 mol) in dried THF (30 mL) at –78 °C. The mixture was stirred at the same temperature for 5 min, after which a solution of diethyl maleate **98** (9.4 mL, 0.058 mol) in dry THF (10 mL) was added. The reaction mixture was slowly warmed to RT and stirring continued for 16 h. The reaction was quenched with Na_2S (4 mL) and the resulting mixture was stirred vigorously for 1 h. The aqueous layer was separated and extracted into EtOAc (3 × 50 mL), and the combined organic layers were washed with saturated brine and dried over $MgSO_4$ and concentrated. The residue was purified over silica gel (hexane: EtOAc; 7:3) to give the title product **99** (5.4 g, 50%) as a colourless oil.

$\boldsymbol{\delta_H}$ (400 MHz, $CDCl_3$) 4.15-4.10 (4H, q, J = 7.2 Hz, OCH_2), 3.60 (s, 2H, 2 × CH_3) and 1.20-1.16 (t, J = 7.2 Hz, 6H, 2 × CH_3); $\boldsymbol{\delta_c}$ (400 MHz, $CDCl_3$) 165.6 (C=O), 61.7 (OCH_2), 52.4 (CH), 13.8 (2 × CH_3); ***m/z*** (ESI^+) 211.01 [$M+Na^+$] (100). These data were in accordance with the literature.[2,3]

(±) *Threo* diethyl 2-(benzyl(methyl)amino)-3-hydroxysuccinate *rac*-100.

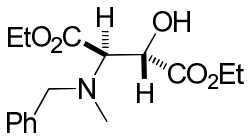

rac-**100**

A solution of *N*-benzylmethylamine (7.74 mL, 0.06 mol) was added dropwise to a suspension of *rac*-**99** (9.7 g, 0.05 mol) in EtOH (60 mL). The solution was stirred at reflux for 15 h, and then the excess of benzylmethylamine and EtOH were removed under reduced pressure. The residue was purified over silica gel (hexane:EtOAc; 6:4) to give the title compound *rac*-**100** (14.2 g, 92%) as colourless oil.

$\boldsymbol{\delta_H}$ (400 MHz, $CDCl_3$) 7.30-7.27 (5H, m, Ar-H), 4.55 (1H, d, *J* = 7.5 Hz, CHOH), 4.32-4.17 (4H, m, OCH_2), 3.92-3.72 (2H, q, *J* = 7.1 Hz, CH_2), 3.68 (1H, d, *J* = 7.5 Hz, CHN), 2.35 (3H, s, NCH_3) and 1.34-1.30 (6H, t, *J* = 7.4 Hz, 2 ×CH_3); $\boldsymbol{\delta_c}$ (400 MHz, $CDCl_3$) 171.8 (C=O), 169.4 (C=O), 138.4 (Ar C), 128.8 (Ar CH), 128,8 (Ar CH), 128.4 (Ar CH), 128.4 (Ar CH), 127.3(Ar CH), 69.5 (COH), 66.8 (CHN), 61.5 (OCH_2), 60.8 (OCH_2), 59.8 (CH_2), 38.6 (NCH_3) and 14.3 (2 x CH_3); **IR** (nujol mull) $\boldsymbol{\upsilon_{max}/cm^{-1}}$ 3472, 1732, 1572, 1458, 1372, 1258, 1151, 1098 and 1025; ***m/z*** (ESI^+) 332.00 [$M+Na^+$] (100), HRMS (ES^+): Found 332.1474. Calcd. For $[M+Na]^+$ $C_{16}H_{23}NO_5Na$, 332.1474.

(±) *Threo* Diethyl 2-(benzyl(methyl)amino)-3-fluorosuccinate *rac*-101.

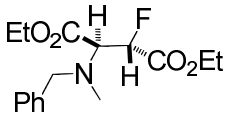

rac-**101**

Deoxo-fluor^{TM} (8.34 mL, 0.03 mol) was added to a solution of *rac*-**100** (4 g, 0.01 mol) in dry DCM (20 mL) at RT. The solution was stirred for 15 h at RT, and then the excess of Deoxo-fluor^{TM} was quenched with saturated $NaHCO_3$ solution to pH 7. The reaction mixture was extracted into EtOAc (3 x 50 mL) and the combined organic layers were dried with $MgSO_4$. The residue was purified over silica gel (hexane: EtOAc; 9:1) to give the title compound *rac*-**101** (2.71 g, 87%) as a pale yellow oil.

$\boldsymbol{\delta_H}$ (400 MHz, $CDCl_3$) 7.23-7.15 (5H, m, Ar H), 5.39 (1H, dd, *J* = 4.0, 47.9 Hz, CHF), 4.26-4.11 (4H, m, OCH_2), 3.89 (1H, dd, *J* = 4.0, 31.7 Hz, CHN), 3.87-3.76 (2H, q, *J* = 13.5 Hz, CH_2), 2.41 (3H, s) and 1.27-1.24 (6H, m, 2 x CH_3); $\boldsymbol{\delta_c}$ (400 MHz, $CDCl_3$) 168.9 (C=O), 167.9 (C=O), 139.1 (Ar C), 128.6 (Ar CH), 128.6 (Ar CH), 128.2 (Ar CH), 128.2 (Ar CH), 127.1, (Ar-C), 91.8 (d, *J* = 191.5 Hz, CHF), 66.31 (d, *J* = 18.6 Hz, CHN), 61.7 (OCH_2), 60.2 (OCH_2), 60.1 (CH_2), 39.3 (NCH_3) and 14.3 (2 ×CH_3); δ_F {^{1}H} (400MHz, $CDCl_3$): -199.3 (1F, s, C(3)HF); **IR** (nujol mull) $\boldsymbol{\upsilon_{max}/cm^{-1}}$ 1742, 1677, 1574, 1455, 1375, 1271, 1131, 1093, 1035, 798 and 738; ***m/z*** (ESI^+) 334 [M+Na^+] (100). HRMS (ES^+): Found 334.1431. Calcd. For [M+Na]$^+$ $C_{16}H_{22}NO_4FNa$, 334.1434.

(±) *Threo* diethyl 2-fluoro-3-(methylamino)succinate *rac*-102.

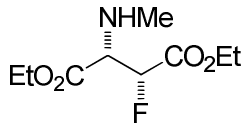

rac-**102**

10 % of Palladium on activated carbon (30 mg) was added into a solution of *rac*-**101** (3.2 g, 0.01 mol) in EtOH (20 mL) and stirred at RT in the presence of hydrogen gas. The reaction mixture was followed by TLC until the reaction had gone to completion and filtered through celite. The reaction mixture was extracted into EtOAc (3 x 50 mL) and dried with $MgSO_4$. Concentration of the reaction crude to give the title compound *rac*-**102** (1.6 g, 87%) as a colourless oil.

$\boldsymbol{\delta_H}$ (300 MHz, $CDCl_3$) 5.17 (1H,dd, *J* = 2.4, 47.7 Hz, CHF), 4.30-4.15 (4H, m, OCH_2), 3.61 (1H, dd, *J* = 2.4, 31.4 Hz, CHN), 2.36 (3H, s, NCH_3) and 1.27-1.22 (6H, m, 2 x CH_3); $\boldsymbol{\delta_c}$ (300 MHZ, $CDCl_3$) 170.2 (C=O), 167.4 (C=O), 90.8 (d, *J* = 189.7 Hz, CHF), 64.3 (d, *J* = 20.2 Hz, CNR), 61.8 (OCH_2), 61.7 (OCH_2), 35.6 (NCH_3) and 14.0 (CH_3); $\boldsymbol{\delta_F}$ {^{1}H} (400MHz, $CDCl_3$): -204.3 (1F, s, C(3)HF); **IR** (nujol mull) $\boldsymbol{\upsilon_{max}/cm^{-1}}$ 1741, 1693, 1577, 1455, 1373, 1260, 1131, 1074, 1035, 795 and 738; ***m/z*** (ESI$^+$) 222.0 [M+H$^+$] (100). HRMS (ES$^+$): Found 244.0961. Calcd. For [M+Na]$^+$ $C_9H_{16}NO_4$ FNa, 244.1000.

(±) *Threo* (*2S,3R*)-3F NMDA HCl *rac*-73.

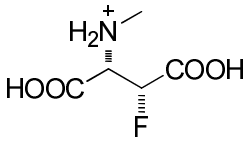

rac-**73**

A few drops of EtOH was added into a solution of *rac*-**102** (1.6 g, 7.23 mmol) until complete dissolution, followed by adding HCl (4M, 4 mL). The reaction mixture was heated under refluxed for 48 h and the reaction was then diluted with DCM (30 mL) and concentrated under reduced pressure to give the title compound *rac*-**73** (480 mg, 30%) as a pale yellow oil.

$\boldsymbol{\delta_H}$ (300 MHz, $CDCl_3$) 5.47-5.32 (1H, dd, *J* = 45.1 Hz, CHF), 4.31-4.22 (1H, dd, *J* = 27.4 Hz, CHN) and 2.69 (3H, NCH_3); $\boldsymbol{\delta c}$ (300 MHz, $CDCl_3$) 171.0 (C=O), 168.6 (C=O), 87.9 (d, *J* = 189.5 Hz), 62.5 (d, *J* = 21.7 Hz, CHN) and 32.3 (NCH_3); $\boldsymbol{\delta_F}$ {^{1}H} (300 MHz, $CDCl_3$): -196.38 (1F, s, C(3)HF). ***m/z*** (ESI^-) 164 [$M\text{-}H^+$] (100). HRMS (ES^-): Found 164.0359. Calcd. For $[M\text{-}H]^-$ $C_5H_7NO_4F$, 164.0369.

meso Dibenzyl (*2S,3R*)-oxirane-2,3-dicarboxylate 104.[4]

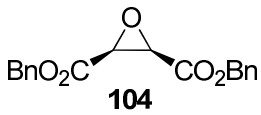

104

Oxalyl chloride (13.5 mL, 0.16 mol) was added to a solution of *cis*-epoxy succinic acid **103** (10.0 g, 0.07 mol) in dry THF at 0 °C. The mixture was stirred at the same temperature for 1 h and then slowly warmed to RT and heated at reflux for another 2 h. The crude product was obtained after solvent evaporation and was used without purification for the subsequent reaction. Catalytic amount of DMF was added to the crude product in dry THF (40 mL) at 0 °C. Benzyl bromide (18.0 mL, 0.15 mol) was added into the reaction mixture and followed by dropwise of pyridine (5 mL) over 20 min. The resulting mixture was slowly warmed to RT and left to stir for 16 h. The aqueous layer was separated and extracted into ethyl acetate (3 × 50 mL), and the combined organic layers were washed with saturated brine and dried over $MgSO_4$. Concentration under reduced pressure and purification over silica gel (hexane: EtOAc; 8:2) afforded the title product **104** as a colourless oil (20.1 g, 86%).

$\boldsymbol{\delta_H}$ (300 MHz, $CDCl_3$) 7.40-7.34 (10H, m, Ar H), 5.13 (2H, s, OCH_2), 3.77 (s, 2H, CH); $\boldsymbol{\delta c}$ ($CDCl_3$) 134.5 (Ar C), 128.7 (Ar CH), 128.7 (Ar CH), 128.6 (Ar CH), 128.6 (Ar CH), 67.6 (CH) and 52.6 (OCH_2); ***m/z*** (ESI^+) 334.9 [$M+Na^+$] (100). HRMS (ES^+): Found 335.0896 Calcd. For $[M+Na]^+$ $C_{18}H_{16}O_5$ Na, 335.0890. These data were in accordance with the literature.[4]

(±) *Threo* dibenzyl 2-(benzyl(methyl)amino)-3-hydroxysuccinate *rac*-105.

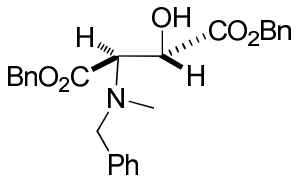

rac-**105**

A solution of *N*-benzylmethylamine in ethanol (4.64 mL, 0.036 mol) was added dropwise to a suspension of **104** (10.0 g, 0.03 mol) in ethanol (60 mL). The solution was stirred at reflux for 15 h, and then the excess of *N*-benzylmethylamine and EtOH were removed under reduced pressure. The residue was purified over silica gel (hexane:EtOAc; 6:4) to give the title compound *rac*-**105** (12.5 g, 92%) as a pale yellow oil.

$\boldsymbol{\delta_H}$ (300 MHz, $CDCl_3$) 7.42-7.26 (15H, m, Ar H), 5.31-5.14 (4H, m, OCH_2), 4.72 (1H, d, *J* = 7.6 Hz, CHOH), 3.98-3.75 (1H, q, CH_2), 3.84 (2H, d, *J* = 7.6 Hz, CHN), 2.38 (3H, s, NCH_3); $\boldsymbol{\delta_c}$ (300 MHz, $CDCl_3$) 171.7 (C=O), 169.3 (C=O), 138.3 (Ar C), 135.5 (Ar C), 128.8 (Ar CH), 128.8 (Ar CH), 128.6 (Ar CH), 128.6 (Ar CH), 128.5 (Ar CH), 128.5 (Ar CH), 128.4 (Ar CH), 127.4 (Ar CH), 69.6 (COH), 67.3 (CHN), 66.5 (2 × OCH_2), 59.6 (CH_2), 38.7 (NCH_3); **IR** (nujol mull) $\boldsymbol{\upsilon_{max}/cm^{-1}}$; 3472, 1732, 1572, 1458, 1372, 1258, 1151, 1098 and 1025; ***m/z*** (ESI^+) 456.0 [$M+Na^+$] (100), HRMS (ES^+): Found 456.1787. Calcd. For $[M+Na]^+$ $C_{26}H_{27}NO_5Na$, 456.1781.

(±) *Threo* dibenzyl 2-(benzyl(methyl)amino)-3-fluorosuccinate *rac*-106.

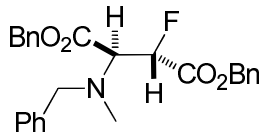

rac-**106**

Deoxofluor^{TM} (5.65 mL, 26.3 mmol) was added into a solution of *rac*-**105** (4 g, 8.77 mmol) in dry DCM (20 mL) at RT. The solution was stirred for 15 h at RT, and then the excess of Deoxofluor^{TM} was quenched with saturated $NaHCO_3$ solution to pH 7. The reaction mixture was extracted into EtOAc (3 x 50 mL) and dried with $MgSO_4$. The residue was purified over silica gel (hexane: EtOAc; 9:1) to afford the title compound *rac*-**106** (3.37 g, 84%) as a pale yellow oil.

$\boldsymbol{\delta_H}$ (300 MHz, $CDCl_3$) 7.42-7.25 (15, m, Ar-H), 5.59 (1H, dd, *J* = 3.77, 47.9 Hz, CHF), 5.36-5.19 (4H, m, OCH_2), 4.06 (1H, dd, *J* = 3.8, 31.9 Hz), 4.00-3.83 (2H, q, *J* = 13.5 Hz, CH_2), 2.51 (3H, s, NCH_3); $\boldsymbol{\delta_c}$ (300 MHz, $CDCl_3$) 168.0 (C=O), 167.7 (C=O), 139.3 (Ar C), 135.7 (Ar CH), 135.2 (Ar CH), 129.1 (Ar CH), 129.0 (Ar CH), 128.9 (Ar CH), 128.7 (Ar CH), 128.6 (Ar CH), 127.5 (Ar CH), 92.0 (d, *J* = 192.2 Hz, CHF), 67.8 (OCH_2), 67.3 (OCH_2), 66.8 (d, *J* = 36.6 Hz, CHN), 60.5 (CH_2), 38.8 (NCH_3); $\boldsymbol{\delta_F}$ {^{1}H} (400MHz, $CDCl_3$): -198.6 (1F, s, C(3)HF); **IR** (nujol mull) $\boldsymbol{\upsilon_{max}/cm^{-1}}$ 1744, 1691, 1576, 1458, 1376, 1270, 1141, 1094, 1037, 796 and 739; ***m/z*** (ESI^+) 458.00 [M+Na^+], (60). HRMS (ES^+): Found 458.1744. Calcd. For [M+Na]$^+$ $C_{26}H_{26}NO_4FNa$, 458.1738.

(±) *Threo* (*2S,3R*)-3F NMDA HCl *rac*-73.

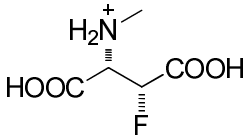

rac-**73**

10 % Palladium on activated carbon was added into a solution of *rac*-**106** (1.6 g, 3.67 mmol) in ethyl acetate (20 mL) and stirred at RT in the presence of hydrogen gas. The reaction mixture was followed by TLC until the reaction had gone completion and then filtered through celite. The reaction mixture was extracted into EtOAc (3 x 50 mL). Concentration under reduced pressure and followed by addition of HCl (1M, 0.1 mL) to give the title compound *rac*-**73** as pale yellow oil (517 mg, 86%).

$\boldsymbol{\delta_H}$ (300 MHz, $CDCl_3$) 5.40 (1H, dd, *J* = 45.1 Hz, CHF), 4.27 (1H, dd, *J* = 27.4 Hz, CHN) and 2.69 (3H, s, NCH_3); **δc** (300 MHz, $CDCl_3$) 171.0 (C=O), 168.6 (C=O), 87.9 (d, *J* = 189.5 Hz, CHF), 62.5 (d, *J* = 21.7 Hz, CHN), and 32.3 (NCH_3); $\boldsymbol{\delta_F}$ {^{1}H} (300MHz, $CDCl_3$): -196.38 (1F, dd, C(3)HF). m/z (ESI^-) 164 [$M\text{-}H^+$] (100). HRMS (ES^-): Found 164.0359. Calcd. For $[M\text{-}H]^-$ $C_5H_7NO_4F$, 164.0369.

Mixture of diastereoisomers dibenzyl –hydroxy -3-(methyl (*S*)-1-phenylethyl)amino) succinate (*S*)-107 and (*S*)-108.

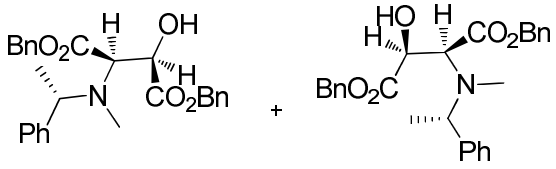

(*S*)-**107** (*S*)-**108**

A solution of (*S*)-(-)-*N*, α-dimethylbenzylamine (19.70 mL) was added dropwise to a suspension of **104** (10.0 g, 0.07 mol) in DMF (10 mL) and the resulting solution was stirred at reflux for 4 h. The reaction mixture was worked up with saturated $NaHCO_3$ solution (3 × 50 mL) and the aqueous layer was washed with ethyl acetate (3 × 50 mL). Solvent evaporation and purification over silica gel (hexane:EtOAc; 8:2) to give the mixture of diastereoisomers (*S*)-**107** and (*S*)-**108** (26.5 g, 85%) as a pale yellow oil.

Data for the mixture of diastereoisomers (*S*)-**107** and (*S*)-**108:** $\boldsymbol{\delta_H}$ (300MHz, $CDCl_3$) 7.41-7.21 (30H, m), 5.33-5.00 (8H, m, OCH_2), 4.63 (1H, d, *J* = 8.3 Hz, CHOH), 4.52 (1H, d, *J* = 8.6 Hz, CHOH), 4.16 (1H, d, *J* = 8.4 Hz, CHN), 3.98 (2H, q, *J* = 6.7 Hz , CH), 3.91 (2H,q, *J* = 6.4 Hz , CH), 3.69 (1H, d, *J* = 8.5 Hz, CHN), 2.43 (3H, s, NCH_3), 2.21 (3H, s, NCH_3); $\boldsymbol{\delta_c}$ (300 MHz, $CDCl_3$) 171.3 (C=O), 169.4 (C=O), 143.1 (Ar C), 128.7 (Ar CH), 128.6 (Ar CH), 128.5 (Ar CH), 128.3 (Ar CH), 128.2 (Ar CH), 127.6 (Ar CH), 127.3 (Ar CH), 127.1 (Ar CH), 68.8 (CHOH),68.5 (CHOH), 67.3 (CHN), 67.0 (CHN), 66.7 (2 × OCH_2), 66.6 (2 × OCH_2), 63.0 (NCH), 62.6 (NCH), 35.7 (NCH_3), 33.7 (NCH_3), 21.1 (CH_3) and 20.5 (CH_3Ph); **IR** (nujol mull) $\boldsymbol{\upsilon_{max}/cm^{-1}}$ 3470, 1731, 1572, 1448, 1362, 1253, 1150, 1097 and 1020; m/z (ESI^+) 470.1 [$M+Na^+$] (100), HRMS (ES^+): Found 470.1943. Calcd. For $[M+Na]^+$ $C_{27}H_{29}NO_5Na$, 470.1938.

Mixture of diastereoisomers dibenzyl 2-hydroxy -3-(methyl((*R*)-1-phenylethyl)amino) succinate (*R*)-108 and (*R*)-107.

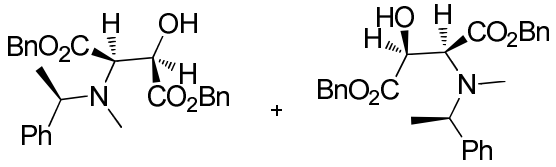

(*R*)-**108** + (*R*)-**107**

Mixture of diastereoisomer (*R*)-**108** and (*R*)-**107** was synthesized as described for (*S*)-**107** and (*S*)-**108**. Compound (*R*)-**108** and (*R*)-**107** (27.8 g, 89%) was synthesized as a pale yellow oil.

Data for the mixture of diastereoisomers (*R*)-**108** and (*R*)-**107**: $\boldsymbol{\delta_H}$ (300 MHz, $CDCl_3$) 7.41-7.21 (30H, m), 5.33-5.00 (8H, m, OCH_2), 4.63 (1H, d, *J* = 8.3 Hz, CHOH), 4.52 (1H, d, *J* = 8.6 Hz, CHOH), 4.16 (1H, d, *J* = 8.4 Hz, CHN), 3.98 (2H, q, *J* = 6.6 Hz , CH), 3.91 (2H,q, *J* = 6.4 Hz, CH), 3.69 (1H, d, *J* = 8.5 Hz, CHN), 2.43 (3H, s, NCH_3), 2.21 (3H, s, NCH_3); $\boldsymbol{\delta}$**c** ($CDCl_3$) 171.3 (C=O), 169.4 (C=O), 143.1 (Ar C), 128.7 (Ar CH), 128.6 (Ar CH), 128.5 (Ar CH), 128.3 (Ar CH), 127.6 (Ar CH), 127.3 (Ar CH), 127.1 (Ar CH), 68.8 (CHOH),68.5 (CHOH), 67.3 (CHN), 67.0 (CHN), 66.7 (2 × OCH_2), 66.6 (2 × OCH_2), 63.0 (NCH), 62.6 (NCH), 35.7 (NCH_3), 33.7 (NCH_3), 21.1 (CH_3) and 20.5 (CH_3); **IR** (nujol mull) $\boldsymbol{\upsilon_{max}/cm^{-1}}$3470, 1731, 1572, 1448, 1362, 1253, 1150, 1097 and 1020; ***m/z*** (ESI^+) 470.1 [$M+Na^+$], 100%), HRMS (ES^+): Found 470.1943. Calcd. For $[M+Na]^+$ $C_{27}H_{29}NO_5Na$, 470.1938.

(-) Dibenzyl 2-fluoro-3- (methyl ((*S*)- 1-phenylethyl)amino) succinate (*S*)-**109** or (*S*)-**110**.

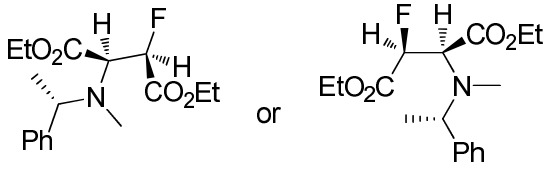

(*S*)-**109** (*S*)-**110**

Deoxofluor™ (5.76 ml, 26.8 mmol) was added to a solution of (*S*)-**107** and (*S*)-**108** (4 g, 8.94 mmol) in dry DCM (20 mL) at RT. The solution was stirred for 15 h at RT, and then the excess of Deoxofluor™ was quenched with saturated $NaHCO_3$ solution to pH 7. The reaction mixture was extracted into EtOAc (3 x 50 mL) and the combined organic layers were dried with $MgSO_4$. The residue was purified over silica gel (hexane: EtOAc; 9:1) to give either one of the stereoisomer of (*S*)-**109** or (*S*)-**110** (3.37 g, 43%) as a pale yellow oil.

Data for either (*S*)-**109** or (*S*)-**110**: $\boldsymbol{[\alpha]_D}$ – 69.5 (c 0.6, D_2O); $\boldsymbol{\delta_H}$ (400 MHz, $CDCl_3$) 7.38-7.05 (15, m, Ar-H), 5.40 (1H, dd, *J* = 4.6 Hz, 48.4 Hz, CHF), 5.27 (4H, m, OCH_2), 3.90 (1H, dd, *J* = 4.3, 32.4 Hz, CHN), 3.95 (1H, q, *J* = 6.3 Hz, CH), 2.66 (3H, s, NCH_3) and 1.58 (3H, s, CH_3); $\boldsymbol{\delta_c}$ (400 MHz, $CDCl_3$) 129.6 (Ar CH), 128.6 (Ar CH), 128.4 (Ar CH), 128.3 (Ar CH), 127.5 (Ar CH), 91.5 (d, *J* = 231.8 Hz, CHF), 67.2 (d, *J* = 49.9 Hz, CHN), 63.1 (CH), 35.2 (NCH_3), 21.3 (CH_3); δ_F {^{1}H} (400MHz, $CDCl_3$): -195.7 (1F, s, C(3)HF); **IR** (nujol mull) $\boldsymbol{\upsilon_{max}/cm^{-1}}$ 2986, 1609, 1451, 1327, 1276, 1163, 1096, 1073, 800 and 751; ***m/z*** (ESI^+) 472.1 [M+Na^+] (30). HRMS (ES^+): Found 472.1900. Calcd. For [M+Na]$^+$ $C_{27}H_{28}NO_4$ FNa, 458.1895.

(+) Dibenzyl 2- fluoro-3- (methyl((*R*)-1- phenylethyl)amino) succinate (*R*)-110 or (*R*)-**109**.

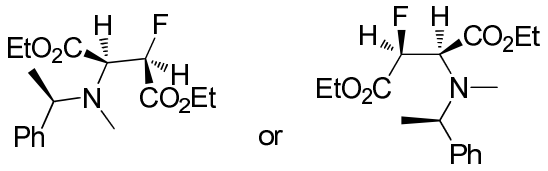

(*R*)-**113** (*R*)-**112**

The stereoisomer of dibenzyl 2-fluoro-3-(methyl((*R*)-1-phenylethyl)amino)succinate (*R*)-**110** or (*R*)-**109** was synthesized as described for (*S*)-**109** or (*S*)-**110**.

Data for either (*R*)-**110** or (*R*)-**109**: $[\alpha]_D$ + 52.2 (c 0.6, D_2O); δ_H (300 MHz, $CDCl_3$) 7.38-7.05 (15, m, Ar H), 5.40 (1H, dd, *J* = 4.6, 48.4 Hz, CHF), 5.27 (4H, m, OCH_2), 3.90 (1H, dd, *J* = 4.3, 32.4 Hz, CHN), 3.95 (1H, q, *J* = 6.8 Hz, CH), 2.66 (3H, s, NCH_3) and 1.58 (3H, s, CH_3); δ_c (300 MHz, $CDCl_3$) 129.0 (Ar C), 128.6 (Ar CH), 128.4 (Ar CH), 128.3 (Ar CH), 127.5 (Ar CH), 91.5 (d, *J* = 231.8 Hz, CHF), 67.2 (d, *J* = 49.9 Hz, CHN), 63.1 (CH), 35.2 (NCH_3), 21.3 (CH_3Ph); δ_F {^{1}H} (400MHz, $CDCl_3$): -195.7 (1F, s, C(3)HF); **IR** (nujol mull) υ_{max}/**cm**$^{-1}$ 2986, 1609, 1451, 1327, 1276, 1163, 1096, 1073, 800 and 751; ***m/z*** (ESI^+) 472.1 [M+Na^+] (30). HRMS (ES^+): Found 472.1900. Calcd. For [M+Na]$^+$ $C_{27}H_{28}NO_4$ FNa, 458.1895.

Threo (2*R*, 3*S*)- or (2*S*, 3*R*)- 3-fluoro NMDA HCl (-)-73.

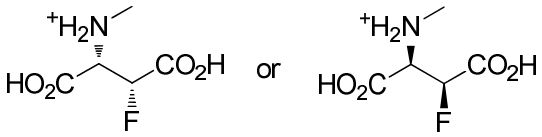

(-)-**73**

10 % Palladium on activated carbon (30 mg) was added to a solution of (*S*)-**109** or (*S*)-**110** (1.6 g, 3.67 mmol) in ethyl acetate (20 mL) and stirred at RT in the presence of hydrogen gas. The reaction mixture was followed by TLC until the reaction had gone to completion and filtered through celite. The reaction mixture was then extracted into EtOAc (3 x 50 mL). Concentration of the reaction crude and HCl (1M, 0.1 mL) was added to give either one of the stereoisomer (-) (*2R,3S*)- or (-) (*2S,3R*)-3-fluoro NMDA HCl **73** (517 mg, 85 %) as a pale yellow oil.

[α]$_D$ -2.1 (c 1.0, D_2O); **δ_H** (500 MHz, $CDCl_3$) 5.39 (1H, dd, *J* = 45.1 Hz, CHF), 4.26 (1H, dd, *J* = 27.4 Hz, CHN) and 2.69 (3H, NCH_3); **δ_c** ($CDCl_3$) 171.0 (C=O), 168.6 (C=O), 87.9 (d, *J* = 189.5 Hz, CHF), 62.5 (d, *J* = 21.7 Hz, CHN), and 32.3 (NCH_3); **δ_F** {^{1}H} (400MHz, $CDCl_3$): -196.38 (1F, s, C(3)HF). m/z (ESI$^-$) 164 [M-H$^+$] (100). HRMS (ES$^-$): Found 164.0359. Calcd. For [M-H]$^-$ $C_5H_7NO_4F$, 164.0369.

Threo (2*S*,3*R*)- or (2*R*,3*S*)- 3-fluoro NMDA HCl (+)-73.

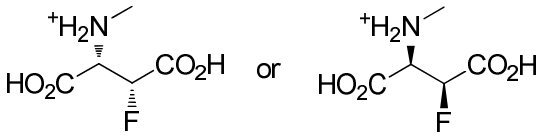

(+)-**73**

10 % Palladium on activated carbon (30 mg) was added to a solution of (*R*)-**110** or (*R*)-**109** (1.6 g, 3.67 mmol) in ethyl acetate (20 mL) and stirred at RT in the presence of hydrogen gas. The reaction mixture was followed by TLC until the reaction had gone completion and then filtered through celite. The reaction mixture was then extracted into EtOAc (3 x 50 mL). Concentration of the crude reaction and HCl (1M, 0.1 mL) was added to give either one of the stereoisomer (+) (2*S*,3*R*)- or (+) (2*R*,3*S*)-3-fluoro NMDA HCl (+)-**73** (517 mg, 85%) as a pale yellow oil.

[α]$_D$ + 2.9 (c 1.0, D_2O); **δ_H** (300 MHz, $CDCl_3$) 5.39 (1H, dd, *J* = 45.1 Hz, CHF), 4.26 (1H, dd, *J* = 27.4 Hz, CHN) and 2.69 (3H, NCH_3); **δ_c** (300 MHz, $CDCl_3$) 171.0 (C=O), 168.6 (C=O), 87.9 (d, *J* = 189.5 Hz, CHF), 62.5 (d, *J* = 21.7 Hz, CHN), and 32.3 (NCH_3); **δ_F** {^{1}H} (400MHz, $CDCl_3$): -196.38 (1F, s, C(3)HF). ***m/z*** (ESI$^-$) 164 [M-H$^+$] (100). HRMS (ES$^-$): Found 164.0359. Calcd. For [M-H]$^-$ $C_5H_7NO_4F$, 164.0369

Triethyl oxalocitrolactone ester 91[5]

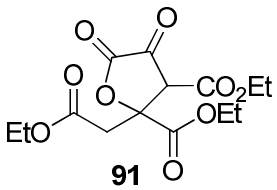

91

HCl in diethyl ether (1M, 0.1 mL) was added to a solution of **89** (0.2 g, 0.6 mmol) in ether (20 ml) and stirred at RT in the presence of argon. Concentration of the reaction crude gave the title compound **91** (0.1 g, 51%) as a colourless oil.

$\boldsymbol{\delta_H}$ (400 MHz, $CDCl_3$) 4.32-4.00 (6H, m, 3 × CH_2), 3.68 (1H, s, CH), 2.46 (2H, s, CH_2) and 1.36-1.23 (9H, m, 3 × CH_3); $\boldsymbol{\delta_c}$ (400 MHz, $CDCl_3$) 62.3 (CH_2), 61.2 (CH_2), 58.4 (CH_2), 52.8 (CH), 31.9 (CH_2) and 14.0 (3 × CH_3). m/z (ESI^-) 329 [$M\text{-}H^+$] (100). These data were in accordance with the literature.[5]

3-(3-(Trifluoromethyl)phenyl)propanoic acid 144.[6]

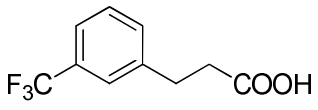

144

10 % Palladium on activated carbon (40 mg) was added to a solution of **140** (10.0 g, 0.04 mol) in EtOH (20 ml) and stirred at RT in the presence of hydrogen gas. The reaction was monitored by TLC until the reaction had gone completion and then filtered through celite. The reaction mixture was extracted into EtOAc (3 x 50 mL). Concentration of the reaction crude gave the title compound **144** (8.5 g, 98%) as a colourless oil.

$\boldsymbol{\delta_H}$ (400 MHz, $CDCl_3$) 11.9 (1H, s, COOH), 7.52-7.43 (4H, m, Ar-H), 3.04 (2H, t, *J* = 7.4 Hz, CH_2) and 2.74 (2H, t, *J* = 7.6 Hz, CH_2); $\boldsymbol{\delta_c}$ (400 MHz, $CDCl_3$) 179.60 (C=O), 141.0 (Ar C), 131.7 (Ar CH), 129.0 (Ar CH), 125.0 (Ar CH), 123.3 (Ar CH), 35.5 (CH_2) and 30.2 (CH_2); $\boldsymbol{\delta_F}$ {^{1}H} (400MHz, $CDCl_3$): -63.11 (3F, s, CF_3); **IR** (nujol mull) $\boldsymbol{\upsilon_{max}/cm^{-1}}$ 3354, 2998, 1708, 1484, 1414, 1275, 1110, 888, 827 and 764. m/z (ESI^-) 217 [M-H^+] (100). These data were in accordance with the literature.[6]

3-(3-(trifluoromethyl)phenyl)propan-1-ol 145.[6]

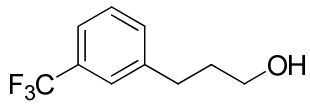

145

Lithium aluminium hydride (11.3 g, 0.03 mol) was added to a solution of **144** (5.0 g, 0.02 mol) in dry THF (30 mL). The reaction mixture was heated at reflux for 1 h. The reaction mixture was quenched with saturated KOH solution (15 mL) and washed with EtOAc (3 x 50 mL). Concentration of the organic layers and purified over silica gel to give the title compound **145** (3.87 g, 95%) as a colourless oil.

$\boldsymbol{\delta_H}$ (400 MHz, $CDCl_3$) 7.49-7.38 (4H, m, Ar-H), 3.67 (2H, t, J = 6.6 Hz, CH_2OH), 2.78 (2H, t, J = 7.7 Hz, CH_2) and 1.91 (2H, m, CH_2); $\boldsymbol{\delta_c}$ (400 MHz, $CDCl_3$) 142.8 (Ar C), 131.8 (Ar CH), 128.7 (Ar CH), 125.0 (Ar CH), 122.7 (Ar CH), 61.6 (COH), 33.9 (CH_2) and 30.2 (CH_2); $\boldsymbol{\delta_F}$ {^{1}H} (400MHz, $CDCl_3$): -63.06 (3F, s, CF_3); **IR** (nujol mull) $\boldsymbol{\upsilon_{max}/cm^{-1}}$ 3353, 2997, 1484, 1318, 1273, 1100, 908, 824 and 754. *m/z* (GC-MS) 204 $M^{+\cdot}$ (40). These data were in accordance with the literature.[6]

3-(3-(trifluoromethyl)phenyl)propanal 146.[6]

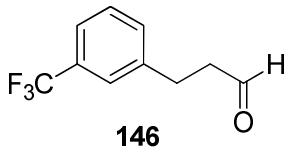

146

DMP (12.7 g, 0.03 mol) was added into a solution of **145** (5.0 g, 0.02 mol) in DCM (20 mL) at 0 °C and was slowly warmed to RT. After 1 h, the reaction was quenched with saturated $NaHCO_3$ solution (30 ml). The aqueous layer was washed with EtOAc (3 x 50 mL) and the combined organic layers were concentrated under reduced pressure. Purification over silica gel (hexane: EtOAc; 9:1) afforded the title compound **146** (2.4 g, 60%) as a colourless oil.

$\boldsymbol{\delta_H}$ (400 MHz, $CDCl_3$): 9.74 (1H, s, CHO), 7.39 (4H, m, Ar-H), 2.93 (2H, t, *J* = 7.6 Hz, CH_2) and 2.74 (2H, t, *J* = 7.6 Hz, CH_2); $\boldsymbol{\delta_c}$ ($CDCl_3$) 143.2 (Ar C), 128.6 (Ar CH), 127.88 (Ar CH), 125.5 (Ar CH), 125.5 (Ar CH), 37.4 (CH_2) and 31.1 (CH_2); $\boldsymbol{\delta_F}$ {^{1}H} (400MHz, $CDCl_3$): -63.13 (3F, s, CF_3); **IR** (nujol mull) $\boldsymbol{\upsilon_{max}/cm^{-1}}$ 3006, 2988, 1613, 1485, 1330, 1275, 1165, 913, 801 and 750. ***m/z*** (ESI^+) 202 [M^+] (40). These data were in accordance with the literature.[6]

(*R*)-2-fluoro-3-(3-(trifluoromethyl)phenyl)propanal (*R*)-148.

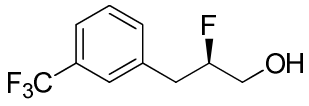

(*R*)-**148**

N-Fluorobenzenesulfonimide (7.80 g, 0.02 mol) and (5*R*) -(+)-2,2,3-trimethyl-5-benzyl-4-imidazolidinone dichloroacetic acid salt (516 mg, 15 % mol) was added to a solution of **146 (**2.0 g, 9.9 mmol) in THF/Isopropanol (9:1) at –15 °C. The reaction was monitored by chiral phase GC-MS until all the starting material was consumed. After 16 h, lithium aluminium hydride (564 mg, 0.01 mol) was added into the reaction and continued stirring for 1 h. The reaction mixture was quenched with $NaHCO_3$ solution (30 ml) at –15 °C. The aqueous layer was washed with $(NH_4)_2SO_4$ and partitioned with EtOAc (3 x 50 mL). The combined organic layer was concentrated under reduced pressure and purified over silica gel (hexane: EtOAc; 7:3) to give the title compound (*R*)-**148** (2.4 g, 80%) as a pale yellow oil.

$[\alpha]_D$ + 9.55 (c 2.0, $CHCl_3$); **δ_H** (300 MHz, $CDCl_3$): 7.43 (5H, m, Ar-H), 4.71 (dm, *J* = 48.5 Hz, CHF), 3.67 (2H, m, CH_2) and 2.97 (2H, m, CH_2); **δ_c** (300 MHz, $CDCl_3$) 132.7 (Ar CH), 129.0 (Ar CH), 125.9 (Ar CH), 123.7 (Ar CH), 94.8 (d, *J* = 172.8 Hz, CHF), 64.1 (d, *J* = 22.2 Hz, COH) and 37.2 (d, *J* = 21.6 Hz, CH_2); **δ_F** {^{1}H} (400MHz, $CDCl_3$): -63.1 (3F, s, CF_3), -189.0 (1F, s, CHF). ***m/z*** (ESI^-) 203 ($M\text{-}F^-$, 40%); **IR** (nujol mull) **υ_{max}/cm^{-1}** 3353, 2934, 1461, 1328, 1199, 1072, 908, 835 and 752. ***m/z*** (CI^+) 203.07 [$M\text{-}F^-$] (100). HRMS (CI^+): Found 203.0684. Calcd. For $(M\text{-}F)^-$ $C_{10}H_{10}OF_3$, 203.0668.

(*S*)-2-Fluoro-3-(3-(trifluoromethyl)phenyl)propan-1-ol (*S*)-148.

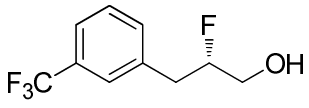

(*S*)-**148**

Compound (*S*)-**148** was prepared following the procedure for (*R*)-**148**, starting with **146**. The product was obtained as a pale yellow oil (2.4 g, 80 %). Spectra data were identical to (*R*)-**148**; $[\alpha]_D$ −14.4 (c 2.1, $CHCl_3$); ***m/z*** (CI^+) 203.07 [M-F^-] (100). HRMS (CI^+): Found 203.0684. Calcd. For [M-F]$^-$ $C_{10}H_{10}OF_3$, 203.0668.

(2*R*,1'*R*)-2-Fluoro Cinacalcet HCl 123.

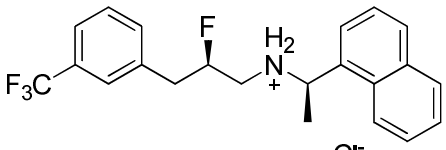

(2*R*,1'*R*)-**123**

Trifluoromethanesulfonic anhydride (0.71 mL, 3.4 mmol) was added to a solution of Et_3N (0.33 mL, 4.5 mmol) and DMAP (27.9 mg, 0.2 mmol) in dry DCM (30 mL) at 0 °C. (*R*)-(**148**) **(**500 mg, 2.2 mmol) was added into the reaction mixture through cannula and was left to stir for 2 h at 0 °C. The reaction mixture was subsequently warmed to RT and continued stirring for 16 h. The reaction was quenched with saturated $NaHCO_3$ solution (30 ml) and the aqueous layer was washed with EtOAc (3 x 50 mL). The combined organic layers were concentrated under reduced pressure to afford the crude mixture of (*R*)-**149**. The crude mixture (*R*)-**149** was used for the next reaction without purification.

(*R*)-1-(1-napthyl)ethylamine (0.11 ml, 0.7 mmol) was added into a solution of (*R*)-**149** (200.0 mg, 0.6 mmol) in toluene (15 mL) and the reaction was heated at reflux for 16 h. After 16 h, the reaction mixture was concentrated under reduced pressure. Purification over silica gel (hexane: EtOAc; 8:2) to afford the title compound (2*R*,1'*R*)-**123** (199.5 mg, 95%) as a pale yellow oil. HCl in diethyl ether (0.1 mL, 1M) was added into (2*R*,1'*R*)-**123** to afford the hydrochloride salt.

$[\alpha]_D$ + 4.4 (c 1.0, $CHCl_3$); δ_H (400 MHz, $CDCl_3$): 8.02-7.22 (11H, m, Ar-H), 5.07 (dm, *J* = 47.9 Hz, CHF), 4.92-4.85 (1H, q, *J* = 6.4 Hz, CHMe), 2.85-2.72 (4H, m, 2×CH_2) and 1.64 (3H, d, *J* = 5.8 Hz, CH_3); δ_c (400 MHz, $CDCl_3$) 133.9 (Ar C), 132.6 (Ar CH), 131.0 (Ar C), 129.1 (Ar CH), 128.9 (Ar CH), 128.5 (Ar CH), 126.5 (Ar CH), 126.0 (Ar CH), 125.8 (Ar CH), 123.8 (Ar CH), 122.3 (Ar CH), 92.9 (d, *J* = 172.8 Hz, CF), 54.1 (CH), 49.8 (d, *J* = 22.2 Hz, CH_2), 39.0 (d, *J* = 20.9 Hz, CH_2) and 22.5 (CH_3); δ_F

{^{1}H} (400 MHz, $CDCl_3$): -63.0 (3F, s, CF_3), -184.2 (1F, s, CF); **IR** (nujol mull) υ_{max}**/cm^{-1}** 2985, 1453, 1329, 1207, 1074, 1026, 801 and 750. ***m/z*** (ESI^+) 398 [$M+Na^+$] (30). HRMS (ES^+): Found 376.1676. Calcd. For $[M+H]^+$ $C_{10}H_{10}OF_3$, 376.1683.

(2*S*,1'*R*)-2-fluoro Cinacalcet HCl 124.

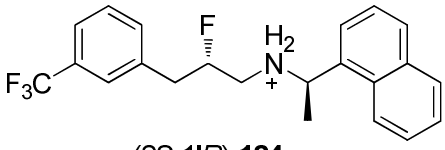

(2S,1'*R*)-**124**

Trifluoromethanesulfonic anhydride (0.3 mL, 1.8 mmol) was added to a solution of Et_3N (0.33 mL, 4.5 mmol) and DMAP (15 mg, 0.1 mmol) in dry DCM (30 mL) at 0 °C. (*S*)-**148 (**258 mg, 1.2 mmol) was added into the reaction mixture through a cannula and was left to stir for 2 h at 0 °C. The reaction mixture was subsequently warmed to RT and stirring continued for 16 h. The reaction was quenched with saturated $NaHCO_3$ solution (30 ml) and the aqueous layer was washed with EtOAc (3 x 50 mL). The combined organic layers were concentrated under reduced pressure to afford (*S*)-**149** as a crude mixture.

The crude mixture (*S*)-**149** was used for the next reaction without purification. (*R*)-1-(1-napthyl)ethylamine (0.2 ml, 1.8 mmol) was added into a solution of (*S*)-**149** (245 mg, 0.7 mmol) in toluene (15 mL) and the reaction was heated at reflux for 16 h. After 16 h, the reaction mixture was concentrated under reduced pressure. Purification over silica gel (hexane: EtOAc; 8:2) to give the title compound (2*S*,1'*R*)-**124** (207 mg, 78%) as a pale yellow oil. HCl in diethyl ether (0.1 mL, 1 M) was added into (2*S*,1'*R*)-**124** to afford the hydrochloride salt.

[α]$_D$ – 8.0 (c 0.6, $CHCl_3$); **δ_H** ($CDCl_3$): 8.22-7.39 (11H, m, Ar-H), 5.39 (dm, *J* = 49.2 Hz, CHF), 5.20-5.14 (1H, q, *J* = 6.7 Hz, CHMe), 3.17-2.79 (4H, m, 2$\times$$CH_2$) and 1.61 (3H, d, *J* = 6.7 Hz, CH_3); **δ_c** ($CDCl_3$) 138.2 (Ar C), 134.4 (Ar CH), 133.1 (Ar CH), 131.6 (Ar CH), 129.4 (Ar CH), 129.2 (Ar CH), 128.0 (Ar CH), 126.4 (Ar CH), 126.1 (Ar CH), 125.9 (Ar CH), 123.9 (Ar CH), 123.9 (Ar CH), 123.4 (Ar CH), 123.1 (Ar CH), 94.6 (d, *J* = 171.6 Hz, CHF), 54.1 (CH), 51.1 (d, *J* = 21.5 Hz, CH_2) and 39.5 (d,

J = 21.6 Hz, CH_2) and 23.9 (CH_3); $\boldsymbol{\delta_F}$ (400 MHz, $CDCl_3$): -63.1 (3F, s, CF_3), -183.6 (1F, s, CF). ***m/z*** (ESI$^+$) 398 [M+Na$^+$] (30). HRMS (ES$^+$): Found 376.1688. Calcd. For [M+H]$^+$ $C_{10}H_{10}OF_3$, 376.1683.

3-(3-(Pentafluorosulfur)phenyl)benzyl bromide 154.

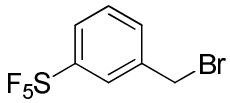

154

Phosphorus tribromide (4.5 mL, 0.05 mol) was added to a solution of **153** (10.0 g, 0.04 mol) in EtOH (20 mL) at RT. After 3 h, the reaction was work-up with $NaHCO_3$ at 0 °C. The aqueous layer was washed with ethyl acetate (3 ×50 mL) and the organic layer was combined. Concentration under reduce pressure and purification over silica gel (hexane: EtOAc; 9:1) to afford the title compound **154** (9.0 g,76%) as a pale yellow oil.

$\boldsymbol{\delta_H}$ (300 MHz, $CDCl_3$) 7.81-7.45 (4H, m, Ar-H) and 4.52 (2H, s, CH_2); $\boldsymbol{\delta_c}$ (300 MHz, $CDCl_3$) 132.1 (Ar CH), 129.2 (Ar CH), 126.5 (Ar CH), 125.9 (Ar CH) and 31.6 (CH_2); $\boldsymbol{\delta_F}$ (400MHz, $CDCl_3$): 62.2 (1F, d, J = 150.1 Hz, F_{eq}) and 83.3 (4F, q, F_{axial}); **IR** (nujol mull) $\boldsymbol{\upsilon_{max}/cm^{-1}}$ 3027, 2984, 1493, 1319, 1158, 1027, 913, 827 and 7549. ***m/z*** (CI) 278 [M-F^-] (55). HRMS (CI^+): Found 276.9302. Calcd. For $[M-F]^+$ $C_7H_6SF_4Br$, 276.9310.

3-(3-(Pentafluorosulfur)phenyl)propanoic acid 155.

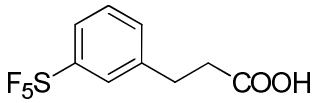

155

Diethyl malonic (2.5 mL, 0.01 mol) and sodium hydride (404.0 mg, 0.01 mol) was added to a solution of **154** (5.0 g, 0.01 mol) in a dry THF (50 mL) at –78 °C. After 1 h of stirring, the reaction mixture was subsequently warmed to RT and stirring continued for 16 h. After all the starting material was consumed, as confirmed by TLC analysis, the reaction was quenched with hydrochloric acid (10 mL) in an ice-cooled water bath. The aqueous layer was washed with ethyl acetate (3 ×50 mL) and the combined organic layers were concentrated under reduced pressure. The crude product was used for the next reaction without purification.

NaOH (6 M, 30 mL) and EtOH (5 mL) were added to the reaction mixture, which was then heated at reflux. After 16 h, the reaction was worked-up with concentrated HCl solution to pH 2 at 0 °C and the reaction mixture was extracted into ethyl acetate (3 ×50 mL). The organic layers were combined and the crude product was concentrated under reduced pressure. The crude product was used for the next stage without further purification.

Concentrated HCl (4M, 30mL) was added to the crude product from the aforementioned reaction and the reaction mixture was heated at reflux. After 16 h, the reaction mixture was quenched with saturated $NaHCO_3$ solution at 0 °C and acidified with concentrated HCl solution until pH 2. The reaction mixture was extracted into ethyl acetate (3 × 100 mL). The combined organic layers were concentrated under reduced pressure and purification over silica gel (hexane/ethyl acetate; 8:2) afforded the title compound **155** (2.3 g, 50%) as a colourless oil.

$\boldsymbol{\delta_H}$ (300 MHz, $CDCl_3$) 7.65-7.41 (4H, m, Ar-H) 3.06 (2H, t, J = 7.7 Hz, CH_2) and 2.76 (2H, t, J = 7.7 Hz, CH_2); δ_c (300 MHz, $CDCl_3$) 141.0 (Ar C), 131.8 (Ar CH), 129.0 (Ar CH), 125.0 (Ar CH), 123.3 (Ar CH), 35.5 (CH_2) and 30.2 (CH_2); $\boldsymbol{\delta_F}$ (400MHz, $CDCl_3$): 62.4 (1F, d, J = 149.5 Hz, F_{eq}) and 83.9 (4F, q, F_{axial}); **IR** (nujol mull) υ_{max}/cm^{-1} 3353, 3006, 1484, 1313, 1272, 1109, 886, 827 and 764. ***m/z*** (ESI^+) 299 [$M+Na^+$] (50). HRMS (ESI^+): Found 299.0141. Calcd. For $[M+Na]^+$ $C_9H_9SF_5O_2$, 299.0136.

3-(3-(Pentafluorosulfur)phenyl)propan-1-ol 156.

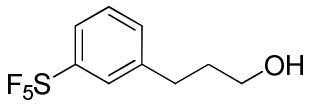

156

Lithium aluminium hydride (206 mg, 5.4 mmol) was added to a solution of **155** (1.0 g, 3.6 mmol) in THF (30 mL). The reaction mixture and heated under reflux for 1 h. The reaction mixture was quenched with saturated $NaHCO_3$ (15 mL). The reaction mixture was extracted into EtOAc (3 x 50 mL). Concentration of the reaction crude to give the title compound **156** (848.8 mg, 90%) as a colourless oil.

$\boldsymbol{\delta_H}$ (400 MHz, $CDCl_3$) 7.61-7.38 (4H, m, Ar-H) 3.7 (2H, *t*, *J* = 6.3 Hz, CH_2) 2.82 (2H, t, *J* = 7.8 Hz, CH_2) and 1.93 (2H, m, CH_2); $\boldsymbol{\delta_c}$ (400 MHz, $CDCl_3$) 131.6 (Ar CH), 128.6 (Ar CH), 125.7 (Ar CH), 123.5 (Ar CH), 61.8 (COH), 33.9 (CH_2) and 31.9 (CH_2); $\boldsymbol{\delta_F}$ (400 MHz, $CDCl_3$): 62.4 (1F, d, *J* = 149.8 Hz, F_{eq}) and 84.4 (4F, q, F_{axial}); **IR** (nujol mull) $\boldsymbol{\upsilon_{max}/cm^{-1}}$ 3351, 2937, 1434, 1328, 1274, 1110, 918, 824 and 744. ***m/z*** (CI^+) 243 [M-F^-] (100). HRMS (CI^+): Found 243.0464. Calcd. For $[M-F]^+$ $C_9H_{11}OF_3S$, 243.0467.

3-(3-(pentafluorosulfur)phenyl)propanal 157.

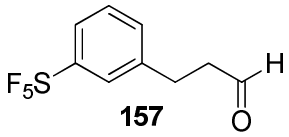

157

Dess-Martin Periodinane (1.9 g, 4.58 mmol) was added to a solution of **156 (**0.8 g, 3.0 mmol) in dry DCM (20 mL) at 0 °C and the reaction mixture was slowly warmed to RT. After 1 h of stirring, the reaction was quenched with saturated $NaHCO_3$ solution (30 mL). The aqueous layer was washed with EtOAc (3 x 50 mL) and the combined organic layers were concentrated under reduced pressure. Purification over silica gel (hexane: EtOAc; 9:1) gave the title compound **157** (0.7 g, 90%) as a colourless oil.

$\boldsymbol{\delta_H}$ (400 MHz, $CDCl_3$) 9.76 (1H, s, CHO), 7.52-7.29 (4H, m, Ar-H) 2.95 (2H, t, *J* = 7.4 Hz, CH_2) and 2.76 (2H, t, *J* = 7.4 Hz, CH_2); $\boldsymbol{\delta_c}$ (400 MHz, $CDCl_3$) 200.3 (C=O), 141.6 (Ar C), 131.6 (Ar CH), 128.9 (Ar CH), 125.8 (Ar CH), 124.0 (Ar CH), 44.9 (CH_2) and 27.8 (CH_2); $\boldsymbol{\delta_F}$ (400MHz, $CDCl_3$): 62.4 (1F, d, *J* = 150.09 Hz, F_{eq}) and 84.1 (4F, q, F_{axial}); **IR** (nujol mull) $\boldsymbol{\upsilon_{max}/cm^{-1}}$ 3006, 1710, 1484, 1435, 1275, 1100, 828, 805 and 783. ***m/z*** (CI^+) 241 [M-F^-] (100). HRMS (CI^+): Found 241.0310. Calcd. For $[M-F]^+$ $C_9H_9OF_3S$, 243.0310.

3''-SF_5- Cinacalcet HCl 137.

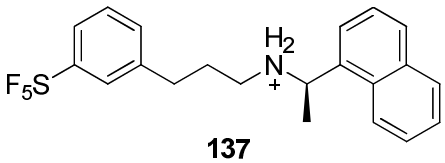

137

(*R*)-1-(1-Napthyl)ethylamine (0.15 mL, 0.9 mmol) was added to a solution of **157** (0.2 g, 0.7 mmol) in THF and stirred at RT for 5 h. Sodium triacetoxyborohydride (0.19 mg, 0.9 mmol) was then added into the reaction mixture and stirring continued for 16 h at RT. The reaction was concentrated under reduced pressure. Purification over silica gel (hexane: EtOAc; 8:2) and followed by addition of HCl in diethyl ether (0.1 mL, 1M) to give to the title compound **137** (0.28 g, 90%) as a colourless oil.

$[\alpha]_D$ +14.0 (c 0.4, $CHCl_3$); **δ_H** (400 MHz, $CDCl_3$): 8.15-7.38 (11H, m, Ar-H), 5.11 (1H, brm, CH), 2.69 (2H, brm, CH_2), 2.47 (2H, brm, CH_2), 2.19 (2H, brm, CH_2) and 1.91 (3H, d, *J* = 6.0 Hz, CH_3); **δ_c** (400 MHz, $CDCl_3$) 141.0 (Ar C), 133.8 (Ar C), 132.0 (Ar C), 131.3 (Ar C), 130.6 (Ar CH), 129.6 (Ar CH), 129.5 (Ar CH), 128.7 (Ar CH), 127.4 (Ar CH), 126.3 (Ar CH), 126.1 (Ar CH), 125.6 (Ar CH), 125.0 (Ar CH), 123.8 (Ar CH), 121.2 (Ar CH), 53.5 (C), 45.4 (CH_2), 32.6 (CH_2), 27.3 (CH_2) and 21.3 (CH_2); **δ_F** (400 MHz, $CDCl_3$): 62.4 (1F, d, *J* = 150.09 Hz, F_{eq}) and 84.0 (4F, q, F_{axial}); **IR** (nujol mull) **υ_{max}/cm^{-1}** 2925, 2848, 1275, 1261, 845, 805 and 750. ***m/z*** (ESI^+) 416 [$M+H^+$] (100). HRMS (ES^+): Found 416.1469. Calcd. For $[M+H]^+$ $C_{21}H_{23}NF_5S$, 416.1471.

Cinacalcet HCl 117.[6]

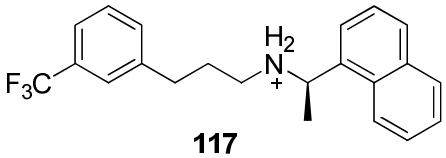

117

Cinacacet HCl was synthesized following a published method[6], starting with **140**. This product was obtained as a pale yellow oil (2.4 g, 80%). $[\alpha]_D$ +8.7 (c 1, $CHCl_3$) lit. $[\alpha]_D$ +10.0 (c 1, $CHCl_3$); δ_H (400 MHz, $CDCl_3$): 8.12-7.21 (11H, m, Ar-H), 4.57 (1H, q, CH), 2.71-2.46 (4H, m, 2×CH_2) and 1.75 (3H, d, J = 6.44 Hz, CH_3); δ_F {^{1}H} (400 MHz, $CDCl_3$): -63.0 (3F, s, CF_3). ***m/z*** (ESI^+) 416 [$M+H^+$] (100). These data were in accordance with the literature.[6]

5.3 GC-MS analysis for determination of enantiopurity of product (*R*)-147 and (*S*)-147.

Chiral phase GC-MS analysis was achieved using a Betadex^{TM} 120 fused silica capillary column (30 m × 0.25 mm i.d., 0.25 μM film thickness). The conditions used for GC-MS analysis of (*R*)-**147** were: oven held at 80 °C for 20 min, then a gradient at 20 °C/min to 150 °C, 250 °C injector temperature; 100:1 split ratio, 1.0 mL/min flow. The GC-MS chromatogram presented in **Figure 5.1** shows a major peak at the retention time of 36.24 min, which corresponds to (*R*)-**147** ($[M]^{+\cdot}$, ***m/z*** = 220, while the minor peak shown at the retention time of 33.16 min was assigned to be the difluorinated compound ($[M]^{+\cdot}$, m/z = 238). The enantiomeric ratio of (*R*)-**147** determined from the chiral phase GC-MS was found to be 99%ee. The MS (EI) spectra of the peak at 33.16 (**Figure 5.2**) and 36.24 min (**Figure 5.3**) showed an identical fragment pattern of *m/z* = 159, which corresponds to $[M\text{-}CHFCHO]^{+}$ of the (*R*)-**147** and **151**.

Retention time (min)	Area (units)	Ratio
33.16	68530.3	1
36.24	1370606	20

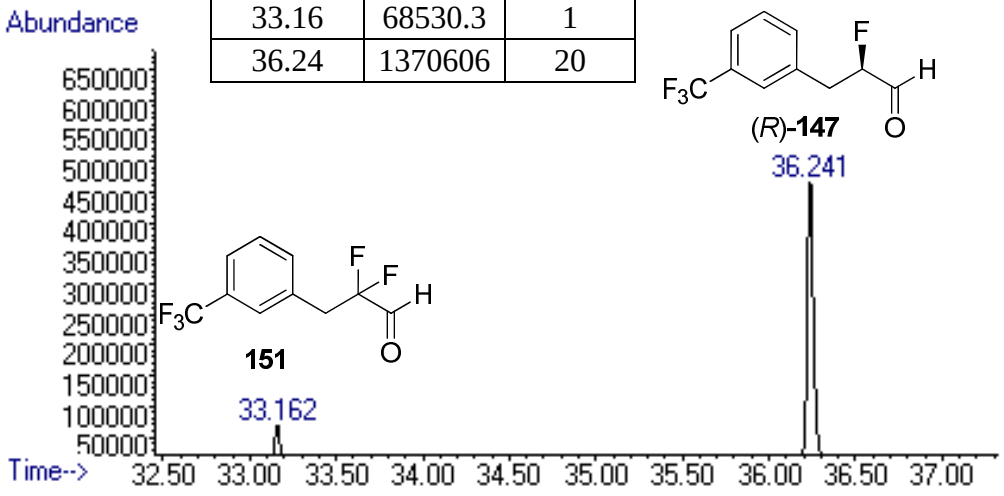

Figure 5.1. The chiral phase GC chromatogram of the crude (*R*)-**147**. (99 % ee): oven start at 80 °C held for 20 min, the gradient at 20 °C/min to 150 °C), 250 °C injector temperature, 100:1 split ratio, 1.0 mL/min flow.

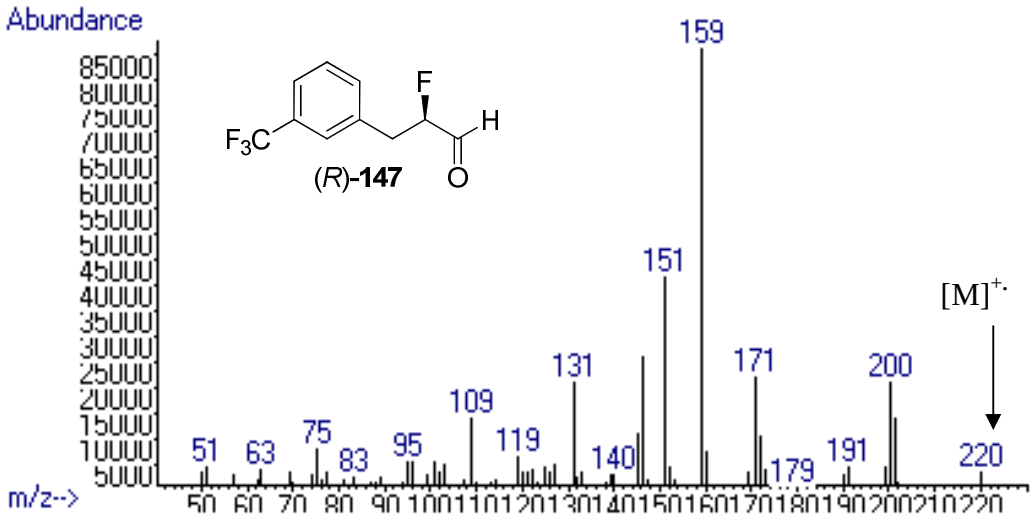

Figure 5.2. Mass spectrum of the GC peak at 36.2 min showing the presence of (*R*)-**147**.

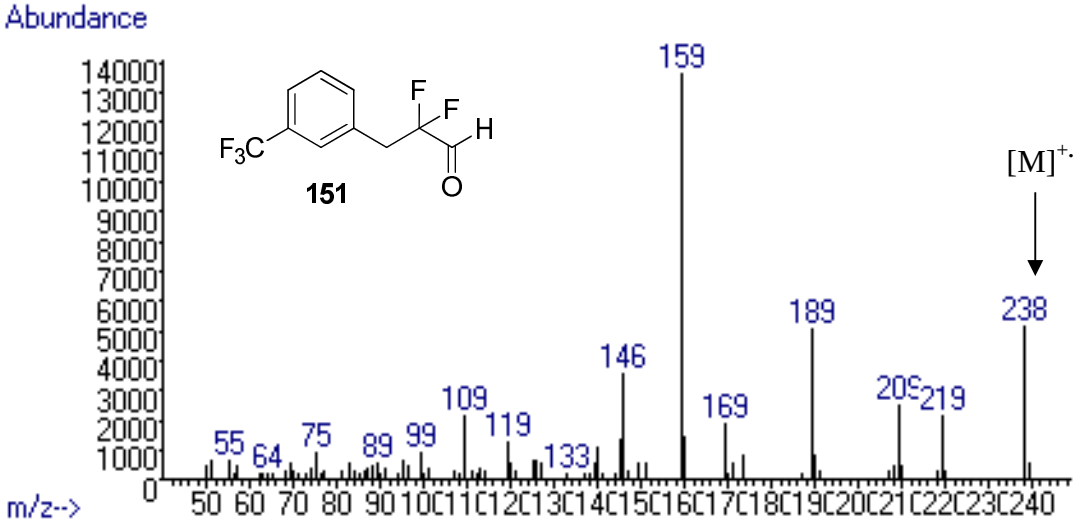

Figure 5.3. Mass spectrum of the GC peak at 33.1 min showing the presence of **151**.

A similar procedure was applied to the other enantiomer (*S*)-**147**. The GC-MS chromatogram presented in **Figure 5.4** showed a major peak at retention time 36.26 min, which corresponded to (*S*)-**147** ($[M]^{+\cdot}$, ***m/z*** = 220), while the minor peak at retention time 33.17 min was assigned to the difluorinated compound **151** ($[M]^{+\cdot}$, m/z = 238). The enantiomeric ratio of (*S*)-**147** determined from the chiral phase GC-MS was found to be 99%. The MS (EI) spectra of the peak at 36.26 min (**Figure 5.5**) was found to have identical fragment pattern with the **Figure 5.3**, with (***m/z*** = 159 $[M\text{-}CHFCHO]^{+\cdot}$, ***m/z*** = 200 $[M\text{-}F^{-}]$, ***m/z*** = 220 $[M]^{+\cdot}$), confirms that (*S*)-**147** are enantiomer of each other.

Retention time (min)	Area (units)	Ratio
33.17	71268.4	1
36.26	1187808	16.7

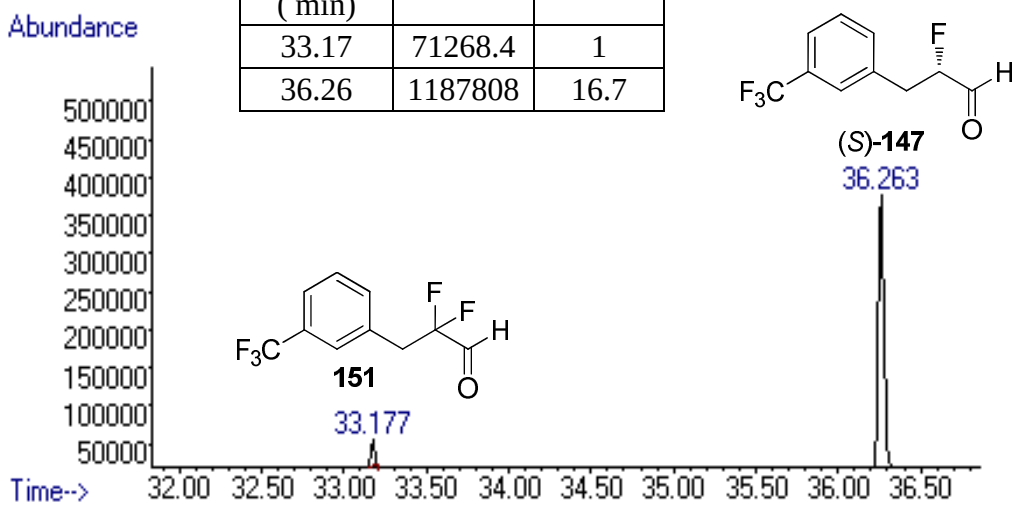

Figure 5.4. The chiral phase GC chromatogram of the crude (*S*)-**147**. (99 % ee): oven start at 80 °C held for 20 min, the gradient at 20 °C/min to 150 °C), 250 °C injector temperature, 100:1 split ratio, 1.0 mL/min flow.

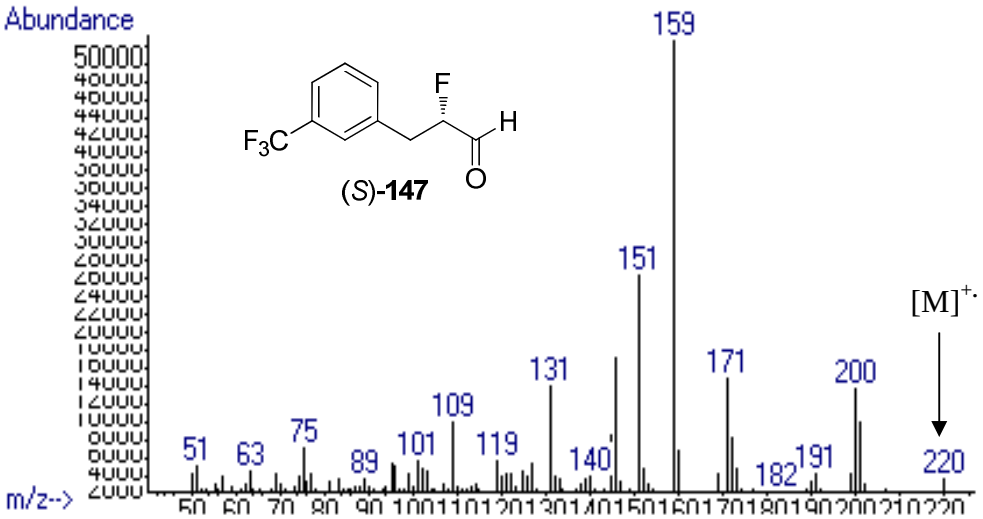

Figure 5.5. Mass spectrum of the GC peak at 36.2 min showing the presence of (*S*)-**147**.

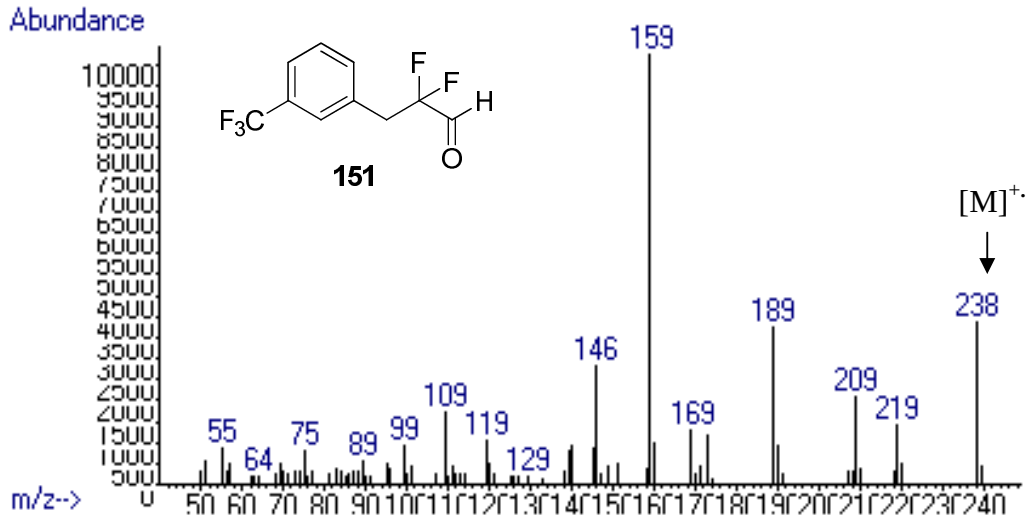

Figure 5.6. Mass spectrum of the GC peak at 33.1 min showing the presence of **151**.

References:

[1] M. E. V. Dort, Y. W. Jung, P. S. Sherman, M. R. Kilburn and D. M. Wieland, *J. Med. Chem.*, 1995, **38**, 810-815.

[2] O. M. Cohn, C. Moore and H. C. Taljaard, *J. Chem. Soc. Perkin Trans.1*, 1988, **9**, 2663-2674.

[3] R. Shlomo and K. Moshe, *J. Org. Chem.*, 1990, **55**, 5155-5159.

[4] R. Cysewski, M. Kwit, B. Warzajtis, U. Rychlewska and J. Gawroński, *J. Org. Chem.*, 2009, **74**, 4573-4583.

[5] L. Claisen and H. Hori, *Ber. Chem.*, 1891, **24**, 120.

[6] X. Wang, Y. Chen, R. Crockett, J. Briones, T. Yan, C. Orihuela, B. Zhi and J. Ng, *Tetrahedron Lett.*, 2004, **45**, 8355-8358.

Appendix 1

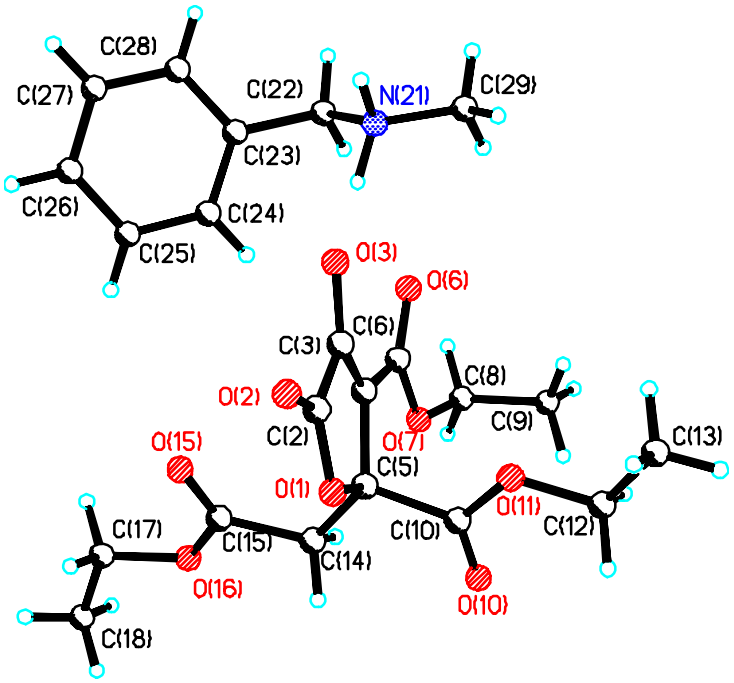

Table 1. Crystal data and structure refinement for **93**

Identification code	pcdh16	
Empirical formula	C22 H29 N O9	
Formula weight	451.46	
Temperature	93(2) K	
Wavelength	0.71073 Å	
Crystal system	Triclinic	
Space group	P-1	
Unit cell dimensions	a = 9.595(9) Å	α= 94.97(2)°.
	b = 9.918(10) Å	β= 92.058(12)°.
	c = 13.558(11) Å	γ = 112.66(2)°.
Volume	1182.9(19) $Å^3$	
Z	2	
Density (calculated)	1.268 Mg/m^3	
Absorption coefficient	0.099 mm^{-1}	
F(000)	480	
Crystal size	0.30 x 0.10 x 0.10 mm^3	
Theta range for data collection	2.56 to 25.39°.	

Index ranges	-10<=h<=11, -11<=k<=11, -13<=l<=16
Reflections collected	7410
Independent reflections	4168 [R(int) = 0.1465]
Completeness to theta = 25.30°	96.6 %
Absorption correction	Multiscan
Max. and min. transmission	1.000 and 0.740
Refinement method	Full-matrix least-squares on F^2
Data / restraints / parameters	4168 / 2 / 298
Goodness-of-fit on F^2	1.299
Final R indices [I>2sigma(I)]	R1 = 0.1447, wR2 = 0.3596
R indices (all data)	R1 = 0.1635, wR2 = 0.3995
Extinction coefficient	0.11(3)
Largest diff. peak and hole	0.632 and -0.447 e.$Å^{-3}$

Appendix 2

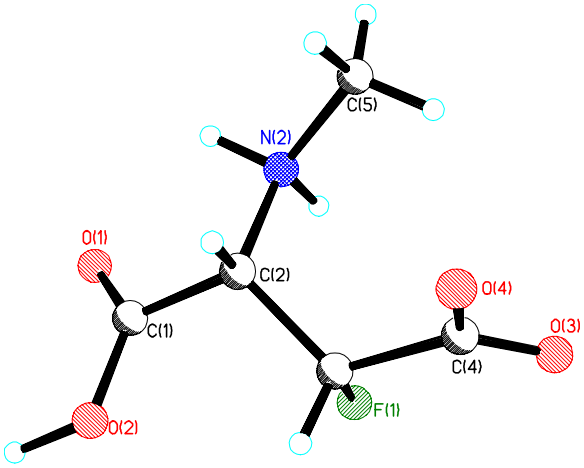

Crystal data and structure refinement for **(-)-73**

Empirical Formula	$C_5H_9ClFNO_4$
Formula Weight	201.58
Crystal Color, Habit	colorless, needle
Crystal Dimensions	0.100 X 0.030 X 0.010 mm
Crystal System	triclinic
Lattice Type	Primitive
Lattice Parameters	a = 5.064(2) Å b = 5.638(2) Å c = 6.877(3) Å α = 110.97(2) ^{o} β = 98.24(2) ^{o} γ = 105.14(2) ^{o} V = 170.75(11) $Å^3$

Space Group	P1 (#1)
Z value	1
D_{calc}	1.960 g/cm^3
F_{000}	104.00
μ(CuKα)	50.302 cm^{-1}

Appendix 3

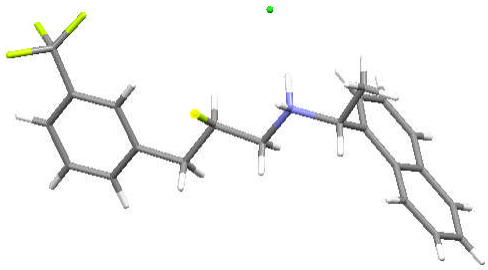

Table 1. Crystal data and structure refinement for (*R*,*R*)-**139**.

Identification code	pcdh27	
Empirical formula	C22 H22 Cl F4 N	
Formula weight	411.86	
Temperature	173(2) K	
Wavelength	1.54178 Å	
Crystal system	Orthorhombic	
Space group	P2(1)2(1)2(1)	
Unit cell dimensions	a = 7.2710(4) Å	α= 90°.
	b = 13.0197(6) Å	β= 90°.
	c = 22.3322(11) Å	γ = 90°.
Volume	2114.11(18) $Å^3$	
Z	4	
Density (calculated)	1.294 Mg/m^3	
Absorption coefficient	1.967 mm^{-1}	
F(000)	856	
Crystal size	0.12 x 0.05 x 0.05 mm^3	
Theta range for data collection	3.93 to 68.06°.	
Index ranges	-8<=h<=8, -15<=k<=15, -26<=l<=26	
Reflections collected	26693	
Independent reflections	3740 [R(int) = 0.0433]	
Completeness to theta = 67.00°	98.3 %	
Absorption correction	Multiscan	
Max. and min. transmission	1.000 and 0.723	
Refinement method	Full-matrix least-squares on F^2	
Data / restraints / parameters	3740 / 2 / 250	
Goodness-of-fit on F^2	1.039	

Final R indices [I>2sigma(I)]	R1 = 0.0704, wR2 = 0.1892
R indices (all data)	R1 = 0.0726, wR2 = 0.1918
Absolute structure parameter	0.05(3)
Largest diff. peak and hole	0.972 and -0.609 e.Å^{-3}

Appendix

Conferences attended:

1. *24-26th April* 2009, *3rd European* Symposium *on Bio-Organic Chemistry. Gregynog, Powys, Wales (UK)*: Visitor.

2. *9-10 September 2010, 10th Annual RSC Fluorine Subject Group Postgraduate Meeting, Durham (UK)*: Oral presentation.

3. *3rd May 2011, 22nd SCI regional graduate symposium on novel organic chemistry, Edinburgh (UK)*: Oral presentation.

4. *14th December 2011, 40th Scottish Regional Meeting of the Organic Division of the Royal Society of Chemistry, Glasgow (UK)*: Visitor.